AD-A139 592 IMPURITY AND DEFECT INTERACTIONS IN GAAS(U) WASHINGTON 1/2
UNIV ST LOUIS MO SEMICONDUCTOR RESEARCH LAB
C M WOLFE ET AL. 29 FEB 84 WU/SRL-64422-22
UNCLASSIFIED N00014-80-C-0762 F/G 20/12 NL

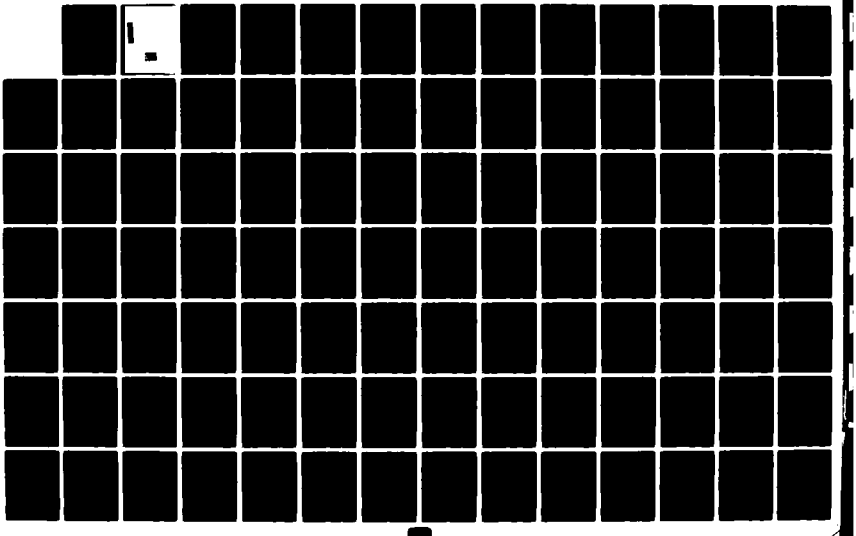

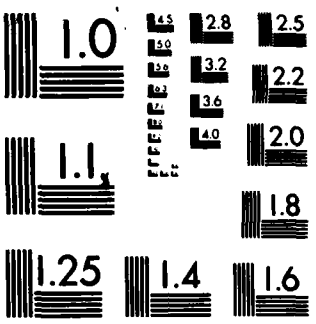

Unclassified

SECURITY CLASSIFICATION OF THIS PAGE (When Data Entered)

(12)

REPORT DOCUMENTATION PAGE		READ INSTRUCTIONS BEFORE COMPLETING FORM
1. REPORT NUMBER	2. GOVT ACCESSION NO.	3. RECIPIENT'S CATALOG NUMBER
4. TITLE (and Subtitle) Impurity and Defect Interactions in GaAs		5. TYPE OF REPORT & PERIOD COVERED Final Technical Report 1 Aug 1980 to 31 Dec 1983 6. PERFORMING ORG. REPORT NUMBER WU/SRL-64422-22
7. AUTHOR(s) Charles M. Wolfe, et al.		8. CONTRACT OR GRANT NUMBER(s) N00014-80C-0762
9. PERFORMING ORGANIZATION NAME AND ADDRESS Semiconductor Research Lab Box 1127 Washington University St. Louis, MO 63130		10. PROGRAM ELEMENT, PROJECT, TASK AREA & WORK UNIT NUMBERS PE61153N PR021-02-03 NR243-032
11. CONTROLLING OFFICE NAME AND ADDRESS Office of Naval Research Code 414 Arlington, VA 22217		12. REPORT DATE 29 February 1984 13. NUMBER OF PAGES 175
14. MONITORING AGENCY NAME & ADDRESS(if different from Controlling Office)		15. SECURITY CLASS. (of this report) Unclassified 15a. DECLASSIFICATION/DOWNGRADING SCHEDULE

16. DISTRIBUTION STATEMENT (of this Report)

Approved for public release; distribution unlimited.

17. DISTRIBUTION STATEMENT (of the abstract entered in Block 20, if different from Report)

18. SUPPLEMENTARY NOTES

ONR Scientific Officer
Telephone: (202) 696-4218

19. KEY WORDS (Continue on reverse side if necessary and identify by block number)

GaAs, impurities, defects, complexes, epitaxy, ion implantation, Cr redistribution, impurity incorporation, complex formation, lineshape analysis, carrier scattering.

20. ABSTRACT (Continue on reverse side if necessary and identify by block number)

This work was initiated to examine interactions among impurities and defects in GaAs which produce problems in the fabrication of high-speed integrated circuits. For this purpose various aspects of impurity and defect identification, interaction, redistribution, incorporation, and carrier scattering were investigated.

DD FORM 1 JAN 73 1473 EDITION OF 1 NOV 65 IS OBSOLETE

Unclassified

SECURITY CLASSIFICATION OF THIS PAGE (When Data Entered)

TABLE OF CONTENTS

APPENDICES

1. RESEARCH OBJECTIVES

The purpose of this work was to investigate the interactions among impurities, defects, and complexes in GaAs which adversely affect the yield and performance of high-speed GaAs integrated circuits. To achieve this objective the following experimental approach was employed: Impurities were introduced into GaAs by doping during epitaxial growth and by ion-implantation into bulk samples. Annealing was performed under controlled atmospheres with applied fields. The resulting samples were characterized by a combination of low and high temperature resistivity and Hall measurements, differential capacitance measurements, far and near infrared photoconductivity measurements, photoluminescence, and secondary ion mass spectroscopy. These data were then analyzed with impurity incorporation, redistribution, complex formation, and other models.

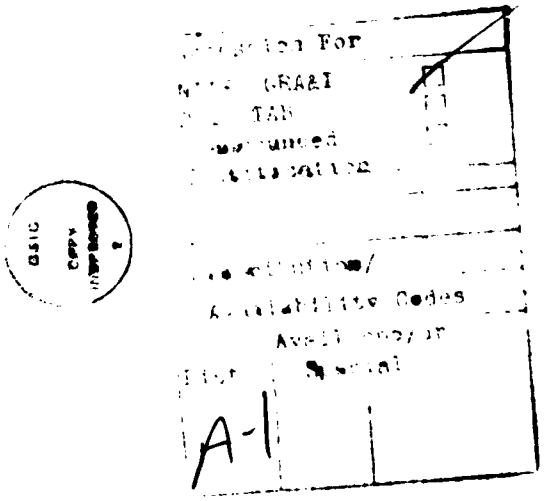

2. SUMMARIZED RESULTS

The results of these measurements and analyses are summarized below. For more details on any subject the reader is referred to the appropriate section in the Appendices.

2.1 IDENTIFICATION OF IMPURITIES

With the availability of high-purity GaAs from a variety of epitaxial growth techniques, improved donor identifications were made by far infrared photoconductivity measurements. Samples grown by $AsCl_3$-H_2 VPE, $AsCl_3$-N_2 VPE, AsH_3 VPE, LPE, MBE, and MOCVD were examined and the common residual donors were identified. (See Section A.1).

Photothermal ionization spectroscopy was also used to determine the residual donor species present and their relative concentrations in the highest purity MBE n-GaAs reported. Data were obtained for samples grown in two different MBE growth reactors; one using elemental As and the other using cracked AsH_3 as the arsenic source. In spite of the substantial differences between growth systems, the donor backgrounds were quite similar. (Section A.2).

Far infrared photoconductivity measurements on Si doped GaAs grown by molecular beam epitaxy (MBE) indicated that the impurity peak previously assigned to Si was incorrect. Data leading to the new identification were obtained and the results leading to the earlier identification were reexamined. Implications of the new identification on the importance of Si as a residual donor in GaAs grown by various techniques were obtained. (Section A.3).

Photothermal ionization data for undoped and S-doped epitaxial GaAs grown by metalorganic chemical vapor deposition (MOCVD) provided a positive identification of the S donor. This identification was unambiguous because S is not a significant residual impurity in the undoped MOCVD GaAs used for these measurements. Implications of

the new identification for the importance of S as a residual donor in epitaxial GaAs prepared by various other growth techniques were found. (Section A.4).

Unintentionally-doped samples grown by LPE in graphite boats in seven different laboratories were characterized using variable temperature photoluminescence and photothermal ionization spectroscopy. The dominant residual donor was always S, with Sn, Pb, and Si donors also observed. The main residual acceptors were Si and C but Mg and Ge were also present. It was found that the residual amphoteric impurities Si and Ge incorporate preferentially as acceptors while residual Pb and Sn incorporate preferentially as donors. The results suggest that S may be the main volatile donor species removed from the melt by baking. (Section A.5).

An analytical study of the impurities in trimethylgallium (TMGa) and subsequent correlation of the effect of these impurities on resulting GaAs films grown by metalorganic chemical vapor deposition (MOCVD) was performed. The effects of using fractional distillation techniques to improve the quality of TMGa and to help isolate and identify major source impurities in TMGa were examined. Photothermal ionization data were obtained which show the residual donor species present and their relative concentrations in the epitaxial layers. Correlations of the residual donor concentrations with TMGa preparation were obtained. It was demonstrated that high purity GaAs with $\mu_{77K} \simeq 125{,}000$ $cm^2/V\text{-sec}$ can be grown by MOCVD using repurified trimethylgallium and arsine source materials. (Section A.6).

2.2 REDISTRIBUTION OF IMPURITIES AND DEFECTS

The distribution of impurities incorporated in epitaxial layers during their growth was determined by diffusion due to concentration gradients and by drift in the built-in

electric field. This problem was previously treated in the approximation that the impurities reach their equilibrium distribution during growth. We extended this calculation to treat impurity drift and diffusion under non-equilibrium conditions, a situation much more characteristic of most realistic growth conditions. In the new calculation, the solution of the Shockley-Poisson problem is exact and the boundary condition at the growth interface is an approximation based on the electrostatics of surface states. The new calculation also permits consideration of outdiffusion from the substrate, a phenomenon of technological significance. It is also capable of modeling variations of source impurity concentration and growth rate during epitaxial growth. Calculations modeling n-type GaAs epitaxy of practical interest were obtained. (Section B.1).

A model of Cr in GaAs which is consistent with a large body of experimental data was developed. It relies on spectroscopic models and on our interpretation of redistribution and electrical data, all of which indicate the existence of Cr complexes. The existence of rapidly diffusing interstitial Cr donors was assumed and justified. The model offers a unified picture of the effects of implantation on the Cr profile. It contains mechanisms for compensation and redistribution, which offer an explanation of the semi-insulating properties of Cr doped GaAs and of the two apparently incompatible classes of diffusion and anneal data. The redistribution depends on how the Cr was incorporated and on the vacancy concentration profiles. A study of representatives of the two classes of redistribution data provided an estimate of the lower limit of interstitial Cr diffusion constant and of the vacancy diffusion lengths in GaAs. (Section B.2).

During the annealing of ion-implanted Cr-doped GaAs, Cr often redistributes and accumulates at the surface.

Although this behavior has been attributed to strain fields and other mechanisms, the widths of these accumulation regions suggest that electric fields due to surface states are a limiting factor in Cr redistribution. For this reason we developed a thermodynamic model for Cr redistribution which takes into account the electric field due to surface states. A qualitative fit to SIMS data on annealed unimplanted GaAs samples was obtained with this model. We also used applied voltages during annealing to modify the amount of band bending and Cr buildup at the surface. This experiment indicated that the accumulated ions were positively charged. We concluded from these experiments that electric fields play a significant role in the redistribution of Cr at GaAs surfaces. (Section B.3).

For ion-implanted samples systematic differences were found between annealing conditions where the Cr is observed to redistribute and the conditions where it does not. When Cr redistribution was observed, we separated electrical from chemical and/or strain interactions. The results indicated that electrical interactions are at least a limiting factor and in most cases a dominant factor in Cr redistribution. Thus, Cr redistribution in ion implanted samples can be minimized or eliminated by annealing at temperatures such that the background free carrier concentration screens out any internal electric fields. (Section B.4).

2.3 INCORPORATION OF IMPURITIES AND DEFECTS

The incorporation of Group IV impurities as donors and as acceptors in high purity epitaxial GaAs was investigated using photothermal ionization spectroscopy and variable temperature photoluminescence to detect donors and acceptors respectively. Samples from several sources of high purity LPE, $AsCl_3$-VPE, AsH_3-VPE, MOCVD, and MBE grown GaAs were measured to establish the typical residual impurities present and their relative concentrations. For AsH_3-VPE, MOCVD, and

MBE GaAs, impurity incorporation data were obtained as a function of III/V ratio. The relative incorporation of amphoteric impurities as donors and acceptors was compared to the model of Teramoto (1972) for LPE and its extension to $AsCl_3$-VPE by Ashen et al. (1975). (Section C.1).

To directly examine possible impurity interactions or complexing in GaAs, multiply-doped epitaxial layers were prepared. Samples doped both homogeneously and inhomogeneously with H_2O and H_2S exhibited effects which indicate that: (1) H_2O produces free carrier compensation and deep donor behavior; and (2) H_2O affects the incorporation and/or diffusion of sulfur. Experiments were performed to obtain more insight into these interactions. (Section C.2).

2.4 INTERACTIONS AMONG IMPURITIES AND DEFECTS

We calculated the correlation function for a pair of specific particles making nearest-neighbor jumps in a simple-cubic lattice. Short-ranged interactions were included by allowing one jump rate when the particles are separated and arbitrary jump rates into and out of configurations where the particles are nearest neighbors. This correlation function was then used to calculate the effects of particle repulsion (or attraction) on T_1(I-I), the motionally altered spin relaxation time due to the dipolar interaction between the hopping particles. The frequency or magnetic-field dependence of this relaxation time is not what one would expect from simply doctored second-moment arguments. (Section D.1).

The electrostatic effects on the energy of a hydrogenic donor complex in the presence of an externally applied magnetic field were investigated. A complex was defined as an impurity of net charge one whose charge distribution is not equivalent to a single simple point charge. The results were examined with respect to photoconductivity measurements of the 1s-2p shallow donor lines in GaAs. A study of these

far infrared photoconductivity donor spectra in a magnetic field indicated several features which were inconsistent with a second order Stark-shifted lineshape. It appears that many of the shallow donors have lower symmetry than the atoms they replace. This could be due to donor atoms displaced from simple substitutional sites or hydrogenic donor complexes. (Section D.2).

The effects of fluctuations in the Coulomb potential due to charged impurities in high-purity n-type III-V semiconductors were examined at low temperatures. Assuming that charged donors and acceptors are randomly distributed at high temperatures, we concluded that the donors are selectively filled at low temperatures leaving non-random distributions of charged and filled donors. The potential fluctuations from these distributions can approximately account for a number of experimental observations on low-temperature high-purity GaAs including the apparent decrease of donor binding energy with increasing impurity concentration observed in Hall measurements, the sharpness and temperature dependence of the 1s-2p transition along with the diffuse 1s-conduction band edge observed in photoconductivity experiments, and the fact that experimentally observed photoconductivity lineshapes are narrower than those previously predicted. (Sections D.3 and D.4).

We also calculated the second-order shifts in the energies of the 1s and $2p_{-1}$ states of hydrogenic donors in a magnetic field due to electric fields and combination of electric and strain fields in a piezoelectric medium. The results indicate a possible explanation of different line shapes and linewidths associated with different donors as observed in far infrared photoconductivity experiments on GaAs. (Section D.5).

2.5 ELECTRON SCATTERING FROM IMPURITIES AND DEFECTS

The magnetic-field dependence of the Hall factor was investigated theoretically and experimentally. The theory

included arbitrary band structure, carrier degeneracy, and wave functions assuming isotropic media and carriers behaving as spinless Fermions without energy-level quantization. Comparisons between theory and experiments on high-purity GaAs from the low magnetic-field limit to the classical high magnetic-field limit agree to within 0.8 percent. This result indicates that the concentrations of electrically active impurities and defects can be obtained from Hall measurements with a high degree of reliability. (Sections E.1 and E.2).

Static strains in piezoelectric semiconductors give rise to an electric field or potential which can have an effect on the electrical properties of the material. We calculated the electric potential due to the strain field arising from a random distribution of point defects. This potential contributes a term to the mobility that is proportional to $T^{1/2}$ and a Hall factor of 1.10. Crude estimates of strain strengths indicate that this scattering mechanism may contribute significantly to the mobility of electrically rather pure III-V semiconductors below room temperature when neutral impurity concentrations are greater than $10^{18} cm^{-3}$. The mechanism may also constitute a dominant one in the mobility of some III-V alloys at fairly low temperatures. The existence of strain induced electric potentials also provides at least a possible mechanism whereby different donors can have different lineshapes as measured in photoconductivity expermiments. (Section E.3).

Suitability of the Born approximation and the Boltzmann equation was demonstrated for the scattering of free-carrier electrons by random-alloy atomic potentials in semiconductor alloys. Composition dependences of alloy-scattering potential strengths were hypothesized and electron scattering rates were derived. "Order parameters" were derived from scattering theory and compared to those derived previously

from statistical and thermodynamic arguments. The treatment was generalized to include ternary, quaternary, and lattice-matched alloys which, in general, show more complicated order-parameter dependencies than the previously known $x(1-x)$ dependence for ternary zincblende-alloys. The results are also applicable to dilute alloys such as those produced by neutral impurities. Electron-momentum relaxation-rate expressions were obtained, including non-parabolic Kane bands and admixed wave functions appropriate to small energy-gap semiconductors. Electron drift mobility, as determined by alloy scattering, was derived in the effective-mass limit which shows that any short-range alloy potential yields the experimentally observed $1/\sqrt{m^{*5}}T$ dependence reported in the literature. An effective-charge model for alloy scattering was compared to experiments on $Al_xGa_{1-x}As$. The magnitude of the effective charge on isolated Al atoms in GaAs was found to be 0.145 electron charges. (Section E.4).

3. PERSONNEL

The personnel who worked directly on various aspects of Contract N00014-80C-0762 are listed below with their titles and affiliations:

Name	Title	Affiliation
Charles M. Wolfe	Sachs Professor of Electrical Engineering	Washington Univ.
Peter A. Fedders	Professor of Physics	Washington Univ.
James H. Burgess	Professor of Physics	Washington Univ.
Gregory E. Stillman	Professor of Electrical Engineering	Univ. of Illinois
Camellia M.L. Yee	Research Assistant	Washington Univ.
Roger T. Green	Research Assistant	Washington Univ.
Elizabeth A. Patten	Research Assistant	Washington Univ.
Thomas S. Low	Research Assistant	Univ. of Illinois
Brian J. Skromme	Research Assistant	Univ. of Illinois

The students who have received or will receive degrees for work performed on this contract are as follows:

Name	Degree	Date
Camellia M.L. Yee	D.Sc.	August 1983
Roger T. Green	D.Sc.	May 1984
Thomas S. Low	Ph.D.	May 1984
Brian J. Skromme	Ph.D.	August 1984

4. PUBLICATIONS

1. P.A. Fedders, "Effects of Interactions Between Hopping Particles on T_1 Relaxation Rates at Low Concentrations", Phys. Rev. B 25, 78 (1982).

2. P.A. Fedders, "Electrostatic Effects of Hydrogenic Donor Complexes on Magneto-Optical Spectra", Phys. Rev. B 25, 3846 (1982).

3. T.S. Low, G.E. Stillman, and C.M. Wolfe, "Identification of Residual Donor Impurities in Gallium Arsenide", Proc. 1981 Int. Symp. GaAs and Related Compounds (Inst. Phys., London, 1982) p. 143.

4. T.S. Low, G.E. Stillman, A.Y. Cho, H. Morkoc, and A.R. Calawa, "Spectroscopy of Donors in High-Purity GaAs Grown by Molecular Beam Epitaxy", Appl. Phys. Lett. 40, 611 (1982).

5. H. Rohdin, M.W. Muller, and C.M. Wolfe, "Impurity Redistribution During Epitaxial Growth", J. Electron. Mat. 11, 517 (1982).

6. T.S. Low, G.E. Stillman, D.M. Collins, C.M. Wolfe, S. Tiwari, and L.F. Eastman, "Spectroscopic Identification of Si Donors in GaAs", Appl. Phys. Lett. 40, 1034 (1982).

7. T.S. Low, G.E. Stillman, T. Nakanisi, T. Udagawa, and C.M. Wolfe, "Photothermal Ionization Identification of Sulfur Donors in GaAs", Appl. Phys. Lett. 41, 183 (1982).

8. P.A. Fedders, "Potential Fluctuations in High-Purity n-Type III-V Semiconductors", J. Appl. Phys. 53, 6154 (1982).

9. D.L. Rode, C.M. Wolfe, and G.E. Stillman, "Magnetic Field Dependence of the Hall Factor of Gallium Arsenide", Proc. 1982 Int. Symp. GaAs and Related Compounds, (Inst. Phys., London, 1983) p.569.

10. B.J. Skromme, T.S. Low, and G.E. Stillman, "Spectroscopic Characterization Studies of the Residual Donors and Acceptors in High-Purity LPE GaAs", Proc. 1982 Int. Symp. GaAs and Related Compounds, (Inst. Phys., London, 1983) p.485.

11. T.S. Low, B.J. Skromme, and G.E. Stillman, "Incorporation of Amphoteric Impurities in High Purity GaAs", Proc. 1982 Int. Symp. GaAs and Related Compounds, (Inst. Phys., London, 1983) p. 515.

12. P.A. Fedders, "Coulomb Potential Fluctuations in High-Purity n-Type III-V Semiconductors", Proc. 1982 Int. Symp. GaAs and Related Compounds, (Inst. Phys., London, 1983) p. 545.

13. P.A. Fedders, "Strain Scattering of Electrons in Piezoelectric Semiconductors", J. Appl. Phys. 54, 1804 (1983).

14. Camellia M.L. Yee, P.A. Fedders, and C.M. Wolfe, "The Effect of Electric Fields on Cr Redistribution at GaAs Surfaces", Appl. Phys. Lett. 42, 377 (1983).

15. H. Rohdin, M.W. Muller, and C.M. Wolfe, "A Model of Cr in GaAs", J. Phys. Chem. Solids 44, 1049 (1983).

16. D.L. Rode and P.A. Fedders, "Electron Scattering in Semiconductor Alloys", J. Appl. Phys. 54, 6425 (1983).

17. D.L. Rode, C.M. Wolfe, and G.E. Stillman, "Magnetic-field Dependence of the Hall Factor for Isotropic Media", J. Appl. Phys. 54, 10 (1983).

18. P.A. Fedders, "Energy Shift of Hydrogenic Donors in a Magnetic Field due to Electric and Strain Fields", Phys. Rev. B 27, 4799 (1983).

19. Camellia M.L. Yee, K.B. Nichols, P.A. Fedders, C.M. Wolfe, and Y.S. Park, "Chromium Redistribution in Ion-Implanted GaAs", Solid-State Elect. 27, 513 (1984).

20. R.T. Green, D.K. Walker, and C.M. Wolfe, "An Improved Method for the Electrochemical C-V Profiling of InP and GaAs", submitted to J. Electrochem. Soc.

5. MEETING TALKS

1. C.M. Wolfe, "Amphoteric Dopants and Compensation in GaAs", Workshop on Shallow Impurities in Semiconductors, Wright-Patterson AFB, Ohio, 21-22 May 1981.

2. G.E. Stillman, "Identification of Shallow Donors in GaAs", Workshop on Shallow Impurities in Semiconductors, Wright-Patterson AFB, Ohio, 21-22 May 1981.

3. H. Rohdin, M.W. Muller, and C.M. Wolfe, "Impurity Redistribution During Epitaxial Growth", Electronic Materials Conference, Santa Barbara, Calif., 24-26 June 1981.

4. T.S. Low, G.E. Stillman, and C.M. Wolfe, "Identification of Residual Donor Impurities in GaAs", Int. Symp. GaAs and Related Compounds, Oiso, Japan, 20-23 September 1981.

5. C.M. Wolfe, "Impurity Complexing in GaAs", Materials Research Meeting, Tokyo, Japan, 24 September 1981.

6. H. Rohdin, M.W. Muller, and C.M. Wolfe, "A Model of Cr in GaAs", Workshop on Compound Semiconductor Microwave Materials and Devices, Scottsdale, Arizona, 22-23 February 1982.

7. T.S. Low, G.E. Stillman, and C.M. Wolfe, "Identification of Residual Donor Impurities in Gallium Arsenide", Workshop on Compound Semiconductor Microwave Materials and Devices, Scottsdale, Arizona, 22-23 February 1982.

8. Camellia M.L. Yee, R.T. Green, P.A. Fedders, and C.M. Wolfe, "Cr-Redistribution at GaAs surfaces", Electronic Materials Conf., Fort Collins, Colorado, 23-25 June 1982.

9. R.T. Green, Camellia M.L. Yee, and C.M. Wolfe, "Impurity Interactions in Vapor-Phase Epitaxial GaAs", Electronic Materials Conf., Fort Collins, Colorado, 23-25 June 1982.

10. T.S. Low, B.J. Skromme, and G.E. Stillman, "Spectroscopic Characterization of Residual Donors and Acceptors in High Purity MOCVD GaAs", Electronic Materials Conf., Fort Collins, Colorado, 23-25 June 1982.

11. D.L. Rode, C.M. Wolfe, and G.E. Stillman, "Magnetic Field Dependence of the Hall Factor of Gallium Arsenide", Int. Symp. GaAs and Related Compounds, Albuquerque, New Mexico, 19-22 September 1982.

12. B.J. Skromme, T.S. Low, and G.E. Stillman, "Spectroscopic Characterization Studies of the Residual Donors and Acceptors in High-Purity LPE GaAs", Int. Symp. GaAs and Related Compounds, Albuquerque, New Mexico, 19-22 September 1982.

13. T.S. Low, B.J. Skromme, and G.E. Stillman, "Incorporation of Amphoteric Impurities in High Purity GaAs", Int. Symp. GaAs and Related Compounds, Albuquerque, New Mexico, 19-22 September 1982.

14. P.A. Fedders, "Coulomb Potential Fluctuations in High-Purity n-Type III-V Semiconductors", Int. Symp. GaAs and Related Compounds, Albuquerque, New Mexico, 19-22 September 1982.

A. IDENTIFICATION OF IMPURITIES

Inst. Phys. Conf. Ser. No. 63: Chapter 4
Paper presented at Int. Symp. GaAs and Related Compounds, Japan, 1981

A.1 Identification of residual donor impurities in gallium arsenide

T.S. Low and G.E. Stillman
Electrical Engineering Research Laboratory, Materials Research Laboratory, and Coordinated Science Laboratory
University of Illinois at Urbana-Champaign, Urbana, Illinois 61801

C.M. Wolfe
Semiconductor Research Laboratory, Washington University
St. Louis, Missouri 63130

Abstract Residual donor species in high purity $AsCl_3$-VPE, AsH_3-VPE, LPE, MBE and MO-CVD GaAs have been detected using photothermal ionization spectroscopy, and typical relative donor concentrations for each technique have been determined. These data are compared with earlier results and the current status of donor identification in GaAs is assessed.

1. Introduction

The nearly hydrogenic energy level spectra of residual donors in high purity GaAs have been studied by several groups using photothermal ionization spectroscopy. Since the donor ground state energy differs slightly from the value predicted from hydrogenic theory, and since this difference is donor species dependent, each hydrogenic transition in a photothermal ionization spectrum contains several closely spaced peaks. Each peak corresponds to a particular donor species present, and has an amplitude which is a measure of the relative concentration of that donor species. This multiplet structure is most easily resolved at high magnetic fields (about 5 T) in the hydrogenic 1s-2p(m=-1) transition. For this reason, all the spectra which appear in this paper show only this transition. The successful application of photothermal ionization spectroscopy requires that $N_D \leq 10^{15}$ cm^{-3} to avoid donor interaction. Photothermal ionization spectra have been recorded for high purity GaAs produced by $AsCl_3$-VPE, AsH_3-VPE, LPE, MBE and MO-CVD growth techniques. The residual donors observed in such unintentionally doped GaAs are for the most part characteristic of the growth technique employed, and independent of the laboratory in which the samples were prepared. Electrical properties of the samples whose spectra are shown in the figures are given in Table 1.

2. $AsCl_3$-VPE Growth Technique

Results on high purity VPE growth of GaAs prior to 1970 have been reviewed previously (Wolfe *et al.* 1970). At that time the only VPE technique that had produced high purity GaAs was the $AsCl_3$-Ga-H_2 vapor phase system. Epitaxial material with carrier concentrations of $n_{77} \approx 5 \times 10^{13}$ cm^{-3} and liquid nitrogen mobilities of $\mu_{77} \approx 200{,}000$ cm^2/Vs could be routinely produced. Because of the successful growth of extremely high purity GaAs by the $AsCl_3$-Ga-H_2 VPE system, much of the early donor identification work was done with material prepared by this technique. Wolfe *et al.* (1976) doped with Si, Ge, Sn, Pb, S, Se and Te by adding a small amount of the dopant in elemental form to the Ga melt. They also attempted to dope with O by adding Ga_2O_3 to the melt, and with C by placing a high purity graphite source near the growing layer. By comparing the spectra of the lightly doped samples with those of unintentionally doped samples grown in the same

0305-2346/82/0063-0143 $02.00

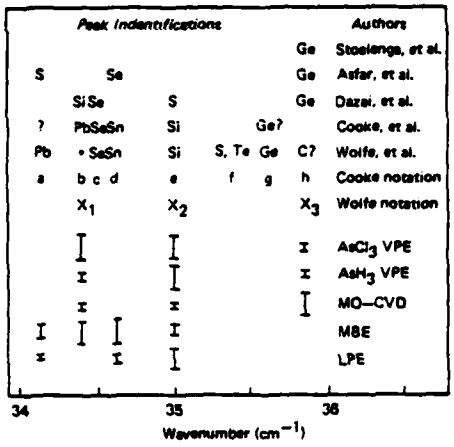

Fig.1 Characteristic donor peaks for GaAs grown by various techniques and several author's identifications. Vertical line heights indicate typical relative concentrations. (B=5.25 T).

reactor, identifications of spectral peaks in the 1s-2p(m=-1) transition with their chemical donor species could be made with reasonable certainty for Si, Ge, Sn, Pb, S, and Se. The identifications of C, and Te were considered tentative, while O was apparently not incorporated as a donor. These identifications and the well established photothermal ionization peak positions are shown in Fig.1.

A spectrum for an undoped $AsCl_3$-Ga-H_2 sample is shown in Fig.2(a). The peaks X_1, X_2, and X_3 are the residual donors characteristic of this growth technique and the relative concentrations of these donors, indicated by the peak heights, are also typical.

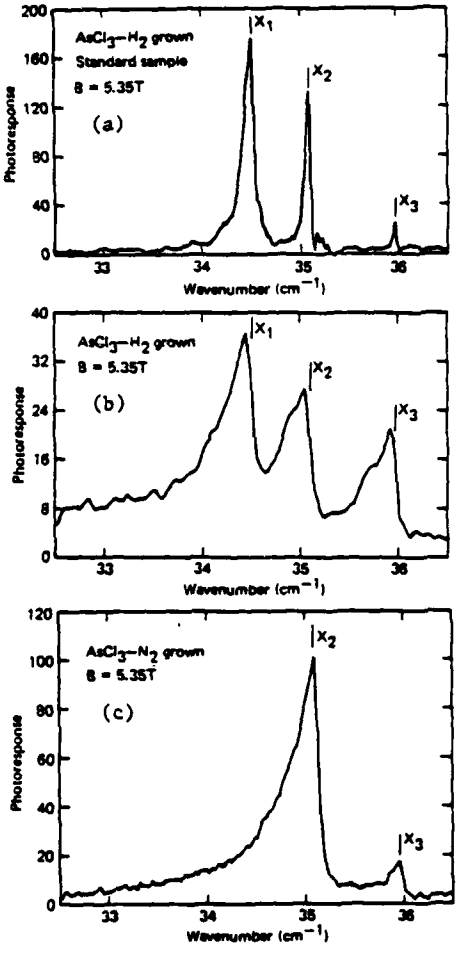

Fig.2 Spectra of $AsCl_3$ grown samples.

A variation of the $AsCl_3$-Ga-H_2 technique, in which N_2 is used as the carrier gas instead of H_2, has been explored by Dazai, et al. (1974). Ozeki et al. (1977) grew samples using both techniques and found that, while samples grown with the H_2 carrier gas showed the usual three residual donors X_1,X_2, and X_3, samples grown with N_2 as the carrier gas showed no evidence of X_1. These workers kindly loaned us samples, one grown with H_2, and one grown with N_2 carrier gas. Spectra for these samples appear in Fig.2(b) and 2(c) respectively. Since the position of the 1s-2p(m=-1) transition changes with magnetic field, all three of the spectra in Fig.2 were taken leaving the superconducting magnet in persistent mode, to facilitate comparison of peak positions between our standard sample in Fig.2(a) and the other two samples. These measurements confirm the results of Ozeki et al. (1977)

that X_1 is suppressed in the $AsCl_3$-Ga-N_2 VPE growth system.

3. AsH_3-VPE Growth Technique.

While the chloride vapor phase growth technique has produced the highest purity GaAs, the hydride (AsH_3-Ga-HCl-H_2) growth technique is advantageous for the growth of GaInAsP alloys. Kennedy (1979) has produced high purity GaAs epitaxial layers with μ_{77}=167,000 cm^2/Vs and more recently samples with μ_{77}=200,000 cm^2/Vs have been grown by Abrokwah (1981). Photothermal ionization spectra for several samples provided by both have shown the residual donors to be X_1, X_2 and X_3, with X_2 being dominant while the concentrations of X_1 and X_3 are sometimes quite small. A spectrum for a typical hydride VPE sample, grown by Kennedy is shown in Fig.3. The positions of the markers for X_1, X_2 and X_3, which appear in this and all the other figures were determined by comparison with a spectrum taken for our standard sample at precisely the same magnetic field.

4. LPE Growth Technique.

There has been considerable effort in the LPE growth of high purity GaAs. Cooke, et al. (1978) and Stradling (1981) examined both undoped samples and samples doped with Sn, Pb, and Se, and confirmed the identifications for these dopants made by Wolfe et al. (1976). The residual donors they observed in undoped LPE material from three different laboratories corresponded to Pb, Sn and X_2 in roughly the ratios of 1:2:3. An example of spectra for high purity LPE GaAs samples grown by Tiwari and Eastman (1979) is shown in Fig.4. As reported by Cooke et al. (1978) and also Morkoç, et al.(1980) the dominant residual donors in these samples are Sn and X_2 with a smaller concentration of Pb. In addition a peak due to X_1 is resolved in this spectrum, and while this is the first observation of X_1 in LPE GaAs, the proximity of the X_1 and Sn peaks and the typically large residual Sn concentrations in LPE material may have prevented its observation in earlier work. In the spectrum of another undoped LPE GaAs sample grown by Abrokwah (1980) Pb was absent and only traces of X_1 and Sn were detected leaving X_2 as the single dominant residual donor.

5. MBE Growth Technique.

High purity unintentionally doped GaAs grown by MBE using a metallic As source is p-type. Using Sn doping Morkoç and Cho (1977) produced a 27 μm

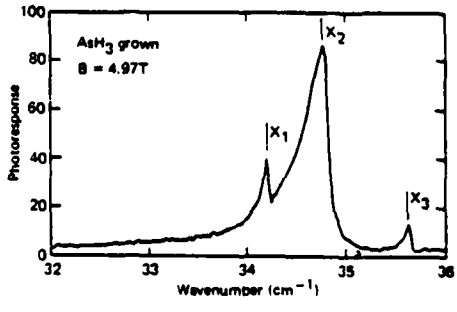

Fig.3 Photothermal ionization spectrum for Kennedy's AsH_3-VPE sample.

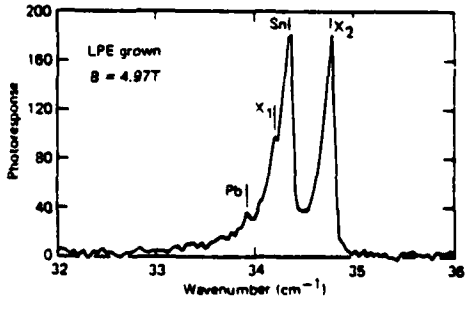

Fig.4 Photothermal ionization spectrum for Tiwari's et al LPE sample.

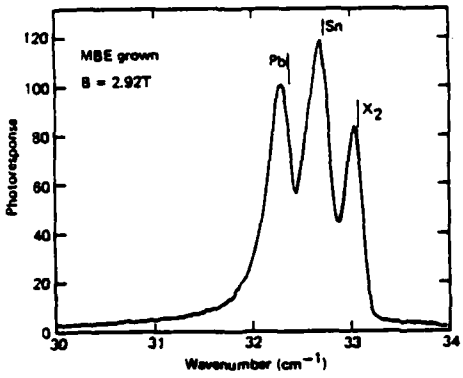

Fig.5 Photothermal ionization spectrum for Calawa's MBE sample.

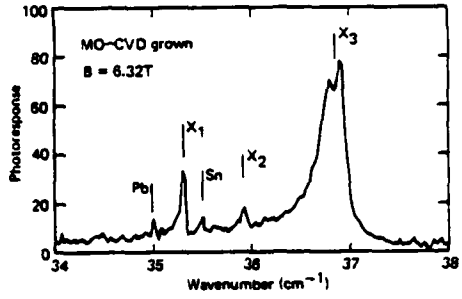

Fig.6 Photothermal ionization spectrum for Dapkus' et al MO-CVD sample.

thick n-type sample with a carrier concentration of $4x10^{14}$ cm^{-3} and μ_{77}= 105,000 cm^2/Vs. The spectrum of this sample showed Pb, possibly X_1, and X_2, in addition to the intentionally added Sn. MBE samples grown by Collins (1981) using a metallic As source but Si instead of Sn doping showed pronounced X_1 and smaller X_2 peaks in their photothermal ionization spectra. Unintentionally doped MBE samples grown by Calawa (1981) using As provided by cracking AsH_3 as it entered the growth chamber were also measured. The layers grown in this way were n-type. Photothermal ionization spectra for these samples (see Fig.5) showed the presence of Pb, Sn and X_2, while X_1 was observed clearly in only one of the samples. The presence of Sn in these spectra is probably a result of previous use of Sn as a dopant in the same growth chamber.

6. MO-CVD Growth Technique.

The first report of high purity GaAs growth by MO-CVD was by Seki et al. (1976) who used triethylgallium as the metalorganic source to grow samples with μ_{77}=125,000 cm^2/Vs. Dapkus et al. (1981) subsequently prepared MO-CVD samples with μ_{77} as high as 125,000 cm^2/Vs using a trimethylgallium source. Spectra recorded in our laboratory for ten such unintentionally doped samples showed the dominant donor to be X_3. Only a trace of Pb was observed in one sample, while X_1, Sn and X_2 were seen in concentrations which varied and occasionally became comparable to that of X_3, depending on growth parameters and source material. An example spectrum for this high purity MO-CVD material is shown in Fig.6. These results are to be compared with the earlier measurement of an alkyl grown sample by Cooke et al. (1978) who observed only Pb and X_3 in the ratio of 7 to 10.

7. Current State of Donor Identification

There is general agreement in the literature on the energy at which photothermal ionization peaks occur, and for Pb, Sn and Se the association of peaks with their chemical donor species is fairly well established. There is controversy however, over the identification of some of the other peaks observed in GaAs.

In the work of Wolfe et al. (1976) the peak X_1 could not be correlated with a chemical donor species and, because this peak had not been observed in

high purity LPE material, it was suggested that it might involve a stoichiometric defect (i.e. a Ga vacancy (Stillman et al. 1976)). Recent annealing experiments on high purity GaAs have tended to support this identification (Stradling 1981). However, the presence of X_1 in undoped material grown in the $AsCl_3$-H_2 system, and its absence in that grown by the $AsCl_3$-N_2 system of Ozeki et al. (1977) suggest that X_1 might be associated with Si, in view of the expected role of H_2 in Si incorporation reactions. These authors observed the peak X_1 in a Si doped $AsCl_3$-N_2 grown sample and also observed a correlation between the appearance of X_1 and the presence of a Si peak in photoluminescence. Also, the MBE samples grown by Collins (1981) in which Si doping was used to render the samples n-type, showed a dominant X_1 peak and a small X_2 peak in their spectra, and larger carrier concentration (indicating heavier Si doping) correlated with a larger ratio of X_1 to X_2 peak heights. These results and those of Ozeki et al. (1977) are convincing evidence for the association of X_1 with Si.

In their earlier work, Wolfe et al. (1976) observed an increase in relative amplitude and broadening of the X_2 peak in their Si doped sample as compared with a control sample grown in the same $AsCl_3$-H_2 reactor. Ozeki et al. (1977) on the basis of a similar increase in amplitude and broadening attributed X_2 to S. Samples doped by adding elemental S to the Ga melt of an $AsCl_3$-H_2 reactor, show a new peak between X_2 and X_3 as shown in Fig.7, but samples doped using H_2S, grown in a similar $AsCl_3$-H_2 system and measured in our laboratory, show only X_1, X_2 and X_3. Asfar et al. (1980) identified S with a peak at lower energy than X_1 in H_2S doped $AsCl_3$-H_2 grown material.

The peak X_3 was tentatively correlated with C by Wolfe et al. (1976) but Ozeki et al.(1977) concluded that C was not incorporated in GaAs as a donor and observed an increase of the amplitude of this X_3 peak after doping with Ge. Stoelenga et al. (1978) and Asfar et al. (1980) have performed neutron transmutation doping (which is expected to produce only Se and Ge donors) on samples which subsequently showed an increase in the amplitude of the peak X_3. Since the position of the Se peak is well established this is further evidence that X_3 is associated with Ge. The earlier Ge doping experiments of Wolfe et al. (1976) and Cooke et al. (1978) seemed to indicate that the Ge peak occured below X_3 in energy but recent experiments in our laboratory suggest that the peak observed was due to line-shape effects and that the true position of the Ge peak probably coincides with the peak X_3.

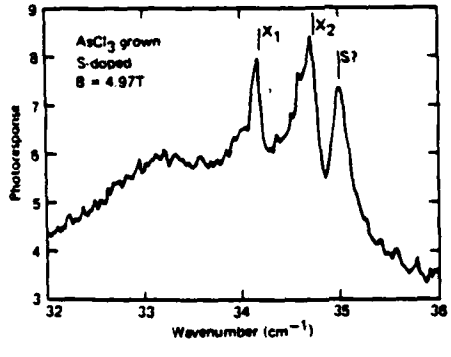

Fig.7 Spectrum for Wolfe's $AsCl_3$-H_2 grown S doped sample.

Considerable work obviously remains to obtain absolute identification of the donor impurities in GaAs and in particular to identify the source of the residual impurities in the various growth techniques. The present results and identifications pose many interesting and new problems concerning impurity incorporation in epitaxial GaAs. For example, if X_1 is due to Si, then Si is not a significant residual donor impurity in LPE GaAs. If X_3 is due to Ge, neglecting the possible degeneracy C and Ge, then Ge is the dominant residual donor in MO-CVD GaAs. If X_2 is due to S as identified by Ozeki et al. (1977), then the two

other peaks attributed to S by Stillman et al. (1976) and Asfar et al. (1980) remain unexplained. In spite of these complications and uncertainties, photothermal ionization spectroscopy is the only characterization method that can reliably distinguish and identify the electrically active chemical donor species present in high purity epitaxial GaAs.

The authors gratefully acknowledge collaboration of J Abrokwah, C Bozler, A R Calawa, A Cho, D M Collins, P D Dapkus, L F Eastman, J Kennedy, G L McCoy, H Morkoç, M Ozeki, and A Shibatomi, who provided samples. We would also like to thank R A Stradling for many helpful and stimulating discussions, to acknowledge the support and encouragement of H Lessoff, and M Yoder in this work, and to acknowledge the assistance of B Payne J Gladin, and G Morris in preparation of the manuscript. This work was supported by ONR under Contract No N00014-80-C-0762 and N00173-79-C-0184.

Table 1 Electrical Properties

Fig.	Sample	μ_{77} (cm^2/Vs)	n_{77} (cm^{-3})	t(μm)
2(a)	$AsCl_3$-H_2 VPE (Wolfe)	201,000	4.5×10^{13}	56
2(b)	$AsCl_3$-H_2 VPE (Ozeki et al)	95,000	3.0×10^{13}	20
2(c)	$AsCl_3$-N_2 VPE (Ozeki et al)	132,000	2.0×10^{13}	20
3	AsH_3 VPE (Kennedy)	137,000	7.0×10^{13}	26
4	LPE (Tiwari et al.)	129,000	1.2×10^{14}	14
5	MBE (Calawa)	108,000	6.3×10^{13}	5
6	MO-CVD (Dapkus et al)	106,000	2.1×10^{14}	30
7	$AsCl_3$-H_2-S VPE (Wolfe)	74,000	9.3×10^{14}	83

References

Abrokwah J, 1980, private communication.
Abrokwah J, 1981, private communication.
Asfar M N, Button K J, McCoy G L, 1980 Inst Phys Conf Ser No 56,pp 547-555.
Calawa A R, 1981, Appl Phys Lett, 38, pp 701-703.
Collins D M, 1981, private communication.
Cooke R A, Houlte R A, Kirkman R F, Stradling R A, 1978, J Phys D, 11, pp 945-953.
Dapkus P D, Manasevit K L, Hess K L, Low T S, Stillman G E, to be published in J Cryst Growth.
Dazai K, Ihara N, Ozeki M, 1974, Fujitsu Sci Tech, J 10, pp 125-143.
Kennedy J, 1979 private communication.
Morkoç H, Cho A Y, 1979, J Appl Phys, 50, pp 6413-6416.
Morkoç H, Eastman, L F, Woodard D, 1980, Thin Solid Films, 71, pp 245-248.
Ozeki M, Kitahara K, Nakai K, Shibatomi A, Dazai K, Okawa S, Ryuzan O, 1977, Jpn J Appl Phys, 16, #9, pp 1617-1622.
Seki H, Kookitu A, Ohta K. Fujimoto M, 1976, Jpn J Appl Phys 15, pp 11-17.
Stillman G E, Wolfe C M, Korn D M, 1976, Proc 13th Int Conf Phys Semi, pp 623-626.
Stoelenga J H M, Larsen D M, Walukiewicz W, Bozler C O, 1978, J Phys Chem Solids, 39, pp 873-877.
Stradling R A, 1981 private communication.
Tiwari S, Eastman L F, 1979 private communication.
Wolfe C M, Stillman G E, 1970, (Inst Phys Conf Ser No 9) pp 3-17.
Wolfe C M, Stillman G E, Korn D M, 1976, (Inst Phys Conf Ser No 33b) pp 120-128.

A.2 Spectroscopy of donors in high purity GaAs grown by molecular beam epitaxy

T. S. Low and G. E. Stillman
Electrical Engineering Research Laboratory,[a] Materials Research Laboratory, and Coordinated Science Laboratory, University of Illinois at Urbana–Champaign, Urbana, Illinois 61801

A. Y. Cho[b] and H. Morkoc
Department of Electrical Engineering and Coordinated Science Laboratory, University of Illinois at Urbana–Champaign, Urbana, Illinois 61801

A. R. Calawa
Lincoln Laboratory, Massachusetts Institute of Technology, Lexington, Massachusetts 02173

(Received 2 December 1981; accepted for publication 12 January 1982)

Photothermal ionization spectroscopy has been used to determine the residual donor species present and their relative concentrations in the highest purity molecular beam epitaxial (MBE) *n*-GaAs yet reported. Data are presented for samples grown in two different MBE growth reactors: one using elemental As and the other using cracked AsH_3 as the arsenic source. In spite of the substantial differences between growth systems, the donor backgrounds are quite similar.

PACS numbers: 72.20.Jv

Molecular beam epitaxy (MBE) of III-V semiconductors is of great interest for semiconductor device applications because of its capability for producing highly uniform layers with precisely controlled thicknesses and doping profiles. For some applications, such as field-effect transistor (FET) buffer layers and undoped layers in high electron mobility transistors, it is also important to be able to grow high purity material. In this letter we report photothermal ionization measurements of the shallow donor species present in high purity MBE GaAs samples grown in two different laboratories.

Photothermal ionization spectroscopy[1] is a technique which can be used to detect the donor species present and measure their concentrations relative to the total donor concentration in high purity semiconductor samples. The extrinsic photoconductivity spectrum of a high purity *n*-type GaAs sample consists of sharp peaks at energies corresponding to transition energies of the hydrogenic donors. Because different donor species have slightly different ground-state energies but nearly identical excited-state energies, each hydrogenic transition has associated with it a closely spaced multiplet of peaks. Each peak in the multiplet corresponds to a hydrogenic transition of a particular donor species. The relative amplitudes of the peaks are a measure of the relative concentrations of the corresponding donor species. The narrow linewidth and large amplitude of the $1s$-$2p(m = -1)$ transition at high magnetic fields make it especially suitable for resolving the closely spaced peaks of the individual donor species. The $1s$-$2p(m = -1)$ transition energies change substantially with changing magnetic field so, to permit comparison of the peaks observed in a given sample with donor identifications in the literature, the spectrum of that sample is compared to the spectrum of a well characterized reference sample taken at precisely the sample magnetic field. This is accomplished by operating the superconducting magnet in persistent mode while both spectra are recorded. The reference sample used in this work is an ultrapure $AsCl_3$-VPE GaAs sample grown by Wolfe, which has a liquid-nitrogen temperature mobility of $\mu_{77} = 201\,000\ \mathrm{cm^2/Vs}$ and a carrier concentration of $n_{77} = 4.5 \times 10^{13}\ \mathrm{cm^{-3}}$.[2] The three peaks present in the spectra of this sample, labeled X_1, X_2, and X_3, correspond to the three characteristic residual donors present in high purity GaAs grown by this technique.[3] Since many of the early donor identification experiments were done using $AsCl_3$-VPE material, the energies of peaks corresponding to different donor species relative to the energies of X_1, X_2, and X_3 are fairly well known.[4,5]

Hall effect data for the MBE samples described here[6,7] show them to be the highest purity GaAs prepared by this technique which has yet been reported. Sample A-147 was grown by Morkoc and Cho who reported a liquid-nitrogen temperature mobility of $105\,000\ \mathrm{cm^2/Vs}$ and a carrier concentration of $4 \times 10^{14}\ \mathrm{cm^{-3}}$ for the 27-μm-thick layer.[6] The MBE system used to grow this sample used an elemental As source, and undoped GaAs grown in this way is generally *p* type with $p \simeq 10^{14}\ \mathrm{cm^{-3}}$. In order to produce an *n*-type sample it was necessary to lightly dope the sample with Sn. The details of the substrate preparation, growth procedure, and precautions for obtaining high purity have been described elsewhere.[6,8] Samples MBE-91 and MBE-92 were grown by Calawa[7] in an MBE system which used an AsH_3 cracking furnace in place of the usual effusion cell As source. Undoped samples grown in this way are *n* type and so no intentional doping was required. The details of the cracking furnace and growth procedure for these samples have also been described previously.[7] The liquid-nitrogen temperature mobilities, and carrier concentrations corrected for both surface and interface depletion in these 5-μm-thick samples are[7,9] $\mu_{77} = 90\,000\ \mathrm{cm^2/Vs}$, $n_{77} = 2.7 \times 10^{14}\ \mathrm{cm^{-3}}$, and $\mu_{77} = 110\,000\ \mathrm{cm^2/Vs}$, $n_{77} = 2.4 \times 10^{14}\ \mathrm{cm^{-3}}$ respectively.

For extremely pure samples in which the photothermal ionization peaks are separated by more than a linewidth in

[a] Department of Electrical Engineering, University of Illinois.
[b] Permanent address: Bell Laboratories, Murray Hill, New Jersey 07974.

 0003-6951/82/070611-03$01.00

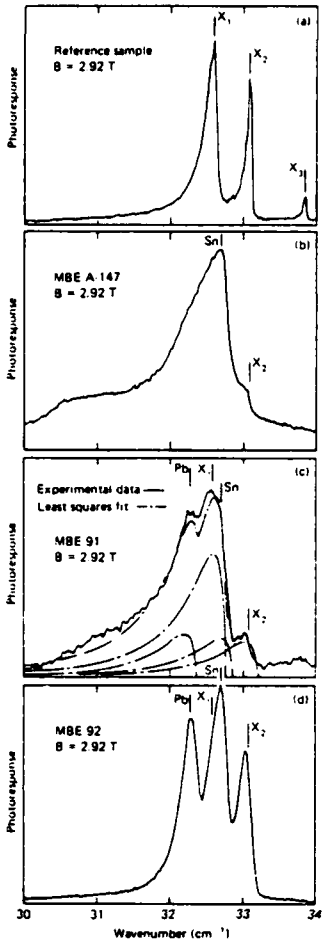

FIG. 1. Photothermal ionization spectra of the 1s-2p($m = -1$) transitions for the MBE samples and the reference sample at a magnetic field of 2.92 T.

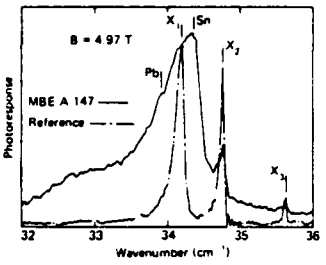

FIG. 2. Photothermal ionization spectrum of the 1s-2p($m = -1$) transitions for MBE sample A-147 and the reference sample at a magnetic field of 4.97 T.

energy, the relative amplitudes of the peaks are expected to correspond to the relative concentrations of donor species present. In less pure and/or more compensated samples, as the concentration of charged centers (ionized acceptors and compensated donors in an n-type sample) increases, the peaks broaden due to the electric fields and field gradients[10] from these charged centers, until the linewidth becomes comparable to the peak separations. The photoresponse at the energy of a peak of a certain donor species is then no longer simply proportional to the concentration of that species, but is related also to the concentration of donors associated with adjacent peaks. This is the case for the spectrum of MBE-91 in Fig. 1(c). Because the photoresponse at the energy of the Pb peak is largely due to the contributions of the low energy tails of the Si and Sn peaks, the relative amplitude of the Pb peak is substantially larger than the relative concentration of Pb donors. In order to obtain a quantitative estimate of the concentrations of the various donor species for each sample reported here, a function $f(\epsilon)$ of the form

$$f(\epsilon) = \sum_{i=1}^{4} \alpha_i P(\beta[\epsilon - \epsilon_i])$$

was fitted to the envelope of the 1s-2p($m = -1$) transitions using a least-squares minimization technique. Each term in $f(\epsilon)$ is a peaked function whose amplitude α_i is interpreted as a relative concentration of the ith donor species. The function $P(\epsilon)$ was derived from a fit to the 1s-2p($m = -1$) line shape calculation by Larsen.[10] The values of α_i and β were adjusted for a best fit while the peak positions ϵ_i were determined from the spectra of Figs. 1(a) and 1(d). The width scale β was constrained to be the same for each peak because the inohomogeneous broadening[10] of peaks is expected to be the same for each donor species in a uniformly doped sample, independent of its relative concentration. The resulting best $f(\epsilon)$ and the individual terms of $f(\epsilon)$ are plotted for MBE-91 along with the experimental data in Fig. 1(c). The total donor and acceptor concentrations for the samples reported here were determined using the Hall mobility analysis of Wolfe *et al.*[11] The relative concentrations for the various donor species present in each sample could then be expressed as the absolute concentrations shown in Table I.

Photothermal ionization spectra for sample A-147 and for the reference sample, both recorded at a magnetic field of 4.97 T, are shown in Fig. 2. As expected from the intentional Sn doping of this sample, the dominant peak in its spectrum occurs at an energy which has been previously associated with Sn by Wolfe *et al.*[4] and Cooke *et al.*[5] The smaller peak at higher energy corresponds to X_2. The peak X_2 was originally associated with Si by Wolfe *et al.*[4] but subsequent doping experiments by Ozeki *et al.*[12] and in our laboratory[13] have indicated that X_1 is Si, while Ozeki *et al.*[12] have associated X_2 with S. The shoulder on the low energy side of the dominant Sn peak occurs at an energy which has been associated with Pb by Wolfe *et al.*[4] and Stradling.[14] In a homogeneously doped sample, the peak width in energy at a given fraction of

TABLE I. Impurity concentrations derived from the photothermal ionization spectra and the Hall mobility analysis of Wolfe *et al.*[11]

	Impurity concentrations ($\times 10^{14}$ cm^{-3}).						
Sample	N_D (total)	N_A (total)	N_D(Pb)	$N_D(X_1 = \text{Si})$	N_D(Sn)	$N_D(X_2)$	$N_D(X_3)$
Reference	0.89	0.45	...	0.47	...	0.36	0.06
A-147	5.8	1.8	<0.3	<0.3	3.9	1.3	<0.1
MBE-91	4.9	3.9	0.9	2.5	0.8	0.7	<0.2
MBE-92	3.4	2.8	0.8	<0.15	1.3	1.2	...

the full peak height should be the same for all peaks. This width, taken at 75% of the full peak heights, is over three times larger for the Sn peak than the X_2 peak, and this suggests that another unresolved donor (possibly X_1 = Si) may be contributing to the low energy tail of the Sn peak.

Photothermal ionization spectra for samples MBE-91, MBE-92, A-147, and the reference sample, recorded at a magnetic field of 2.92 T, are shown in Fig. 1. The maximum photoresponse in the spectrum of MBE-91 is at the energy of X_1 = Si, but if only Si were present in this sample, the photoresponse would drop off more sharply for energies above that of the maximum. The additional photoresponse on the high energy side of the Si peak is probably due to Sn, especially in view of the presence of a Sn peak in the spectrum of MBE-92. At still higher energy there is a small peak coincident in energy with X_2 and possibly also with X_3, while at lower energy there is a peak at the energy associated with Pb.

The photothermal ionization spectrum for MBE-92 in Fig. 1(d) shows the clear presence of Pb, Sn, and X_2, and the fact that the Sn peak is slightly broader relative to its amplitude than either the Pb or X_2 peak, suggests there may be a slight amount of X_1 = Si present. The presence of Sn in the unintentionally doped samples MBE-91 and MBE-92 may be due in part to the previous one of Sn as an n-type dopant in the MBE growth chamber. Several growth runs were made between the use of Sn and the growth of MBE-91 and MBE-92, however, and so passivation of the walls of the growth chamber may have minimized this contribution of Sn. Samples MBE-91 and MBE-92 were grown under indentical conditions except for the temperature of the AsH_3 cracking furnace. Calawa[7] correlated an increase in net carrier concentration for samples grown with increasing cracking furnace temperature and attributed it to Si donors provided by the hot quartz walls of the cracking furnace. This idea is substantiated by the donor concentrations derived from the fits to the spectra of MBE-91 and MBE-92. In MBE-91, grown with a cracking furnace temperature of 690 °C, the concentration of X_1 = Si donors is over half of the total donor concentration, while in MBE-92, grown with the lower cracking furnace temperature of 610 °C, and having a lower total donor concentration, the presence of X_1 = Si donors is barely discernable. The concentrations of Pb, Sn, and X_2 donors, however, are similar for both samples (see Table I).

In conclusion, the photothermal ionization data presented here for high purity MBE GaAs samples grown in different laboratories and using substantially different growth techniques show remarkably similar donor backgrounds. Peaks associated with Pb, Si, Sn, and S are present in each of the MBE samples measured. The X_3 donor, if present at all in these samples, has a concentration at least a factor of 20 smaller than the total donor concentration. The absence of X_3, which has been associated with both C (Ref. 4) and Ge (Refs. 15 and 16) in the literature, is interesting because it is one of the characteristic residual donor species present in $AsCl_3$-H_2 VPE, $AsCl_3$-N_2 VPE, and AsH_3 VPE grown GaAs[3,4,12] and it is the dominant residual donor species in MOCVD grown GaAs.[3,5,17] In contrast, the Pb donor is absent in unintentionally doped GaAs grown by all of the above techniques except MBE.

The authors gratefully acknowledge C. M. Wolfe for many helpful discussions and for providing the reference sample used in this work. We would also like to acknowledge the support of H. Lessoff and M. N. Yoder and to thank B. L. Payne, R. T. Gladin, and G. E. Morris for their assistance in preparation of the manuscript. This work was supported by ONR under Contract Nos. N00014-80-C-0762 and N00173-79-C-0184.

[1] G. E. Stillman and C. M. Wolfe, in *Semiconductors and Semimetals*, edited by R. K. Willardson and A. C. Beer (Academic, New York, 1977), Vol. 12, pp. 169–290.
[2] C. M. Wolfe (private communication).
[3] T. S. Low, G. E. Stillman, and C. M. Wolfe, *Proc. Sym. GaAs and Related Compounds*, Oiso, 1981 (to be published).
[4] C. M. Wolfe, G. E. Stillman, and D. M. Korn, *Proc. Sym. GaAs and Related Compounds, St. Louis, 1976* (Institute of Physics, London), pp. 120–128.
[5] R. A. Cooke, R. A. Hoult, R. F. Kirkman, and R. A. Stradling, J. Phys. D **11**, 945 (1978).
[6] H. Morkoc and A. Y. Cho, J. Appl. Phys. **50**, 6413 (1979).
[7] A. R. Calawa, Appl. Phys. Lett. **38**, 701 (1981).
[8] A. Y. Cho and J. R. Arthur, *Progress in Solid State Chemistry* (Pergamon, New York, 1975), Vol. 10, pp. 157–191.
[9] A. Chandra, C. E. C. Wood, D. W. Woodard, and L. F. Eastman, Solid State Electron. **22**, 645 (1979).
[10] D. M. Larsen (private communication); Phys. Rev. B **13**, 1681 (1976).
[11] C. M. Wolfe, G. E. Stillman, and J. O. Dimmock, J. Appl. Phys. **41**, 504 (1970).
[12] M. Ozeki, K. Kitahara, K. Nakai, A. Shibatomi, K. Dazai, S. Okawa, and O. Ryuzan, Jpn. J. Appl. Phys. **16**, 1617 (1977).
[13] T. S. Low, G. E. Stillman, D. M. Collins, C. M. Wolfe, S. Tiwari, and L. F. Eastman (unpublished).
[14] R. A. Stradling (private communication).
[15] J. H. M. Stoelenga, D. M. Larsen, W. Walukiewicz, and C. O. Bozler, J. Phys. Chem. Solids **39**, 873 (1978).
[16] M. N. Asfar, K. J. Button, and G. L. McCoy, *Proc. Sym. GaAs and Related Compounds, 1980* (Inst. of Physics, London), pp. 547–555.
[17] P. D. Dapkus, H. M. Manasevit, K. L. Hess, T. S. Low, and G. E. Stillman, J. Cryst. Growth **55**, 10 (1981).

A.3 Spectroscopic identification of Si donors in GaAs

T. S. Low and G. E. Stillman
Electrical Engineering Research Laboratory,[a] Materials Research Laboratory and Coordinated Science Laboratory, University of Illinois, Urbana, Illinois 61801

D. M. Collins
Solid State Laboratory, Hewlett Packard Laboratories, Palo Alto, California 94304

C. M. Wolfe
Semiconductor Research Laboratory, Washington University, St. Louis, Missouri 63130

S. Tiwari and L. F. Eastman
School of Electrical Engineering, Cornell University, Ithaca, New York 14853

(Received 8 February 1982; accepted for publication 30 March 1982)

Photothermal ionization measurements on Si-doped GaAs grown by molecular beam epitaxy (MBE) have indicated that the previous identification of the Si donor peak was incorrect. Data leading to the new identification are presented and the results leading to the earlier identification are re-examined. Implications of the new identification for the importance of Si as a residual donor in epitaxial GaAs grown by various techniques are discussed.

PACS numbers: 72.20.Jv

Silicon is widely believed to be an important residual impurity in GaAs prepared by several growth techniques. The results of many experiments on the growth of high purity GaAs have been explained in terms of the influence of various growth parameters on the incorporation of Si. Most such experiments have relied on Hall effect data and on the tacit assumption that only changes in Si incorporation are important in determining changes in the carrier concentration. Since Si is neither the only residual acceptor[1] nor the only residual donor[2] present in high purity GaAs grown by a wide variety of techniques, it is necessary to specifically measure the concentration of electrically active Si in order to assess the role of Si as a residual impurity. Photothermal ionization spectroscopy can detect the donor species present in a high purity semiconductor sample and measure their relative concentrations from the amplitudes of the corresponding spectral peaks. Carefully controlled doping experiments have been performed by several research groups[3-5] to identify various donor species with the associated photothermal ionization peaks. Such experiments are difficult because of the small range of donor concentrations between that of the purest GaAs which can be grown by a given technique, and that for which impurity interactions[6] and other effects[7] degrade the spectra by broadening and distorting the spectral peaks. In this letter we report photothermal ionization measurements made on Si-doped GaAs grown by molecular beam epitaxy (MBE) which have resulted in the identification of Si donors with a spectral peak different from that previously associated with Si.[8]

Si-doped samples 1 and 2 were grown at Hewlett–Packard Laboratories on (100) undoped semi-insulating LEC substrates in a Varian GEN/II MBE system equipped with liquid nitrogen cryoshrouds. All source materials were evaporated from pyrolytic boron nitride (PBN) crucibles, contained in high purity source furnaces in which the heated zones are comprised of only Ta and PBN. An elemental As source was used, and undoped MBE GaAs prepared in this way is generally p type with $p \simeq 10^{14}$ cm^{-3}.[9] Doping with elemental Si to produce the n-type samples required for the measurements produces a Si donor concentration which dominates the small background concentration of other donors and acceptors present in undoped material. The only materials other than Ga, As, and Si, which had been previously evaporated in this MBE system, were Al and Be (a p-type dopant). The layers were grown with a substrate temperature of 585 °C at a rate of 1 μm/h. The electrical properties of these samples and the other samples reported in this work, corrected for surface and substrate depletion,[10] are shown in Table I.

Photothermal ionization spectra for samples 1 and 2 and for reference sample 1 are shown in Fig. 1. These spectra show the $1s$-$2p(m = -1)$ transitions of the various donor species present, and were recorded at precisely the same magnetic field ($B = 2.92T$) by operating the superconducting magnet in the persistent mode. The three peaks in the spectrum of the ultrapure $AsCl_3$-H_2 vapor phase epitaxial (VPE) grown reference sample 1, labeled X_1, X_2, and X_3, correspond to the three characteristic residual donors present in GaAs grown by this technique. At a given magnetic field, the energies of these peaks provide a reference for identifying the peaks in the spectra of other samples.

The spectra of both Si-doped samples 1 and 2 contain two peaks which have the typically observed asymmetric line shape predicted by Larsen.[6] In both spectra, the large peak corresponds with X_1 in the reference spectrum, while the smaller peak corresponds with X_2. The slight downshift in the peak energies of the MBE spectra with respect to those in the reference spectrum is often observed in samples of this doping level. The dominance of the X_1 peak in the spectra for these Si-doped MBE samples by itself strongly suggests the association of Si donors with the X_1 peak, but further evidence is provided by the absolute donor concentrations in these samples. The relative concentrations of X_1 and X_2 do-

[a] Department of Electrical Engineering, University of Illinois.

 0003-6951/82/121034-03$01.00

TABLE I Hall effect data and impurity concentrations derived from spectra and Hall mobility analysis.

Sample	μ_{77}(cm^2/V s)	Impurity concentrations ($\times 10^{14}$ cm^{-3}) N_D(total)	N_A(total)	N_D(Pb)	$N_D(X_1 = \text{Si})$	N_D(Sn)	$N_D(X_2 = \text{Si})$	$N_D(X_3)$
1	74 300	9.7	3.2	...	7.3	...	2.4	...
2	71 700	11.3	3.7	..	9.0	...	2.3	...
3	129 000	2.8	1.6	$\lesssim 0.1$	$\lesssim 0.1$	1.3	1.3	...
Ref.1	201 000	0.89	0.45	...	0.47	...	0.36	0.06
Ref. 2	207 000	0.43	0.13	...	0.8	0.14	0.14	0.08

nors were derived from the relative peak amplitudes in the spectra. Absolute concentrations could then be calculated from the total donor concentration using the 77-K Hall effect data and the method of Wolfe *et al.*[11] In the more heavily doped sample 2, the concentration of X_1 donors is 1.23 times larger than in sample 1, but the concentration of X_2 donors is essentially the same in both samples. This is interpreted to mean that the concentration of $X_1 = \text{Si}$ donors increases with increasing doping while the background of X_2 donors remains constant. It is also interesting to note, in view of the amphoteric nature of Si in GaAs, that the total acceptor concentration in the more heavily doped sample 2 is 1.16 times that of sample 1. The identification of the X_1 peak with Si is consistent with the work of Ozeki *et al.*[4]

The data which led to the earlier identification of peak X_2 with Si by Wolfe *et al.*[8] are shown in spectra (a) and (b) of Fig. 2. In these experiments the photothermal ionization spectrum of a Sn-doped $AsCl_3$-H_2 VPE grown GaAs control sample was compared to that of a sample which was prepared identically except that Si was added to the Ga melt. On the basis of the larger amplitude and width of the X_2 peak in the Si-doped sample, the X_2 peak was identified with Si donors.

The new identification of Si with X_1 can be reconciled with the data of Wolfe *et al.*[8] by examining the region of the spectra of Fig. 2 in the vicinity of X_1. While the X_2 peaks have the typically observed low energy tail predicted by Larsen,[6] the shapes of the X_1 peaks in both spectra (a) and (b) are anomalous. The photoresponse drops precipitously for energies less than that of the X_1 peaks, and after a sharp notch, forms the broad wing noted by Wolfe *et al.*[8] Spectrum (c) in Fig. 2 is that of reference sample 2, in which all peaks have the predicted line shape.[6] Careful comparison of these spectra shows that the X_1 peak in the reference spectrum (c) corresponds not with the peaks in spectra (a) and (b), labeled as X_1 by Wolfe *et al.*,[8] but with the notches in photoresponse just below these peaks. Photothermal ionization peaks having a sharply peaked component slightly above the usual peak energy and a broad wing well below the usual peak energy have been observed previously, particularly for the larger amplitude peaks (i.e., higher concentration donors). Space does not permit a thorough discussion of this effect and related experiments,[12] and the details of the phenomenon are not yet fully understood, but we believe the anomalous peak shape is caused by an absorption by the corresponding (in this case $X_1 = \text{Si}$) donors near the substrate-epilayer interface. This absorption does not contribute significantly to the photoconductive response, but reduces the intensity of far infrared light within the sample at the peak energy, so that a sharp notch is observed in the associated photothermal ionization peak. In the absence of this absorption, the X_1 peaks in both spectra would have the more typical shape of X_2 and substantially larger amplitudes, indicative of the actual relative concentrations of $X_1 = \text{Si}$. The greater width of the X_2 peak in the spectrum of the Si-doped sample is the result of increased Stark broadening caused by the additional charged centers (ionized acceptors and compensated donors) introduced by the Si doping. The broad wing observed in both spectra is interpreted as the usual Stark broadened low energy tail of the X_1 peak, distorted by the absorption. As expected from this interpretation,

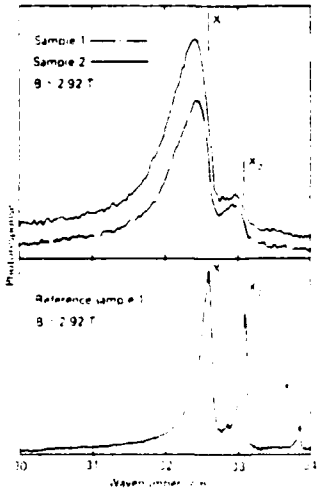

FIG. 1. Photothermal ionization spectra of the $1s$-$2p(m = -1)$ transitions for the Si-doped MBE samples 1 and 2, and for reference sample 1.

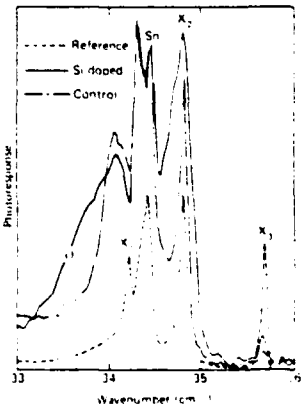

FIG. 2. Photothermal ionization spectra of the $1s$-$2p(m = -1)$ transitions for the Si-doped and control samples of Ref. 8, and for reference sample 2 ($B = 5.00$ T).

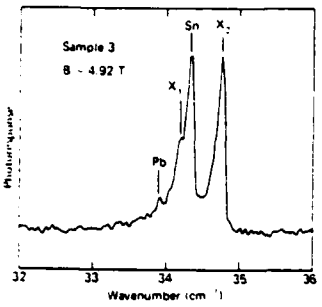

FIG. 3. Photothermal ionization spectrum of the high purity LPE grown sample 3, showing the X_1 = Si peak in addition to the usual Pn, Sn, and X_2 peaks.

its width is also greater in the spectrum of the Si-doped sample.

The identification of Si with X_1 instead of X_2 in photothermal ionization spectra has important implications with regard to the role of Si as a residual donor in GaAs grown by liquid phase epitaxy (LPE). Until recently X_1 was never observed in LPE GaAs, and this led to the suggestion that this peak might be due to a stoichiometric defect complex.[13] The only residual donor peaks previously observed in LPE materials were identified as Pb,[3,5,14] Sn,[3,15,16] and X_2, which is often the dominant peak in the spectra, and which has been associated with S.[4,12] The earlier identification of Si with X_2 fit well with the expectation that reduction of hot SiO_2 by H_2 in the LPE reactor would lead to incorporation of Si into the melt, and subsequently into the growing epilayer,[17,18] and that this mechanism was the dominant contribution to residual donors in LPE GaAs. The present identification of Si with X_1, together with the previous photothermal ionization data for LPE GaAs,[2,5,19] indicates not only that Si is not the dominant residual donor, but that it is usually present in undetectably small concentrations relative to the other residual donor species. Figure 3 shows the spectrum of the high purity LPE GaAs sample 3, which was grown at Cornell University. Peaks corresponding to the usual Pb, Sn, and X_2 donors are clearly visible in this spectrum, but a small peak at the energy of X_1 = Si was also reproducibly observed. Most of the photoresponse at the energy of X_1 is due to the low energy tail of the Sn peak and so the relative concentration of X_1 is quite small. The proximity of the X_1 and Sn peaks in energy and the fact that the residual Sn concentration is usually much larger than the concentration of X_1 donors observed here may account for the fact that this is the first report of the X_1 peak in the photothermal ionization spectra of undoped LPE GaAs.

The identification of Si with X_1 instead of X_2 also has implications with regard to the role of Si as a residual donor in GaAs grown by various other techniques. In AsH_3 VPE grown GaAs the residual donors are X_1, X_2, and X_3, as in $AsCl_3$-H_2 VPE, but the concentrations of X_1 and X_3 are lower, and X_2 is dominant.[2] In MBE GaAs grown with an elemental As source and using Sn as the n-type dopant, both X_1 and X_2 are present but the concentration of X_1 is low,[20] while if AsH_3 is cracked in a SiO_2 furnace to provide the As, the amplitude of the X_1 = Si peak increases with increasing cracking furnace temperature.[20] In metalorganic chemical vapor deposited (MOCVD) grown GaAs the relative concentrations of various residual donors including X_1 and X_2 deduced from photothermal ionization measurements have been correlated with various growth parameters and purification techniques from the metalorganics.[21] These results indicate that the residual X_1 = Si donor concentration can be made negligible in MOCVD GaAs.

In conclusion, on the basis of photothermal ionization measurements on Si-doped MBE GaAs samples, an identification of Si with the spectral peak X_1 has been made. This identification together with previous photothermal ionization data indicates that Si is not an important residual donor in high purity LPE GaAs, and also necessitates a reevaluation of the importance of Si as a residual donor in epitaxial GaAs grown by a variety of other techniques.

The authors gratefully acknowledge the support of H. Lessoff and M. N. Yoder, and thank B. L. Payne, R. T. Gladin, and G. E. Morris for their assistance in preparation of the manuscript. This work was supported by ONR under Contract Nos. N00014-80-C-0762 and N00173-C-0184.

[1] D. J. Ashen, P. J. Dean, D. T. J. Hurle, J. O. Mullin, A. M. White, and P. D. Greene, J. Phys. Chem. Solids **36**, 1041 (1975).
[2] T. S. Low, G. E. Stillman, and C. M. Wolfe, GaAs Conf. Proc. Sym. GaAs and Related Compounds, Oiso, 1981 (to be published).
[3] C. M. Wolfe, G. E. Stillman, and D. M. Korn, Inst. Phys. Conf. Ser. No. 33b, 120 (1976).
[4] M. Ozeki, K. Kitahara, K. Nakai, A. Shibatomi, K. Dazai, S. Okawa, and O. Ryuzan, Jpn. J. Appl. Phys. **16** (9), 1617 (1977).
[5] R. A. Cooke, R. A. Houlte, R. F. Kirkman, and R. A. Stradling, J. Phys. D **11**, 945 (1978).
[6] D. M. Larsen, Phys. Rev. B **13**, 1681 (1976).
[7] T. S. Low, G. E. Stillman, C. M. L. Yee, and C. M. Wolfe (unpublished).
[8] C. M. Wolfe, D. M. Korn, and G. E. Stillman, Appl. Phys. Lett. **24**, 78 (1974).
[9] H. Morkoç and A. Y. Cho, J. Appl. Phys. **50**, 6413 (1979).
[10] A. Chandra, C. E. C. Wood, D. W. Woodard, and L. F. Eastman, Solid State Electron. **22**, 645 (1979).
[11] C. M. Wolfe, G. E. Stillman, and J. O. Dimmock, J. Appl. Phys. **41**, 504 (1970).
[12] T. S. Low and G. E. Stillman (unpublished).
[13] G. E. Stillman, C. M. Wolfe, and D. M. Korn, Proc. 13th Int. Conf. Phys. of Semiconductors, Rome, pp. 623–626 (1977).
[14] R. A. Stradling (private communication).
[15] H. R. Fetterman, J. Waldman, C. M. Wolfe, G. E. Stillman, and C. D. Parker, Appl. Phys. Lett. **21**, 434 (1972).
[16] R. A. Stradling, L. Eaves, R. A. Houlte, N. Miura, P. E. Simmonds, and C. C. Bradley, Proc. of the Fourth Int. Symp. on GaAs, Inst. Phys. London, 1973, p. 65.
[17] M. W. Weiner, J. Electrochem. Soc. **119**, 496 (1972).
[18] H. G. B. Hicks and P. D. Green, Inst. Phys. Conf. Ser. No. 9, Bristol and London 92 (1971).
[19] H. Morkoç, L. F. Eastman, and D. Woodard, Thin Solid Films **71**, 245 (1980).
[20] T. S. Low, G. E. Stillman, H. Morkoç, A. Y. Cho, and A. R. Calawa, Appl. Phys. Lett. **40**, 611 (1982).
[21] P. D. Dapkus, H. M. Manasevit, K. L. Hess, T. S. Low, and G. E. Stillman, J. Cryst. Growth **55**, 10 (1981).

A.4 Photothermal ionization identification of sulfur donors in GaAs

T. S. Low and G. E. Stillman
Electrical Engineering Research Laboratory,[a] Materials Research Laboratory, and Coordinated Science Laboratory, University of Illinois, Urbana, Illinois 61801

T. Nakanisi and T. Udagawa
Electronics Equipment Division, Toshiba Corporation, 1 Komuakai Toshiba-cho Saiwai-ku, Kawasaki, Japan

C. M. Wolfe
Semiconductor Research Laboratory, Washington University, St. Louis, Missouri 63130

(Received 22 April 1982; accepted for publication 4 May 1982)

Photothermal ionization data for undoped and S-doped epitaxial GaAs grown by metalorganic chemical vapor deposition (MOCVD) are presented which permit the positive identification of the S donor. This identification is unambiguous because S is not a significant residual impurity in the undoped MOCVD GaAs used for these measurements. Implications of the new identification for the importance of S as a residual donor in epitaxial GaAs prepared by various other growth techniques are discussed.

PACS numbers: 81.15.Gh

Sulfur is frequently used as an *n*-type dopant in both bulk and epitaxial GaAs. It incorporates readily and can be introduced into the epitaxial layer in a variety of ways depending on the growth technique. Sulfur has also been suspected as a possible residual donor in high-purity GaAs, but this suspicion has not been verified because of the several conflicting spectroscopic identifications of the S donor in previously reported photothermal ionization measurements.

The best method for the detection and identification of donor impurities in high-purity GaAs is photothermal ionization spectroscopy.[1] This technique can detect the residual donor species present in high-purity samples, and also determine the relative concentrations of the different donor species from the amplitudes of the corresponding spectral peaks. Carefully controlled doping experiments have been performed by several research groups[2–4] to identify various photothermal ionization peaks with the associated donor species. Such experiments are difficult because of the small donor concentration range between the purest GaAs which can be grown, and that for which impurity interactions[5] degrade the spectra by broadening and distorting the spectral peaks. Doping experiments performed by three separate research groups using similar growth techniques have resulted in the association of as many distinct spectral peaks with S donors.[2,4,6,7] In this letter we present photothermal ionization measurements on undoped and S-doped GaAs prepared by metalorganic chemical vapor deposition (MOCVD) which positively identify the $1s$–$2p(m = -1)$ photothermal ionization peak due to sulfur. This identification is unambiguous because S is not a prominant residual donor in the high-purity MOCVD GaAs used for these measurements. Together with earlier photothermal ionization data for GaAs grown by a variety of techniques in many different laboratories, this identification indicates that S donors comprise a substantial fraction of the total residual donor concentration in high-purity GaAs grown by both graphite[8,9] and silica[3] boat liquid phase epitaxy (LPE), by $AsCl_3$-H_2,[2,4,8] $AsCl_3$-N_2,[4,8] and AsH_3-HCl-H_2[8] vapor phase epitaxy (VPE), by molecular beam epitaxy (MBE),[10,11] and in some high-purity GaAs grown by MOCVD.[8,12,13]

The undoped and S-doped MOCVD samples were grown in a $(CH_3)_3Ga$-AsH_3 growth system, and the S doping was accomplished by introduction of H_2S into the gas stream. Further details of the techniques used for growth of this high-purity MOCVD GaAs have been described previously.[14] Photothermal ionization spectra for the MOCVD samples and for the $AsCl_3$-H_2 VPE reference sample are shown in Fig. 1. These spectra, which were recorded at precisely the same magnetic field ($B = 3.89$ T) by operating the superconducting magnet in the persistent mode, show the $1s$–$2p(m = -1)$ transitions of the various donor species present. The three peaks labeled X_1, X_2, and X_3 in the spectrum of the reference sample in Fig. 1(d), correspond to the three characteristic residual donors present in GaAs grown by the $AsCl_3$-H_2 VPE technique. At a given magnetic field, the energies of these peaks provide a reference for identifying the peaks in the spectra of the other samples. Quantitative relative concentrations can be derived from the spectra,[11] and absolute donor concentrations can then be calculated using the Hall mobility analysis of Wolfe *et al.*[15] Impurity concentrations calculated in this way for these samples are given in Table I.

The spectrum of the undoped sample 1 in Fig. 1(a) shows the dominant X_1 donor peak typical of high-purity undoped MOCVD GaAs[8,12,13] and much smaller peaks corresponding to Sn and X_2. There is some uncertainty regarding the identification of the donor species responsible for the X_1 peak. Photothermal ionization measurements on $AsCl_3$ VPE grown GaAs doped with Ge by adding the dopant in elemental form of the Ga melt,[4,13] and also by neutron transmutation doping,[8,16] have indicated that Ge donors contribute a peak at or near X_1 in energy. However, Ge acceptor peaks are absent from the photoluminescence spectra of MOCVD samples showing the dominant X_1 donor peak.[17] Earlier experiments resulted in the tentative identification of X_1 with carbon donors.[2] For the purposes of the present work however, the importance of the spectrum of sample 1 is

[a] Department of Electrical Engineering.

 0003-6951/82/02183-03$01.00

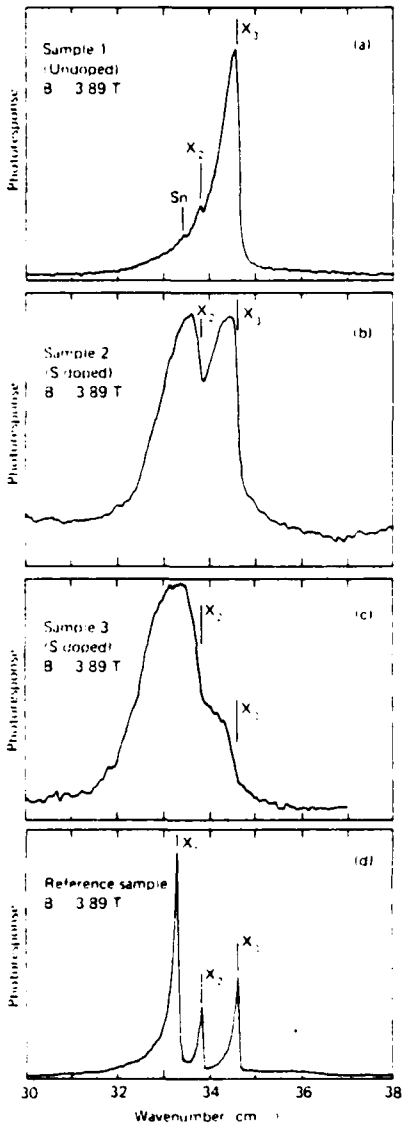

FIG. 1. Photothermal ionization spectra of the $1s$–$2p(m = -1)$ transitions for the undoped and two S-doped MOCVD samples, and for the $AsCl_3$-H_2 VPE reference sample, demonstrating the increase in X_2 donor concentration with S doping.

that it is typical of high-purity undoped MOCVD GaAs, showing primarily X_3 donors and very little else.

The spectrum of the more lightly S-doped sample 2 shown in Fig. 1(b) contains two peaks, with each having the typically observed asymmetric line shape predicted by Larsen.[5] The peak at lower energy corresponds to X_2 in the reference spectrum while the higher energy peak corresponds to the dominant MOCVD residual donor X_3. In spite of the approximately equal amplitudes of the X_2 and X_3 peaks in the spectrum of sample 2, the actual concentration of X_2 donors is only 0.43 times that of the X_3 donors (see Table I), because a substantial fraction of the photoresponse at the energy of X_2 is due to the low-energy tail of the X_3 peak.

The spectrum of the more heavily S-doped sample 3 is shown in Fig. 1(c). Again the two peaks present correspond to X_2 and X_3 in the reference sample, but the X_2 donors are present at substantially larger concentration than in sample 2. The concentrations of X_3 donors in the two samples are nearly equal, however. The increase in peak widths and slight downshift in peak energies observed in Fig. 1 as the S doping increases are explained by the increasing Stark broadening of the $1s$–$2p(m = -1)$ transition caused by the electric fields due to charged centers (compensated donors and ionized acceptors) as described by Larsen.[5] Such behavior is frequently observed in samples of this doping level.

As noted above, the concentration of X_2 donors in the undoped MOCVD sample 1 is quite small. The appearance of X_2 donors at significant levels in the spectrum of the S-doped samples 2 and 3, and the increase in the observed concentration of X_2 donors with increasing S doping, clearly indicate that S donors are responsible for the X_2 peak. This identification confirms that of Ozeki *et al.*,[4] made using $AsCl_3$-N_2 VPE grown GaAs, in which the characteristic residual donors are X_2 and X_3. The larger relative amplitude of the X_2 photothermal ionization peak in a S-doped sample as compared with similarly grown undoped samples led these workers to identify X_2 with the S donor.

As mentioned above, however, photothermal ionization peaks other than X_2 have been previously identified with the sulfur donor. The photothermal ionization spectrum of the S-doped $AsCl_3$-H_2 VPE grown sample 4 is shown in Fig. 2. This is the same sample used in a previous attempt to identify the spectral peak corresponding to S donors.[2,7] Doping of this sample was accomplished by adding elemental S to the Ga melt. The $1s$–$2p(m = -1)$ transitions include the usual residual donor peaks X_1, X_2, and possibly X_3, but there is an additional peak present above X_2 in energy. Although this peak does not have the characteristic shape expected for the shallow donor transitions,[5] it was nevertheless attributed to S donors.[2,7] Photothermal ionization peaks having a notch at the usual $1s$–$2p(m = -1)$ transition energy with a sharply peaked component at slightly higher energy and a

TABLE I. Impurity concentrations ($\times 10^{14}$ cm^{-3}).

Sample	μ_{77}(cm^2/Vs)	N_D(total)	N_A(total)	$N_D(X_1 = \mathrm{Si})$	N_D(Sn)	$N_D(X_2 = S)$	$N_D(X_3)$
reference	151 000	1.61	1.20	0.91	a	0.29	0.41
1	95 900	4.84	3.56	a	0.15	0.31	4.38
2	59 000	15.2	6.3	a	a	4.6	10.6
3	49 000	19.6	9.9	a	a	10.0	9.6
4	74 000	12.0	2.6	b	b	b	b

[a] Not detected.
[b] Not determined (see text).

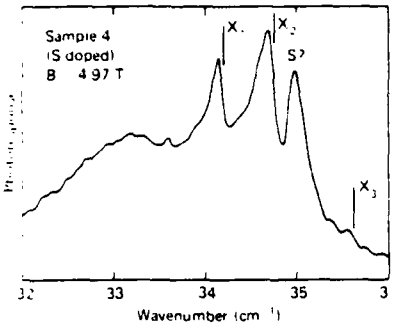

FIG. 2. Photothermal ionization spectrum of the $1s$–$2p(m = -1)$ transitions in the S-doped $AsCl_3$-H_2 VPE sample 4, showing the anomalously shaped peak originally attributed to S donors.

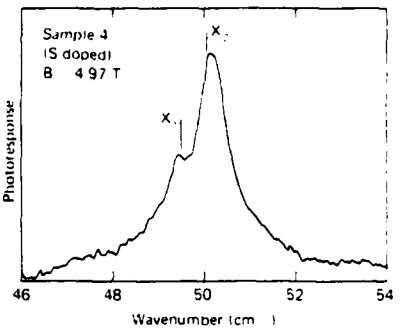

FIG. 3. Photothermal ionization spectrum of the $1s$–$2p(m = 0)$ transitions in the S-doped $AsCl_3$-H_2 VPE sample 4 showing the large amplitude of the X_2 peak and the absence of any peak of higher energy than X_2 corresponding with the peak labeled S? in Fig. 2.

broader wing at lower energy have been observed previously,[18] particularly for the larger amplitude peaks (i.e., higher concentration donors). The mechanism which produces this peak shape is not yet fully understood, but because of the anomalous shape of the peak attributed to S and its proximity to X_2, it now seems likely that the peaks labeled X_2 and S in Fig. 2 may actually be the high- and low-energy components of a single notched peak associated with X_2 = S donors. Further evidence for this is provided by examination of the $1s$–$2p(m = 0)$ transition, in which the notched peak shape has never been observed. Figure 3 shows the photothermal ionization spectrum in the region of the $1s$–$2p(m = 0)$ transition for sample 4. The smaller peak corresponds closely with the energy of X_1 in the $1s$–$2p(m = 0)$ transition of the reference spectrum. The existence of a single large amplitude peak near the energy of X_2 in the $1s$–$2p(m = 0)$ transition of the reference spectrum supports the notched peak interpretation of the $1s$–$2p(m = -1)$ spectrum in Fig. 2.

In another identification of S donors, Afsar *et al.*[6] used a H_2S-doped $AsCl_3$-H_2 VPE grown sample to associate S donors with a peak below X_1 in energy. This peak is nearly coincident with a peak previously attributed to Pb donors by Wolfe *et al.*[2] and Stradling,[19] from measurements of $AsCl_3$-H_2 VPE and LPE samples, respectively. The presence of this peak in the spectrum of the S-doped sample of Afsar *et al.*[6] is especially difficult to understand in view of the absence of such a peak in the spectra of S-doped $AsCl_3$ VPE samples grown by Bozler,[20] Ozeki *et al.*,[4] and Wolfe *et al.*[2] It is interesting to note, however, in view of the present identification of X_2 as S, and the fact that amplitude of the X_2 peak is generally somewhat smaller than that of the residual X_1 in undoped $AsCl_3$-H_2 VPE grown GaAs prepared in several different laboratories[2,8,13] [cf. Fig. 1(d) reference sample], that the largest peak in the spectrum of the S-doped sample of Afsar *et al.*[6] is the X_2 peak.

In conclusion, on the basis of photothermal ionization measurements on undoped and S-doped MOCVD grown GaAs samples, the spectral peak X_2 has been positively identified with S donors. This unambiguous identification is made possible by the near absence of X_2 donors in the undoped control sample. Together with previous photothermal ionization data, this identification indicates that S comprises a substantial fraction of the total donor concentration in undoped high-purity GaAs prepared by a wide variety of growth techniques.

The authors gratefully acknowledge T. H. Miers of Motorola Incorporated for providing the reference sample used in this work, and also C. O. Bozler of M. I. T. Lincoln Laboratory for providing several H_2S-doped samples. The authors also acknowledge the support of H. Lessoff and M. Yoder, and thank B. L. Payne, R. T. Gladin, and G. E. Morris for their assistance in preparation of the manuscript.

[1] G. E. Stillman and C. M. Wolfe, in *Semiconductors and Semimetals*, edited by R. K. Willardson and A. C. Beer (Academic, New York, 1977), Vol. 12, pp. 169–290.
[2] C. M. Wolfe, G. E. Stillman, and D. M. Korn, *GaAs and Related Compounds, St. Louis, 1976*, Conf. Ser. No. 33b (Institute of Physics, London, 1977), pp. 120–128.
[3] R. A. Cooke, R. A. Hoult, R. K. Kirkman, and R. A. Stradling, J. Phys. D **11**, 945 (1978).
[4] M. Ozeki, K. Kitahara, K. Nakai, A. Shibatomi, K. Dazai, S. Okawa, and O. Ryuzan, Jpn. J. Appl. Phys. **16**, 1617 (1977).
[5] D. M. Larsen, Phys. Rev. B **13**, 1681 (1976).
[6] M. N. Afsar, K. J. Button, and G. L. McCoy, *GaAs and Related Compounds, Vienna 1980*, Conf. Ser. No. 56 (Institute of Physics, London, 1981), pp. 547–555.
[7] G. E. Stillman, C. M. Wolfe, and D. M. Korn, *Proceedings of the 13th International Conference on Physics of Semiconductors*, 1976 (Rome, 1976), pp. 623–626.
[8] T. S. Low, G. E. Stillman, and C. M. Wolfe, *GaAs and Related Compounds, Oiso, 1981* (Institute of Physics, London, 1982) (to be published).
[9] H. Morkoç, L. F. Eastman, and D. Woodard, Thin Solid Films **71**, 245 (1980).
[10] T. S. Low, G. E. Stillman, D. M. Collins, C. M. Wolfe, S. Tiwari, and L. S. Eastman, Appl. Phys. Lett. **40**, 1034 (1982).
[11] T. S. Low, G. E. Stillman, H. Morkoç, A. Y. Cho, and A. R. Calawa, Appl. Phys. Lett. **40**, 611 (1982).
[12] P. D. Dapkus, H. M. Manasevit, K. L. Hess, T. S. Low, and G. E. Stillman, J. Cryst. Growth **55**, 10 (1981).
[13] T. S. Low and G. E. Stillman (unpublished).
[14] T. Nakanisi, T. Udagawa, A. Tanaka, and K. Kamei, J. Cryst. Growth **55**, 255 (1981).
[15] C. M. Wolfe, G. E. Stillman, and J. O. Dimmock, J. Appl. Phys. **41**, 504 (1970).
[16] J. H. M. Stoelenga, D. M. Larsen, W. Walukiewicz, and C. O. Bozler, J. Phys. Chem. Solids **39**, 873 (1978).
[17] T. S. Low, B. Ji Skromme, G. E. Stillman, P. D. Dapkus, K. L. Hess, and H. M. Manasevit (unpublished).
[18] T. S. Low, G. E. Stillman, C. M. L. Yee, and C. M. Wolfe (unpublished).
[19] R. A. Stradling (private communication).
[20] C. O. Bozler (private communication).

Inst. Phys. Conf. Ser. No. 65: Chapter 6
Paper presented at Int. Symp. GaAs and Related Compounds, Albuquerque, 1982

A.5 Spectroscopic characterization studies of the residual donors and acceptors in high-purity LPE GaAs

B J Skromme, T S Low, and G E Stillman

Electrical Engineering Research Laboratory
Materials Research Laboratory and Coordinated Science Laboratory
University of Illinois at Urbana-Champaign, Urbana, Illinois 61801

Abstract. Unintentionally-doped samples grown by LPE in graphite boats in seven different laboratories have been characterized using variable temperature photoluminescence and photothermal ionization spectroscopy. The dominant residual donor is always found to be S, with Sn, Pb, and Si donors also observed. The main residual acceptors are Si and C but Mg and Ge are also present. It is found that the residual amphoteric impurities Si and Ge incorporate preferentially as acceptors while residual Pb and Sn incorporate preferentially as donors. The results suggest that S may be the main volatile donor species removed from the melt by baking.

1. Introduction

The ability to grow high purity layers of GaAs using liquid-phase epitaxy (LPE) is important for various device applications such as FET buffer layers p-i-n photodetectors, and Gunn-effect devices. Accurate determination of the residual impurity species present in such layers is a necessary prerequisite to identifying the sources of impurities in the growth system and to the characterization and control of the growth process. In the present study, the complementary techniques of variable temperature photoluminescence (PL) and photothermal ionization spectroscopy were used to identify the residual acceptors and donors, respectively, in high purity LPE layers from several different laboratories. The dominant residual impurity species are identified and the incorporation of residual donors and acceptors in the same samples is correlated to study the behavior of amphoteric impurities in LPE. Comparisons are made with the behavior of these elements as intentional dopants.

2. Experimental

The samples used in this study were prepared in various laboratories using the graphite slider-boat technique, with the exception of the samples from Hughes grown using the infinite solution technique (Kamath et al. 1977) and the sample from the Forschungsinstitut grown in a graphite tipping boat. Hall-effect data for these samples are presented in Table I.

Photoluminescence measurements were performed over the temperature range 1.6-20 K with the sample freely suspended in liquid or gaseous He. The excitation was provided by 5145 Å light from an Ar^+ laser at power levels $\lesssim$ 1W. For measurements above 4.2 K, 1 mW of power was used. The luminescence was detected with a resolution of about 0.2 Å using a 1m

0305-2346/83/0065-0485 $02.25

Table I Electrical Characteristics

Source	$\mu_{77}(cm^2/Vs)$	$n_{77}(cm^{-3})$
Cornell (S Tiwari and L F Eastman)	137,000	$1.8 \cdot 10^{14}$
Forschungsinstitut der DBP/FTZ (E Kuphal)	136,000	$2.9 \cdot 10^{13}$
HP (C A Stolte)	130,000	$9.0 \cdot 10^{13}$
Honeywell (J K Abrokwah)	98,400	$1.2 \cdot 10^{14}$
Hughes (D E Holmes and G S Kamath)	58,000	$7.9 \cdot 10^{14}$
Max-Planck Institut (E Bauser)	140,000	$4.7 \cdot 10^{13}$
University of Illinois (G E Bulman)	47,300	$1.1 \cdot 10^{14}$

spectrometer, cooled S-1 photomultiplier tube, and D.C. detection. The spectra are uncorrected for detector response.

The technique of photothermal ionization spectroscopy is described in detail elsewhere (Stillman et al. 1977). A Fourier transform spectrometer was used as a tunable, high resolution (0.06 cm^{-1}) far-infrared light source to excite the 1s-2p(m=-1) transitions of the shallow hydrogenic donor species with the sample placed in a uniform magnetic field of up to 6.7 T. As the photon energy is tuned though the 1s-2p(m=-1) transition energies of the various donor species which are present, peaks are observed in the electrical conductivity of the sample whose amplitudes are proportional to the relative concentrations of the donor species, as long as the peaks are sufficiently well separated. The donor species present were determined by a comparison of the spectrum of each sample with that of a well characterized reference sample (μ_{77}=201,000 cm^2/Vs, $n_{77}=4.5 \cdot 10^{13}$ cm^{-3}) recorded at precisely the same magnetic field.

3. Photoluminescence Spectra

The near band-edge PL spectrum of GaAs at low temperature can be broadly divided into three regions: the exciton region, the band-to-acceptor region, and the deep region. The exciton region of a typical high-purity sample is shown in Fig. 1. The lines due to the recombination of free and

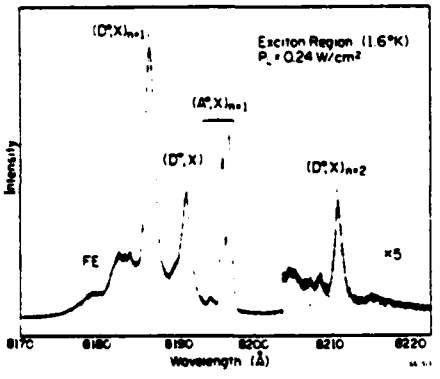

Fig. 1 PL spectrum of H.P. SB-957 (Exciton Region)

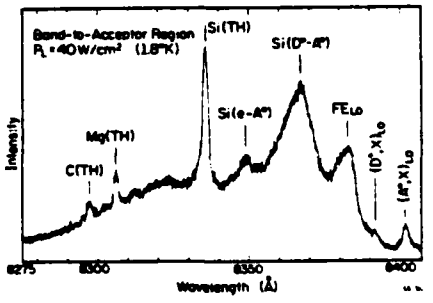

Fig. 2 PL spectrum of H.P. SB-957 (Two-hole transitions)

bound excitons are labeled using the notation of Heim and Hiesinger (1974). The narrow linewidths of the exciton spectrum are useful in assessing sample purity but little information on the nature of the acceptor species is provided. Of much greater use are the "two-hole" (TH) replicas of the (A°,X) peaks at lower energy, as shown in Fig. 2.

The two-hole replicas result when the neutral acceptor is left in its first excited state and are therefore separated by nearly the full chemical shift for different acceptors (Ashen et al. 1975). The peak positions of the unresolved doublets in Fig. 2 at 8297.3 Å (1.49387 eV), 8305.9 Å (1.49232 eV), and 8335.7 Å (1.48699 eV) correspond to within .06 meV or better of those reported by Ashen et al. (1975) for C, Mg, and Si-doped crystals, respectively, enabling a positive identification of those acceptors. Broader bands corresponding to the conduction band-to-acceptor (e-A°) and donor-to-acceptor (D°-A°) peaks for Si acceptors are also observed in this spectrum, as well as LO phonon replicas of several of the exciton lines.

At much lower excitation intensities the (e-A°) and (D°-A°) peaks of 4 different acceptors can be resolved in this sample, as shown in the spectra of Fig. 3 at two different temperatures. The relative decline in the strengths of the (D°-A°) peaks and the enhancement of the (e-A°) peaks for each acceptor at the higher temperature is due to increased thermal ionization of the shallow donors. The observed peak energies of the (e-A°) transitions at 7 K are 1.4931 eV, 1.4914 eV, 1.4851 eV, and 1.4781 eV for the C, Mg, Si, and Ge acceptors, respectively, and the corresponding (D°-A°) peak energies at 2 K are 1.4891 eV, and 1.4875 eV, 1.4814 eV, and 1.4746 eV. The values of the (e-A°) peak positions are all in accord with Ashen's values to within 1 meV or better.

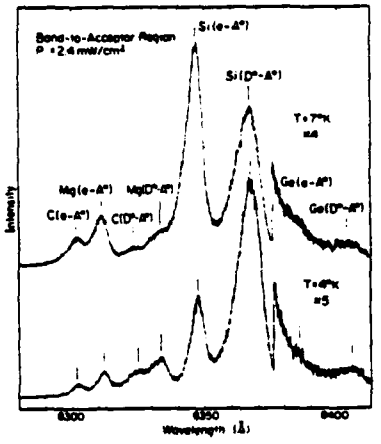

Fig. 3 PL spectrum of H.P. SB-957 (Band-to-acceptor region)

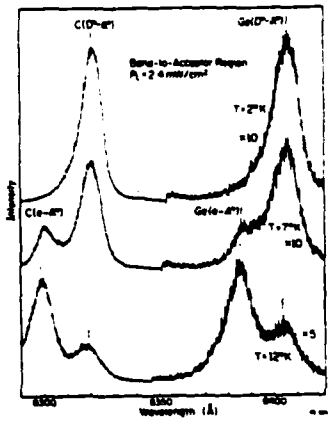

Fig. 4 PL spectrum of Hughes 12-11-79 (Band-to-acceptor region)

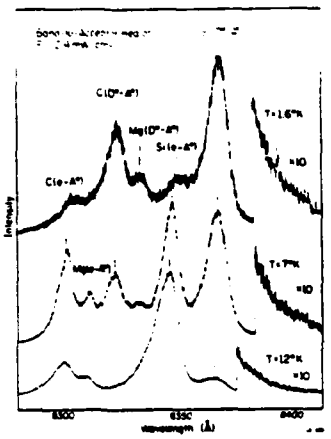

Fig. 5 PL spectrum of Honeywell 251 (Band-to-acceptor region)

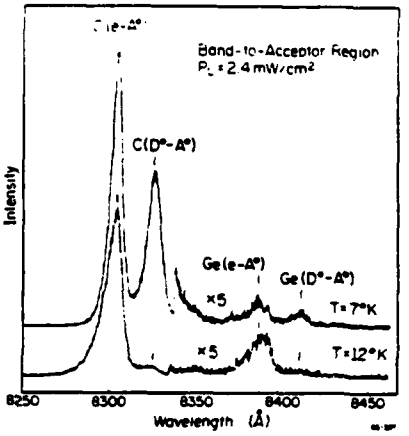

Fig. 6 PL spectrum of Max-Planck sample (Band-to-acceptor region)

The band-to-acceptor regions of three other samples as a function of temperature are shown in Figs. 4, 5, and 6. The complete absence of Si and Mg in the samples of Fig. 4 and 6 is quite striking when compared to Figs. 3 and 5. A summary of the relative concentrations of shallow acceptors in all of the measured samples, as estimated from the relative heights of (D°-A°)peaks at 1.6 K, is given in Fig. 7. This method of estimating relative concentrations favors the shallower acceptors somewhat, since their more extended wave functions increase the (D°-A°) recombination rate. A similar plot of donor concentrations is given for comparison in Fig. 8 (see next section). Marked similarities and contrasts are apparent on comparing the spectra of Fig. 7, most notably the complete absence of Si in the first three samples.

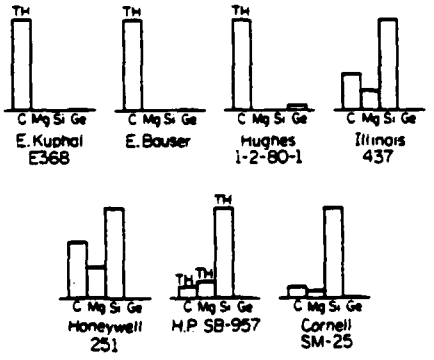

Fig. 7 Relative concentrations of shallow acceptors (TH denotes two-hole transition observed)

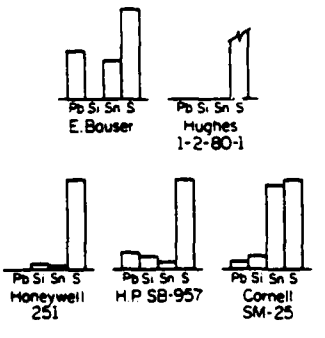

Fig. 8 Relative concentrations of shallow donors

The deep acceptors Mn and Cu were observed in nearly all of the samples studied, as illustrated for a typical sample in Fig. 9. Various TA and LO-phonon replicas of the deep acceptor peaks are also observed. Deep Sn acceptors were identified in the two samples from Cornell, but only by means of the neutral Sn acceptor-bound exciton line at 1.5071 eV. The deep Sn acceptor peaks were apparently obscured by interference from the Cu acceptor peaks, which occur at very nearly the same energy. No Sn acceptors were detected in any of the other samples.

4. Photothermal Ionization Spectra

The photothermal ionization spectrum of a high purity LPE sample is shown in Fig. 10. The multiplet of peaks corresponds to the fine structure of the 1s-2p(m=-1) transition of the donors in a high magnetic field. Each peak in the multiplet corresponds to a different donor species, the separation of the peaks resulting from the central-cell corrections to the ionization energy calculated from the hydrogenic approximation for shallow donors. The narrow linewidths of these peaks is indicative of the very high purity of this sample. The dominant peak in this spectrum is X_2, which was originally thought to be Si (Wolfe et al. 1977) but more recently has been shown to be S by Low et al. (1982a) and Ozeki et al. (1977). The identifications of the lines marked Pb and Sn are based on back-doping experiments performed by Wolfe et al. (1977), Cooke et al. (1978), and Stradling (1981). Early work indicated that the X_1 peak which appears in this spectrum might be associated with a Ga vacancy complex (Wolfe et al. 1977), but more recent studies by Ozeki et al. (1977) and Low et al. (1982b) have shown it to be due to Si donors. Notably absent in this spectrum is the X_3 peak, which was originally attributed to C donors (Wolfe et al. 1977). More recent work by Ozeki et al. (1977), Stoelenga et al. (1978), Afsar et al. (1981), and Low and Stillman (1982c) suggests that X_3 is actually due to Ge donors. The experiments of Ozeki et al. (1977) concluded that C does not incorporate as a donor in GaAs.

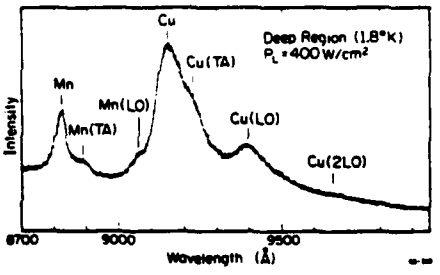

Fig. 9 PL spectrum of Max-Planck sample (Deep region)

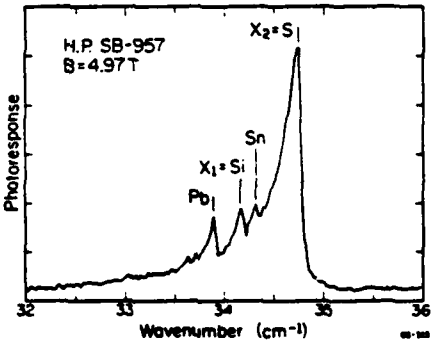

Fig. 10 Photothermal ionization spectrum of H.P. SB-957

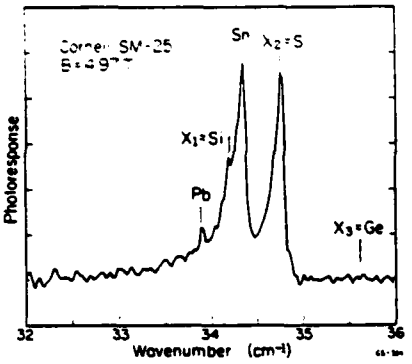

Fig. 11 Photothermal ionization spectrum of Cornell SM-25

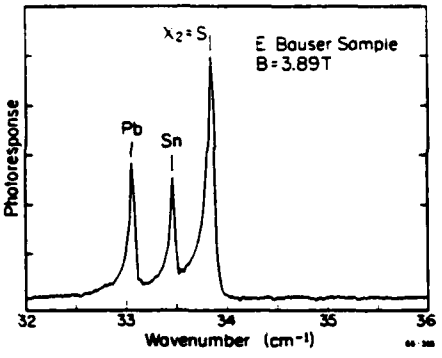

Fig. 12 Photothermal ionizaton spectrum of Max-Planck sample

Photothermal ionization spectra for two other samples are shown in Figs. 11 and 12 for comparison. The latter spectrum displays the narrowest linewidths of any of the LPE samples we have measured to date, even at the lower magnetic field. A comparison of the relative donor concentrations in the measured samples is given in Fig. 8. The spectrum of the Hughes sample was broadened by impurity interactions so that it was impossible to resolve donors other than S. The concentrations in this figure were estimated from relative peak heights, correcting for contributions from the low energy tails of adjacent peaks. It is seen that in all cases the dominant donor is S followed by Sn, Pb, and lastly Si in order of decreasing relative concentrations.

5. Discussion

It is of interest to compare our results to previous studies. While O has often been proposed to be the dominant shallow donor species in LPE GaAs (see, e.g. Solomon 1969 and Nanishi 1978), no spectroscopic evidence for this contention has ever been presented and in light of the current donor identifications it clearly contradicts the present results. Similar remarks can be made concerning early speculation that C was the dominant donor (Morkoç and Eastman 1976). Kang and Greene (1969) correctly hypothesized that S might be the dominant donor, based on the temperature dependence of the residual doping and the presence of 0.2 ppm of S in the graphite crucible used for growth, but no spectroscopic evidence was obtained. The only previous spectroscopic studies (Cooke et al. 1978 and Morkoç et al. 1980) concluded that Si was the dominant donor, with lower levels of Pb and Sn present (although the latter identifications were not considered definite.) Those studies are consistent with our results if the present identification of X_2 = S is applied to their data.

The previous photoluminescence study of Ashen et al. (1975) identified C and Si as the dominant acceptors in LPE samples grown in either quartz or graphite boats, with traces of Ge also frequently seen. Zschauer (1973) found the dominant PL acceptor peaks for samples grown in vacuum in various types of boats to be those now known to be due to C (Ashen et al. 1975). Our PL results are largely in accord with the previous studies, but the observation of significant levels of Mg in four of our samples is

interesting given that residual Mg acceptors have never previously been reported in LPE material. The report of Zn acceptors in LPE samples by Morkoç et al. (1980) must be considered highly questionable in light of the present data and the fact that their spectra did not separately resolve the (e-A°) and (D°-A°) transitions of the different acceptors.

Correlations of the residual acceptor and donor species in undoped LPE samples have not previously been reported. A comparison of Figs. 7 and 8 indicates that the residual Si incorporates predominantly as acceptors in these samples, which were all grown at temperatures << 860°C. This result is in agreement with compensation studies of intentionally Si-doped samples (Hicks and Greene 1971) and with theoretical predictions of the behavior of Si in GaAs (Teramoto 1972). The importance of Si donors in LPE samples grown at low temperatures is in fact so minor that they were only very recently observed for the first time by Low and Stillman (1982d) for one of the samples in the present study. The residual Ge exhibits similar behavior in accord with its well known behavior as an uncompensated p-type dopant in LPE. On the other hand, Sn is found to incorporate primarily as a donor, since Sn acceptors are observed only in the samples with the largest concentration of Sn donors (Cornell). Doping experiments with Sn produced similar conclusions (Kang and Greene 1969). Apparently Pb incorporates exclusively as a donor. The n-type behavior of Sn and Pb under Ga-rich growth conditions can be understood theoretically on the basis of their larger covalent radii (Teramoto 1972). Incorporation of amphoteric impurities is discussed in more detail elsewhere (Low et al. 1983).

The source of the residual impurities in LPE is at present poorly understood. Contamination with S might occur from the graphite boats but Cooke et al. (1978) found S to be generally dominant in samples grown at STL in quartz boats. The dominance of S donors in the samples we measured and its extremely high volatility suggest that it may be the principle n-type dopant removed from the melt by baking. Removal of Si from the melt would result in fewer acceptors. The well-known recontamination effect on the melt when the growth system is opened (Morkoç and Eastman 1976) might result from S contamination from the atmosphere. The presence of Si and C acceptors has been ascribed to interactions among the components of the growth system (Mattes et al. 1975), but C acceptors have been observed even in samples grown in non C-containing apparatus (Ashen et al. 1975). Recent work has indicated that Pd-diffused H_2 may contain significant amounts of CO (Stevenson et al. 1977); another possible source of C is contamination from the substrate. The absence of Si acceptors in some samples would seem to contradict the conventional model involving reduction of the quartz walls of the reactor, but more work is needed here. It has been suggested that Pb contamination might result from atmospheric pollution (Stradling 1981); the source of the Mg and Ge is unknown.

6. Conclusions

It was found that S is the dominant donor in LPE GaAs, contrary to previous reports of C, O, and Si. Lower levels of Pb, Sn, and Si donors were observed. The dominant acceptors were Si and C with smaller amounts of Mg and Ge. The residual impurity Sn incorporates mainly as donors, Pb incorporates exclusively as a donor, and Si and Ge mainly as acceptors. The principle donor removed from the melt by baking is probably S. The present results form the foundation for future studies which are necessary to firmly identify the sources of the residual impurities.

7. Acknowledgments

The authors are greatly indebted to the following for the provision of samples: J K Abrokwah, E Bauser, G E Bulman, L F Eastman, D E Holmes, G S Kamath, E Kuphal, C A Stolte, S Tiwari. We are also grateful to B L Payne, R MacFarlane, and R T Gladin for their expert assistance in the preparation of the manuscript. Financial support was provided by ARO under Contract DAAG 29-82-K-0059, by ONR under Contract N00173-79-C-0184, and by JSEP under Contract N00014-79-C-0424.

8. References

Afsar M N, Button K J, and McCoy G L 1981 GaAs and Related Compounds 1980 (Inst. Phys. Conf. Ser. 56) pp 547-555
Ashen D J, Dean P J, Hurle D T J, Mullin J B, and White A M 1975 J. Phys. Chem. Solids 36 1041
Cooke R A, Hoult R A, Kirkman R F, and Stradling R A 1978 J. Phys. D11 945
Heim U and Hiesinger P 1974 Phys. Stat. Sol. b66 461
Hicks H G B and Greene P D 1971 GaAs and Related Compounds 1970 (Inst. Phys. Conf. Ser. 9) pp 92-99
Kamath G S, Ewan J, and Knechtli R C 1977 IEEE Trans. Electron. Devices 24 473
Kang C S and Greene P E 1969 GaAs and Related Compounds 1968 (Inst. Phys. Conf. Ser. 7) pp 18-21
Low T S, Stillman G E, Nakanisi T, Udagawa T and Wolfe C M 1982a Appl. Phys. Lett. 41 183
Low T S, Stillman G E, Collins D M, Wolfe C M, Tiwari S, and Eastman L F 1982b Appl. Phys. Lett. 40 1034
Low T S and Stillman G E 1982c unpublished
Low T S and Stillman G E 1982d *GaAs and Related Compounds* 1981 (Inst. Phys. Conf. Ser. 63) pp 143-148
Low T S, Skromme B J, and Stillman G E, 1983 GaAs and Related Compounds 1982 this volume
Mattes Brenton L, Houng Yu-Min, and Pearson Gerald L 1975 J. Vac. Sci. Technol. 12 869
Morkoç Hadis and Eastman Lester F 1976 J. Cryst. Growth 36 109
Morkoç H, Eastman L F and Woodard D 1980 Thin Solid Films 71 245
Nanishi Yasushi 1978 Jpn. J. Appl. Phys. 17 1177
Ozeki M, Kitahara K, Nakai K, Shibatomi A, Dazai K, Okawa S, and Ryuzan O 1977 Jpn. J. Appl. Phys. 16 1617
Solomon R 1969 GaAs and Related Compounds 1968 (Inst. Phys. Conf. Ser. 7) pp 11-17
Stevenson D A, Mattes B L, and Dun H 1977 Tech. Rep. CMR-77-4, Stanford University, unpublished
Stradling R A 1981 private communication
Stillman G E, Wolfe C M, and Dimmock J O 1977 Semiconductors and Semimetals ed. R K Willardson and A C Beer (New York: Academic) 12 pp 169-290
Stoelenga H H M, Larsen D M, Walukiewicz W, and Bozler C O 1978 J. Phys. Chem. Solids 39, 873
Teramoto I 1972 J. Phys. Chem. Solids 33 2089
Wolfe C M, Stillman G E, and Korn D M 1977 GaAs and Related Compounds 1976 (Inst. Phys. Conf. Ser. 33b) pp 120-128
Zachauer, K-H 1973 GaAs and Related Compounds 1972 (Inst. Phys. Conf. Ser. 17) pp 3-10

Journal of Electronic Materials, Vol. 11, No. 6, 1982

A.6 AN ANALYTICAL EVALUATION OF GaAs GROWN WITH COMMERCIAL AND REPURIFIED TRIMETHYLGALLIUM*

K. L. Hess, P. D. Dapkus,* H. M. Manasevit,**
Microelectronic Research and Development Center
Rockwell International, Thousand Oaks, CA 91360

and

T. S. Low, B. J. Skromme, and G. E. Stillman
Department of Electrical Engineering
University of Illinois, Urbana, IL 61801

(Received May 17, 1982)

An analytical study of the impurities in trimethylgallium (TMGa) and subsequent correlation of the effect of these impurities on resulting GaAs films grown by metalorganic chemical vapor deposition (MOCVD) is presented. The effects of using fractional distillation techniques to improve the quality of TMGa and to help isolate and identify major source impurities in TMGa is detailed. Photothermal ionization data are presented which show the residual donor species present and their relative concentrations in the epitaxial layers. Correlations of the residual donor concentrations with TMGa preparation are made. It is demonstrated that high purity GaAs with $\mu_{77K} \approx 125{,}000$ $cm^2/V\text{-sec}$ can be grown by MOCVD using repurified trimethylgallium and arsine source materials.

Key words: metalorganic chemical vapor deposition, epitaxial growth, gallium arsenide, fractional distillation, photothermal ionization, photoluminescence.

* Work supported in part by the U.S. Naval Research Laboratory on Contract No. N00173-80-C-0066.
** Rockwell International/Microelectronics Research and Development Center, Anaheim, CA 92803.

Introduction

The metalorganic chemical vapor deposition (MOCVD) process has become an important III-V epitaxial growth technology for electronic and opto-electronic devices. Since the first demonstration of MOCVD for GaAs by Manasevit (1) in 1968, work has included efforts to improve the quality of the material and utilize it in state-of-the-art devices. Areas of major success have been solar cells (2,3), heterojunction lasers (4-8), quantum well heterostructures (9-12), and FET's (13,14).

Despite these successes, the purity of GaAs grown by MOCVD has been variable and an examination of residual impurity incorporation in GaAs grown by MOCVD was undertaken. The initial investigations, which have been previously reported (15) focused on the effect of growth parameters on the purity of GaAs grown by MOCVD using commercially available source materials. The investigation led to significantly improved high purity GaAs with 77K mobilities $\approx 87{,}000$ $cm^2/V\text{-}s$ from "selected" source materials and a procedure for comparing the different reactant materials. An investigation of the impurities in the metalorganic starting materials and the correlation of these impurities with the resulting GaAs film properties was lacking. This paper reports the results of such an investigation.

Sources of both TMGa and arsine (AsH_3) are known to contribute substantial amounts of electrically active impurities to GaAs and GaAlAs (16-19). By working with commercial vendors of AsH_3, significantly improved AsH_3/H_2 sources have been prepared. The state of affairs with TMGa is less well developed.

Based on our experience with TMGa, it was our belief that a carefully designed purification system combined with proper handling techniques would yield TMGa of the desired quality and reproducibility for use in routine growth of high purity GaAs ($N_D + N_A < 10^{15}$ cm^{-3}). Toward this goal, a fused quartz purification system was designed and built to purify metalorganic compounds. An investigation of appropriate techniques for distilling the TMGa, impurity analyses to assess the purity of the resulting TMGa, and correlation with the quality of the resulting MOCVD grown GaAs are reported here.

Experimental Procedures

Repurification Apparatus and Techniques

The purification of commercially available TMGa was performed in a specially designed fused quartz apparatus. A schematic diagram of the apparatus is shown in Figure 1. The major components of this apparatus include a high efficiency packed fractional distillation column, a multipurpose chemical vacuum line, and an argon gas purifier for delivering argon gas with purities in excess of 99.9999% (R. D. Mathis, Argon Gas Purifier). Argon served as the inert gas blanket under which the atmospheric pressure distillations could be performed.

The quartz distillation apparatus consisted of the following functional units: (1) distillation pot, (2) packed fractionation column, (3) automatic liquid dividing head, (3) product receiver and fraction cutter, and (4) metal alkyl collection receivers. A quartz/stainless steel inlet sidearm permitted gravity transfer of the reactive TMGa into the distillation pot directly from the vacuum line.

The fractionation of the TMGa source materials was performed in a three-foot long vacuum-jacketed and silvered column which operated adiabatically throughout its length. The internal column dimensions (12 mm I.D.) permitted efficient contacting of the rising TMGa vapors and returning

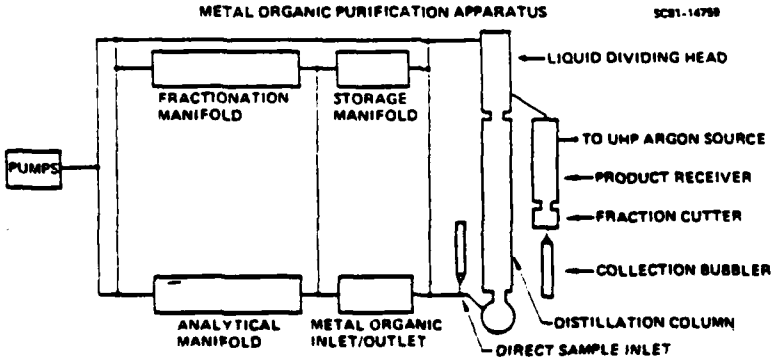

Fig. 1 Metalorganic purification apparatus.

reflux and tended to maximize the exchange between heat and material.

The column was packed with ~5100 quartz helices. These helices (4 mm O.D. × 3 mm I.D. × 1.5 mm thick), having a large surface area/volume ratio, were capable of equilibrating a large volume of vapor/liquid per unit time, because of the small liquid hold-up per individual helice, and the efficient throughput provided by the free space of the helice network. The automatic liquid dividing head was also vacuum jacketed and silvered to minimize heat loss during equilibration of the column and recovery of the product. A digital thermocouple assembly monitored the distillate temperature. The entire assembly was coupled to a timer controlled magnetic solenoid that maintained precise control of the reflux ratio during the repurification. The product receiver and fraction cutter were water-cooled. 316 SS electron beam welded source bubblers or high purity quartz bubblers served as receivers.

Atmospheric pressure distillation (argon blanket) was used exclusively in this study because of the high volatility of the TMGa source materials and high degree of impurity separation which could be achieved by this process. Prior to each distillation, the apparatus was evacuated (~10^{-6} Torr) for 24 hrs. The quartz surface was then passivated at room temperature with the vapor of TMGa. Commercially synthesized TMGa was then gravity transferred from the vacuum line into the distillation pot.

Three fractions were collected during each distillation. Selected fractions were analyzed by mass spectroscopy and by growth of GaAs. The column hold-up material and any high boiling contaminants which were concentrated in the still pot were pumped into a -196°C storage bulb on the vacuum line and later fractionated using low temperature/low pressure techniques. Samples of impurities isolated by this technique were subsequently analyzed by mass spectroscopy and/or emission spectroscopy, depending on the volatility of the material.

Characterization Studies

GaAs Transport Properties. The ultimate test for purity of the repurified TMGa was the quality of the GaAs

grown using it. Optimal conditions in the reactor used for these studies have been reported previously (20) and are summarized in Table I. Comparisons were made between the properties of films produced from TMGa prior to repurification and from selected fractions after distillation.

The GaAs samples grown in this study were characterized using van der Pauw geometry Hall effect measurements. These measurements were performed on rectangular samples by contacting them with indium dots around the periphery of the sample. The Hall effect was measured in an automated Hall apparatus utilizing a 5 kG magnetic field. Measurements at 77K were performed by immersing the sample in liquid nitrogen. Temperature dependent measurements (accurate to ±1°C) were made in the same automated apparatus by heating the sample immersed in the vapors from liquid nitrogen.

Donor and Acceptor Spectroscopy. Photothermal ionization spectroscopy (21) was used to identify the specific donor species present and measure their concentrations relative to the total donor concentration. The narrow linewidth and large amplitude of the 1s - 2p (m = -1) hydrogenic donor transition at high magnetic fields make it especially suitable for resolving the closely spaced peaks of the individual donor species. The 1s - 2p (m = -1) transition energies change substantially with changing magnetic field, so, to permit comparison of the peaks observed in a given

Table I. High Purity GaAs Grown by MOCVD With Repurified Trimethylgallium

MOCVD Growth Parameters

Parameter	APMOCVD	LPMOCVD
Reactor Pressure	760 torr	70 torr
Total Gas Flow	4 lpm	1 lpm
AsH_3/H_2 Flow	500 ccpm	500 ccpm
$H_2/(CH_3)_3Ga$ Flow	15 ccpm	10 ccpm
$(CH_3)_3Ga$ Source (°C)	0°C	-12°C
Growth Temperature	600°C	575-600°C
Growth Rate	0.166 μm/min	0.055 μm/min

sample with donor identifications in the literature, the spectrum of that sample is compared to the spectrum of a well-characterized reference sample, taken at precisely the same magnetic field. This is accomplished by operating the superconducting magnet in persistent mode while both spectra are recorded. The reference sample used in this work is an ultra pure $AsCl_3$-VPE GaAs sample grown by C. M. Wolfe at M.I.T. Lincoln Laboratory, which has a liquid nitrogen temperature mobility of $\mu_{77K} = 201{,}000$ cm^2/Vs and a carrier concentration of $n_{77} = 4.5 \times 10^{13}$ cm^{-3} (22). The three peaks present in the spectra of this sample, labeled X_1, X_2, and X_3 correspond to the three characteristic residual donors present in high purity GaAs grown by this technique (23,24). Since many of the early donor identification experiments were done using $AsCl_3$-VPE material, the energies of peaks corresponding to different donor species relative to the energies of X_1, X_2, and X_3 are fairly well known (23,24).

The photothermal ionization spectra presented here were recorded at 4.2K in a magnetic field of 65 kG. The rather well-established 1s - 2p (m = -1) donor transition energies at which spectral peaks are observed for this magnetic field, and the identification of these peaks with the associated donor species are shown in Table II. Some controversy exists concerning the identification of some of these peaks, particularly for the X_3 peak, which dominates the donor spectra of all the MOCVD GaAs samples measured, but most of the identifications are fairly well established. Through controlled doping experiments by various research groups, the X_3 peak has been associated with both C (23) and Ge donors (26,27,28), and it may be that both of these donor species contribute peaks at or near X_3. The photoluminescence data and mass spectrometric data presented here suggest that the dominant donor species producing the X_3 peak in these samples may be C and not Ge.

Photoluminescence measurements were made at temperatures from 1.8K to 20K, using 5145Å excitation light from an Ar^+ laser, in order to identify the residual acceptors present in MOCVD grown GaAs. Data were interpreted by comparison with the back-doping experiments of Ashen et al (29).

Table II. Energy of 1s-2p (m = -1) Transition (65 kG) for Various Donors in GaAs

Donor	Energy
Pb	35.0 cm^{-1}
X_1 = Si(1)	35.3 cm^{-1}
Se	35.42 cm^{-1}
Sn	35.50 cm^{-1}
X_2 = S(2)	35.90 cm^{-1}
C(3)	36.82 cm^{-1}
X_3 Ge(3)	36.7 cm^{-1}

(1) X_1 was originally thought to be a complex involving a Ga vacancy (23), but more recently has been identified as Si by Ozeki et al (26) and Low et al (34).
(2) X_2 was originally thought to be Si (23) but more recently has been identified as S by Ozeki et al (26) and Low et al (35).
(3) There is some ambiguity in the identification of C and Ge donors. Recent work (26,27,28) identified the X_3 peak of Wolfe et al (23) as due to Ge.

Mass and Emission Spectroscopy (Qualitative). The mass spectra of the TMGa source materials and isolated contaminants were recorded on a low resolution Hitachi-Perkin Elmer RMU-6D magnetic sector mass spectrometer. Metal and non-metal micro-impurities were identified by emission spectroscopy with an Applied Research dc arc grating spectrometer. Both of these measurements were performed at a commercial testing laboratory.

Experimental Results

Evaluation of As-Received TMGa Source Materials

Two sources of TMGa of particular interest from different vendors were analyzed by growth of GaAs films and by mass spectroscopy prior to repurification. The electrical transport properties of undoped GaAs films grown with these two sources are summarized in Table III. The GaAs grown with the TMGa-A source is low purity with μ_{77K} = 30,000

Table III. Electrical Properties of GaAs Grown by MOCVD With As-Received Trimethylgallium Source Materials

Property	Source-A		Source-B	
Mobility at 77K[a]	29,800	32,500	87,500	89,400[b]
$(N_D - N_A)$ at 77K	2.9×10^{15}	3.4×10^{15}	2.4×10^{15}	3.9×10^{15}
$AsH_3/(CH_3)_3Ga$	~40/1	~103/1	~40/1	~103/1
Technique	APMOCVD	LPMOCVD	APMOCVD	LPMOCVD

[a] Film thickness for all samples ~20 μm.
[b] μ(77°K) = 108,000 cm^2/V-sec at growth temperature ~575°C.

cm^2/V-sec and a relatively high residual doping density ($N_D - N_A \sim 3 \times 10^{15}$ cm^{-3}).

In comparison, the GaAs films grown with the TMGa-B source were high quality with $\mu_{77K} \approx 90,000$ cm^2/V-sec and a residual doping density ($N_D - N_A \sim 3 \times 10^{15}$ cm^{-3}) which is approximately an order of magnitude lower than that obtained from the TMGa-A source.

Both TMGa samples were first analyzed for major contaminants by low resolution mass spectroscopy. Both source materials exhibited all four cracking patterns characteristic of TMGa with the correct isotopic ratio distribution for the two stable gallium isotopes (Ga^{71} 40%; Ga^{69}, 60%). These results indicate the absence of any associated gallium species; i.e., parent trimer ions $[Ga(CH_3)_3]_3^+$. There were no molecular or fragment ions characteristic of any other Group III metal alkyl contaminants.

Methyl iodide was identified to be the major contaminant in the TMGa-A source material. Although the synthetic history of the TMGa-A batch is unknown, it is possible to rationalize the presence of the CH_3I on the basis of commonly used syntheses of TMGa. Three routes are summarized in Table IV. All three methods involve CH_3I in quantities which are greater than stoichiometric. Since the boiling point of CH_3I is ~42°C, it is quite possible that an inefficient fractional distillation would result in a poor separation of the methyl iodide contaminant from the trimethylgallium (BP ~55°C). The origin of low molecular weight

Table IV. Possible Synthetic Routes to TMGa-A Source Material

- Alkylation of magnesium/gallium alloy

$$6CH_3I + (Mg_3Ga_2)\ \text{Alloy} \xrightarrow{\ddot{O}} 3MgI_2 \downarrow + 2(CH_3)_3Ga$$

- Grignard alkylation of gallium tri-iodide

$$CH_3I + Mg \xrightarrow[I_2]{\ddot{O}} CH_3MgI\ \text{(ether complex)}$$

$$3CH_3MgI\ \text{(ether complex)} + GaI_3 \xrightarrow{\ddot{O}} 3MgI_2 \downarrow + (CH_3)_3Ga$$

- Redox alkylation of gallium mono-iodide

$$2CH_3Li + GaI + CH_3I \xrightarrow{\ddot{O}} (CH_3)_3Ga + 2LiI \downarrow$$

hydrocarbons which were detected in the as-received TMGa-A source material is unknown. It is possible that the apparatus used to synthesize the TMGa and/or contain the final product for shipment was degreased with hydrocarbon solvents. Inefficient thermal vacuum outgassing of this equipment could certainly lead to such contamination. Moisture on the surface of the synthesis apparatus and/or containment bubblers could easily account for the methane found. A trace amount of CH_3OH was found during the mass spectrometric analysis of the TMGa-B source material, but could not be present as a contaminant owing to its immediate reaction with TMGa. It most likely is generated by surface reactions of $CH_3^{\bullet}$ in the mass spectrometer.

Repurification of TMGa-A Samples

To distill sample TMGa-A, the quartz still pot was charged with ~110 grams of TMGa-A. After equilibration for several hours at ~55.47°C, three major fractions of color-

less TMGa liquid were collected over a period of ~240 min; the first, ~34 grams over a temperature range of 55.47°C-55.64°C; the second, ~40 grams over a temperature range of 55.67°C-56.32°C; and the third, over an interval of 56.37°C-57.80°C. Vacuum distillation of the residuals in the column and still pot left a yellow-brown viscous oily residue at the bottom of the still pot. Pumping on this oil for ~2 days through a -50°C bath into a -196°C trap in series condensed an oil of low volatility at -50°C, and left a solid brown-yellow residue in the pot.

The second fraction of repurified TMGa-A was characterized by MOCVD crystal growth and mass spectroscopy. The involatile pot residue was analyzed by mass spectroscopy and emission spectroscopy.

To distill sample TMGa-B, the still pot was charged with ~83 grams of TMGa-B. The liquid was canary yellow in color. After equilibrating the apparatus for several hours at ~55.61°C, fractionation was begun. Three major fractions of colorless TMGa liquid were collected over a period of 405 min; the first, ~28 grams over a temperature range of 55.61°C-55.64°C; the second, ~40 grams from 55.64-55.68°C; and a third, ~10 grams over an interval of 55.68°C-55.71°C. Vacuum distillation of the residuals in the column and still pot left a (white/yellow) solid. Pumping on this solid for ~2 days through a -50°C bath into a -196°C trap in series did not change the appearance of the pot residue but condensed a colorless material of low volatility at -50°C.

The second fraction of repurified TMGa-B was characterized by MOCVD crystal growth and mass spectroscopy. The involatile pot residue was examined by emission spectroscopy. The -50°C bath material was analyzed by emission spectroscopy.

Characterization of Repurified TMGa-A

The transport properties of undoped GaAs films grown with the repurified TMGa sources are summarized in Table V. The data indicate that repurification of the TMGa-A via one distillation improved the 77K mobility of the films by a factor of about three and reduced the donor concentration by one order of magnitude.

Table V. Electrical Properties of GaAs Grown by MOCVD With Purified Trimethylgallium Source Materials

Property	Source A		Source-B	
Mobility at 77K[a]	76,200	65,000	68,400	106,000
$(N_D - N_A)$ at 77K	3.8×10^{14}	3.9×10^{14}	5.5×10^{13}	2.1×10^{14}
$AsH_3/(CH_3)_3Ga$	~40/1	~103/1	~40/1	~103/1
Technique	APMOCVD	LPMOCVD	APMOCVD	LPMOCVD

[a] film thickness for all samples ~20 um

The repurification of TMGa-B via one distillation did not seem to introduce additional major contaminants into the material. The electrical properties of the films grown were equivalent or slightly better than those previously obtained with the same source. It is possible that the background impurity concentration is being limited by impurities in the arsine at this purity level, and no conclusive statement concerning a possible improvement of source TMGa-B by redistillation is possible.

The photothermal ionization spectra for films grown with TMGa-A and TMGa-B sources, both before and after repurification of the TMGa, are shown in Figures 2 and 3. The relative concentrations of residual donors in these samples were determined from the relative peak amplitudes in the spectra. Absolute concentrations could then be calculated using the 77K Hall effect data and the analysis of mobility data presented by Wolfe et al (30). Donor concentrations determined in this way for the samples of Figures 2 and 3 are shown in Table VI.

In the spectrum of sample 1, grown with the TMGa-A source before repurification, the donor peaks are severely broadened because of the large impurity concentration and the resulting impurity interactions (31). The residual donors in this spectrum include the usual X_3, and probably Sn at lower energy. The purity of sample 2, grown with the same TMGa-A source after repurification is considerably improved, as indicated by the 77K Hall effect data in Table VI. The improvement in purity is also apparent in the

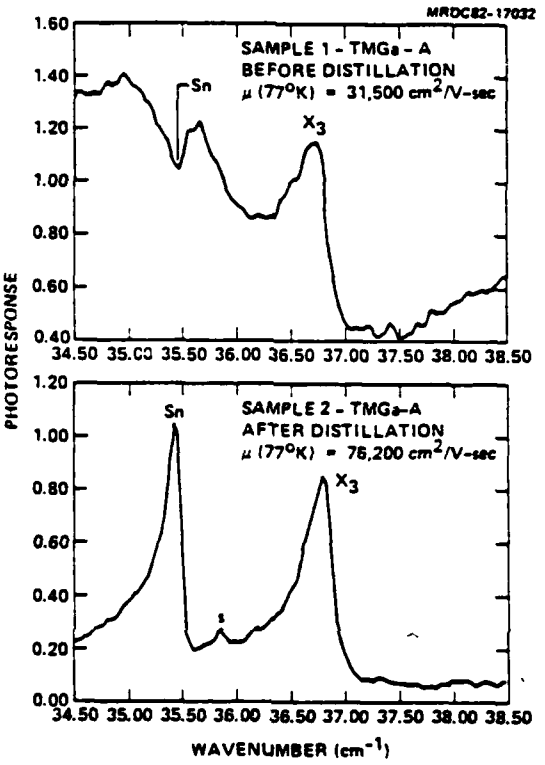

Fig. 2 Photoconductivity spectra of GaAs grown with TMGa-A before and after distillation.

photothermal ionization spectrum of Figure 2, in which peaks due to the usual residual X_3 as well as Sn and a much smaller concentration of S are clearly resolved.

An improvement in purity of the GaAs grown with the TMGa-B source after repurification is observed in the spectra of Figure 3. In both samples 3 and 4, the higher concentration X_3 donors dominate the spectra. The relative concentrations of both Si, and also S, are lower in sample 4, grown with repurified TMGa-B. In sample 4, traces of Pb, and Sn, are also observed, at concentrations which would have been below the detection limit in the less pure sample 3, grown with unpurified TMGa-B.

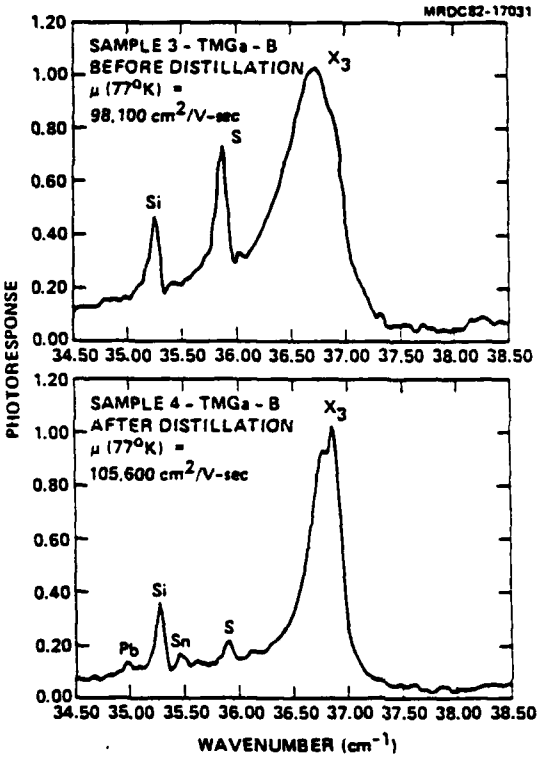

Fig. 3 Photoconductivity spectra of GaAs grown with TMGa-B before and after distillation.

Table VI. Impurity Concentrations × 10^{14} cm^{-3}

Sample	μ_{77}(cm^2/Vs)	N_D(Pb)	N_D(Si)	N_D(Sn)	N_D(S)	N_D(X_3)
1	31,500	*	*	*	*	*
2	76,200	—	—	4.0	0.9	2.9
3	98,100	—	1.9	—	2.0	2.4
4	105,600	0.41	0.97	0.46	0.55	2.25
5	87,000	—	—	—	0.72	5.8

*Spectrum was not suitable for determination of relative donor concentrations.

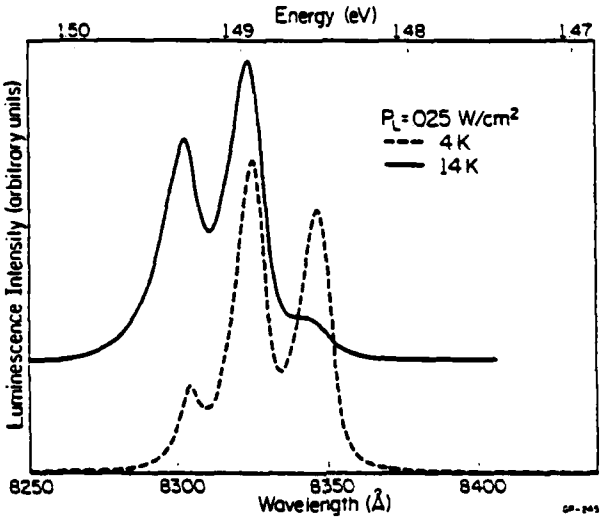

Fig. 4 Photoluminescence spectra for high purity MOCVD sample.

Photoluminescence spectra taken at two different temperatures, for a high purity MOCVD sample grown with TMGa-B before distillation (sample 5 in Table VI) are shown in Figure 4. The 1.4855 eV peak is due to donor to Zn acceptor pair (P) transitions, the 1.4930 eV peak results from conduction band to C acceptor (B-A) recombination, and the 1.4893 peak is the overlap of the (P) peak due to C and the (B-A) peak due to Zn. The 1.4855 eV peak in MOCVD GaAs was tentatively ascribed to Si (B-A) transitions in preliminary 4K photoluminescence measurements, the observed decrease in amplitude of this peak with increasing temperature (see Figure 4) is characteristic of (P) and not (B-A) transitions (29), and the absence of any Si (P) peak at low temperatures indicate that Si acceptors are absent in this sample. Strong, sharp doublet lines at 1.49373 eV, 1.49391 eV, and 1.49026 eV, 1.49046 eV were also observed at higher excitation levels at 2K corresponding to the two-hole transitions of excitons bound to C and Zn acceptors, respectively (29). No two-hole transition doublets were observed for Si acceptor bound excitors, confirming the absence of Si acceptors. The 1.4888 eV exciton line due to deep O donors, which is usually observed in $AsCl_3$ VPE material (29), was also absent from the spectra of the MOCVD samples.

Spectra on several other MOCVD samples showed quite similar spectra, with C and Zn acceptors present at varying relative levels. The spectrum of sample 2 in Table VI, the lowest purity sample measured, showed only C acceptors and Zn was undetectable.

The absence of Ge acceptors in the photoluminescence data for this MOCVD GaAs and the clear presence of C acceptors, suggest that the dominant donor species producing the X_3 peak in the photothermal ionization spectra may be C and not Ge. This conclusion is also supported by the absence of Ge in any of the mass spectrometric data for the source material and pot residues presented here. It could be argued, however, that the conditions under which the MOCVD growth occurs (e.g., the large As/Ga ratio and rather low growth temperatures) might preferentially incorporate amphoteric impurities like Ge as donors rather than acceptors (32,33), and so Ge donors could account for the X_3 photothermal ionization peak and still be absent in the photoluminescence spectra. A more detailed correlation of such spectra with the parameters of MOCVD growth is required in order to understand the relative incorporation of these amphoterics.

Spectrometric analyses of the pot residues are presented in Table VII. These data indicate that tin is a significant impurity in the particular batch of TMGa-A evaluated and provides confirmation of the photothermal ionization data. The very high silicon content found in the TMGa-B pot residue suggests that the distillation process concentrated this particular contaminant in the pot and is partly responsible for the apparent significant reduction of silicon in GaAs films grown with repurified TMGa-B observed in the photothermal ionization spectra.

The presence of arsenic in the TMGa-B residue is not difficult to understand if one considers the fact that the source material and bubbler had been used for ~24 months in the GaAs MOCVD growth apparatus prior to the repurification experiment. The exit of the bubbler was directly interfaced with the mixing manifold of the reactor. Since very low flows of H_2 passed through the bubbler (10-15 ccpm), it may be that some back diffusion of AsH_3 into the bubbler took place with subsequent formation of a less volatile addition complex. Such material would tend to concentrate in the

Table VII. Spectrometric Analyses of Pot Residues

TMGa-A Repurification			TMGa-B Repurification	
Mass Spectrometric (Qualitative)	Emission Spectrometric (Weight %)		Emission Spectrometric (Weight %)	
CH_3I	Ga	74	Ga	47
	Sn	0.011	Sn	<0.006 (ND)
$(CH_3)_3Ga$	B	<0.004 (ND)	As	2.6
	Si	0.035	Si	15
$R_1-\ddot{O}-R_2$	Mg	0.0029	Mg	0.0025
	Fe	0.0038	Fe	0.46
	Co	0.00056	Al	0.20
	Ag	<0.0001 (ND)	Cu	0.0072
	Ni	<0.001 (ND)	Ag	<0.003 (ND)
	Ca	0.0024	Ni	0.069
	Cr	<0.0002 (ND)	Ca	0.0036
	Al	0.0038	Cr	0.024
			Ti	0.0062
			Mn	0.11

(ND) This element was not detected; the limit of detection for this analysis was less than the amount stated in the table above.

Table VII

still pot during the low temperature distillation and eventually manifest itself as one of the nonvolatile components of the residue. The lack of any such arsenic in the TMGa-A residue may be due to the limited number of MOCVD experiments performed with that particular bubbler prior to distillation of the TMGa.

The presence of an ether linkage ($R_1-\ddot{O}-R_2$) and CH_3I in the TMGa-A residue lends further support to the synthetic history of TMGa-A proposed in Table IV. The presence of significant amounts of Mn, Fe, Ni, and Cr in the TMGa-B residue suggests that these elements may derive from the stainless steel bubbler used to contain the TMGa throughout the 24-month period prior to repurification. These particular elements are major components of series 300 AISI austenitic stainless steels. The absence of Mn, Ni, and Cr

in the TMGa-A residue and presence of only ~0.0038 weight percent Fe lends credence to the speculation that leaching effects may be realized over extended time durations. The TMGa-A material was exposed to the stainless steel container environment for only a short period of time before repurification.

Qualitative mass spectrometric analyses were performed on the repurified TMGa source materials. The data indicate that after one fractional distillation, only trace amounts of CH_3I remained in the TMGa-A source material. Methane and other low molecular weight hydrocarbons were still present in about the same relative concentration levels as originally found in the TMGa-A source material. This suggests that the number of plates required to separate these carbon contaminants from TMGa is greater than that characteristic of the packed column used in this study. It seems likely that the use of a spinning band column would help correct this separation problem because of an increase in the diffusion coefficient of the vapor due to the turbulence created by rotation of the band.

Unidentified m/e-104 and m/e-73 peaks were detected in the TMGa-B source material after distillation. These peaks were originally thought to come from the compound trimethylsilylmethyl ether, $(CH_3)_3SiOCH_3$. However, closer examination of the mass spectrum indicated that the characteristic fragmentation pattern of the trimethylsilyl group, $(CH_3)_3Si$, was absent. This group breaks to give a large peak at m/e-58 due to loss of one of the methyl groups from the highly-branched silicon atom, and this is always the largest peak in this heavy ion group and would have been the base peak in the spectrum. The mass spectrum of such a silicone contaminant would also be expected to give very large rearrangement peaks at m/e-34, m/e-45, m/e-59 with formulae $(SiH_3)^+$, $(SiCH_3H_2)^+$, and $[Si(CH_3)_2H]^+$ which are formed from the $Si(CH_3)_3$ end of the molecule by elimination of methyl groups with replacement of a single hydrogen atom for every methyl lost. A series of peaks would also have been expected at m/e-47, m/e-61, and m/e-75 due to the addition of the oxygen atom to the above ions. The characteristic isotope abundances for the heavy isotopes of silicon (Si^{28}, 92.2%; Si^{29}, 4.7%; Si^{30}, 3.1%) were also absent. The absence of any detectable volatile silicon compounds in the repurified TMGa materials seems to suggest that any contam-

inating reactions between $(CH_3)_3Ga$ and the SiO_2 network are minimal and that high purity quartz is a suitable agent in which repurification and possibly storage of TMGa can be done.

Mass spectrometric analysis of the TMGa-A column hold-up material (trapped at -50°C) showed the presence of an ether R_1-O-R_2 in addition to undistilled TMGa-A. A corresponding analysis of the TMGa-B column hold-up material (-50°C bath) indicated that nitropropane was present as a contaminant. Nitropropane is a commonly used industrial solvent and could have been used to clean the original TMGa-B source bubbler prior to filling by the vendor. Its boiling point of ~132°C dictates its concentration in the column hold-up and subsequent isolation during vacuum distillation at -50°C.

An emission analysis was also performed on the TMGa-B -50°C trap material, and the results are summarized in Table VIII. The large decrease in the amount of silicon found in the -50°C trap residue compared to that detected in the pot residue indicates that the silicon contaminant is basically nonvolatile. As would be expected, the concentration of major transition metal micro-impurities Fe, Ni, Cr, and Mn is quite small (as compared to that found in the TMGa-B residue) presumably due to the absence of delocalized electron ligands which would impart more volatility to these metal contaminants.

Emission spectrographic results for TMGa-A and TMGa-B vapors which were hydrolyzed/oxidized at the exit to the distillation apparatus during the repurification process established the presence of metal micro-impurities (ppm range) in the gas phase during the distillation of TMGa source materials. Quantitative elimination of these impurities would require very sophisticated techniques, such as those used during the laser repurification of silane.

Characterization of Arsine Source Material

A sample of arsine/hydrogen used during this study was analyzed by mass spectroscopy and gas chromatography for gas composition. The gas composition agreed with the vendor's analysis. Emission spectrometric analysis of the arsenic powder resulting from pyrolysis of the arsine in a quartz

Table VIII. TMGa-B -50°C Bath Material Emission Analysis

Emission Spectrometric (weight percent)	
Ga	19
Si	0.31
Al	0.84
As	Trace <0.03
B	0.0022
Mg	0.0089
Mn	0.00067
Fe	0.036
Cr	0.00025
Ni	0.0085
Sn	Trace <0.001
Cu	0.00098
Ag	0.00041
Ti	0.00062
Ca	0.068

chamber at 600°C showed arsenic to be the major constituent. Germanium, tin and zinc were not detected. Trace copper (<0.00006 wt%) was detected.

Evaluation of Distilled TMGa-B with Specially Prepared Arsine/Hydrogen Source Material

Arrangements were made with the vendor of AsH_3-in-H_2 materials to prepare three different cylinders of AsH_3/H_2 from the same AsH_3 source, the cylinders to represent a head, middle, and tail fraction of the pure AsH_3. Analysis was then made of the light organic compounds of each AsH_3 fraction in its cylinder before mixing with UHP-H_2 and subsequent analysis of the mixture. The results are summarized in Table IX. The "inferiority" of the head fraction was demonstrated when undoped films were grown with 77K mobilities of only $\mu_{77K} = 50,000$ $cm^2/V\text{-}s$ with a net carrier concentration of $(N_D - N_A) = 1.8 \times 10^{15} m^{-3}$. The middle fraction led to films with $(N_D - N_A) = 1.5\text{-}3.5 \times 10^{14}$ cm^{-3} and $\mu_{77K} = 70,000$ $cm^2/V\text{-}s$.

The electrical transport properties of undoped GaAs films grown using the tail fraction of AsH_3/H_2 are summarized in Table X. The 77K mobilities of ~125,000 cm^2/V-sec attest to the high quality AsH_3-in-H_2 in this tail fraction and indicate the value of fractionating the AsH_3 as well as the TMGa when extremely high purity layers are needed for specific device fabrication.

Table IX. Compositional Analyses of Special Prepared AsH_3/H_2 Mixtures

Components	Concentration Head	Middle	Tail
AsH_3 (99.9995%)	10.09%	10.0%	9.98%
N_2	<1 ppm	<1 ppm	<1 ppm
O_2	<1 ppm	<1 ppm	<1 ppm
Ar	<1 ppm	<1 ppm	<1 ppm
CH_4	<1 ppm	<1 ppm	<1 ppm
CO	<1 ppm	<1 ppm	<1 ppm
CO_2	<1 ppm	<1 ppm	<1 ppm
H_2 (99.9999%)	Balance	Balance	Balance
Light Organic Analysis[a]			
CH_4	0.06 ppm	0.05 ppm	ND <0.003 ppm
C_2H_4 and/or C_2H_2	0.06 ppm	0.02 ppm	0.01 ppm
C_2H_6	0.02 ppm	0.02 ppm	0.01 ppm
C_4's	ND <0.04 ppm	ND <0.04 ppm	0.04 ppm
C_5's	ND <0.04 ppm	ND <0.04 ppm	0.04 ppm

[a] Organic analysis of the pure AsH_3 after its transfer to the individual mixture cylinders and before addition of the UHP-H_2.

Table X. High Purity GaAs Grown by MOCVD with Repurified TMGa-B and Tail Fraction AsH_3

Property	LPMOCVD	APMOCVD
Mobility at 77K	125,000	104,000
$(N_D - N_A)$ at 77K	4.8×10^{13}	1.1×10^{11}
$AsH_3/(CH_3)_3Ga$	103/1	40/1

Conclusions

We have demonstrated that controlled fractional distillation with a packed column is an effective technique for improving the quality of commercially available trimethylgallium source materials. However, this technique does not separate low molecular weight aliphatic hydrocarbons or gas phase metal/nonmetal micro-impurities from trimethylgallium. Fractional distillation has helped to isolate and identify major source impurities in these source materials.

The photothermal ionization measurements show that, in the purest MOCVD samples, a single impur'ty species dominates the residual donor concentration. Together with the photoluminescence measurements and mass spectrometric data, these measurements suggest that this donor species is C and not Ge, but this assignment should be regarded as tentative. The residual shallow acceptors present, as determined by photoluminescence, were C and usually Zn in varying relative concentrations. Finally, high purity GaAs with μ_{77K} = 125,000 $cm^2/V\text{-}s$ can be realized using repurified TMGa and AsH_3 source materials.

References

1. H. M. Manasevit and W. I. Simpson, J. Electrochem. Soc. 116 1725 (1969).
2. R. D. Dupuis, P. D. Dapkus, R. D. Yingling and L. A. Moudy, Appl. Phys. Lett. 31, 201 (1977).
3. N. J. Nelson, K. K. Johnson, R. L. Moon, H. A. Vander Plas and L. W. James, Appl. Phys. Lett. 33, 26 (1978).
4. R. D. Dupuis and P. D. Dapkus, Appl. Phys. Lett. 31, 466 (1977).
5. R. D. Dupuis and P. D. Dapkus, Appl. Phys. Lett. 32, 437 (1978).
6. E. J. Thrush and J. E. A. Whiteaway, in: Proc. 8th Intern. Symp on GaAs and Related Compounds, Vienna, 1980. Inst. Phys. Conf. Ser. 56 (Inst. Phys., London, 1981), p. 337.
7. R. D. Dupuis, Appl. Phys. Lett. 35, 311 (1979).
8. R. D. Dupuis and P. D. Dapkus, Appl. Phys. Lett. 32, 473 (1978).
9. R. D. Dupuis, P. D. Dapkus, N. Holonyak, Jr., E. A. Rezek and R. Chin, Appl. Phys. Lett. 33, 596 (1978).

10. R. D. Dupuis, P. D. Dapkus, R. M. Kolbas and N. Holonyak, Jr., Solid State Commun. 27, 531 (1978).
11. J. J. Coleman and P. D. Dapkus, Appl. Phys. Lett. 37, 15 (1980).
12. R. D. Dupuis, P. D. Dapkus, N. Holonyak, Jr., E. A. Rezek, and P. Chin, Appl. Phys. Lett. 32, 295 (1978).
13. T. Shino, S. Yanagauki, Y. Yamada, K. Arai, K. Kamei, T. Chigira, and T. Nakanisi, Electron. Lett. 17, 738 (1981).
14. K. Kamei, H. Kawasaki, T. Chigira, T. Nakanisi, K. Kawabuchi, and M. Yoshimi, Electron. Lett. 17, 450 (1981).
15. H. M. Manasevit, P. D. Dapkus, K. L. Hess, and J. J. Yang, 22nd Annual Electron. Mater. Conf., Ithaca, N.Y., 1980.
16. Y. Seki, K. Tanno, K. Iida, and E. Ichiki, J. Electrochem. Soc. 122, 1108 (1975).
17. T. Nakanisi, T. Udagawa, A. Tanaka, and K. Kamei, J. Crystal Growth 55, 255 (1981).
18. G. B. Stringfellow and G. Hom, Appl. Phys. Lett. 34, 794 (1981).
19. G. B. Stringfellow and H. T. Hall, Jr., J. Electron. Mater. 8, 201 (1979).
20. P. D. Dapkus, H. M. Manasevit, K. L. Hess, T. S. Low, and G. E. Stillman, J. Crystal Growth 55, 10 (1981).
21. G. E. Stillman and C. M. Wolfe, in Semiconductors and Semimetals, Vol. 12 edited by R. K. Willardson and A. C. Beer, (Academic Press 1977), pp. 169-290.
22. C. M. wolfe, private communication, 1979.
23. C. M. Wolfe, G. E. Stillman and D. M. Korn, in: Proc. Symp. on GaAs and Related Compounds, St. Louis, 1976, (Inst. Phys., London, 1977) p. 120-128.
24. T. S. Low, G. E. Stillman, C. M. Wolfe, Proc. Sym. GaAs and Related Compounds, Oiso, 1981 (to be published).
25. R. A. Cooke, R. A. Hoult, R. F. Kirkman, R. A. Stradling, J. Phys. D: Appl. Phys. vol. 11, 945 (1978).
26. M. Ozeki, K. Kitahara, K. Nakai, A. Shibatomi, K. Dazai, S. Okawa and O. Ryuzan, Japan, J. App. Phys. 16, 1617 (1977).
27. H. H. M. Stoelenga, D. M. Larsen, W. Walukiewcz and C. O. Bozler, J. Phys. Chem. Solids, 39, 873 (1978).
28. M. N. Asfar, K. J. Button, G. L. McCoy, Proc. Sym. GaAs and Related Compounds, 1980 (Inst. of Physics, London) pp. 547-555.

29. D. J. Ashen, P. J. Dean, D. T. J. Hurle, J. O. Mullin, A. M. White, and P. D. Greene, J. Phys. Chem. Solids, 36, 1041 (1975).
30. C. M. Wolfe, G. E. Stillman, and J. O. Dimmock, J. Appl. Phys. 41, 504 (1970).
31. D. M. Larsen, Phys. Rev. B, 13, 1681 (1976).
32. Y. G. Chai, R. Chow, and C. E. C. Wood, Appl. Phys. Lett. 39, 800 (1981).
33. I. Teramoto, J. Phys. Chem. Solids, 33, 2089 (1972).
34. T. S. Low, G. E. Stillman, D. M. Collins, C. M. Wolfe, S. Tiwari and L. F. Easton, Appl. Phys. Lett, 1 April 1982 (to be published).
35. T. S. Low, G. E. Stillman (unpublished).

B. REDISTRIBUTION OF IMPURITIES AND DEFECTS

Journal of Electronic Materials, Vol. 11, No. 3, 1982

B.1 IMPURITY REDISTRIBUTION DURING EPITAXIAL GROWTH*

H. Rohdin, M.W. Muller and C.M. Wolfe
Department of Electrical Engineering
Washington University
St. Louis, MO 63130

(Received July 13, 1981)

The distribution of impurities incorporated in epitaxial layers during their growth is determined by diffusion due to concentration gradients and by drift in the built-in electric field. This problem has been previously treated in the approximation that the impurities reach their equilibrium distribution during growth. We have extended this calculation to treat impurity drift and diffusion under non-equilibrium conditions, a situation much more characteristic of most realistic growth conditions. In the new calculation, the solution of the Shockley-Poisson problem is exact and the boundary condition at the growth interface is an approximation based on the electrostatics of surface states. The new calculation also permits consideration of outdiffusion from the substrate, a phenomenon of technological significance. It is also capable of modeling variations of source impurity concentration and growth rate during epitaxial growth. Calculations modeling n-type GaAs epitaxy of practical interest are presented.

Key words: impurity incorporation, impurity redistribution, epitaxial growth, Shockley-Poisson equation, GaAs.

Introduction

The incorporation of impurities in epitaxially grown layers of semiconductors and their subsequent redistribution often leads to impurity and carrier density profiles that are unforeseen and that may be unfavorable for certain applications. Examples are: the formation of high resistance or inverted polarity layers in Gunn devices and the occurrence of high conductivity layers close to the SI-substrate in FET's and IC's.

A model has been proposed by Wolfe and Nichols (1,2) to account for some of these effects. In this model the impurities redistribute by diffusion in concentration gradients, drift in the built-in electric field due to surface states and the doping discontinuity at the layer-substrate interface, and finally due to the growth itself.

In order to model these processes analytically, it was necessary to make several restrictive assumptions, some of which were known to be unrealistic. In particular, it was assumed that the impurity distributions were stationary, that no impurity transport crossed the substrate-epitaxial layer interface, and calculation was restricted to epitaxial layer impurity concentrations so small as not to affect the interfacial electric fields. Therefore, although insight could be gained, especially into the usually neglected effect of the field, no quantitative conclusions could be drawn. In the present work we improve the model, renouncing the less realistic assumptions and providing for the simulation of a greater variety of growth conditions.

New Dynamical Model

With typical ionic diffusion constants and mobilities, and with epitaxial growth rates of technological importance, the impurity distribution does not reach a steady state during epitaxy. Transport of impurities across the epitaxial layer-substrate interface can be an important, even dominant feature of impurity redistribution. If the doping of the epitaxial layer exceeds the intrinsic carrier concentration, redistribution affects the field. These points are accommodated in the new model. Moreover,

although the specific simulations we have carried out so far assume homogeneous initial doping and uniform growth rate, the model is designed to accommodate arbitrary non-uniformities in both space and time.

Assumptions of the Model

1. The material is homogeneous (homoepitaxy).

2. The material is nondegenerate and the electrons and holes are in thermal equilibrium. This implies that the electron and hole concentrations (n and p respectively) satisfy

$$np = n_i^2 \tag{1}$$

where n_i is the intrinsic carrier concentration, and from the absence of carrier current, that the electron concentration and electric field E are related by

$$E = -\frac{kT}{q}\frac{d}{dx}\ln n \tag{2}$$

3. The substrate is semi-infinite, and the potential and field deep in the substrate go to zero.

4. The growth surface is characterized by a fixed surface state concentration. These states are always fully ionized and the field at the surface (x = 0) is constant and determined by the surface charge density, σ_s,

$$\varepsilon E(0,t) = \sigma_s \tag{3}$$

where ε is the total dielectric constant.

5. The ambient phase is ideally stirred; there is no diffusive impurity flow.

6. There are no temperature gradients.

7. All the impurities are fully ionized. This means that the total doping is

$$C = \sum_k z_k N_k \tag{4}$$

where N_k is the concentration of the k^{th} impurity and z_k the number of elementary charges it carries. We have

$$z_k = \begin{cases} +1 \text{ for a simple donor} \\ \\ -1 \text{ for a simple donor} \end{cases}$$

8. The impurities diffuse by a simple non-reactive mechanism. This implies that the flow J_k of the k^{th} impurity, is

$$J_k = - D_k \frac{\partial N_k}{\partial x} + \mu_k E N_k \qquad (5)$$

where the ionic mobility μ_k for the k^{th} impurity is given by the Einstein relation

$$\mu_k = B_k \frac{z_k q}{kT} D_k \qquad (6)$$

B_k is a numerical factor which depends on the diffusion mechanism (3, pp. 92-99):

$$B_k = \begin{cases} 1.27 \text{ for a vacancy mechanism} \\ \\ 1.0 \text{ for interstitial diffusion} \end{cases}$$

The continuity equation for the k^{th} impurity is

$$\frac{\partial N_k}{\partial t} = - \frac{\partial J_k}{\partial x} \qquad (7)$$

without generation or recombination terms.

9. The surface conductance which determines the outdiffusion from the growth surface and has the dimensions of velocity (4), is much smaller than the growth velocity. The implication of this assumption will be discussed below, in connection with the surface continuity

condition of the impurity fluxes. It implies that a hypothetical distribution coefficient, k_{eff}, defined in the absence of surface fields and concentration gradients would be equal to unity (5, p. 9).

10. The high-temperature impurity distribution is frozen in upon cooling.

Critique of the Assumptions

For some of the assumptions the validity is determined by how the growth situation is set up; for others by what types of impurities are used. Most electronically useful materials are nondegenerate especially at growth temperatures. Also, many impurities are fully ionized, even at room temperature. During growth this is true for an even larger class of impurities. If the chemistry of any reactive diffusion mechanism present were well understood, the model could be extended to include this but we have not attempted such an extension here.

The assumption of a constant surface field is an approximation. In principle one should fix neither the potential nor the field at the surface, but instead one should use a self-consistent solution taking into account the energy dependence of the surface state density, a quantity about which little is known at growth temperature. We shall see below that for common growth conditions the choice of boundary condition made here is not critical.

There is very little information on the surface conductance of impurities in GaAs. It is known to be very small for Sb diffusing from Ge (4), and a tentative analysis of recent data on the diffusion of Cr from GaAs (6) yields a value of ≈1μm/h, consistent with our assumption.

Whether the last assumption is valid or not depends on the temperature dependence of the diffusion coefficients, but in most instances the combination of temperature dependence and rapid cooling rate will make this a very good approximation.

In summary, the assumptions made here are not very restrictive, and the model should be useful to simulate

a wide variety of growth processes. It is to be understood, of course, that we model only planar growth. Lateral growth and edge effects are excluded from consideration.

Governing Equations

We make the following normalizations:

Position x expressed in terms of the intrinsic Debye length L_{Di}

$$L_{Di} = \sqrt{\frac{\varepsilon kT}{q^2 n_i}}$$

Potential ψ expressed in terms of

$$\psi_0 = \frac{kT}{q}$$

Electric field E expressed in terms of

$$E_0 = \frac{\psi_0}{L_{Di}}$$

Concentrations n, p, N_k, C expressed in terms of the intrinsic carrier concentration n_i.

Time t expressed in some convenient unit t_0.

Diffusion constants D_k expressed in terms of

$$D_0 = \frac{L_{Di}^2}{t_0}$$

Growth velocity v expressed in terms of

$$v_0 = \frac{D_0}{L_{Di}}$$

Impurity flow J_k expressed in terms of

$$J_0 = n_i v_0$$

The Electric Field Problem

The electrostatic potential ψ is obtained by solving Poisson's equation, which for a one dimensional nondegenerate semiconductor with the mobile carriers in thermal equilibrium reads (7)

$$\frac{\partial^2 \psi}{\partial x^2} = 2 \sinh (\psi_c + \psi) - C. \tag{8}$$

This will be referred to as the Shockley-Poisson equation (SPE). It has been written with partial derivatives although it is valid only for a static situation. The reason is that the potential and field will change in time due to the redistribution, but only so slowly that an electrostatic approach is valid. The electric field is

$$E = - \frac{\partial \psi}{\partial x} .$$

The boundary conditions for our semiinfinite case are

$$\frac{\partial \psi}{\partial x} (0,t) = - \frac{\sigma_s}{\epsilon E_0} , \tag{9a}$$

$$\psi(\infty,t) = 0 . \tag{9b}$$

The constant ψ_c is given by

$$\psi_c = \sinh^{-1} \left(\frac{C_0}{2} \right) \tag{10}$$

where $C_0 = C(\infty,t)$ independent of time.

From the potential the electron and hole concentrations can be obtained

$$n = n(\infty)e^{\psi} \; ; \quad p = \frac{1}{n} = p(\infty)e^{-\psi} \; . \tag{11}$$

The conductivity σ in units of $q\mu_n n_i$ is

$$\sigma = n + \frac{\mu_p}{\mu_n} p \; . \tag{12}$$

The Redistribution Problem

If we put the origin ($x = 0$) at the moving growth surface the impurity flow is

$$J_k = - D_k \frac{\partial N_k}{\partial x} + z_k B_k D_k E N_k + v N_k \; . \tag{13}$$

The continuity equation (7) can then be written

$$\frac{\partial N_k}{\partial t} = D_k \frac{\partial^2 N_k}{\partial x^2} - z_k B_k D_k \frac{\partial}{\partial x} \left\{ E N_k \right\} - v \frac{\partial N_k}{\partial x} \; . \tag{14}$$

The initial condition is

$$N_k(x,0) = N_{0k}(x) \; . \tag{15}$$

The boundary conditions are

$$N_k(\infty,t) = N_k(\infty,0) = N_{0k}(\infty) \; , \tag{16}$$

$$- D_k \frac{\partial N_k}{\partial x}(0,t) + \left\{ z_k B_k D_k E(0,t) + v(t) \right\} N_k(0,t) = v(t) N_{ak}(t) \; , \tag{17}$$

where $N_{ak}(t)$ is the concentration in the ambient phase. This last expression reflects the continuity of the flow. It is here that the surface conductance (assumption 9) has been neglected.

The electric field problem and the redistribution problem constitute a system of two coupled second-order differential equations, one ordinary and intrinsically very nonlinear, the other partial and nonlinear in the sense that the field depends in a complicated way on all the impurity concentrations. Without making severe simplifications this calls for numerical methods.

Numerical Method

To study the time evolution of the impurity redistribution we make stepwise calculations of the concentrations using the field at the termination of the last step. At each discrete time we recalculate the concentration with halved steps until the result converges, or until the time step is no longer larger than a preset minimum. This minimum time interval is determined from the requirement that the model be macroscopic. For each time step we have two two-point boundary condition problems: one for the field and once that is know, the redistribution.

These are solved by finite difference schemes (8), in the field case combined with a quasilinearization (9) scheme. The infinity-boundary is picked sufficiently deep in the substrate. Both the concentrations and the field/potential vary rapidly over short distances while being almost constant in large parts of the studied region. This necessitates a variable mesh technique which has to be dynamical because of the moving growth interface. Details of the numerical methods will be reported later.

Results for GaAs at 1000K

We have chosen, as an initial application of the model, to simulate two epitaxial growth processes in which the effect of the interfacial fields might be significant. They are:

1) growth of lightly doped n-type GaAs on a heavily n-type substrate; and
2) growth of moderately doped n-type GaAs on a compensated semi-insulating substrate.

These processes are interesting because they are representative, respectively, of the technologies for fabricating Gunn effect devices and MESFET material. We have chosen realistic values of initial impurity concentrations and of growth velocity, and what we believe are reasonable estimates of ionic mobilities and diffusion coefficients (10). The resulting impurity concentration profiles show some striking inhomogeneities, especially in the distribution of minority species. In the two runs that we have simulated in detail, these inhomogeneities do not generate harmful conductivity profiles. It is possible, on the basis of these results, however, to recognize combinations of parameters that may prove troublesome in applications.

Before discussing the numerical simulations in detail, we can point out some features that they have in common. We assume a high temperature acceptor-like surface state density as calculated by Wolfe and Nichols (2) of $N_s = 6.3 \times 10^{11}$ cm^{-2}. The surface electric field associated with the corresponding charge density is $E_s = -8.6 \times 10^4$ Vcm^{-1}. In Figures 1-14 all concentrations are given in units of the measured (11) 1000K intrinsic carrier concentration of $n_i = 6 \times 10^{16}$ cm^{-3}, distances in units of the intrinsic Debye length $L_{Di} = 3.2 \times 10^{-2}$ μm, potential in units of $kT/q = 86.2$ mV, electric field in units of $kT/qL_{Di} = 2.66 \times 10^4$ Vcm^{-1} and time in minutes. The resulting units of diffusion constant and velocity are, respectively, $D_0 = 1.75 \times 10^{-13}$ cm^{2}s^{-1} and $v_0 = 1.94$ μmh^{-1}.

We find that, for any reasonable growth velocity, the growth interface rather quickly outruns any effects associated with the substrate-layer interface. This means that the interfacial field rapidly divides into two regions. The chief effect of the field region associated with the growth surface, after the initial growth stage, is to establish a surface concentration profile. If, as is usual, the growth rate is held constant, this profile does not change. The surface field can, of course, have important effects on distribution coefficients and complex formation. These processes are not modeled here, but one important differential surface effect on donors and acceptors does result from the fact that the growth velocity is greater than the rate of ionic drift in the surface field. Because of this, the electric field term in the boundary condition equation (17), which discriminates between donors and

acceptors, is small compared with the growth velocity term, and both donors and acceptors develop a positive concentration gradient immediately adjacent to the surface. As soon as the surface moves away, the field becomes important, generating a donor accumulation (negative concentration gradient) and an acceptor depletion (positive concentration gradient). Since these two effects operate in the same direction for acceptors, in opposite directions for donors, the acceptor depletion beneath the growth surface tends to be more pronounced than the donor accumulation. This tendency can be seen in the concentration profiles of the incorporated impurities on all the figures, which also show the minute surface region of "inverted concentration gradient" of the donors.

The separation of the two interfacial field regions has another interesting, and not a priori obvious bearing

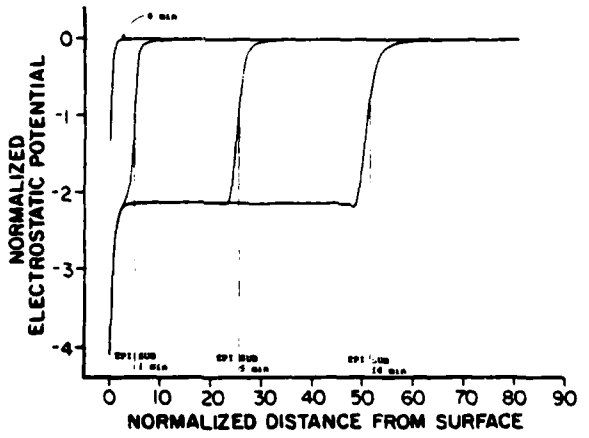

Figure 1. The electrostatic potential for the growth case listed in Table I, after 0, 1, 5, and 10 minutes of growth.

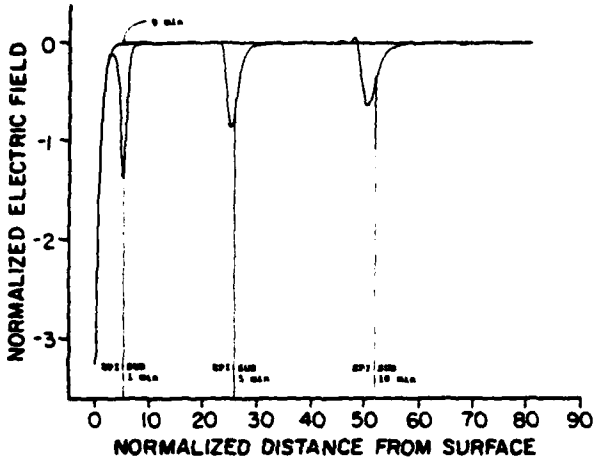

Figure 2. The electric field for the growth case listed in Table I, after 0, 1, 5, and 10 minutes of growth.

on the growth surface boundary condition. We have assumed a fixed surface field, and we find that, after the initial stage, the surface potential remains effectively constant (Figures 1 and 9). Obviously the converse would be true as well. Thus, knowledge of the actual, and poorly understood, high temperature surface state energy distribution which determines the relation between surface field and potential, is not essential for a realistic simulation. For some of the impurity profiles ripples occur. These are numerical artifacts.

Growth on n^+ Substrate (Table I)

When the n-type substrate is more heavily doped than the epitaxial layer, the interfacial electric field points from the substrate to the epitaxial layer (Figures 1 and 2). The substrate is partially compensated, its donors (Figure 3)

Table I. First n-GaAs growth simulation;
Lightly doped epitaxial layer on heavily doped substrate.

v = 10 μm/h

No.	Impurities				Conc	D	B
	Donor	Acceptor	Substrate	Epilayer	(cm^{-3})	(cm^2/s)	
1	x		x		1×10^{18}	1×10^{-14}	1.27
2		x	x		5×10^{17}	1×10^{-13}	1.27
3	x			x	1×10^{15}	1×10^{-14}	1.27
4		x		x	2.5×10^{14}	1×10^{-13}	1.27

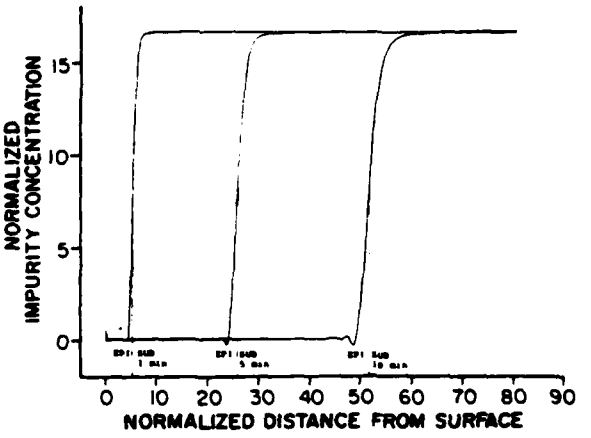

Figure 3. The distribution of impurity no. 1 for the growth case listed in Table I, after 1, 5, and 10 minutes.

experience a force pulling them out of the substrate, its acceptors (Figure 4) a force pushing them back. Hence the electric force aids the concentration gradient for the donors, opposes it for the acceptors. If the diffusion constants of the two species are roughly equal, this means that the out diffusion of the acceptors lags behind that of the donors, as can be seen from Figure 8. If, as would be true for example for Se doping, the acceptors are an order of magnitude more mobile than the donors, we find (Figure 7) that very little charge separation occurs.

The opposite effect is experienced by the donors (Figure 5) and acceptors (Figure 6) grown into the epitaxial layer. Here interfacial field and concentration gradient drive the acceptors in the same, the donors in opposite directions. The somewhat surprising concentration profiles of Figures 5 and 6 result from this interaction. These profiles can be understood when it is realized that

the field is mostly confined to the more lightly doped epitaxial region. Hence, while it influences only the edge of the substrate impurity profiles, it can cause a pileup of donors, and "eat a hole" into the distribution of acceptors, in the epitaxial layer.

The dominant effect in these simulations is the field-aided outdiffusion of donors from the substrate. Since this species has a concentration from one to three orders of magnitude greater than any other, it blots out the variation of all the minority species, so far as the resulting room temperature carrier concentration is concerned. The effect posited by Wolfe and Nichols (1,2) to account for an interfacial high resistivity layer would be expected to occur if the substrate donors were effectively immobile. Then either the separation of incorporated epitaxial layer donors and acceptors (species 3 and 4 in

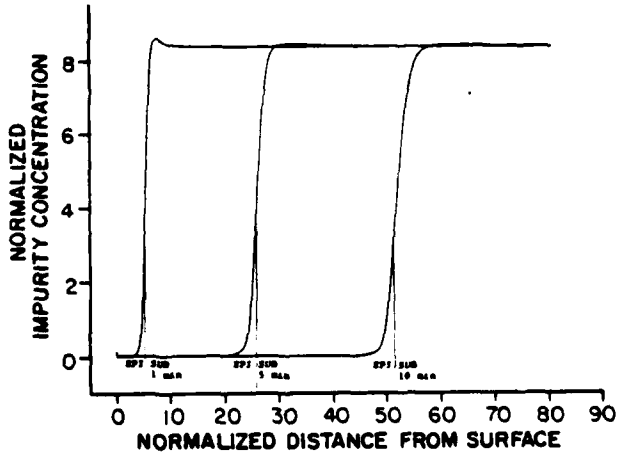

Figure 4. The distribution of impurity no. 2 for the growth case listed in Table I, after 1, 5, and 10 minutes.

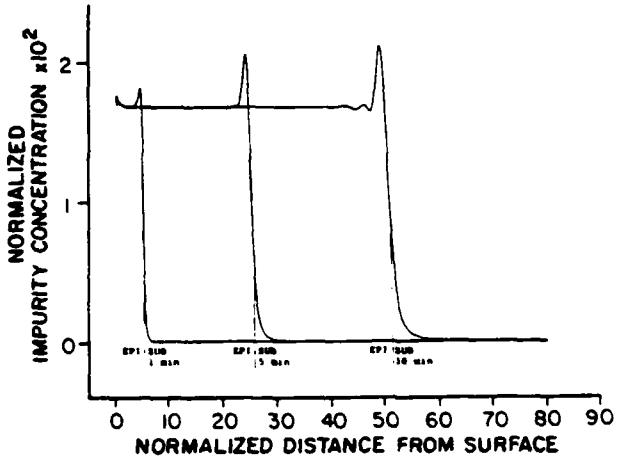

Figure 5. The distribution of impurity no. 3 for the growth case listed in Table I, after 1,5, and 10 minutes.

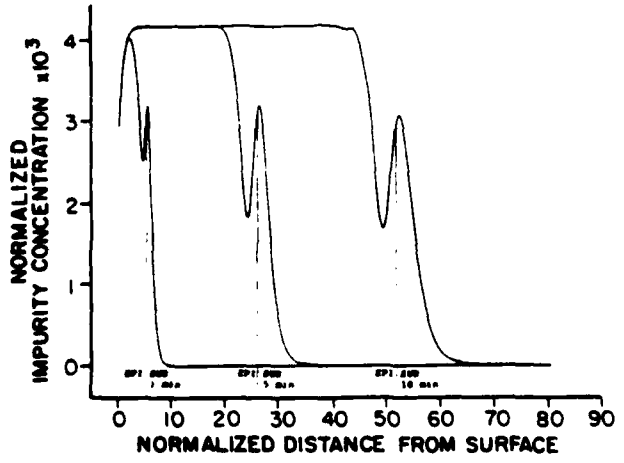

Figure 6. The distribution of impurity no. 4 for the growth case listed in Table I, after 1,5, and 10 minutes.

Figure 7), or outdiffusion of partially compensating substrate acceptors could produce a thin nearly intrinsic or polarization reversed layer.

Growth on a Compensated Semi-Insulating Substrate (Table II)

We have attempted to model a Cr-compensated substrate as follows: A concentration of $8\times10^{16}cm^{-3}$ slowly diffusing ($D = 10^{-14}$ cm^2s^{-1}) residual donors (for example Si^+) is compensated by 1×10^{17} cm^{-3} Cr of which 90% are totally immobile substitutional acceptors, 10% mobile ($D = 10^{-12}$ cm^2 s^{-1}) interstitial donors. The epitaxial layer grown on this substrate incorporates 1×10^{17} cm^{-3} slowly diffusing ($D = 10^{-14}$ cm^2 s^{-1}) donors and 2.5×10^{16} cm^{-3} an order of magnitude more mobile acceptors, giving a net n-type doping of 7.5×10^{16} cm^{-3}. With this concentration, barely

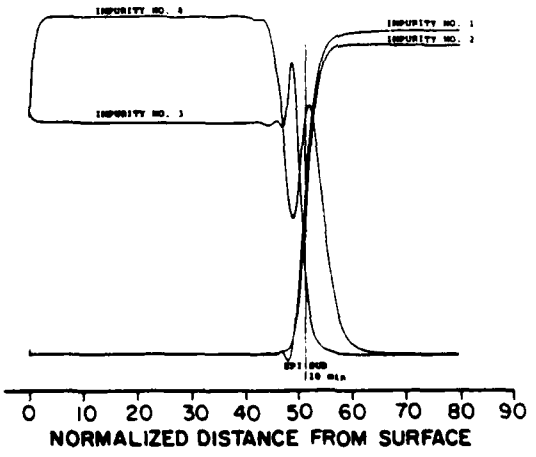

Figure 7. Superposition of the impurity profiles after 10 minutes for the growth case listed in Table I. (The impurity concentrations are plotted to different scale).

Table II. Second n - GaAs growth simulation;
Moderately doped epitaxial layer on semi-insulating substrate.

$v = 10$ μm/h

	Impurities				Conc	D	B
No.	Donor	Acceptor	Substrate	Epilayer	(cm^{-3})	(cm^2/s)	
1	x		x		8×10^{16}	1×10^{-14}	1.27
2	x		x		1×10^{16}	1×10^{-12}	1.0
3	x			x	1×10^{17}	1×10^{-14}	1.27
4		x		x	2.5×10^{16}	1×10^{-13}	1.27

The substrate is initially semi-insulating due to Cr acceptors with a concentration 9×10^{16} cm^{-3}. These are assumed to be fixed.

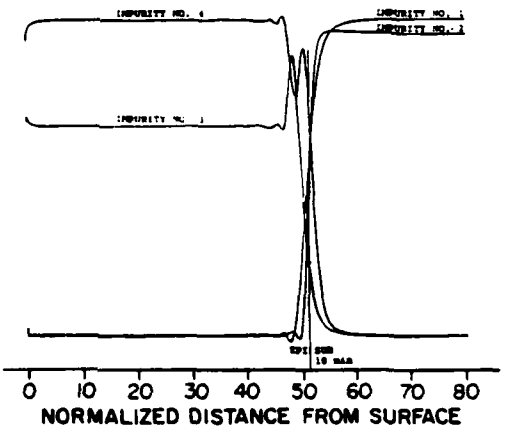

Figure 8. Same as Figure 7 but for a slightly different growth case with $D_1 = D_2 = D_3 = D_4 = 10^{-14}$ cm^2/s.

in excess of the intrinsic concentration of 6×10^{16} cm^{-3} at 1000K, the epitaxial layer-substrate interfacial potential (Figure 9) and field (Figure 10) are quite small and they modify the diffusion only slightly. The chief effect of the impurity redistribution comes from the outdiffusion of donors (Figure 12) and the preferential indiffusion of acceptors (Figure 14), which turns the substrate slightly p-type near the interface. As a result, upon cooling to room temperature, the Debye shielding length is reduced below what it would be without redistribution and the carrier concentration falls off considerably more steeply.

The epitaxial material for use in MESFET's and IC's is frequently one to two orders of magnitude more lightly doped than in our numerical example. Such epitaxial layers are intrinsic at 1000K, and their growth on SI substrates

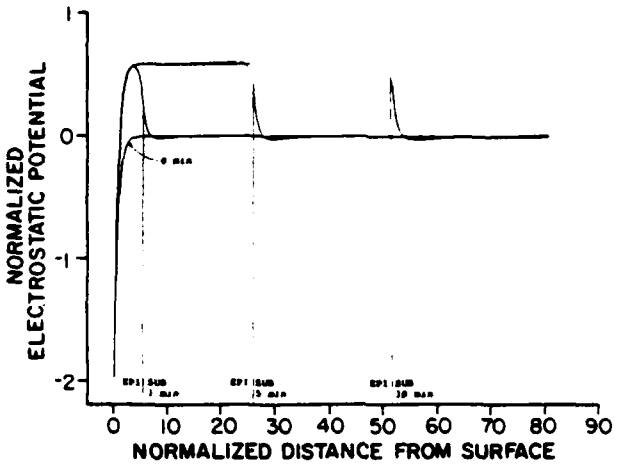

Figure 9. The electrostatic potential for the growth case listed in Table II, after 0, 1, 5, and 10 minutes of growth.

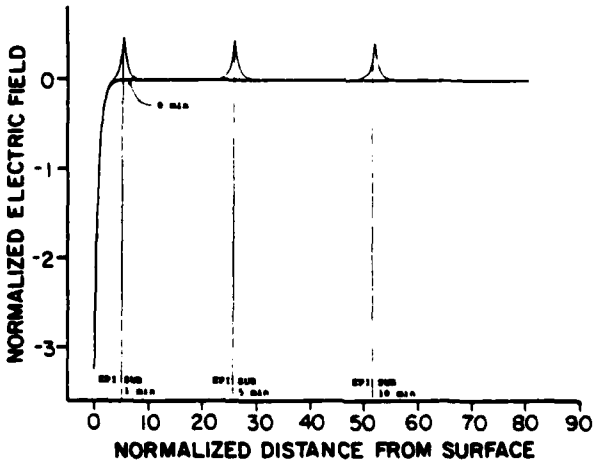

Figure 10. The electric field for the growth case listed in Table II, after 0, 1, 5, and 10 minutes of growth.

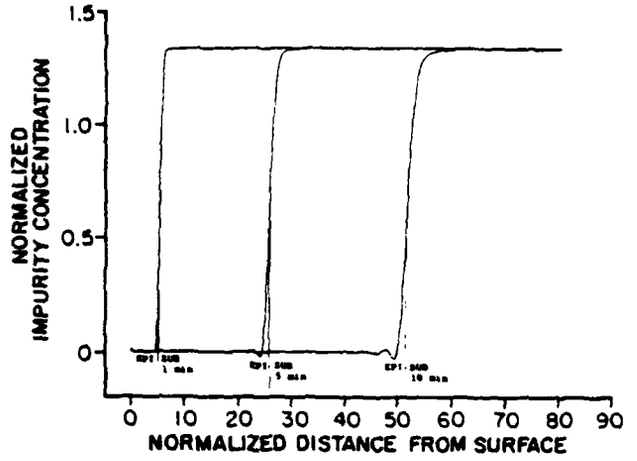

Figure 11. The distribution of impurity no. 1 for the growth case listed in Table II after 1, 5, and 10 minutes.

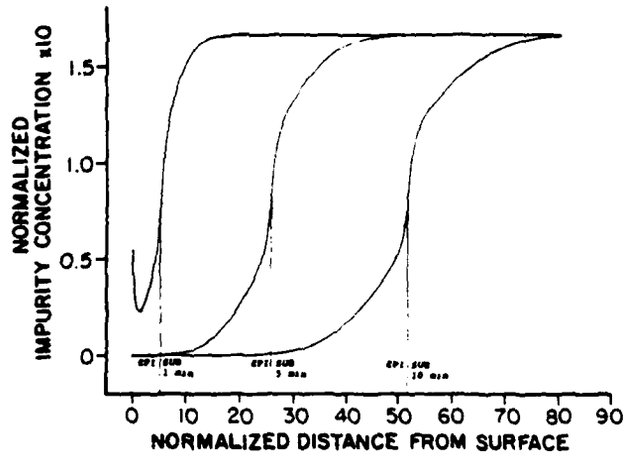

Figure 12. The distribution of impurity no. 2 for the growth case listed in Table II after 1, 5, and 10 minutes.

would occur without an interfacial field. Under these conditions preferential diffusion (12) of donors from a heavily compensated substrate, as shown in Figure 11, could produce a high conductivity layer at the interface.

Conclusions and Applications

The results we have obtained so far indicate that our model is a versatile instrument for the study of ionic diffusion and drift. We have demonstrated that even under very simple epitaxial growth conditions ionic redistribution can produce fairly complicated impurity density profiles. We have already mentioned that the numerical technique contains options we have not yet used, such as inhomogeneous substrate doping, depletion of the ambient, changes in growth rate, etc.; and that it could be readily modified to include reactive diffusion processes.

In addition to this first application of understanding and interpreting the impurity density profiles that arise with standard epitaxial growth techniques, we can envisage at least two other uses of the model.

By mathematical experimentation we may hope to develop growth and/or processing programs to achieve specified doping and conductivity profiles suited to given functional applications. Such work would require detailed knowledge of ionic mobilities and diffusion constants. The present model may assist in the determination of these parameters by providing detailed quantitative correlations between controlled growth experiments, analysis of the resulting profiles, and numerical simulation. The model, especially if it is modified to include reactive diffusion processes, should also be suitable for the simulation of the annealing and activation of implanted impurities; indeed, because of the absence of a moving boundary, such simulations should be simpler than those of epitaxial growth.

Acknowledgement

We are grateful to Prof. D. L. Elliott for enlightening discussions of numerical techniques.

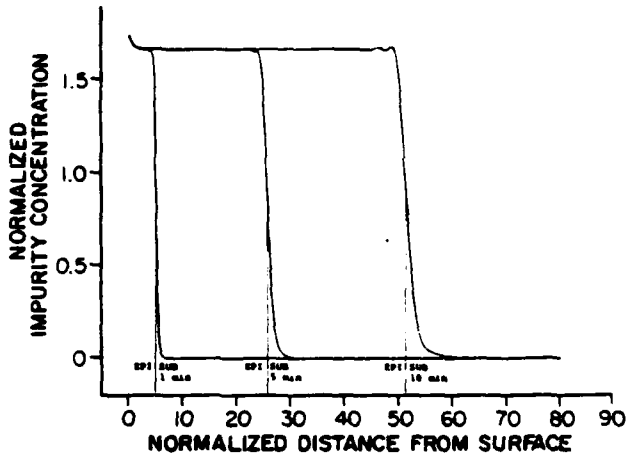

Figure 13. The distribution of impurity no. 3 for the growth case listed in Table II after 1, 5, and 10 minutes.

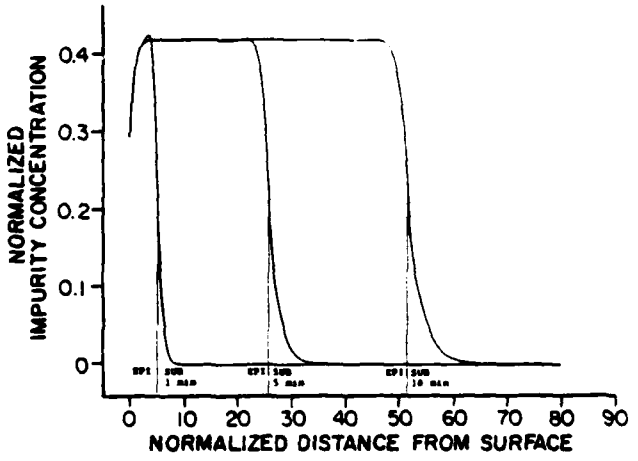

Figure 14. The distribution of impurity no. 4 for the growth case listed in Table II after 1, 5, and 10 minutes.

References

* Supported by ONR Contract N00014-79-C-0840 and ONR Contract N00014-80-C-0762.

1. C.M. Wolfe and K.H. Nichols, Appl. Phys. Lett., Vol. 31, 356 (1977).

2. Final Scientific Report No. 59356-6, Washington University, St. Louis, Mo. (1979).

3. L.A. Girifalco, Atomic Migration in Crystals, Blaisdell Publishing Company, 1964.

4. R.C. Miller and F.M. Smits, Phys. Rev., Vol. 107, 65 (1957).

5. F.A. Kröger, The Chemistry of Imperfect Crystals, 2nd ed., Vol. 1, North-Holland, Amsterdam, 1973.

6. J. Kasahara and N. Watanabe, Jap. J. Appl. Phys., Vol. 19, L151 (1980).

7. W. Shockley, Electrons and Holes in Semiconductors, Van Nostrand, 1950.

8. G.D. Smith, Numerical Solution of Partial Differential Equations, Oxford University Press, New York and London, 1965.

9. L. Fox and D.F. Mayers, Computing Methods for Scientists and Engineers, Clarendon Press, Oxford, 1968.

10. D. Shaw (editor), Atomic Diffusion in Semiconductors, Plenum Press, London and New York, 1973.

11. K.H. Nichols, Camellia M.L. Yee, and C.M. Wolfe, Solid State Electron. 23, 109 (1980).

12. C.M. Wolfe, A.G. Foyt and W.T. Lindley, Electrochem. Tech. 6, 208 (1968).

J. Phys. Chem. Solids Vol. 44, No. 11, pp. 1049–1057, 1983
Printed in Great Britain.

0022-3697/83 $3.00 + .00
Pergamon Press Ltd.

B.2 A MODEL OF Cr IN GaAs

H. ROHDIN†, M. W. MULLER and C. M. WOLFE
Department of Electrical Engineering, Washington University, St. Louis, MO 63130, U.S.A.

(*Received* 31 *August* 1982; *accepted in revised form* 4 *March* 1983)

Abstract—We have developed a model of Cr in GaAs which is consistent with a large body of experimental data. It relies on recent spectroscopic models and on our interpretation of redistribution and electrical data, all of which indicate the existence of Cr complexes. The existence of rapidly diffusing interstitial Cr donors is assumed and justified. The model offers a unified picture of the effects of implantation on the Cr profile. It contains mechanisms for compensation and redistribution, which offer an explanation of the semi-insulating properties of Cr doped GaAs and of the two apparently incompatible classes of diffusion and anneal data. The redistribution depends on how the Cr was incorporated and on the vacancy concentration profiles. A study of representatives of the two classes of redistribution data allows us to estimate a lower limit of interstitial Cr diffusion constant and of the vacancy diffusion lengths in GaAs.

1. INTRODUCTION

Cr-doped GaAs has been studied for some 20 yr. The experimental data that have been generated over this period fall mainly into three categories: spectroscopic results, electrical properties, and redistribution phenomena. Many properties of the GaAs:Cr system are still not well understood. In this paper we present a model consistent with a wide spectrum of experimental data from the three classes.

We start by reviewing indications of Cr interacting with other defects in GaAs, and evidence of the existence of highly mobile interstitial Cr donors. We can then give a unifying picture of the effect of implantation on Cr, and reinterpret the compensation and redistribution mechanisms of Cr in GaAs.

2. INTERACTION OF Cr WITH OTHER DEFECTS

It is becoming increasingly clear that one cannot in general model Cr independently from other defects that are present. We will therefore start with a short survey of experimental data indicating defect interaction with Cr.

2.1 Cr *complexes suggested by spectroscopic data*

White[1a] has assigned excitonic recombination at an isoelectronic Cr-complex $(Cr_{Ga}D_{As})^{\circ}$ as the cause of the observed 0.84 eV photoluminescence line earlier attributed to an internal Cr transition $^5E - {}^5T_2$. This assignment is supported by the Zeeman anisotropy[1b] and by the angular dependence of the optically detected magnetic resonance[1c]. Picoli *et al.*[1d] proposed an interesting alternative: an interstitial Cr coupled with an acceptor A on an arsenic site. This would, according to the authors, explain the 0.575/0.535 eV transition.

2.2 *Interaction suggested by redistribution data*

Favennec *et al.*[2] observed trapping of Cr in GaAs implanted with oxygen. The dose was rather large, which could indicate gettering due to damage. However, implantation of neon under the same conditions (same dose and energy) did not cause a build-up of Cr in the implanted region. The authors give complexing of Cr and O as a possible explanation. Favennec and L'Haridon[3, 1e] implanted Se and Zn into GaAs:Cr. Their results do not indicate any complexing; i.e. no trapping of Cr was observed in the implanted region. Asbeck *et al.*[4] implanted Se and Kr. No trapping of Cr in either case was reported. However, Evans *et al.*[5] did see Cr trapping in the Se implanted region. They used a dose 3 orders of magnitude larger than in the two aforementioned papers. In the latter case the Cr pile-up disappeared and formed again at the surface after further annealing. An interesting case was reported by Magee *et al.*[6]. They annealed GaAs implanted with high doses of B (isoelectronic with Ga). This increased the outdiffusion of Cr, compared to annealing without implantation, and resulted in a stable Cr depletion channel. A small tendency for Cr pile-up at the implant peak was observed for high Cr content. Ne implantation[2] also enhances Cr outdiffusion.

Tuck *et al.*[7] observed that S doping of an epitaxial layer grown on a Cr doped substrate decreases the Cr outdiffusion more than an undoped layer. This indicates some interaction between Cr and S.

It is possible that Cr is sensitive to lattice strain. Clegg *et al.*[8] point out that Cr doping of GaAs reduces the lattice constant. In regions of large concentrations of As vacancies (e.g. at the surface) the lattice constant is larger. The gettering of Cr in such regions may decrease the lattice strain energy. Strain due to interfaces between encapsulants and GaAs may also interact with Cr. Eu *et al.*[9] suggest that the surface pile-up of Cr would be caused by precipitation of Cr at dislocations generated at the

†Present address: Howlett-Packard Laboratories, 1501 Page Mill Road, Palo Alto, CA 94304, U.S.A.

interface. They attribute the generally smaller accumulation of Cr at unencapsulated surfaces to smaller dislocation densities. This contrasts with the behavior in the bulk. Simondet *et al.*[1f] observe that Cr prefers to migrate rather than to precipitate. They perform implantation of Cr and study the redistribution during the post-implantation encapsulated anneal. The Cr peak flattens out and Cr accumulates at the interface and in the encapsulant (silicon nitride). A higher dose of Cr causes more damage, and if Cr had a tendency to precipitate in damaged regions, the Cr peak would disappear at a less rapid rate, if at all. However, at higher doses the Cr shows the same tendency to leave the region of implantation.

2.3 *Interaction suggested by electrical data*

Mullin *et al.*[10] observed that the deep-level-forming species in their samples were present at one percent or less of the total Cr concentration in the crystal. This led them to propose that Cr gives rise indirectly to the species that controls the Fermi level. They mentioned a Cr–O complex as one possibility.

Brozel *et al.*[11] studied the electrical compensation mechanism of Cr in GaAs doped with Cr and Si. Using localized vibrational mode absorption measurements they concluded that there were no signs of near-neighbor Si–Cr pairs. However, they did observe an increase of the Cr concentration when the Si concentration was increased. They actually observed a geometrical adjustment of the Cr concentration to the Si concentration. This behavior certainly indicates some kind of interaction between Cr and Si.

Hobgood *et al.*[12] observed that the post-implantation activation of Si is more efficient when the Cr background is higher. Although this suggested to them a Cr-Si interaction, it does not seem likely that this is due to Cr_{Ga} forming pairs with Si. This is because most of the Si atoms as donors reside on the Ga sublattice where Cr is also thought to reside. This would indicate that a Cr–Si pair is not as favorable as, for example, a Cr–O pair.

3. INTERSTITIAL Cr DONOR

It has been suggested that Cr can exist as an interstitial donor in GaAs[13]. In a paper to be discussed in detail later, Tuck and Adegboyega[4] model their diffusion data, which exhibit exceedingly rapid diffusion of Cr, by invoking a very mobile interstitial Cr-species (Cr_i). We will assume the existence of *very mobile interstitial Cr donors*. There have been experimental data reported which support this. Deveaud and Favennec[15] observed a new PL line in substrates that had been Cr-implanted and annealed, and also in contaminated epitaxial layers; i.e. layers into which Cr had outdiffused from the substrates. A very interesting feature of the latter is that, although the part of the layer into which Cr had outdiffused contained almost as much Cr as the substrate itself, it was not semi-insulating. Furthermore, the new PL line was much stronger than those usually assigned to Cr. The authors suggested that Cr may be located non-substitutionally. Asbeck *et al.*[4] observed a spurious *n*-type layer just below the GaAs–Si_3N_4 interface after encapsulated annealing, and in this region Cr is always observed to accumulate at concentrations above the expected solubility[3, 16]. Andre and LeDuc[17] actually concluded that Cr incorporated into LPE layers form shallow donors, contrary to Cr incorporated during bulk growth. As mentioned in Section 2.1, Picoli *et al.*[1d] argue the formation of (Cr,A)-pairs. With our assumption this seems very likely to be enhanced by an electrostatic interaction.

4. EFFECT OF IMPLANTATION ON Cr

The spectroscopic models invoking Cr complexes appear well justified. The existence of these complexes would certainly affect both redistribution of Cr and the electrical properties of Cr doped GaAs. Actually, successful reinterpretation of both the redistribution and compensation mechanisms in terms of Cr complexes is possible, as we will see in the following sections. In this section we will focus on the cause of Cr redistribution about implants, and present a unifying qualitative interpretation.

The redistribution of implanted Cr discussed above, indicates that Cr is much more prone to outdiffuse and precipitate at the interface, than to be gettered in damaged regions. If Cr actually does accumulate in regions of implantation of a different ion, it is therefore presumably not because Cr is attracted by the damage, but instead due to a direct interaction between Cr and the implanted species. The observed redistribution of Cr upon post-implantation annealing therefore suggests that Cr tends to complex with the column VI elements (probably most strongly with O), but that the barriers to be overcome in the complexing reaction are so large that the material has to be nearly amorphous before this takes place; Simondet *et al.*[1f] point out that doses of about 10^{15} cm^{-2} effectively disorder the material, and it is in this range that trapping is observed. The dependence on the dose is well illustrated in [1g] where implanted S traps Cr for a dose larger than about 10^{14} cm^{-2}. The proposed mechanism also conforms well with the depletion of Cr in regions of B implantation. The damage will undoubtedly produce a large amount of interstitial Cr, which will have to compete with B for Ga sites. Excess interstitial Cr will not accumulate in damaged regions, but instead outdiffuse rapidly, by a mechanism that will be discussed in detail in Section 6.

In summary, Cr does not appear to be attracted, or repelled, by bulk damage caused by implantation. Any accumulation, or depletion, of Cr in implanted regions is likely to occur by an attraction, or effectively a repulsion, by the specific implanted ions. The damage only promotes the processes.

5. COMPENSATION MECHANISM

Our model of Cr in GaAs relies on the existence of ($Cr_{Ga}D_{As}$) complexes, and rapidly diffusing interstitial

Cr donors. Even though the $(Cr_i A)$ complexes were proposed as an alternative to the $(Cr_{Ga} D_{As})$ complexes, it appears likely that both kinds can occur. This would offer an alternative interpretation of the compensation in Cr-doped GaAs. As was first observed by Cronin and Haisty[18], the semi-insulating properties of bulk grown GaAs:Cr are remarkably independent of the Cr concentration added to the melt. This behavior is typically explained[11] by assuming that the deep acceptor level(s) of Cr_{Ga} pin the Fermi level close to the center of the gap. Excess Cr can the precipitate[18].

We suggest the following compensation mechanism: At the high bulk-growth temperatures the residual donors D_{As} are chemically compensated by Cr through the formation of the isoelectronic complex $(Cr_{Ga} D_{As})^{\circ}$. The excess Cr is in the form of isolated Cr_{Ga} and Cr_i. As the ingot is cooled the Cr_i donors flush out because of limited solubility and large diffusion constant. Since the acceptors and the mobile Cr_i donors are oppositely charged, electrostatic attraction between the two species is expected. This will enhance the formation of $(Cr_i A)$ complexes and contribute to good compensation. In addition to giving an alternative interpretation of the semi-insulating properties of GaAs doped with Cr during bulk-growth, this offers an explanation of the enhanced apparent activation of Si in the presence of Cr. Si is amphoteric and the Si-acceptors can be neutralized by rapidly diffusing Cr_i-donors. The same effect can explain the increase of Cr concentration with increasing Si concentration that was observed by Brozel *et al.*[11] even locally.

The compensation mechanism gives a first hint to an understanding of the redistribution properies of Cr in GaAs since we no longer can expect Cr incorporated during high-temperature bulk growth to redistribute in the same way as Cr introduced into the crystal at lower temperatures. The rest of this paper will be devoted to the redistribution problem.

6. REDISTRIBUTION MECHANISM

The foregoing discussion suggests that the problem of Cr redistribution in GaAs is quite complicated. Cr apparently occurs in several different forms: isolated interstitial Cr_i, isolated substitutional Cr_{Ga}, complexed interstitial $(Cr_i A)$, and complexed substitutional $(Cr_{Ga} D_{As})$. Furthermore, there are a number of mechanisms involved in the redistribution: diffusion in concentration gradients, drift of Cr ions in a built-in electric field, quasi-chemical reactions, and gettering in the strain fields of surfaces and dislocations. We expect the following reactions to be dominant:

$$Cr_i + V_{Ga} \rightleftarrows Cr_{Ga}, \tag{1}$$

$$Cr_i + V_{Ga} + D_{As} \rightleftarrows (Cr_{Ga} D_{As}), \tag{2}$$

and

$$Cr_i + A \rightleftarrows (Cr_i A). \tag{3}$$

Three assumptions appear physically weli motivated:

(1) The actual transport of Cr occurs interstitially. The diffusion and drift of the substitutional and complexed Cr are negligible. This is typically assumed for interstitial-substitutional diffusion.

(2) At the usually relatively low processing temperatures there is no formation of $(Cr_{Ga} D_{As})$ complexes since this is a third order process and seems very unlikely to occur after the original formation of the crystal.

(3) The complexes are considerably more strongly bound than the substitutional Cr ions to their sites.

The major technological problem with Cr doped substrates is their apparent irreproducibility. Capless anneal sometimes leads to surface build-up[1h, 9], at other times not[1h, 19], depending on temperature and As overpressure. Capped anneal generally leads to thin surface pile-up[3, 9, 16]. Apart from the surface behavior, however, the different results do not appear to dissimilar; i.e. they are characterized by a thin (1–2 μm) surface depletion of Cr, while the bulk concentration remains unaffected. The really astonishing deviation from most of these results is reported in the experiments conducted by Tuck *et al*[7, 14]. They observed a remarkable penetration and diffusion of Cr in GaAs leading to a uniform Cr concentration throughout hundreds of microns, and a thick (10–20 μm) surface pile-up on both indiffusion and anneal. The uniform bulk concentration was observed to vary exponentially in time. In this section we will focus on this apparent inconsistency.

As was mentioned in the last section, our model indicates that the redistribution depends strongly on how the Cr was incorporated. We will therefore study the two cases of post-growth incorporated Cr as represented by the data of Tuck *et al.*, and Cr incorporated during high temperature bulk growth as represented by the data of Kasahara and Watanabe. The latter are typical of the behavior usually encountered. The results lack the surface build-up, presumably due to stable conditions set by the As overpressure and temperature. In both cases the vacancies will affect the redistribution, and we will therefore discuss the expected vacancy concentration profiles in GaAs. In the analysis we will ignore the drift of Cr in electric and strain fields. This means that we do not model the immediate vicinity of the surface. However we will begin by giving a separate qualitative discussion of the drift of Cr_i in electric fields due to dopant gradients in the bulk.

6.1 *Drift of interstitial* Cr

Drift in built-in electric fields can typically be neglected except at surfaces and interfaces. At free surfaces it is difficult to distinguish between field induced and strain induced built-up. However at an interface between two doping regions in a structurally homogeneous crystal, an anomaly in the Cr distribution is more likely to be caused by the electric field.

It has been observed[20] that Cr outdiffusing during epitaxy from a semi-insulating GaAs:Cr substrate, through an undoped GaAs buffer layer, into a n-GaAs

active layer (electron concentration n), piles up at the buffer layer side of the interface between the epitaxial layers for $n = 10^{17}\,cm^{-3}$, but not for $n = 5 \times 10^{16}\,cm^{-3}$. At the growth temperature of 750°C the intrinsic concentration has been measured[21] to be $6 \times 10^{16}\,cm^{-3}$. That means that for the case where pile-up is observed there is an electric field in the interfacial region between the active layer and the buffer layer. This is mostly confined to the undoped buffer layer and is directed into this. The interfacial pile-up of Cr resembles those of charged impurities reported in [22]. These were caused by the electric field due to doping gradients. The observed Cr pile-up is such that the mobile Cr would have to be positively charged. It is therefore likely that the interstitial Cr actually is a donor as was argued above. The Cr profiles observed by Linh *et al.*[1i] in MBE layers conform qualitatively with this assignment.

6.2 *Vacancy concentration profiles*

In the redistribution model we have outlined, the vacancies play an important role primarily through reaction (1). One possible native mechanism for Ga vacancy production is the process,

$$Ga_{Ga} + I \rightleftarrows V_{Ga} + Ga_i \qquad (4)$$

where I is an interstitial site. A similar reaction would apply to As vacancies. It is also conceivable to have vacancy production at dislocations. In either case the continuity equation for the vacancy concentration C_v can be written (neglecting possible drift),

$$\frac{\partial C_v}{\partial t} = D_v \frac{\partial^2 C_v}{\partial x^2} - \beta C_v + \alpha, \qquad (5)$$

where D_v is the diffusion coefficient. It is not clear what the diffusion mechanism is, but it seems likely that it is similar to that suggested by Swalin[23] for vacancy diffusion in group IV semiconductors. The mechanism would then involve transfer of an atom to a nearby vacancy (for III–V semiconductors, at a next-nearest neighbor site). α is the generation rate, and βC_v the annihilation rate of vacancies due to the dominant mechanism, possibly reaction (4).

At the surface the concentration of vacancies need not be the same as in the bulk since it can be more readily influenced, for instance, by the As overpressure. In the steady state the vacancy concentration profile is

$$C_v^{(s)}(x) = C_v^{(b)} + [C_v^{(s)} - C_v^{(b)}] \exp(-x/L_v), \qquad (6)$$

where $C_v^{(s)}$ is the surface concentration, $C_v^{(b)}$ the bulk concentration, and L_v the vacancy diffusion length given by

$$L_v = \sqrt{D_v/\beta}. \qquad (7)$$

6.3 *Diffusion of* Cr *introduced after bulk growth*

We believe that Tuck *et al.*[7, 14] have reported some of the few experiments that involve essentially only reaction (1). In these experiments radiotracer Cr was diffused into bulk grown GaAs (Cr-doped or n-type) at temperatures well below the growth temperature. Under these circumstances, reaction (2) is not expected to go to the right, and reaction (3) is secondary due to the small number of isolated acceptors. The indiffusing Cr, which is the only Cr that is detected, is thus not expected to interact strongly with the residual impurities.

Tuck and Adegboyega (TA) account for the observed exponential time dependence of the uniform bulk concentration by means of a model[14] involving the non-equilibrium chemistry of substitutional and interstitial Cr and of Ga vacancies. The width of the surface peak permits them to estimate the diffusion constant of Ga vacancies. It is assumed that Cr can exist in GaAs as a highly mobile interstitial species Cr_i, or substitutionally on Ga sites as immobile Cr_s. The reaction converting each species into the other is reaction (1). Only Cr_i is incorporated or desorbed at the surface. For Cr to penetrate to the interior, it must first be converted by reaction (1) to Cr_s. It then diffuses rapidly and can again react with V_{Ga} to form Cr_s. The limit chosen by TA to interpret the experiments assumes that the surface incorporation and conversion reactions are in equilibrium, that the interstitial diffusion is extremely rapid (in effect, instantaneous on the time scale considered), and that the bulk conversion is slow. In addition it is assumed that no vacancies are generated or annihilated in the bulk except through reaction (1). The surface concentration gradients are qualitatively accounted for by the diffusion of V_{Ga}. This vacancy concentration, depleted by reaction (1) during indiffusion of Cr, is replaced by diffusion from the surface, resulting in a surface Cr peak, as observed. In the outdiffusion experiment from a homogeneously vacancy-depleted sampi vacancies also diffuse in from the surface, "pulling" Cr from the interior to supply reaction (1), and again resulting in a surface peak.

We adopt a similar model but with a substantially modified picture of the vacancy dynamics. Unlike TA, we assume that the vacancy concentration is determined by the dominant native mechanism and is always able to reach its steady state, on the time scale of the experiments under study, leading to the vacancy concentration profile (6). This appears to us more consistent with a rather large vacancy diffusion constant, as inferred by TA, than the large departure from equilibrium implied by their interpretation. We could indeed adopt TA's viewpoint in which the vacancy concentration is determined by the diffusing Cr atoms. This would generalize to

$$C_v(x, t) = C_v^{(s)}(x) - [C_s(x, t) - C_s(x, 0)], \qquad (8)$$

where we assume equilibrium initial distribution $C_s(x, 0) = C_v^{(s)}(x)$. We find this limit less plausible. Either approach, however, permits us to extend the validity

of the treatment closer to the surface, and we are able to estimate the Ga vacancy diffusion length from TA's data. We start in Section 6.3.1 by examining rapid diffusion and find that we can deduce a condition on the diffusion constant necessary to keep the concentration uniform. From this we can estimate the lower limit of the diffusion constant for interstitial Cr, again using TA's data. The combined effect of a *homogeneous distribution of interstitial* Cr_i and of the vacancy equilibrium described by eqn (6) on the conversion reaction (1) is to produce a total Cr impurity profile that is to a good approximation proportional to the Ga vacancy profile. This conclusion is used in Section 6.3.3 to obtain a measure of the Ga vacancy diffusion length L_v.

The evolution of the bulk Cr concentration depends in fairly involved fashion on reaction time constants, distribution coefficients, and boundary conditions. We have not obtained a solution for the most general case, but in Section 6.3.2 we study the limit considered by TA and also the limit where the surface conversion reaction is the bottleneck. TA's indiffusion data, which exhibit a large constant surface concentration on indiffusion, indicate incorporation equilibrium, so this must be discarded as a possible bottleneck. The entire process of incorporation, surface conversion of Cr_i into Cr_s, diffusion of Cr_s, generation of Ga vacancies, and conversion between Cr_i and Cr_s in the bulk is illustrated in Fig. 1.

6.3.1 *Rapid diffusion leading to uniform concentration.* We study an atomic species that redistributes in a sample of thickness l by a simple diffusion mechanism. The continuity equation is then

$$\frac{\partial C}{\partial t} = D\frac{\partial^2 C}{\partial x^2}, \tag{9}$$

with boundary conditions set by the surface flux,

$$J(0,t) = -D\frac{\partial C}{\partial x}(0,t) = v[kC_a - C(0,t)], \tag{10a}$$

and

$$J(l,t) = -D\frac{\partial C}{\partial x}(l,t) = -v[kC_a - C(l,t)]. \tag{10b}$$

In these equations $C(x,t)$ and C_a are the concentrations in the sample and in the ambient atmosphere respectively, D is the atomic diffusion constant, k the segregation coefficient and v the surface diffusion velocity. We wish to determine the condition on D that will keep the concentration practically uniform at all times,

$$C(x,t) = C'(t), \tag{11}$$

assuming the consistent initial condition

$$C(x,0) = C'(0). \tag{12}$$

With these initial and boundary conditions, the solution of the diffusion equation is [24]

$$C(x,t) - kC_a = [C'(0) - kC_a]\left[\cos\alpha_1 x + \frac{v}{\alpha_1 D}\sin\alpha_1 x\right] \times \exp(-D\alpha_1^2 t), \tag{13}$$

where α_1 is the first positive root of

$$\tan\alpha l = \frac{2\alpha(v/D)}{\alpha^2 - (v/D)^2}. \tag{14}$$

For $C(x,t)$ to be considered independent of x we must have $\alpha_1 l \ll 1$ and $v/\alpha_1 D \ll 1$. If these conditions are fulfilled, (13) becomes

$$C'(t) = kC_a + [C'(0) - kC_a]\exp(-t/\tau), \tag{15}$$

where

$$\frac{1}{\tau} = \alpha_1^2 D \ll \frac{D}{l^2}. \tag{16}$$

For the root α_1 of (14) we get $\alpha_1^2 = 2v/Dl$, so that $1/\tau = 2v/l$ as expected.

Thus, if the concentration is observed to relax uniformly with the characteristic time τ, (16) sets a lower limit on the diffusion constant,

$$D \gg l^2/\tau. \tag{17}$$

6.3.2 *Bulk Cr concentration.* The continuity equation for the Cr_i concentration C, is not as simple as (9) since Cr_i is also involved in reaction (1). The diffusion of Cr_i is assumed to be fast enough to maintain a uniform concentration and much faster than the rate of the reaction. Under these conditions, the continuity equation becomes

$$\frac{\partial C_i}{\partial t} = D_i\frac{\partial^2 C_i}{\partial x^2} - \frac{\overline{\partial C_i}}{\partial t}, \tag{18}$$

where the bar indicates spacial average. That is, because of the fast diffusion of Cr_i, it is only the global effect of the reaction that matters.

Neglecting diffusion of Cr_s, the continuity equation for the Cr_s concentration C_s is governed entirely by the rate of the reaction (1),

$$\frac{\partial C_s}{\partial t} = -\frac{C_s}{\tau_R^{(s)}} + \frac{\kappa_0^{(s)}}{\tau_R^{(s)}} C_v^{(s)}(x) C_i(t). \tag{19}$$

Fig. 1. Reactions involved in the redistribution of Cr introduced after bulk growth.

This is an alternative to and an extention of TA's continuity equation where we adopt the equilibrium vacancy picture (6), allow for the time dependence of the Cr_i concentration, and superscribe the relaxation time τ_u and the equilibrium constant κ_u with "b" for "bulk". This is done to distinguish these quantities from those associated with the formally identical surface conversion reaction, for which the parameters may be different. This equation will lead to an "outer" solution[25], which does not satisfy the boundary condition that C_i be constant at the surface. At the surface there is a boundary layer in which the outer solution connects with an "inner" solution which falls off rapidly due to finite substitutional diffusion and effects due to strain and fields. This will be neglected here but kept in mind when we estimate the vacancy diffusion length later.

The boundary condition for the Cr, concentration is prescribed by the flux as in the last section. This flux equals the net surface production of Cr, by the surface conversion reaction. There is a surface generation $\sigma_s/\tau_u^{(s)}$ of Cr_i, where σ_s is the surface concentration of Cr_s and $\tau_u^{(s)}$ is the relaxation time analogous to $\tau_u^{(b)}$ in (19) but with superscript "s" referring to the surface. σ_s is constant since we have assumed incorporation equilibrium. Thus, per unit area

$$\sigma_s = k_s C_a d_a, \tag{20}$$

where k_s is the segregation constant for Cr_s, C_a is the Cr concentration in the ambient atmosphere, and d_a is the thickness of an effective surface layer. There is also surface annihilation of Cr_s; i.e. Cr, becomes Cr_s. This process is described by a similar relaxation term, $C_i(t)d_i/\tau_u^{(s)}$, where d_i is analogous to d_a and $\tau_u^{(s)}$ is the relaxation time for this process. We find then

$$J(0, t) = -J(l, t) = v[k_i C_a - C_i(t)], \tag{21}$$

where we have defined the surface diffusion velocity v and segregation constant k_i for Cr_i as

$$v = \frac{d_i}{\tau_u^{(s)}} \tag{22}$$

and

$$k_i = k_s \frac{d_a}{d_i} \tau_u^{(s)} \tau_u^{(s)}, \tag{23}$$

to point out the similarity with the boundary conditions (10) for the problem in the last section. Any direct incorporation of interstitial Cr would only modify v in (22) and k_i in (23).

Equation (18) in its present form is not similar to equation (9), but it will be in the following two limiting cases:

(1) Bulk conversion bottleneck: If conversion from Cr_i to Cr_s in the bulk is so slow that we can neglect $(\partial C_i/\partial t)$ in (18), it becomes identical with (9) by putting $D = D_i$. The estimate (17) of D_i is

$$D_i \gg l^2/\tau_i. \tag{24}$$

However, the observed time constant is presumably $\tau_u^{(b)}$ which is associated with the slow bulk conversion reaction. Thus, $\tau_i \ll \tau_u^{(b)}$ and the estimate of the required magnitude of D_i tends to get larger. On the experimental time scale then,

$$C_i(t) = k_i C_a = C_\infty, \tag{25}$$

and the solution to (19) is

$$C_i(x, t) = \kappa_u^{(b)} C_\infty C_r^{(o)}(x) + [C_i(x, 0) - \kappa_u^{(b)} \times C_\infty C_r^{(o)}(x)] \exp(-t/\tau_u^{(b)}). \tag{26}$$

The total Cr concentration is

$$C(x, t) = C_\infty + C_i(x, t). \tag{27}$$

(2) Surface conversion bottleneck: The bulk conversion is assumed to be in equilibrium,

$$C_i(x, t) = \kappa_u^{(b)} C_r^{(o)}(x) C_i(t), \tag{28}$$

and the spacial average is

$$\bar{C}_i(t) = \kappa_u^{(b)} \bar{C}_r^{(o)} C_i(t). \tag{29}$$

Equation (18) then becomes,

$$\frac{\partial C_i}{\partial t} = \frac{D_i}{1 + \kappa_u^{(b)} \overline{C_r^{(o)}}} \frac{\partial^2 C_i}{\partial x^2}, \tag{30}$$

reducing it to the form of eqn (9). Thus we can apply to eqn (30) the criterion we have developed above for the magnitude of the diffusion constant required to insure uniform C_i eqn (17). The criterion yields

$$\frac{D_i}{1 + \kappa_u^{(b)} \overline{C_r^{(o)}}} > \gg \frac{l^2}{\tau_i}. \tag{31}$$

In this case the observed relaxation time is τ_i but one usually expects $\kappa_u^{(b)} \overline{C_r^{(o)}}$ to be much larger than unity since it is essentially the ration of C_i to C_r. So again the estimate of D_i would tend to get larger than that associated with the observed time constant. The concentration of Cr, becomes

$$C_i(t) = k_i C_a + [C_i(0) - k_i C_a] \exp(-t/\tau_i), \tag{32}$$

and the total Cr concentration is

$$C(x, t) = C_i(t)[1 + \kappa_u^{(b)} C_r^{(o)}(x)]. \tag{33}$$

6.3.3 *Estimate of* Ga *vacancy diffusion length.* No matter which of the conversion reactions is the bottleneck, a plot of $\ln[C(x, t) - C(\infty, t)]$ vs x of TA's data should yield a straight line with a slope $-L_c^{-1}$. If the assumption of vacancy equilibrium is correct the slopes should be independent of time t. The data for such a plot from TA's Figs. 1, 3, 4 and 6 are displayed in our Fig. 2. From this it is apparent that the data points for $x > 10\,\mu$m can be fitted with

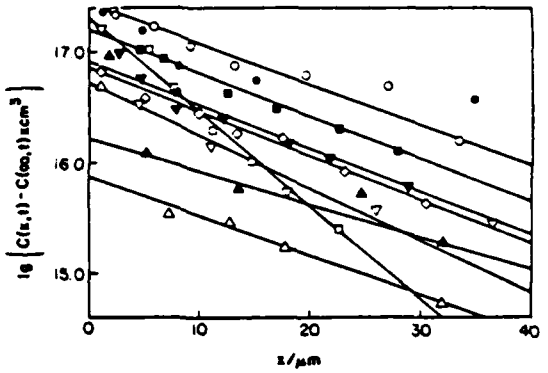

Fig. 2. Some of TA's diffusion data replotted in order to estimate the Ga vacancy diffusion length. The numbers in parenthesis refer to the figures in [14] used. (a) ● 10h, 1100°C, $L_\tau = 11.7\,\mu$m (4). (b) ○ 4h, 1100°C, $L_\tau = 11.7\,\mu$m (1, 4). (c) ■ 3h, 1100°C, $L_\tau = 11.1\,\mu$m (4). (d) ▼ 2h, 1100°C, $L_\tau = 11.1\,\mu$m (4). (e) ▲ 1h, 1100°C, $L_\tau = 14.7\,\mu$m (4). (f) □ 4h, 1000°C, $L_\tau = 5.1\,\mu$m (1). (g) ▽ 4h, 900°C, $L_\tau = 9.1\,\mu$m (1). (h) △ 4h, 800°C, $L_\tau = 12.2\,\mu$m (1). (i) ◇ 1h, 750°C, $L_\tau = 10.9\,\mu$m (6).

straight lines except possibly for the data recorded with the 900°C, 4-hr indiffusion (ling *g*). The 750°C, 1-hr outdiffusion data (line *i*) fall on a straight line all the way to the surface. This is not surprising since there is no large Cr_i surface concentration producing a large gradient in a boundary layer. All the lines except *e* and *f* yield roughly the same value of L_τ,

$$L_\tau(\mathrm{Ga}) = (11 \pm 3)\,\mu\mathrm{m}. \tag{34}$$

The two cases *e* and *f* are responsible for effectively the entire standard deviation of 3 μm. It may be argued that this value of L_τ is not precise. However, there are two important points to be made:

(1) L_τ is essentially time independent (lines *a*, *b*, *c*, *d* and *e*); and

(2) L_τ is essentially temperature independent (lines *b*, *f*, *g* and *h*).

The time independence supports the assumption of vacancy equilibrium The temperature independence is not unexpected if one considers the vacancy production to occur through the reaction (4), and the diffusion mechanism to be of the Swalin kind as discussed earlier. In this case both D_τ and β in expression (7) for L_τ contain an exponential of the activation energy to remove an atom from its substitutional site. If an additional vacancy production mechanism were present, for instance due to a high dislocation density, one would expect L_τ to decrease (β increase). We would also expect temperature dependence and some time dependence since the properties of dislocations can change, for instance by motion. This may be a reason for the anomalous cases.

6.3.4 *Estimate of interstitial* Cr *diffusion constant.* During indiffusion we have

$$C(x, t) = C(x, \infty)[1 - \exp(-t/\tau)], \tag{35}$$

where the timeconstant τ is $\tau_\mu^{(b)}$ if the bulk conversion is the bottleneck and τ_s if the surface conversion is the bottleneck. In the former case we have neglected the concentration of Cr_i compared to the equilibrium concentration of Cr_s. The condition on D_i is

$$D_i \gg l^2/\tau, \tag{36}$$

Plotting $\ln[1 - C(x, t)/C(x, \infty)]$ vs t should yield a straight line with slope $-\tau^{-1}$. In Fig. 3 we show such a plot for $x = \infty$, i.e. in the uniform bulk, where the fit is expected to be best. We used TA's Fig. 4 for indiffusion at 1100°C. The estimated straight line to fit the data points has been drawn, keeping in mind that the relative errors increase as $C(\infty, t)$ approaches $C(\infty, \infty)$. It yields $\tau = 2.1 \times 10^4$ s. In TA's work $l = 0.05$ cm so $l^2/\tau \simeq 10^{-7}$ cm^2/s. A rough lower limit for D_i would be

$$D_i(1100°\mathrm{C}) \gtrsim 10^{-5}\,\mathrm{cm}^2/\mathrm{s}. \tag{37}$$

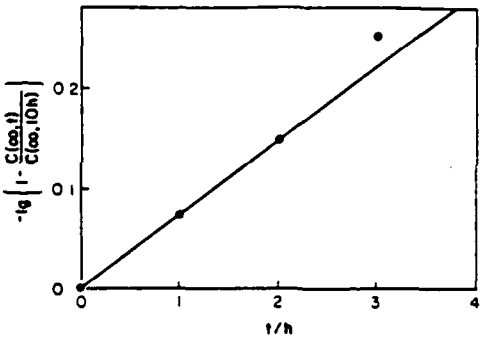

Fig. 3. TA's 1100°C bulk concentration ([14] Fig. 4) plotted as a function of time in order to estimate the associated time constant.

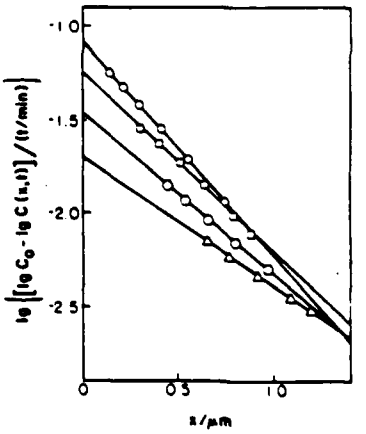

Fig. 4. KW's 850°C anneal data([19)] Fig. 2) replotted in order to estimate the As vacancy deffusion length. (a) ○ 15 min, $L_\tau = 0.38\,\mu$m. (b) □ 30 min, $L_\tau = 0.45\,\mu$m. (c) ○ 60 min, $L_\tau = 0.50\,\mu$m. (d) △ 120 min, $L_\tau = 0.63\,\mu$m.

It is interesting to compare this with the largest conceivable diffusion constant. This occurs when the diffusion is driven by optical phonons with a jump frequency equal to the phonon frequency. For interstitial diffusion in GaAs the optical phonon frequency is $f = 8 \times 10^{12} s^{-1}$. The interstitial jump distance is $\sqrt{3}\,a/4$, where a is the lattice constant (5.65 Å), and

$$D_i(\max) = a^2 f/8 \simeq 3 \times 10^{-3}\ \mathrm{cm^2/s}. \quad (38)$$

The Cr_i diffusion constant is, thus, very large and appears to be quite close to the phonon-driven limit. It is interesting at this point to recall the theory developed by Weiser[26] for interstitial diffusion in the diamond lattice. He found that one would expect some ions of intermediate size interstitially, virtually without any potential barrier between sites. He proposed that this may be the case for Cu in GaAs which would explain its diffusion behavior.

6.4 *Outdiffusion of* Cr *introduced during bulk growth*

The contrasting experimental results that we set out to study are those represented by the data of Kasahara and Watanabe (KW)[19]. These authors perform annealing experiments and study the outdiffusion of Cr from the sample. They model the result assuming substitutional diffusion and a finite surface diffusion velocity. They get good fit far from the surface with an increasing discrepancy between theory and experiment as the surface is approached.

The present model offers an alternative explanation which appears capable of accounting for the results closer to the surface. In the experiments the measured Cr was incorporated during bulk growth. That means that most of the Cr is presumably bound in relatively strong complexes, mostly as $(Cr_{Ga}D_{As})$. We suggest that the dominant redistribution mechanism is the dissociation of these complexes. Note that there is no uniform reduction of the Cr concentration. If the dissociation had occurred throughout the sample, one would expect, in view of the fast diffusion of Cr, inferred in the last section, that the reduction of the Cr concentration would extend further into the sample. The dissociation appears to be catalyzed close to the surface. The defect responsible for this is likely to be native of the GaAs crystal since the surface depletion appears in a variety of samples. The region of the outdiffusion is much thinner than the Cr peak in TA's data, which indicates that Ga vacancies are not directly involved. We therefore suggest that the arsenic vacancies are responsible for the catalysis. An As vacancy adjacent to a $(Cr_{Ga}D_{As})$ complex could very well increase the probability of dissociation which would then be described by

$$(Cr_{Ga}D_{As}) + V_{As} \rightleftarrows Cr_i + D_{As} + V_{Ga} + V_{As}. \quad (39)$$

6.4.1 *Estimate of* As *vacancy diffusion length.* By a technique similar to the one used to analyse TA's data, we can estimate the As vacancy diffusion length from KW's data. We assume that the As vacancy equilibrium is maintained. This appears reasonable since no V_{As} are consumed in the reaction (with the possible exception of the formation of divacancies). We will approximate the equilibrium vacancy profile (6) by

$$C_v^{(e)} = C_v^{(s)} \exp(-x/L_v), \quad (40)$$

since the surface is typically very V_{As} rich. In view of the rapid diffusion of Cr_i, the Cr_i formed will "immediately" result in a uniform distribution. The concentration of Cr_i will be exceedingly small and we can neglect this and the capture by V_{Ga}. With these premises the continuity equation for the total Cr concentration will be

$$\frac{\partial C}{\partial t} = -\gamma(x)C, \quad (41)$$

where $\gamma(x)$ is proportional to the As vacancy concentration. With a uniform initial concentration C_o the solution is

$$C(x, t) = C_o \exp(-\gamma(x)t), \quad (42)$$

with approximation (40) for the As vacancy concentration.

A plot of $\ln[(\ln C(x, t) - \ln C_o)/t]$ vs x should yield a straight line with slope $-L_v^{-1}$. For different times the lines should coincide; i.e. the position and slope should be time independent. We plot the data of KW's Fig. 2 in the described manner in our Fig. 4. In each case (different t) a straight line fits the points very well and we can calculate the average estimated diffusion length and the standard deviation,

$$L_v(\mathrm{As}) = 0.5 \pm 0.1\ \mu\mathrm{m}. \quad (43)$$

The standard deviation represents a reasonable error. The drift of slope and intercept may indicate the extent to which the vacancy equilibrium fails to be maintained.

7. SUMMARY

We have proposed a model for Cr impurities in GaAs that is consistent with a wide variety of experimental observations, including spectroscopic, redistribution and diffusion, and electrical data. This model does not appear to be in conflict with any reported experiments. In particular, it accounts for the excellent compensation that is achieved with Cr doping, and we can reconcile the apparently incompatible but equally reliable diffusion and annealing data that have been reported by different workers. It is also capable of interpreting the observed Cr redistribution about implants during annealing.

By using this model to reinterpret experimental work reported in the literature, we have also established new estimates of several useful parameters for both the impurity and the host crystal.

AD-A139 592 IMPURITY AND DEFECT INTERACTIONS IN GAAS(U) WASHINGTON 3/2
UNIV ST LOUIS MO SEMICONDUCTOR RESEARCH LAB
C M WOLFE ET AL. 29 FEB 84 WU/SRL-64422-22
UNCLASSIFIED N00014-80-C-0762 F/G 20/12 NL

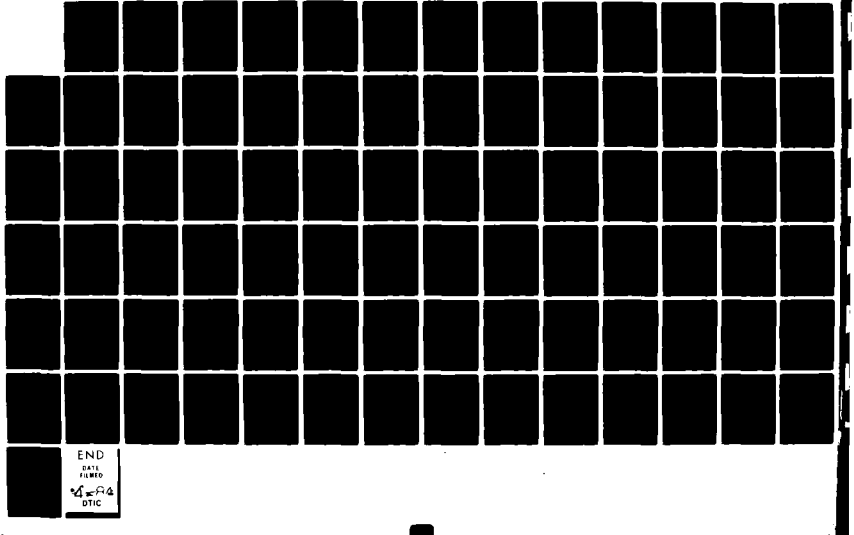

END
DATE FILMED
4-84
DTIC

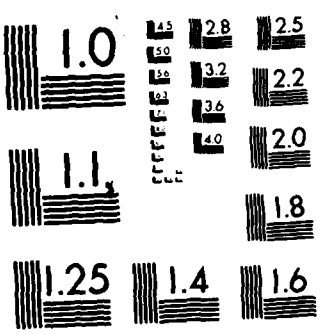

We hope that the model also will be helpful in analysing other experimental data on Cr in GaAs, such as thermal conversion of GaAs:Cr substrates and surface Cr pile-up during heat treatment, and those associated with Cr outdiffusion into epitaxial layers.

Acknowledgements—We are grateful to Dr. M. J. Cardwell for communicating experimental observations prior to publication, and to Dr. P. A. Fedders for helpful discussions. The work was supported by ONR Contracts N00014-79-C-0840 and N00014-80-C-0762.

REFERENCES

1. Rees G. J. (Ed.), *Semi-Insulating III–V Materials*, Shiva, Nottingham (1980). (a) White A. M., p. 3; (b) Eaves L., Englert T., Instone T., Uihlein C., Williams P. J. and Wright H. C., p.145; (c) Killoran N., Cavenett B. C. and Hagston W. E., p. 190; (d) Picoli G., Deveaud B. and Galland D., p. 254; (e) Favennec P. N. and L'Haridon H., p. 130; (f) Simondet F., Venger C, Martin G. M. and Chaumont J., p. 100; (g) Evans C. A., Jr., Hopkins G. C., Norberg J. C., Deline V. R., Blattner R. J., Wilson R. G., Jamba D. M. and Park Y. S., p. 138; (h) Udagawa T., Higashiura M. and Nakanisi T., p. 108; (i) Linh N. T., Huber A. M., Etienne P., Morillot G., Duchemin P. and Bonnet M., p. 206.
2. Favennec P. N., Gauneau M., L'Haridon H., Deveaud B., Evans C. A., Jr. and Blattner R. J., *Appl. Phys. Letters* **38**, 271 (1981).
3. Favennec P. N. and L'Haridon H., *Appl. Phys. Letters* **35**, 699 (1979).
4. Asbeck P. M., Tandon J., Welch B. M., Evans C. A., Jr., and Deline V. R., *IEEE Electron. Device Letters* EDL-1, 35 (1980).
5. Evans C. A., Jr., Deline V. R., Sigmon T. W. and Lidow A., *Appl. Phys. Letters* **35**, 291 (1979).
6. Magee T. J., Ormond R. D., Evans C. A., Jr., Blattner R. J., Malbon R. M., Day D. S. and Sankaran R., *Appl. Phys. Letters* **38**, 559 (1981).
7. Tuck B., Adegboyega G. A., Jay P. R. and Cardwell M. J., *Inst. Phys. Conf. Ser. No.* **45**, 114 (1979).
8. Clegg J. B., Scott G. B., Hallais J. and Mircea-Roussel A., *J. Appl. Phys.* **52**, 1110 (1981).
9. Eu V., Feng M., Henderson W. B., Kim H. B. and Whelan J. M., *Appl. Phys. Letters* **37**, 473 (1980).
10. Mullin J. B., Ashen D. J., Roberts G. G. and Ashby A., *Inst. Phys. Conf. Ser. No.* 33a, 91 (1977)
11. Brozel M. R., Butler J., Newman R. C., Ritson A., Stirland D. J. and Whitehead C., *J. Phys. C.* **11**, 1857 (1978).
12. Hobgood H. M., Eldridge G. W., Barrett D. L. and Thomas R. N., *IEEE Trans. Electron. Devices* **ED-28**, 140 (1981).
13. Broom R. F., *J. Appl. Phys.* **38**, 3483 (1967).
14. Tuck B. and Adegboyega G. A., *J. Phys. D.* **12**, 1895 (1979).
15. Deveaud B. and Favennec P. N., *Solid St. Commun.* **24**, 473 (1977).
16. Huber A. M., Morillot G., Linh N. T., Favennec P. N., Deveaud B. and Toulouse B., *Appl. Phys. Letters* **34**, 858 (1979).
17. Andre E. and Le Duc J. M., *Matl Res. Bull.* **4**, 149 (1969).
18. Cronin G. R. and Haisty R. W., *J. Electrochem. Soc.* **111**, 874 (1964).
19. Kasahara J. and Watanabe N., *Jap. J. Appl. Phys.* **19**, L151 (1980).
20. Cardwell M. J., private communication.
21. Nichols K. H., Yee C. M. L. and Wolfe C. M., *Solid St. Electron* **23**, 109 (1980).
22. Rohdin H., Muller M. W. and Wolfe C. M., *J. Electron. Matl* **11**, 517 (1982).
23. Swalin R. A., In *Atomic Diffusion in Semiconductions* (Edited by D. Shaw), p. 65. Plenum Press, London and New York (1973).
24. Carslaw H. S. and Jaeger J. C., *Conduction of Heat in Solids*. 2nd Edn, p. 114. Oxford University Press (1959).
25. Bender C. M. and Orszag S. A., *Advanced Mathematical Methods for Scientists and Engineers*, Chap. 9. McGraw-Hill, New York (1978).
26. Weiser K., *Phys. Rev.* **126**, 1427 (1962).

B.3 Effect of electric fields on Cr redistribution at GaAs surfaces[a)]

Camellia M. L. Yee, P. A. Fedders, and C. M. Wolfe
Semiconductor Research Laboratory, Washington University, St. Louis, Missouri 63130

(Received 21 October 1982; accepted for publication 30 November 1982)

During the annealing of ion-implanted Cr-doped GaAs, Cr often redistributes and accumulates at the surface. Although this behavior has been attributed to strain fields and other mechanisms, the widths of these accumulation regions suggest that electric fields due to surface states are a limiting factor in Cr redistribution. For this reason we have developed a thermodynamic model for Cr redistribution which takes into account the electric field due to surface states. A qualitative fit to SIMS data on annealed unimplanted GaAs samples can be obtained with this model. We have also used applied voltages during annealing to modify the amount of band bending and Cr buildup at the surface. This experiment indicates that the accumulated ions are positively charged. We conclude from these experiments that electric fields play a significant role in the redistribution of Cr at GaAs surfaces.

PACS numbers: 72.80.Ey, 73.20.Hb, 82.65.Dp

There has been considerable recent interest in the redistribution of Cr in GaAs during annealing processes. A prominent feature of this redistribution is often an accumulation of Cr at the surface. This pileup has been observed under a variety of conditions, and attributed to As vacancies[1-3] or encapsulant strains.[1,4-9] To examine these possibilities it is useful to consider the characteristic lengths associated with Cr buildup. In many cases the cause of a physical phenomenon can be determined from the various length scales associated with different mechanisms. For example, the estimated diffusion length of As vacancies is about 0.5 μm.[10] Although the characteristic lengths associated with surface strain can change with conditions, it is also a long range phenomenon compared to the smaller regions of Cr pileup observed at the surface. In this letter we examine the shortest length scale associated with Cr accumulation, which is apparently due to the electrostatic field caused by surface states.

The characteristic lengths associated with surface Cr buildup as determined from secondary ion mass spectroscopy (SIMS) data in recent literature[6-9,11-14] and from our own annealing experiments are plotted in Fig. 1 as a function of annealing temperature. The characteristic lengths L_i were extracted from the SIMS data with the expression[15]

$$N(r) = n_i \coth^2(r/L_i + \alpha), \tag{1}$$

where $N(r)$ is the impurity profile, n_i the intrinsic carrier concentration, r the distance from the surface, and

$$\alpha = \coth^{-1}\sqrt{n(0)/n_i}. \tag{2}$$

This is the equilibrium profile expected[16] for positively charged impurities in the presence of an electric field due to surface states. Since Cr-doped substrates are nearly intrinsic at typical annealing temperatures,[17] the intrinsic Debye length L_D was also plotted as a function of temperature for comparison. As can be seen in Fig. 1, all the data points lie above or near the intrinsic Debye length curve. This suggested to us that electric fields due to surface states is the limiting factor in the redistribution of Cr near the surface.

To examine this possibility in more detail, an equilibrium thermodynamic model was developed for the behavior of Cr near the surface. Basically, this model consists of a fixed surface charge and charged Cr species that can redistribute. Space charge neutrality is assumed so that the surface charge is exactly compensated by the net charge within the crystal. We also assume a surface area that is large with respect to the sample thickness, so that the problem is one dimensional. The free energy of the system is then minimized to produce an equilibrium distribution of Cr.

The Helmholtz free energy F of a system with two Cr charged species capable of redistributing was examined and is given by

$$\begin{aligned} F = & -q\int V(r)[N^+(r) - N^-(r)]\,dr \\ & + \frac{q}{2}\int \{[N^+(r) - N_0^+] - [N^-(r) - N_0^-]\}v(r-r')\{[N^+(r') - N_0^+] - [N^-(r') - N_0^-]\}dr'dr \\ & + kT\int [N^+(r)\ln N^+(r) + N^-(r)\ln N^-(r)]\,dr + \int \mu[N^+(r) + N^-(r)]\,dr, \end{aligned} \tag{3}$$

where $V(r)$ is the potential due to surface states, $v(r-r')$ the Coulomb potential, μ the chemical potential, r the distance from the surface, $N^+(r)$ the concentration of positive Cr ions, N_0^+ the bulk concentration of positive Cr ions, $N^-(r)$ the concentration of negative Cr ions, and N_0^- the bulk concentration of negative Cr ions. The first integral on the right-hand side of Eq. (3) is the energy due to surface states, while the second term corresponds to the Coulomb interaction among all charges. The third integral is the entropy contribution to the free energy, and the last term is the chemical potential energy.

[a)] Research supported by the Office of Naval Research under Contract No. N00014-80C-0762.

 0003-6951/83/040377-03$01.00

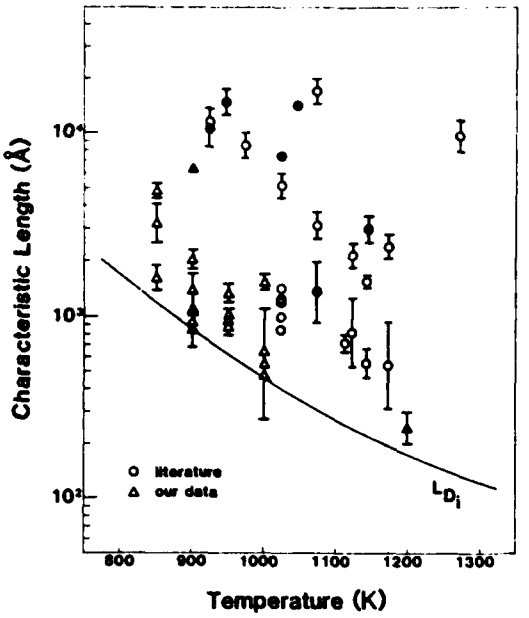

FIG. 1. Comparison of characteristic lengths L, obtained from recent literature and our own experiments with the intrinsic Debye length L_{D_i}. Open symbols indicate encapsulated samples and closed symbols indicate unencapsulated samples.

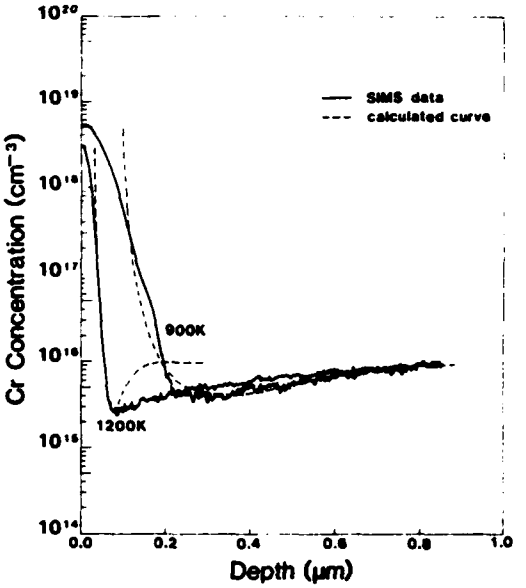

FIG. 2. SIMS data for 900 and 1200-K curve fitted to the two charged species model.

To determine the equilibrium situation, Eq. (3) for the free energy was minimized everywhere. This resulted in a nonlinear differential equation which has an exact solution:

$$t = \frac{1}{2}\int_{x}^{x_0} \frac{dy}{\sqrt{y^3 + (R-1)y^2 \ln y + Ry - (R+1)y^2}}, \quad (4)$$

where

$$t = r/\sqrt{2}L_{D_i} \quad (5)$$

is the normalized distance from the surface,

$$x = N^+(r)/N_0^+ \quad (6)$$

is the normalized Cr concentration,

$$x_0 = x(0) \quad (7)$$

is the normalized surface Cr concentration, and

$$R = N_0^+/N_0^- . \quad (8)$$

The profile for two Cr ions has a pileup at the surface and a dip near the surface in total Cr concentration due to the depletion of $N^-(r)$ near the surface.

To determine how well this model corresponds to an experimental situation, unencapsulated GaAs substrates were annealed in an As overpressure using a boat of InAs held at the same temperature upstream. The InAs has about an order of magnitude higher dissociation pressure than GaAs and has been previously used[18] to stabilize the GaAs surface during annealing. SIMS analyses done on two of these samples are shown in Fig. 2. One of the interesting features of this experimental data is that the characteristic length at 900 K is much larger than that at 1200 K. This behavior is opposite to that expected for As vacancies or surface strain, but in agreement with the temperature dependence of the intrinsic Debye length. The characteristic length at 900 K, however, is about a factor of 7 too large. Both samples show a dip below the bulk level in their profiles which is in qualitative agreement with the behavior for two Cr ions. The total depletion in the 1200-K data, however, is too large to be explained by surface states alone.

The dashed lines in Fig. 2 indicate an attempt to fit Eq. (4) to the experimental data. The ratio R in the model determines the magnitude of the dip when only two charged Cr species are present. If there are neutral Cr atoms N^0 in the material, however, they will tend to mask the dip since SIMS analysis shows the total Cr concentration. The presence of neutral Cr would have no effect in Eq. (4) since it acts only as an added amount of Cr distributed evenly over the sample. It does give us, however, an added parameter that can be adjusted to fit the experimental data. Also, the condition of charge neutrality allows us to determine the surface charge density N_S. The fit shown in Fig. 2 for the 900-K SIMS data corresponds to an R of 5.8×10^{-4}, a surface charge density N_S of 2.8×10^{12} cm^{-2}, and a neutral Cr concentration N^0 of 5.9×10^{15} cm^{-3}. The fit for the 1200-K SIMS data corresponds to an R of 2.0×10^{-4}, and N_s of 5.5×10^{11} cm^{-2}, and an N^0 of 7.4×10^{15} cm^{-3}. The values of N_s obtained in this process can be compared to a previously determined[15] value at 1000 K of 5.1×10^{11} cm^{-2}.

As shown in Fig. 2 the agreement between the model and the experimental data is only qualitative. The reference point used for the curve fitting process was located at the point where the Cr concentration equaled that of the bulk. The calculated curve obtained by this method indicates that the surface on both samples should begin further in the material. This difference in surface location could be due to the presence of an oxide layer on these samples. The presence of surface artifacts is known to cause matrix effects that affect the accuracy of SIMS analysis near the surface.[19,20] Part of the cleaning process for these samples involved a 5:1:1 H_2SO_4:H_2O_2:H_2O etch, which invariably leaves a thin oxide layer on GaAs surfaces. To support this conjecture, the data

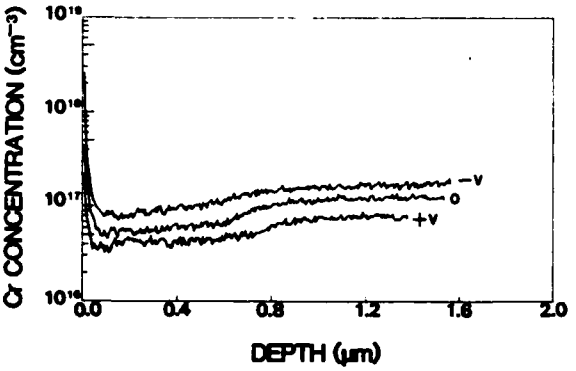

FIG. 3. Cr redistribution as a function of applied voltage.

indicate a thinner oxide layer for the sample annealed at 1200 K which could be explained by greater oxide reduction in a H_2 ambient at higher temperatures.

To investigate further the role that electric fields play in the redistribution of Cr at the GaAs surface, samples were annealed with different applied voltages. Due to the surface states present there is a built-in potential at the surface which causes band bending. By applying a voltage to the surface, the built-in electric field can be altered and the amount of band bending reduced or increased accordingly. If Cr redistribution is electric field dependent, then larger electric fields and band bending due to negative bias should cause larger positively charged Cr pileups at the surface. Conversely, positive applied voltage should reduce the amount of Cr pileup.

For this purpose a metal-oxide-semiconductor (MOS) structure was used to apply various voltages to different areas of the substrate during annealing. Anneals were performed from 800 to 1000 K for two different time periods at each temperature. The SIMS data shown in Fig. 3 are typical of the results obtained. As can be seen, a negative bias on the MOS structure produced a larger buildup of Cr near the surface, while a positive bias reduced the buildup of Cr. This behavior is in agreement with the expected behavior for positively charged Cr. In all the samples, however, the Cr depletion beyond the surface is larger than can be attributed to the effect of surface states. The variation in Cr bulk levels shown in Fig. 3 is probably due to inhomogeneity in bulk Cr concentration among the areas used for voltage contacts.

In conclusion, our results indicate that the electric field caused by surface states is a limiting factor in the redistribution of Cr at the GaAs surface. This is supported by the following observations: (1) the lower limit on the characteristic lengths of the surface regions is very close to the intrinsic Debye length; (2) a thermodynamic model for the redistribution of Cr in the presence of surface states predicts the general shape of the Cr profile; (3) the application of electric fields to the surfaces during annealing changes the magnitude of the Cr buildup.

[1]V. Eu, M. Feng, W. B. Henderson, and H. B. Kim, Appl. Phys. Lett. 37, 473 (1980).
[2]J. B. Clegg, G. B. Scott, J. Hallais, and A. Mircea-Roussel, J. Appl. Phys. 52, 1110 (1981).
[3]T. J. Magee, K. S. Lee, R. Ormond, C. A. Evans, Jr., R. J. Blattner, and C. Hopkins, Appl. Phys. Lett. 37, 635 (1980).
[4]M. Feng, S. P. Kwok, V. Eu, and B. W. Henderson, J. Appl. Phys. 52, 2990 (1981).
[5]A. M. Huber, G. Morillot, N. T. Linh, P. N. Favennec, B. Deveaud, and B. Toulouse, Appl. Phys. Lett. 34, 858 (1979).
[6]C. A. Evans, Jr., V. R. Deline, T. W. Sigmon, and A. Lidow, Appl. Phys. Lett. 35, 291 (1979).
[7]T. J. Magee, K. S. Lee, R. Ormond, R. J. Blattner, and C. A. Evans, Appl. Phys. Lett. 37, 447 (1980).
[8]C. A. Evans, Jr., C. G. Hopkins, J. C. Norberg, V. R. Deline, R. J. Blattner, R. G. Wilson, D. M. Jamba, and Y. S. Park, *Semi-Insulating III-V Materials* (Shiva, Orpington, 1980), p. 138.
[9]F. Simondet, C. Venger, G. M. Martin, and J. Chaumont, *Semi-Insulating III-V Materials* (Shiva, Orpington, 1980), p. 100.
[10]H. Rohdin, M. W. Muller, and C. M. Wolfe, J. Phys. Chem. Solids (to be published).
[11]Y. S. Park (unpublished).
[12]P. K. Vasudev, R. G. Wilson, and C. A. Evans, Jr., Appl. Phys. Lett. 37, 308 (1980).
[13]T. J. Magee, R. D. Ormond, C. A. Evans, Jr., R. J. Blattner, R. M. Malbon, D. S. Day, and R. Sankaran, Appl. Phys. Lett. 38, 559 (1981).
[14]P. N. Favennec, M. Gauneau, H. L'Haridon, B. Deveaud, C. A. Evans, Jr., and R. J. Blattner, Appl. Phys. Lett. 38, 271 (1981).
[15]K. H. Nichols, R. E. Goldwasser, and C. M. Wolfe, Appl. Phys. Lett. 36, 601 (1980).
[16]C. M. Wolfe and K. H. Nichols, Appl. Phys. Lett. 31, 356 (1977).
[17]K. H. Nichols, Ph.D. thesis, Washington University, 1979.
[18]J. Woodall, H. Rupprecht, C. Ransome, T. I. Chappel, and G. Wicks (unpublished).
[19]J. W. Coburn and Eric Kay, Crit. Rev. Solid State Sci. 4, 561 (1974).
[20]Richard E. Honig, Thin Solid Films 31, 89 (1976).

Solid-State Electronics Vol . No . pp . 1984
Printed in Great Britain

0038-1101/84 $3.00 + .00

B.4 CHROMIUM REDISTRIBUTION IN ION-IMPLANTED GaAs†

CAMELLIA M. L. YEE, K. B. NICHOLS,‡ P. A. FEDDERS, and C. M. WOLFE
Washington University, St. Louis, MO 63130, U.S.A.

and

Y. S. PARK
Air Force Avoinics Laboratory, Wright-Petterson Air Force Base, OH 45433, U.S.A.

(*Received* 12 *May* 1983)

Abstract—In this paper we attempt to find systematic differences between the annealing conditions for ion implanted GaAs where Cr is observed to redistribute and the conditions where it does not. For samples where Cr redistribution was observed, we also separate electrical from chemical and/or strain interactions. The results indicate that electrical interactions are at least a limiting factor and in most cases a dominant factor in Cr redistribution. For this reason it appears that Cr redistribution in ion implanted samples can be minimized or eliminated by annealing at temperatures such that the background free carrier concentration screens out any internal electric fields.

NOTATION

Symbol	*Unit*
$N(x)$	cm^{-3}
N	cm^{-3}
$n(X)$	cm^{-3}
n	cm^{-3}
n_0	cm^{-3}
n_i	cm^{-3}, μm
x	μm
L	μm
L_i	μm
d	μm
α	μm^{-2}
β	μm^{-2}
γ	dimensionless
ψ	volt
ϵ	farad/cm
k	joule/K
T	K
q	coul.

INTRODUCTION

During the annealing of ion-implanted Cr-doped GaAs, two major Cr redistribution effects are typically, but not always, observed: one is a pile-up of Cr at the outer surface; the other is some type of redistribution and depletion of Cr in the vicinity of the ion implanted region. The pile-up at the outer surface has been atrributed to As vacancy gradients[1–3], encapsulant strains[1, 4–9], or surface states[10]. The redistribution in the implanted region has been blamed on implantation damage[3, 6–8, 11–14] or a combination of physical and chemical effects[15]. Although these explanations in many instances may be correct, the problem of Cr redistribution in general is not very well understood.

†Research supported by the Office of Naval Research under Contract No. N00014-80C-0762.

‡Now at M.I.T. Lincoln Laboratory, Lexington, MA 02173, U.S.A.

This is not particularly surprising. Ion implanted samples are annealed with and without encapsulants, at different temperatures and pressures, with and without an As overpressure, and under a variety of other conditions. Thus, in some annealing experiments there may be several phenomena producing Cr redistribution, while in others there may be no driving force for Cr migration. Because of this diversity in experimental conditions and potential complexity of causes, it could be very useful to understand the physical mechanisms underlying Cr redistribution. In this paper we attempt to achieve this understanding and provide some guidance for reducing or eliminating the problem of Cr migration.

GENERAL APPROACH

For these purposes we assume that all the Cr redistribution observed by us and others could be caused by some combination of electrical, chemical, or strain interactions between the Cr and the rest of the sample. On the basis of this assumption we then take the following approach: (1) First, we investigate systematic differences between experimental conditions where Cr redistributes and where it does not. (2) Then, we attempt to separate electrical from chemical and/or strain interactions. In principle, item (2) can be achieved due to the different characteristic lengths associated with the possible interactions.

To follow this procedure, it is first necessary to determine the background free carrier concentrations in Cr-doped GaAs samples at typical annealing temperatures. Fig. 1 shows the results of high temperature Hall measurements on three encapsulated Cr-doped GaAs samples. The carrier concentrations were determined from the Hall data using an appropriate four-band model[16]. Also shown, as a dashed line, is the calculated[16] intrinsic carrier concentration for GaAs. A comparison of the data with the

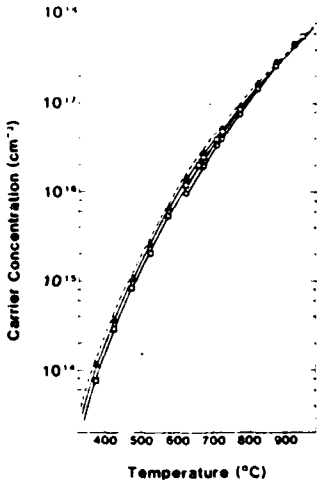

Fig. 1. Measured carrier concentrations in Cr-doped GaAs as a function of annealing temperature. The dashed line is the calculated intrinsic carrier concentration.

dashed line indicates that it is not unreasonable to assume that the background carrier concentration in Cr-doped GaAs is intrinsic under most annealing conditions. Unless indicated otherwise, we make this assumption in the remainder of this work.

Figure 2 shows secondary ion mass spectroscopy (SIMS) data on a, more or less, typically perverse ion-implanted sample in which Cr-redistribution has occurred. In this particular Cr-doped sample, Mg was implanted and annealed for a relatively short time (compared to Cr equilibrium) at a temperature such that the intrinsic concentration, n_i, was at the level indicated. The background Cr concentration, N_{Cr}, is also shown. The other symbols in Figure 2 will be discussed later. Disregarding the bumps and wiggles in the Cr profile, the salient features we are concerned with here are the Cr pile-up at the outer surface and

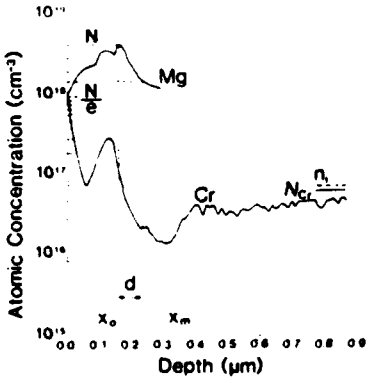

Fig. 2. SIMS profile showing the redistribution of Cr in a GaAs sample ion implanted with Mg. The intrinsic carrier concentration at the annealing temperature, n_i, is indicated by the horizontal dashed line. The uniform Cr concentration before annealing, N_{Cr}, is indicated by the horizontal solid line.

the depletion of Cr under the Mg implant out to about 0.3 μm. As we will discuss later, the Cr peak in the implanted region is probably a nonequilibrium artifact. We will first examine the Cr pile-up at the outer surface.

Surface pile-up

Since almost all of the SIMS data in the literature and all of our data indicate a pile-up of Cr at the outer surface in annealed samples, we could not systematically determine the conditions under which it does not occur [item (1) above]. We, therefore, proceeded to separate possible electrical from chemical and/or strain effects [item (2)]. For this purpose we assumed that the Cr profiles have the form,

$$N(x) = n_0 \coth^2(x/L + \gamma), \tag{1}$$

where x is the distance from the surface, n_0 is the background carrier concentration, L is the characteristic length associated with the profile, and

$$\gamma = \coth^{-1}[(N(0)/n_0)^{1/2}]. \tag{2}$$

This is the equilibrium profile expected[10] for Cr ion migration in an electric field due to surface states with opposing charge. Equations (1) and (2) were derived[17] for otherwise intrinsic material where n_0 is the intrinsic carrier concentration, n_i, and L is the intrinsic Debye length, L_i, where

$$L_i = (2\epsilon kT/q^2 n_i)^{1/2}. \tag{3}$$

The characteristic lengths for surface pile-up, L, were determined from eqns (1) and (2) for a number of our own samples and those of others[6–9, 11, 12, 18] by taking the surface Cr concentrations, $N(0)$, from the SIMS data and assuming that the background carrier concentrations at the annealing temperatures, n_0, were as indicated in Fig. 1. These characteristic lengths are plotted in Fig. 3 versus the Debye lengths at the annealing temperatures, as determined from eqn (3) for each sample. As can be seen, all of the characteristic lengths are either close to or larger than the Debye lengths.

Since the characteristic lengths associated with chemical and strain fields are large compared to those due to electric fields, these data indicate that the Cr surface pile-up is typically due to a combination of electric, chemical, and or strain effects. (Experimental problems, such as surface oxides, beam angle, etc., can produce larger apparent characteristic lengths and cannot be excluded). Also, considering that the characteristic lengths approach the intrinsic Debye lengths but do not go below it, the data indicate that the interaction with surface states is the limiting factor in the redistribution of Cr at the surface. This conclusion is supported by other experiments[19]

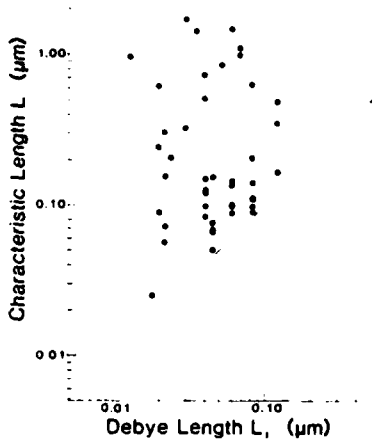

Fig. 3. Characteristic lengths associated with surface Cr pile-up versus intrinsic Debye lengths at the annealing temperature.

IMPLANTED REGION REDISTRIBUTION

A number of annealing experiments have been performed where the Cr in the ion implanted region does not redistribute. For this reason we were able to investigate the differences between these conditions and those where redistribution is observed [item (1) in the approach]. In Fig. 4 we have plotted the peak implanted ion concentration, N, (as determined from SIMS data) divided by the background carrier concentration, n_0, (as obtained from Fig. 1) as a function of annealing temperature for a number of our own and other samples[3, 4, 7, 8, 11–14, 18, 20–24]. The solid circles indicate those samples where Cr was observed to redistribute in the implanted region, while the open circles show those where no redistribution was observed. As can be seen, the dashed line, $N/n_0 = 1$, separates the data fairly well.

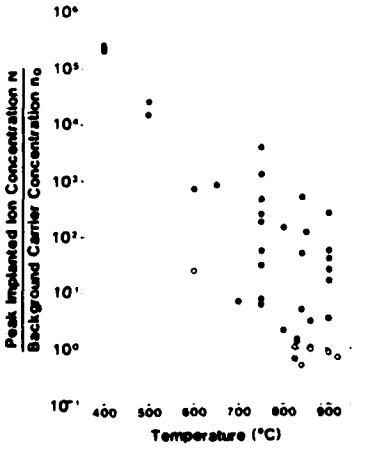

Fig. 4. Peak implanted ion concentration divided by background carrier concentration as a function of annealing temperature. The solid circles indicate those samples where the Cr redistributed, while the open circles show those where no redistribution was observed.

Qualitatively, this behavior can be understood in the following way: (1) During the annealing process the implanted ions are activated, producing free carriers. (2) If the free carrier concentrations produced by the implanted ions are greater than the background carrier concentrations, the carriers diffuse in the concentration gradients, producing internal electric fields in equilibrium. The Cr ions can then migrate in these electric fields, as well as in any chemical or strain fields. (3) If the free carrier concentrations produced by the implanted ions are less than the background carrier concentrations, there are no free carrier gradients and no associated electric fields. That is, the implanted ions are screened by the background carriers. The Cr ions can then only migrate in chemical or strain fields. The data in Fig. 4 indicate that, for most of the samples (not including the high concentration B implants since B is isoelectronic to Ga) *where there is no electric field in the implanted regions, there is no* Cr *redistribution.*

For the samples above the line $N/n_0 = 1$ where Cr redistribution was observed, we now attempt to separate electrical from chemical and/or strain effects [item (2)]. We first assume that the activated implanted ion profile is given by,

$$N(x) = N \exp[-\alpha(x - x_0)^2], \tag{4}$$

where N is the peak ion concentration, α is related to the straggle, and x_0 is the range. We further assume that the free carrier concentration is,

$$n(x) = n \exp[-\beta(x - x_0)^2] + n_0, \tag{5}$$

where n is the peak carrier (electron or hole) concentration, β is related to the standard deviation, and n_0 is the background carrier concentration.

In equilibrium the electrostatic potential produced by the diffusion of free carriers is,

$$\psi(x) = \frac{kT}{q} \ln[n(x)/n_0], \tag{6}$$

and Poisson's equation is,

$$\frac{d^2\psi(x)}{dx^2} = \frac{q}{\epsilon}[n(x) - N(x) - n_0], \tag{7}$$

assuming the free carriers are electrons.

Using eqns (4), (5) and (7) the electric field is maximum at the points x_m determined from,

$$(x_m - x_0)^2 = \frac{\ln(N/n)}{\alpha - \beta} \tag{8}$$

To find N/n in eqn (8) we take the second derivative of eqn (6), which is equal to eqn (7), and evaluate the equality at x_0. The result, assuming β is approxi-

mately equal to α, is,

$$\frac{n}{N} \simeq -\frac{1}{2}\left(\frac{n_0}{N}+\frac{2\alpha\epsilon kT}{q^2N}-1\right) + \frac{1}{2}\left[\left(\frac{n_0}{N}+\frac{2\alpha\epsilon kT}{q^2N}\right)^2+4\frac{n_0}{N}\right]^{1/2}. \quad (9)$$

and β can then be determined from,

$$1+\frac{N}{n_0}\exp\left[\frac{-\alpha\ln\left(\frac{N}{n}\right)}{\alpha-\beta}\right]=\frac{2\beta}{\alpha-\beta}\ln\left(\frac{N}{n}\right), \quad (10)$$

which is obtained from eqns (5), (6) and (8).

Figure 2 illustrates how measured values of $|x_m-x_0|$ are obtained from typical SIMS data and also how values of N and α are determined to calculate values of $|x_m-x_0|$. The points of maximum electric field, x_m, are the regions where the largest amount of Cr depletion is expected. N is taken as the peak concentration and α is found from the distance d where N decreases to $1/e$ of its value by,

$$\alpha=\frac{1}{d^2}. \quad (11)$$

Although few activated ion profiles and no resulting free carrier profiles are Gaussian, as assumed in eqns (4) and (5), the process indicated above represents a reasonably accurate method for characterizing the experimental data. We have calculated exact values of $|x_m-x_0|$ for several profiles using a thermodynamic model[19], and found that this approximate model is accurate to within about 10%.

Figure 5 shows measured versus calculated values of $|x_m-x_0|$ for our own and other[3, 4, 7, 8, 12–14, 20–24] samples. The measured values were taken from the Cr depletion regions farthest from the surface to minimize surface effects. As can be seen, all the measured and calculated values agree to within an order of magnitude or less. We believe this correlation is reasonably good considering the approximate analysis, the potential experimental error, and the possibility of strain in many of the samples.

The data in Fig. 5 were plotted assuming that the background carrier concentrations were intrinsic, $n_0=n_i$, as indicated in Fig. 1 for the Cr-doped samples we measured. There is some indication[5] that, for samples with higher Cr concentrations, the Cr increases the carrier concentrations above the intrinsic values. Figure 6 shows data for the same samples as in Fig. 5, except that $|x_m-x_0|$ was calculated assuming a Cr-increased background, $n_0=n_i+N_{Cr}$. The agreement between measured and calculated values in Fig. 6 is about the same as in Fig. 5, except that fewer points fall balow the line in Fig. 6. This suggests that the electrical interaction is a limiting factor for Cr redistribution in ion implanted regions. Not all of the Cr, however, is expected to yield increases in carrier concentration. Thus, the true picture is probably somewhere between Figs. 5 and 6.

We have not included in Figs. 5 and 6 all of the available data. There are cases for which $|x_m-x_0|$ cannot be measured due to limitations imposed by time and temperature. For long annealing times or high temperatures all mobile charged Cr moves out of the ion implanted region. This leaves one large depletion region superimposed on the depletion region near the surface. In general, this situation cannot be distinguished from that due to surface states alone and $|x_m-x_0|$ cannot be measured.

CONCLUSIONS

In conclusion, our results indicate that, although in some cases chemical and/or strain interactions are important factors, electrical interactions are at least a limiting factor and in most instances a dominant factor in Cr redistribution. Almost all of the SIMS data exhibit Cr pile-up at the outer surface. In this region the electric fields due to surface states appear to be a limiting factor in Cr migration. When this is the only factor, it should be possible to reduce this migration by annealing at temperatures where the

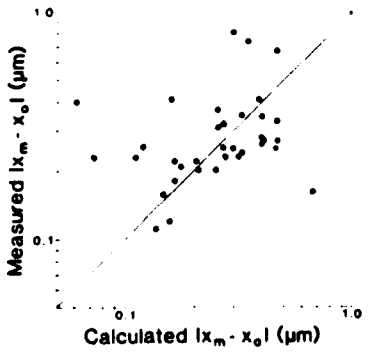

Fig. 5. Measured extent of Cr depletion in ion-implanted regions versus calculated positions of maximum electric field. The data are plotted assuming the background carrier concentration is intrinsic: $n_0=n_i$.

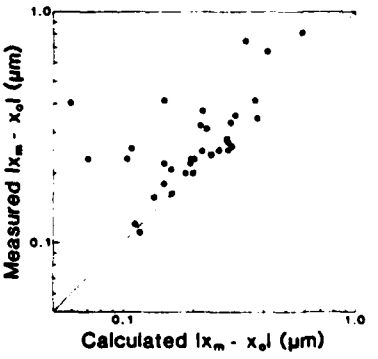

Fig. 6. Measured extent of Cr depletion in ion-implanted regions versus calculated positions of maximum electric field. The data are plotted assuming the Cr adds to the background carrier concentration: $n_0=n_i+N_{Cr}$.

surface states are screened by free charge carriers. In the ion implanted regions, many samples show no Cr redistribution. The annealing conditions for most of these samples are such that the background carrier concentrations are greater than the peak implanted ion concentrations. Thus, it should be possible to reduce or eliminate Cr redistribution by using Fig. 1 to determine the appropriate temperatures for annealing.

REFERENCES

1. V. Eu, M. Feng, W. B. Henderson and H. B. Kim, *Appl. Phys. Lett.* **37**, 473 (1980).
2. J. B. Clegg, G. B. Scott, J. Hallais and A. Mircea-Roussel, *J. Appl. Phys.* **52**, 1110 (1981).
3. T. J. Magee, K. S. Lee, R. Ormond, C. A. Evans, Jr., R. J. Blattner and C. Hopkins, *Appl. Phys. Lett.* **37**, 635 (1980).
4. M. Feng, S. P. Kwok, V. Eu and B. W. Henderson, *J. Appl. Phys.* **52**, 2990 (1981).
5. A. M. Huber, G. Morillot, N. T. Linh, P. N. Favennec, B. Deveaud and B. Toulouse, *Appl. Phys. Lett.* **34**, 858 (1979).
6. C. A. Evans, Jr., V. R. Deline, T. W. Sigmon and A. Lidow, *Appl. Phys. Lett.* **35**, 291 (1979).
7. T. J. Magee, K. S. Lee, R. Ormond, R. J. Blattner and C. A. Evans, *Appl. Phys. Lett.* **37**, 447 (1980).
8. C. A. Evans, Jr., C. G. Hopkins, J. C. Norberg, V. R. Deline, R. J. Blattner, R. G. Wilson, D. M. Jamba and Y. S. Park, *Semi-Insulating III–V Materials*, p. 138. Shiva, Orpington (1980).
9. F. Simondet, C. Venger, G. M. Martin and J. Chaumont, *Semi-Insulating III–V Materials*, p. 100. Shiva, Orpington (1980).
10. K. H. Nichols, R. E. Goldwasser and C. M. Wolfe, *Appl. Phys. Lett.* **36**, 601 (1980).
11. P. K. Vasudev, R. G. Wilson and C. A. Evans, Jr., *Appl. Phys. Lett.* **37**, 308 (1980).
12. T. J. Magee, R. D. Ormond, C. A. Evans, Jr., R. J. Blattner, R. M. Malbon, D. S. Day and R. Sankaran, *Appl. Phys. Lett.* **38**, 559 (1981).
13. T. J. Magee, H. Kawayoshi, R. D. Ormond, L. A Christel, J. F. Gibbons, C. G. Hopkins, C. A. Evans, Jr. and D. S. Day, *Appl. Phys. Lett.* **39**, 906 (1981).
14. M. Feng, V. Eu, H. Kanber and W. B. Henderson, *J. Electron. Mat.* **10**, 973 (1981).
15. M. N. Yoder, *Semi-Insulating III–V Materials* p. 281. Shiva, Orpington (1980).
16. K. H. Nichols, Camellia M. L. Yee and C. M. Wolfe, *Solid-St. Electron.* **23**, 109 (1980).
17. C. M. Wolfe and K. H. Nichols, *Appl. Phys. Lett.* **31**, 356 (1977).
18. P. N. Favennec, M. Gauneau, H. L'Haridon, B. Deveaud, C. A. Evans, Jr. and R. J. Blattner, *Appl. Phys. Lett.* **38**, 271 (1981).
19. Camellia M. L. Yee, P. A. Fedders and C. M. Wolfe, *Appl. Phys. Lett.* **42**, 377 (1983).
20. S. G. Liu, E. C. Douglas, C. P. Wu, C. W. Magnee, S. Y. Narayan, S. T. Jolly, F. Kolondra and S. Jain, unpublished.
21. H. Kanber, M. Feng and J. M. Whelan, *Appl. Phys. Lett.* **40**, 960 (1982).
22. A. Masuyama, M. A. Nicolet, I. Golecki, J. L. Tandon, D. K. Sadana and J. Washburn, *Appl. Phys. Lett.* **36**, 749 (1980).
23. Y. K. Yeo, Y. S. Park and R. Kwor, *J. Appl. Phys.* **53**, 1815 (1982).
24. Y. K. Yeo, Y. S. Park, F. L. Pedrotti and Byung Doo Choe, *J. Appl. Phys.* **53**, 6148 (1982).
25. R. Zucca, *J. Appl. Phys.* **48**, 1987 (1977).

C. INCORPORATION OF IMPURITIES AND DEFECTS

Inst. Phys. Conf. Ser. No. 65: Chapter 6
Paper presented at Int. Symp. GaAs and Related Compounds, Albuquerque, 1982

C.1 Incorporation of amphoteric impurities in high purity GaAs

T.S. Low, B.J. Skromme, and G.E. Stillman

Electrical Engineering Research Laboratory,
Materials Research Laboratory, and Coordinated Science Laboratory
University of Illinois at Urbana-Champaign, Urbana, Illinois 61801

Abstract The incorporation of Group IV impurities as donors and as acceptors in high purity epitaxial GaAs has been investigated using photothermal ionization spectroscopy and variable temperature photoluminescence to detect donors and acceptors respectively. Samples from several sources of high purity LPE, $AsCl_3$-VPE, AsH_3-VPE, MOCVD, and MBE grown GaAs were measured to establish the typical residual impurities present and their relative concentrations. For AsH_3-VPE, MOCVD and MBE GaAs, impurity incorporation data are presented as a function of III/V ratio. The relative incorporation of amphoteric impurities as donors and acceptors is compared with the model of Teramoto (1972) for LPE and its extension to $AsCl_3$-VPE by Ashen et al. (1975).

1. Introduction

The Group IV impurities, namely C, Si, Ge, Sn, and Pb, are expected to behave either as donors or acceptors in GaAs, depending on whether they substitute on Ga or As sites. It is well known that the relative incorporation as donors and acceptors is different for different elements, growth techniques, and growth conditions (e.g. growth temperature, III/V ratio, etc.) Much of this information has come from doping experiments which rely on Hall effect data and the tacit assumption that only changes in dopant incorporation are important in determining changes in carrier concentration and 77 K mobility. The direct measurement of the concentrations of individual impurity species would afford a clearer picture of impurity incorporation, particularly at low concentrations. To this end, photothermal ionization spectroscopy (described in detail by Stillman et al. (1977)), and low temperature photoluminescence have been used to measure the concentrations of donors and acceptors, respectively, in high purity GaAs prepared by a wide variety of growth techniques. The relative donor concentrations were determined from the 1s-2p(m=-1) peak amplitudes at high magnetic fields using the identifications of Wolfe et al. (1976) for Pb, Sn, Se, and of Low et al. (1982 a and b) and Ozeki et al. (1977) for X_1=Si, X_2=S, and X_3=Ge. The relative acceptor concentrations were estimated from the relative amplitudes of the (D^o-A^o) peaks at 2 K under 1 mW excitation from an Ar^+ laser, using the identifications in Ashen et al. (1975). Absolute donor and acceptor concentrations could then be determined using the total N_D and N_A calculated, under the assumption that the shallow impurities dominate the ionized impurity scattering, from the 77 K Hall effect data by the method of Wolfe et al. (1970).

0305-2346/83/0065-0515 $02.25

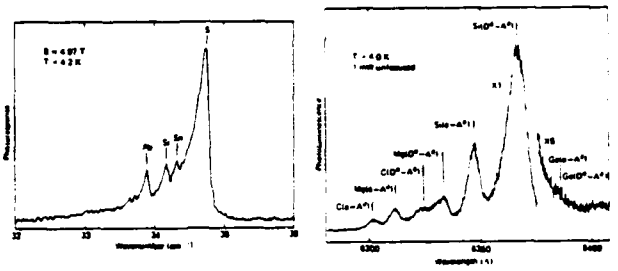

Fig. 1 (a) Photothermal ionization and (b) photoluminescence spectra of Hewlett Packard LPE sample.

2. Amphoteric Impurities in LPE GaAs

The residual shallow impurities in high purity undoped LPE samples from seven different sources were measured (see Skromme et al. 1983a). The photothermal ionization and photoluminescence spectra for the Hewlett Packard sample are shown in Fig. 1 (a) and (b), and are typical of the spectra of the other samples measured. The characteristic LPE residual donors, Pb, X_1=Si, Sn, and X_2=S are present at concentrations of 0.28, 0.22, 0.12 and 1.54 x10^{14}cm^{-3} respectively. The dominance of X_2=S is usual for both graphite (Skromme et al. 1983a) and silica (Cooke et al. 1978) boat grown LPE GaAs. The characteristic LPE residual shallow acceptors, C, Mg, Si and Ge are present at approximate concentrations of 0.13, 0.18, 1.0 and 0.03 x10^{14}cm^{-3} respectively.

The photothermal ionization and photoluminescence data for the LPE samples measured consistently indicated that the Group IV impurities Pb and Sn incorporate preferentially as donors while Si, Ge, and C incorporate preferentially as acceptors. The incorporation of Pb in GaAs grown by $AsCl_3$-VPE is small (Wolfe et al. 1976a) and although Pb doping experiments have associated Pb with a peak coincident with that of Mn deep acceptors, it seems likely that this can be explained by traces of Mn present in the Pb dopant (Bebb et al 1972), and that Pb may not incorporate as an acceptor in GaAs. It should be noted however that the Mn acceptor peak was observed in most of the LPE samples measured. The Pb and Sn donor peaks were sometimes larger in the spectra of the other LPE samples than that shown in Fig. 1 but were always dominated by sulfur. In the two Cornell LPE samples in which Sn was most prominent (nearly equal in concentration to S) traces of Sn acceptors were detected (via the neutral Sn acceptor bound exciton line), but no Sn acceptors could be detected in any of the other LPE samples. It was impossible to determine the Sn acceptor concentration so from this data the incorporation ratio $[Sn_{Ga}]/[Sn_{As}]$ can only be said to be much greater than one. The X_1=Si donor peak was sometimes absent from the photothermal ionization spectra and this correlated with a much smaller levels of the usually dominant Si acceptor detected by photoluminescence. In the three samples for which both Si donor and acceptor concentrations could be accurately measured, (each of which was grown at 700°C) incorporation ratios of $[Si_{Ga}]/[Si_{As}]$ = 0.16, 0.19, and 0.22 were determined. The X_3=Ge donor peak has never been observed in LPE GaAs but small concentrations (0.01-0.10 x10^{14}cm^{-3}) of Ge acceptors were observed in most of the LPE samples measured. The detection limit for X_3=Ge donors in the sample with the largest Ge acceptor concentration can be estimated as about 0.02x10^{14}, and so $[Ge_{Ga}]/[Ge_{As}]$ must be less than about 0.2. Early doping experiments suggested that C donors may contribute a photothermal ionization peak

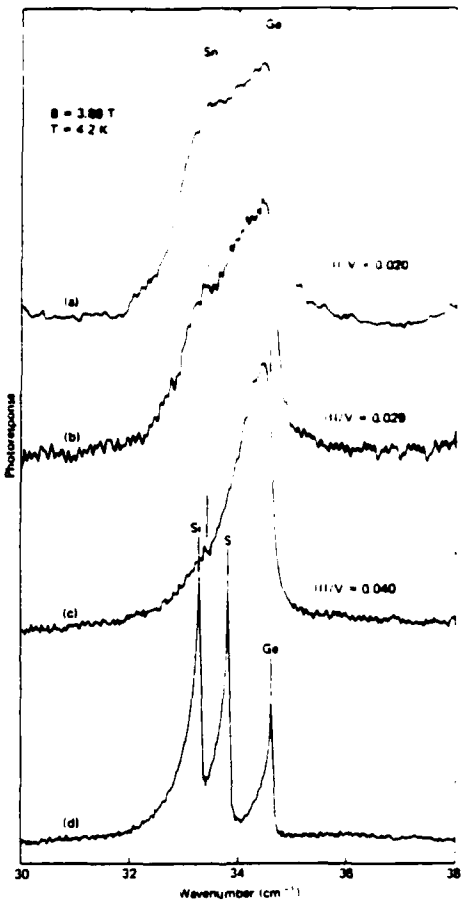

Fig. 2 Photothermal ionization spectra for the Toshiba MOCVD samples (top three plots) in which Sn and Ge donor incorporation was suppressed by increasing the III/V ratio. Lower plot is for the Motorola $AsCl_3$-VPE reference sample.

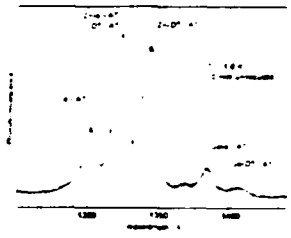

Fig. 3 Photoluminescence spectrum for Motorola $AsCl_3$-VPE sample.

coincident with the X_3-Ge peak (Wolfe et al. 1976). There is evidence to suggest that C does not incorporate as a donor at least in $AsCl_3$-VPE GaAs (Ozeki et al. 1977), but even assuming that C donors do contribute such an X_3 peak, the detection limit for X_3 donors together with the largest concentration of C acceptors detected determine an upper bound on $[C_{Ga}]/[C_{As}]$ in LPE GaAs of about 0.02.

These observations of the relative incorporation of the Group IV impurities $[IV_{Ga}]/[IV_{As}]$ are in qualitative agreement with the well established behavior of Si, Ge and Sn as dopants in LPE deduced from Hall effect data, and have been predicted quantitatively for these impurities in terms of Ga and As activities and the free energy difference $\Delta G_{A/B}$ between IV_{Ga} and IV_{As} site occupation (Teramoto 1972) as:

$$\log ([IV_{Ga}]/[IV_{As}]) = \log (X_{As}^{l}/X_{Ga}^{l}) + \varepsilon/T$$

where ϵ is determined by $\Delta G^{\circ}_{A/B}$ and the heats of solution ΔH^{ℓ}_{Ga} and ΔH^{ℓ}_{As}. The melt mole fractions X^{ℓ}_{As} and X^{ℓ}_{Ga} can be determined at a given growth temperature from the liquidus data of Hall (1963). Using the $\Delta G_{A/B}$ values for Si, Ge, and Sn calculated by Teramoto and the typical growth temperature of 700°C we obtain $[Si_{Ga}]/[Si_{As}] = 0.16$, $[Ge_{Ga}]/[Ge_{As}] = 0.034$, and $[Sn_{Ga}]/[Sn_{As}] = 4.7$, which are in good agreement with our observed results above.

Following Teramoto and using the tetrahedral covalent radii of Pauling (1960) one can calculate $\Delta G_{A/B}$ for both C and Pb as +14.75 kcal/mole and -28.33 kcal/mole, respectively. For a growth temperature of 700°C, we obtain incorporation ratios of $[C_{Ga}]/[C_{As}] = 6.4\times10^{-7}$ and $[Pb_{Ga}]/[Pb_{As}] = 3.0\times10^{+3}$. These numbers should be taken as very approximate in view of the inadequacy of equilibrium thermodynamics to describe the non-equilibrium process of crystal growth, and of the way in which $\Delta G_{A/B}$ is calculated and its sensitivity to choice of covalent radii, but they are in agreement with the observation of Pb as exclusively donors and of C exclusively as acceptors in GaAs. The physical interpretation of these results is, since the "size" of the Ga site is larger than that of As, the

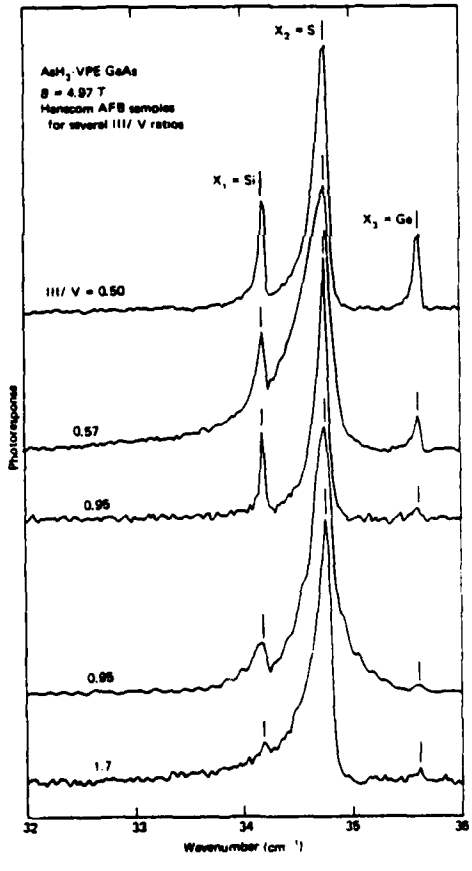

Fig. 4 Photothermal ionization spectra for AsH_3-VPE samples showing suppression of Group IV donors Si and Ge with increasing III/V ratio.

lattice strain energy contribution to $\Delta G^{\circ}_{A/B}$ then forces the smaller C onto As (acceptor) sites, and forces the larger Pb onto Ga (donor) sites.

3. Amphoteric Impurities in $AsCl_3$-VPE GaAs

The residual shallow impurities in several high purity undoped $AsCl_3$-VPE samples from seven different sources were measured. The bottom photothermal ionization spectrum in Fig. 2 for the Motorola sample shows the characteristic $AsCl_3$-VPE residual donors X_1=Si, X_2=S, and X_3=Ge, which are present at concentrations of 0.47, 0.53, and 0.27 $x10^{14}$ cm^{-3} respectively. These same residual donors were observed in the other samples although Si was sometimes more and Ge less prominent. Because of its very high purity the peaks in this sample are extremely well resolved, and so at a given magnetic field it was used as a reference for peak identifications in many of the other samples described in this work. The photoluminescence spectrum for this sample in Fig. 3 shows the typically prominent residual acceptor Zn (0.51 $x10^{14}$ cm^{-3}) and smaller concentrations of C and Ge acceptors (0.17 and 0.10 $x10^{14}$ cm^{-3}). Residual Si acceptors were not detected in this sample but were detected in trace amounts in some of the other samples measured. Residual Ge acceptors were frequently observed at approximately this same concentration and always dominated the traces of Si acceptors when the latter were present. The observed preferential incorporation of Si as donors rather than acceptors is in agreement with the general absence of Si acceptors in the photoluminescence data of Ashen et al. (1975) for undoped $AsCl_3$-VPE GaAs, and is in qualitative agreement with their prediction, under the typical $AsCl_3$-VPE growth conditions of $T_G \approx 750°C$ and $P(AsCl_3) = 6 \times 10^{-3}$ atm, that $[Si_{Ga}]/[Si_{As}] = 1.6 \times 10^{3}$. The arguments of Ashen et al. can be extended to the other Group IV impurities, using the $\Delta G_{A/B}$ values calculated in the manner of Teramoto, giving incorporation ratios which scale for a given growth temperature with those calculated for LPE. We obtain then $[C_{Ga}]/[C_{As}]=1.2x10^{-2}$, $[Ge_{Ga}]/[Ge_{As}]=3.7x10^{+2}$, $[Sn_{Ga}]/[Sn_{As}]=3.9x10^{+4}$, and $[Pb_{Ga}]/[Pb_{As}] = 1.9x10^{+7}$ for the above $AsCl_3$-VPE growth conditions. The measured concentrations Si and Ge donors and acceptors indicate that the calculated incorporation ratios for these elements are substantially too large. These ratios correctly predict however, the conduction type (n or p) when Ge, Si, Sn, Pb (Wolfe et al. 1976a) and C (Ozeki et al, 1977) are used as dopants in $AsCl_3$-VPE, and the dominance observed here of Si and Ge donors over acceptors. In the samples measured which have comparable Si and Ge donor concentrations, they also correctly predict the observed dominance of Ge acceptors over Si acceptors.

4. Amphoterics Impurites in AsH_3-VPE GaAs

The residual shallow impurities in high purity undoped AsH_3-VPE samples from three different sources were determined and these measurements are discussed in more detail by Skromme et al. (1983b). The three residual donors X_1=Si, X_2=S, and X_3=Ge were observed in the samples from each source with X_2=S always dominant, while C and Zn were the dominant shallow acceptors. Both Si and Ge acceptors were observed at low concentrations in the University of Illinois samples but were absent in all the samples from the other two sources. The most striking behavior with respect to Group IV impurities was observed in the Hanscom AFB samples grown under otherwise similar conditions but varying the III/V ratio (i.e. $P(HCl)/P(AsH_3)$). The photothermal ionization spectra of these samples in Fig. 4 show the steady decrease in Group IV donor incorporation (X_1=Si and

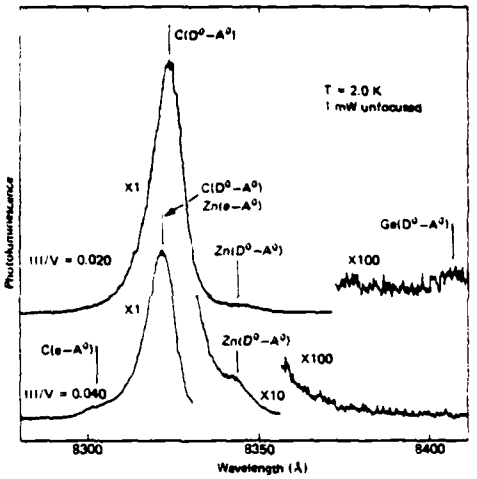

Fig. 5 Photoluminescence spectra for Toshiba MOCVD samples showing decrease of Ge acceptors with increasing III/V ratio.

X_3=Ge) relative to Group VI donor incorporation (X_2=S) as the III/V ratio is increased, until the Group IV donors are barely detectable at III/V = 1.7. A similar but less dramatic trend was observed in photoluminescence for the C_{As} to Zn_{Ga} acceptor incorporation ratio. The ratio $[C_{As}]/[Zn_{Ga}]$ varied from 3.8 to 11 as the III/V ratio was increased from 0.50 to 1.7. These data are consistent with the idea that the gas phase stoichiometry influences the relative impurity incorporation through the relative concentrations of Ga and As vacancies (incorporation sites) on the growing surface. Even in the sample grown with the highest III/V ratio however, neither Si nor Ge acceptors could be detected.

5. Amphoteric Impurities in MOCVD GaAs

High purity undoped MOCVD samples from four different sources were measured and some of this data is decribed in more detail by Low et al (1983c). In all the samples measured X_3=Ge was the dominant residual donor while smaller concentrations of X_1=Si, Sn, X_2=S, and rarely Pb donors were also observed. The dominant residual shallow acceptor was usually C, but Zn was usually prominent and occasionally exceeded C in concentration. Traces of Ge acceptors were occasionally detected. The photothermal ionization spectra of three samples from Toshiba, all grown under similar conditions (T_G = 660°C) but with varying III/V ratio (i.e. P(TMGa)/P(AsH_3)) are shown in the upper three curves Fig. 2. The only two residual donors detected in these samples were Sn and Ge, both from Group IV. The N_D values determined from Hall data steadily decreased from 17.3 to 11.2 to 6.6 x10^{14} cm^{-3} (while N_A remained essentially constant at 4.3, 4.4 and 4.1 x10^{14} cm^{-3}) as the III/V ratio increased from 0.020 to 0.029 to 0.040 respectively. This behavior is similar to that observed in the AsH_3-VPE samples in that Group IV donor incorporation is supressed by increasing the gas phase III/V ratio, and might be interpreted in terms of vacancy incorporation site availability in the same way. It is interesting to note that the Sn donor concentration seems to decrease more rapidly than that of Ge with increasing III/V ratio. No trend was observed in the ratio $[C_{As}]/[Zn_{Ga}]$ (which assumed the values 36, 26, and 38, respectively) as the III/V ratio was increased. Finally, the concentration of Ge acceptors decreased from 6.5 x10^{11} cm^{-3} to 3.6 x10^{11} cm^{-3} to undetectable as the III/V ratio increased, (see Fig. 5) while, consistent with the expected relative vacancy concentrations the

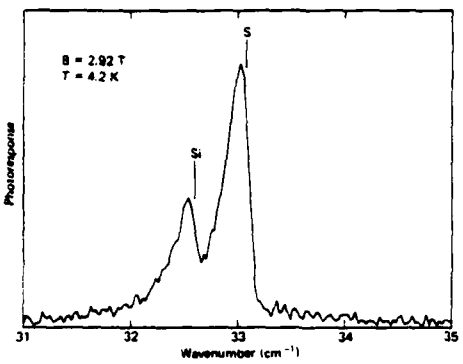

Fig. 6 Typical photothermal ionization spectrum for the Bell Labs MBE samples (grown with P_{As}/P_{Ga}=15).

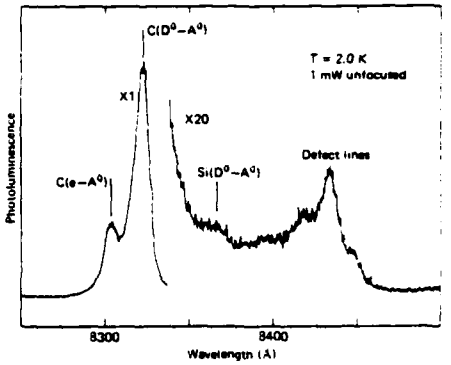

Fig. 7 Photoluminescence spectrum for Bell Labs MBE sample grown with smallest P_{As}/P_{Ga} =15 showing a trace of Si acceptors.

$[Ge_{Ga}]/[Ge_{As}]$ ratio increased from 2.3×10^3 to 3.1×10^3 to $\gtrsim 4 \times 10^3$ respectively. The increase in concentration of both Ge donors and acceptors with decreasing III/V ratio (increasing $P(AsH_3)$) is consistent with the suggestion that the source of the residual impurity Ge in MOCVD GaAs may be the AsH_3 (possibly in the form of GeH_4).

6. Amphoteric Impurities in MBE GaAs

High purity elemental As source grown MBE samples from four sources were measured and some of this data is discussed in more detail by Low et al. (1982 a and d). The dominant and usually the only residual donor detected these samples was X_2=S but the necessity of using Si or Sn dopants to achieve the n-type conduction required for the photothermal ionization measurements would mask their presence as residuals. No donor peak attributable to C was observed in any of these samples but C was the only shallow acceptor detected (with one exception noted below). Several Si doped samples grown at Bell Labs using various growth temperatures (T_G = 600-650°C) and various Ga to As pressure ratios (P_{As}/P_{Ga} = 15 to 25 with P_{Ga} and P_{Si} held constant) were measured, but no strong trends were observed in impurity incorporation. Figure 6 is a photothermal ionization spectrum which is typical of these samples. A small peak not visible in the other Bell samples coincident with Si acceptor (D°-A°) (see Fig. 7) recombination was observed in the sample grown with the lowest P_{As}/P_{Ga}, which is consistent with the expected highest As site availability for Si incorporation.

7. Conclusions

In conclusion, the relative incorporation of the Group IV impurities in high purity GaAs prepared by a variety of growth techniques has been measured. The model of Teramoto (1972) for LPE and its extension of $AsCl_3$-VPE by Ashen et al. (1975) are in qualitative agreement with the observations for all the Group IV elements. In particular the large lattice strain energy contributions to $\Delta G_{A/B}$ for Pb and C are consistent with the failure to conclusively observe C donors or Pb acceptors in

epitaxial GaAs grown by any technique. Finally, the III/V ratio dependences of Group IV incorporation for AsH_3-VPE, MOCVD, and MBE are in qualitiative agreement with the expected influence on concentrations of Ga and As vacancy sites available for impurity incorporation.

The authors gratefully thank the many contributors of samples and in particular; C A Stolte and D M Collins of Hewlett Packard, T H Miers of Motorola, S Tiwari and L F Eastman of Cornell, C M Wolfe of Washington U, T J Roth of University of Illinois, J K Kennedy of Hanscom AFB, T Nakanisi and T Udagawa of Fujitsu, P D Dapkus of Rockwell, and J C M Hwang of Bell Laboratories.

References

Ashen D J, Dean P J, Hurle D T J, Mullin J B, White A M, and Greene P D, 1975, J. Phys. Chem Solids 36, pp 1041-1053

Bebb H B and Williams E W in Semiconductors and Semimetals, edited by R K Willardson and A C Beer (Academic Press 1972) Vol 8, pp 321-419

Cooke R A, Hoult R A, Kirkman R K, and Stradling R A, 1978, J. Phys. D. 11, pp 945-953

Hall R N, 1963, J Electrochem. Soc. 110 p 385

Low T S, Stillman G E, Collins D M, Wolfe C M, Tiwari S, and Eastman L F, 1982a, Appl. Phys. Lett. 40, p 1034

Low T S, Stillman G E, Nakanisi T, Udagawa T, Wolfe C M, 1982b, Appl. Phys. Lett. 1982b 41, pp 183-185

Low T S, Skromme B J, Stillman G E, Dapkus P D Hess K L, Manasevit H M, 1983c J. Electronic Materials (to be published)

Low T S, Stillman G E, Morkoç H, Cho A Y, and Calawa A R, 1982d, Appl. Phys. Lett. 40, p 611

Ozeki M, Kitahara K, Nakai K, Shibatomi A, Dazai K, Okawa S, and Ryuzan O, 1977, Jpn. J. Appl. Phys. 16, pp 1617-1622

Pauling L, The Nature of the Chemical Bond 3rd edition (Cornell University Press 1960), p 246

Skromme B J, Low T S, Stillman G E, 1983a, GaAs and Related Compounds, Albuquerque 1982 (Inst. of Physics London 1983) (to be published)

Skromme B J, Low T S, Roth T J, Stillman G E, Abrokwah J K, Kennedy J K, 1983b, J. Electronic Materials (to be published)

Stillman G E, Wolfe C M, and Dimmock J O, in Semiconductors and Semimetals, edited by R K Willardson and A C Beer (Academic, New York 1977), Vol. 12 pp 169-290

Teramoto I, 1972 J Phys. Chem. Solids 33, pp 2089-2099

Wolfe C M, Stillman G E, and Korn D M, GaAs and Related Compounds, St Louis, 1976, Conf. Ser. No. 33b (Institute of Physics, London, 1977) pp 120-128

Wolfe C M, Stillman G E, and Dimmock J O, 1970, J. Appl. Phys. 41, 504

C.2 EPITAXIAL GROWTH OF GaAs IN THE PRESENCE OF H_2S AND H_2O

In this section we present the results of a study undertaken to determine the interactions between or complexing of multiple dopants in GaAs. The impurities initially studied are sulfur and oxygen. To examine possible interactions, experiments involving the growth and characterization of samples homogeneously and inhomogeneously doped with H_2O and/or H_2S were undertaken. The inhomogeneously doped layers provide self-calibrating samples for subsequent analysis.

C.2.1 HOMOGENEOUSLY DOPED LAYERS

All of the homogeneously doped layers were grown on Cr doped, semi-insulating substrates oriented 2° off {100} towards {110}. An extensive series of growth runs were performed using H_2S(g) diluted to 11 ppm as the only doping source. This series of runs yielded the expected result that sulfur is a well-behaved shallow donor in GaAs. The variation of carrier concentration (given by the effective distribution coefficient) with H_2S flow rate is shown in Fig. 1. Doping levels from $3x10^{15}cm^{-3}$ to $3x10^{17}cm^{-3}$ were reproducibly obtained.

Another series of runs was performed using only H_2O as the doping source. The input partial pressure of H_2O was controlled by a constant temperature bath. The dopant was transported into the reactor by passing H_2 over a bed of solid H_2O for those runs performed with the temperature bath at less than $0^{\circ}C$, and by bubbling H_2 through liquid H_2O for those runs

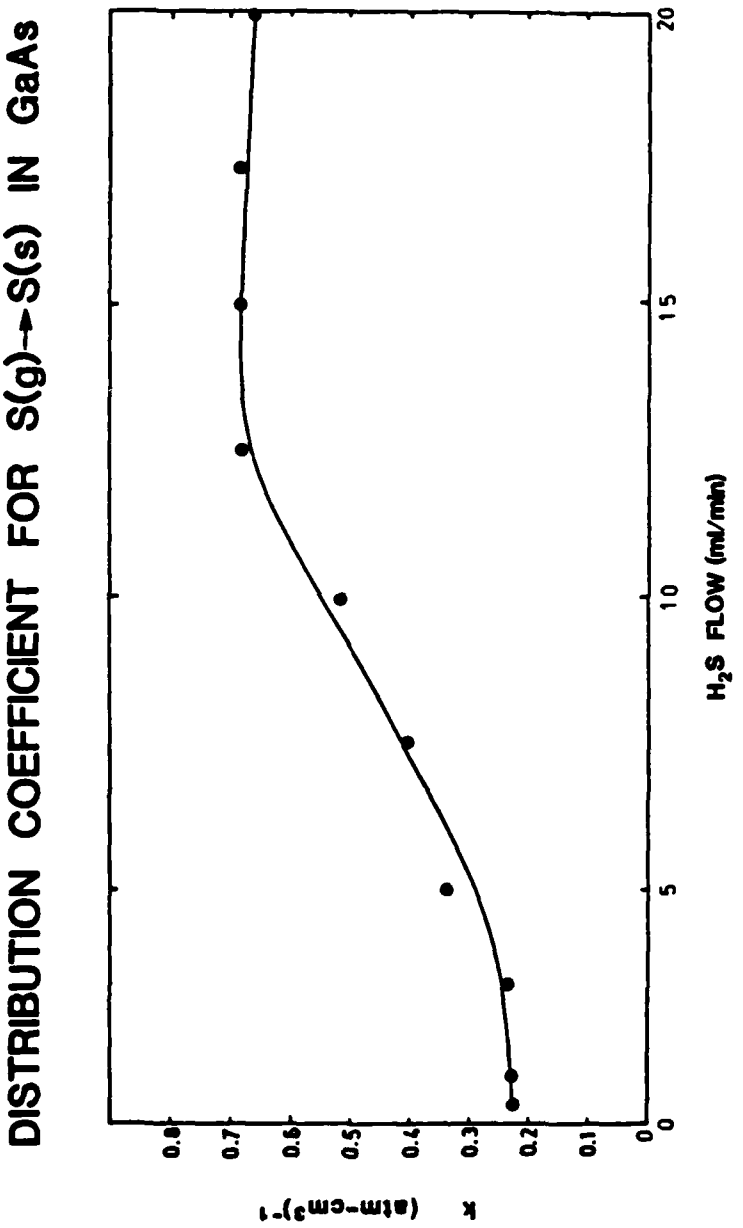
DISTRIBUTION COEFFICIENT FOR S(g)→S(s) IN GaAs
K (atm-cm³)⁻¹
0.8
0.7
0.6
0.5
0.4
0.3
0.2
0.1
0
5
10
15
20
H₂S FLOW (ml/min)

Figure 1

performed with the temperature bath at greater than $0^{\circ}C$. The results of the H_2O doping for the temperature range between $-78^{\circ}C$ and $+24^{\circ}C$ were quite striking. For each run the resulting layer was highly compensated with carrier concentrations ranging from $1x10^{14}cm^{-3}$ at $-78^{\circ}C$ to $8x10^{12}cm^{-3}$ at $24^{\circ}C$.

Growth runs were also performed in which the layers were simultaneously doped with H_2S and H_2O. A series of runs was performed to determine the effect of H_2 flow rate over the $H_2O(s)$. The H_2S flow rate used was 7.5 ml/min and the H_2O source was maintained at a temperature of $-78^{\circ}C$. Fig. 2 shows the effect that varying the gas flow over the $H_2O(s)$ has on the carrier concentration obtained from van der Pauw[1] measurements at 300K and 77K. From these data, two effects are demonstrated.

The first effect to be noticed is the increase in carrier concentration with an increase in flow rate over the H_2O. The second effect can be seen in the freeze-out of carriers at 77K. The last column of Fig. 2 shows the difference between the carrier concentrations at 300K and 77K for each of the flow rates given. This shows that the concentration of carriers freezing out is linearly dependent on the flow rate. Such behavior is indicative of a deep donor.

The effect of increasing the partial pressure of H_2O in the system is similar to increasing the flow rate of H_2 through the H_2O, although a definite upper limit to the obtainable carrier concentration is evidenced. Layers were grown with an H_2S flow of 7.5 ml/min and a H_2+H_2O flow of 5.0 ml/min. The temperature of the H_2O was varied from layer to layer

SULFUR/OXYGEN DOPED HOMOGENEOUS LAYERS

H_2+H_2O flow (ml/min)	concentration (cm^{-3}) n_{300}	n_{77}	$n_{300}-n_{77}$
5	2.5×10^{16}	2.0×10^{16}	0.5×10^{16}
10	3.3×10^{16}	2.2×10^{16}	1.1×10^{16}
15	5.0×10^{16}	3.6×10^{16}	1.4×10^{16}

H_2S flow 7.5 (ml/min)

Figure 2

over the range from -78°C to 24°C. Fig. 3 shows the 300K carrier concentration versus H_2O temperature and partial pressure[2]. At the low end of the temperature range (-78°C), the carrier concentration is about $3x10^{16}cm^{-3}$ which is the same as for layers grown in the absence of H_2O. In the high temperature range the carrier concentration is relatively insensitive to changes in H_2O temperature and remains constant at about $2x10^{17}cm^{-3}$.

C.2.2 SELF-CALIBRATING LAYERS

The self calibrating layer structure used in this work is shown in Fig. 4. N_{D1} and N_{D2} are the dopants added to the layer; in this case N_{D1} and N_{D2} are due to H_2S and H_2O, respectively. The layer is structured into five regions. Regions I and V are the calibration regions in which the chemical and electrical properties of each dopant may be determined independent of any interactions with the other dopant. Regions II and IV are the transition regions for dopants D2 and D1, respectively, which contain the information on how the chemical and electrical concentrations change as a function of concentration of the dopant being switched on or off. Region III is the region in which both dopants are at their maximum levels and the effects of any interactions or complexing should be greatest. Routine analysis of self-calibrating layers consists of SIMS profiling to determine the chemical composition of the layer and C-V profiling to determine the free carrier concentration. The C-V analysis was

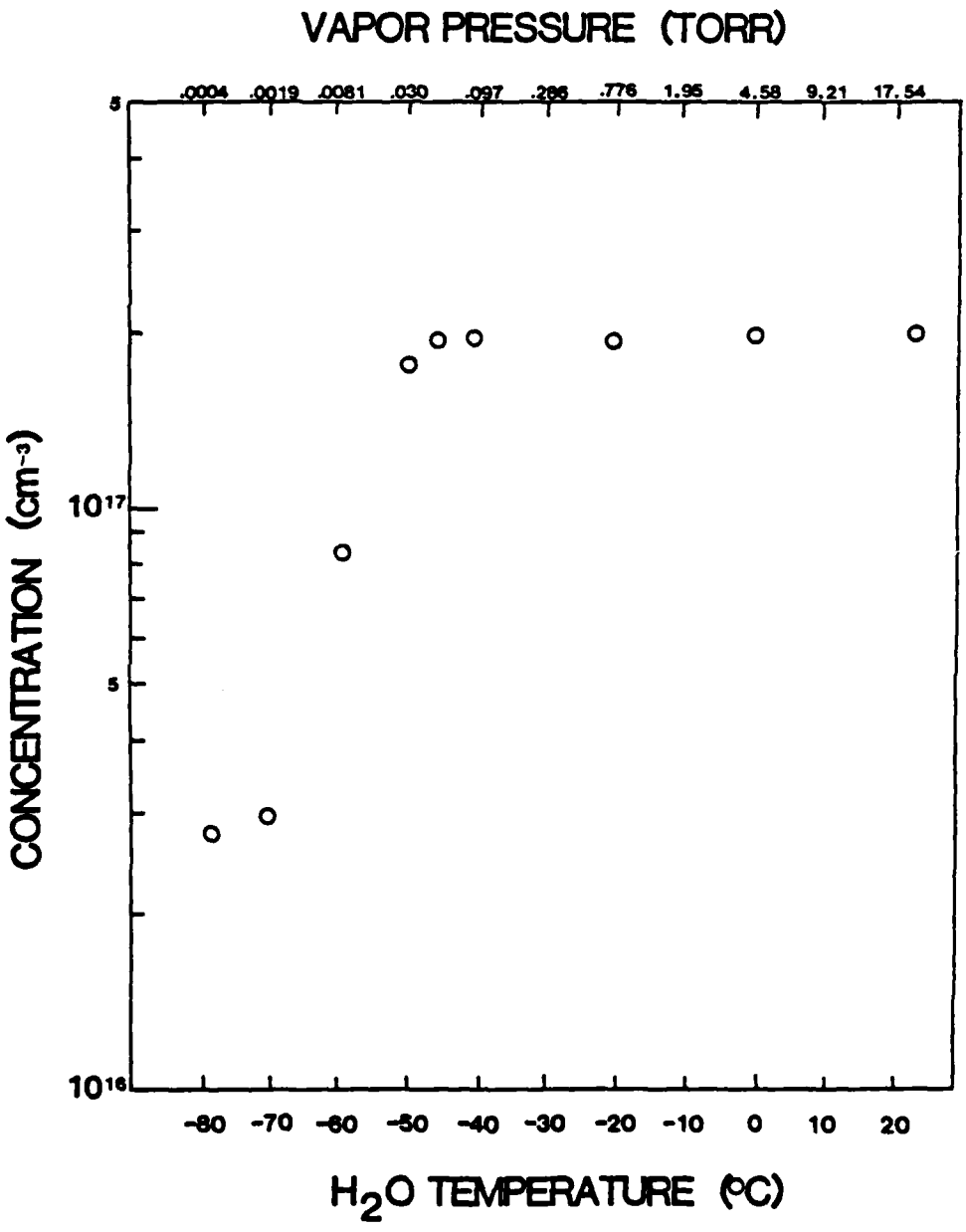

Figure 3. 300K van Der Pauw carrier concentration for layers grown with various levels of H_2O.

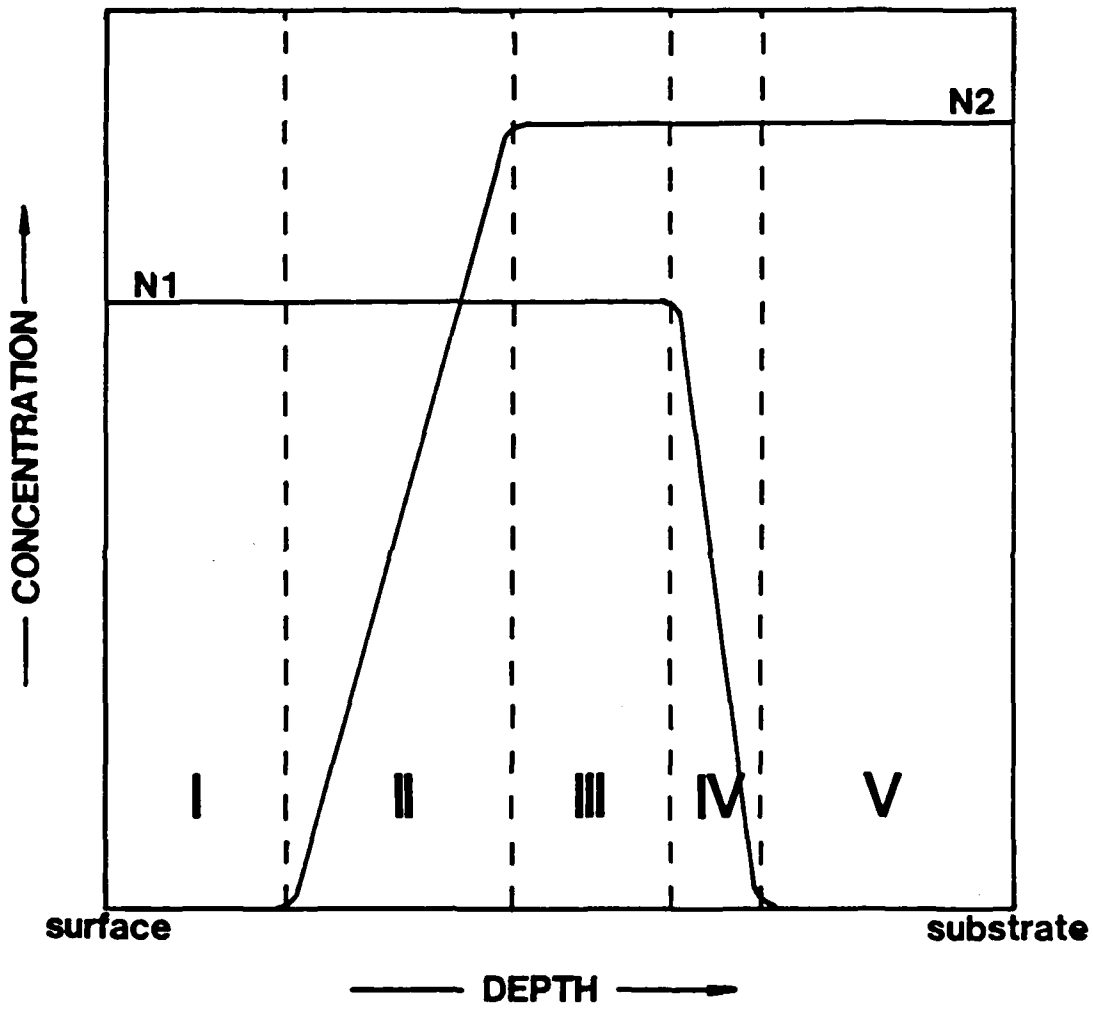

Figure 4. Self-calibrating layer structure.

performed using an electrochemical cell so that thick, heavily doped layers could be examined[4,5,6,7,8].

The self-calibrating layers were grown on Si doped substrates oriented 2° off {100} towards {110} with a carrier concentration between $2x10^{17}cm^{-3}$ and $2x10^{18}cm^{-3}$. The H_2S flow rate, when on, was set for 7.5 ml/min. The flow of H_2+H_2O was 5.0 ml/min with the H_2O temperature ranging from $-78^{\circ}C$ to $24^{\circ}C$. Figs. 5, 6, and 7 show the SIMS and C-V analyses for three samples grown with various input partial pressures of H_2O. In these figures n_i is the intrinsic concentration at the growth temperature[9]. In the H_2S calibration region of all three samples, the free carrier concentration at the growth temperature ($740^{\circ}C$)[9] is between $1x10^{17}cm^{-3}$ and $2x10^{17}cm^{-3}$ which is an order of magnitude higher than the sulfur concentration. This may be due to the influence of a slow turn-off profile for the H_2O as shown in Figs. 6 and 7. A possible effect of the gradual turn-off of H_2O may be seen in the slope of the sulfur profiles in the H_2S calibration region in Figs. 6 and 7. Samples grown without H_2O present or with a very low partial pressure of H_2O exhibit flat sulfur profiles in the calibration region. There are two possible reasons for the dependence of the sulfur profile on the H_2O: (1) the distribution or the diffusion of sulfur in GaAs is altered through some interaction with the H_2O or (2) oxygen incorporated in the layer is detected in the form of O_2 which is indistinguishable from S in normal SIMS analysis[10].

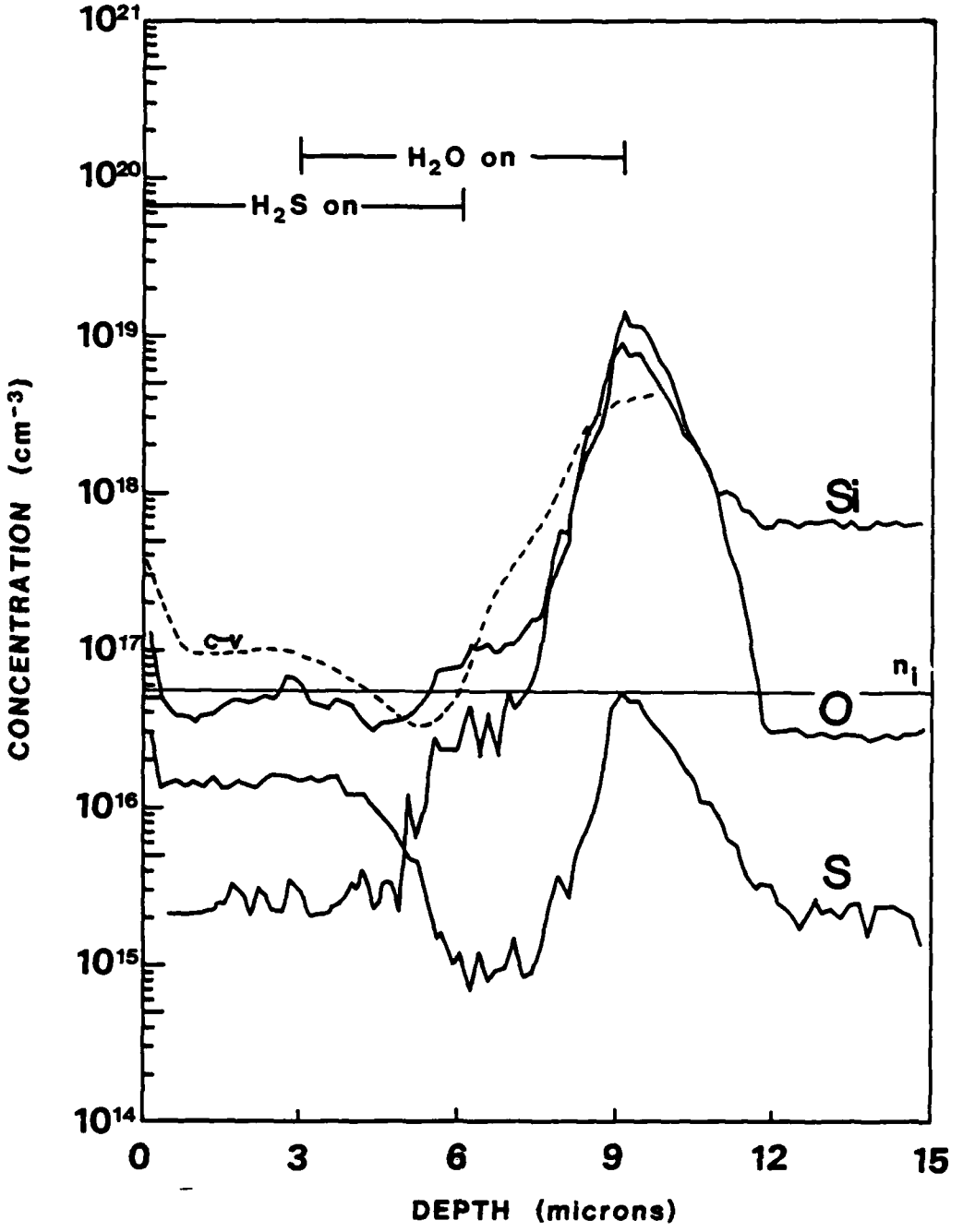

Figure 5. Self-calibrating layer grown with H_2O at -60°C.

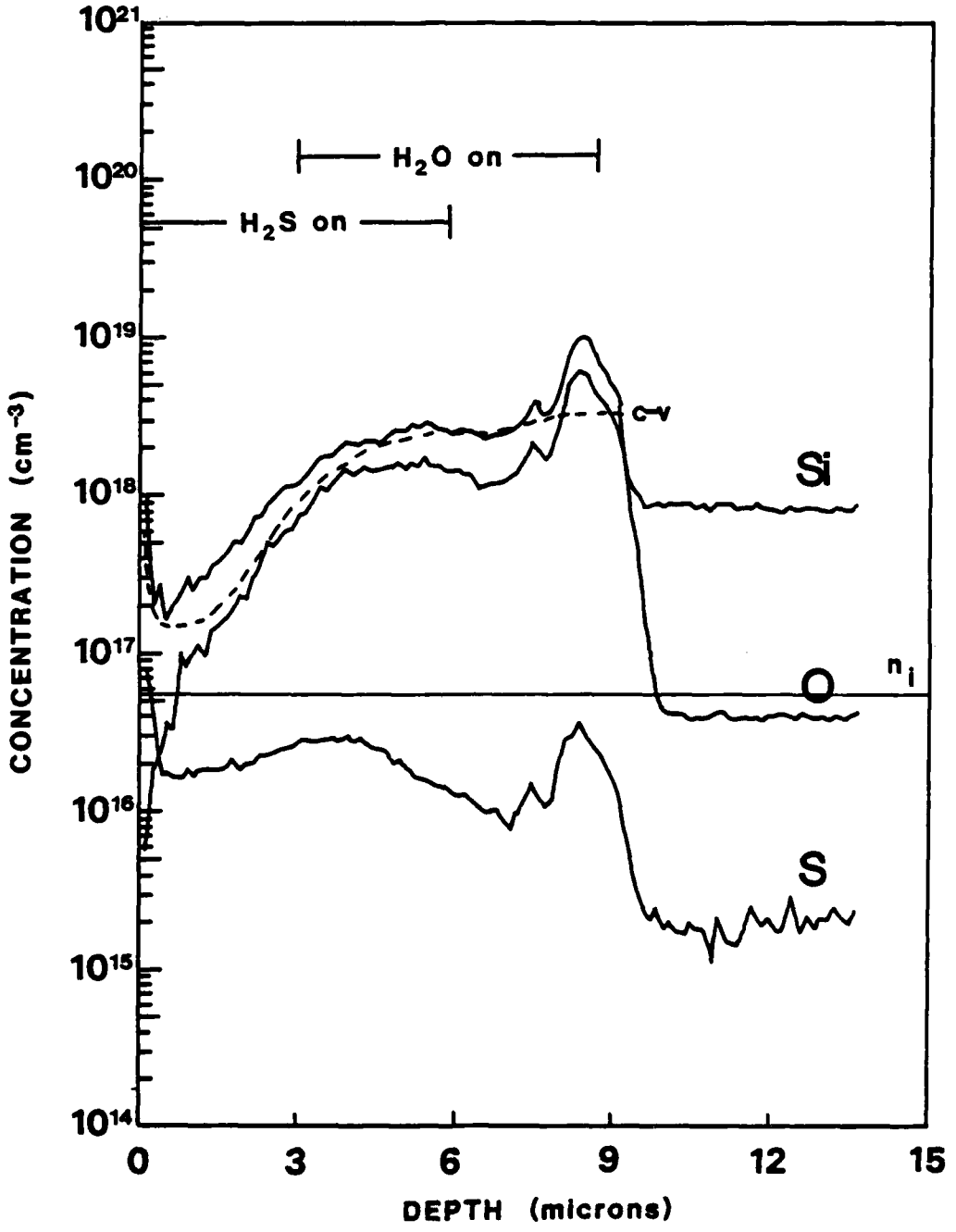

Figure 6. Self-calibrating layer grown with H_2O at -50°C.

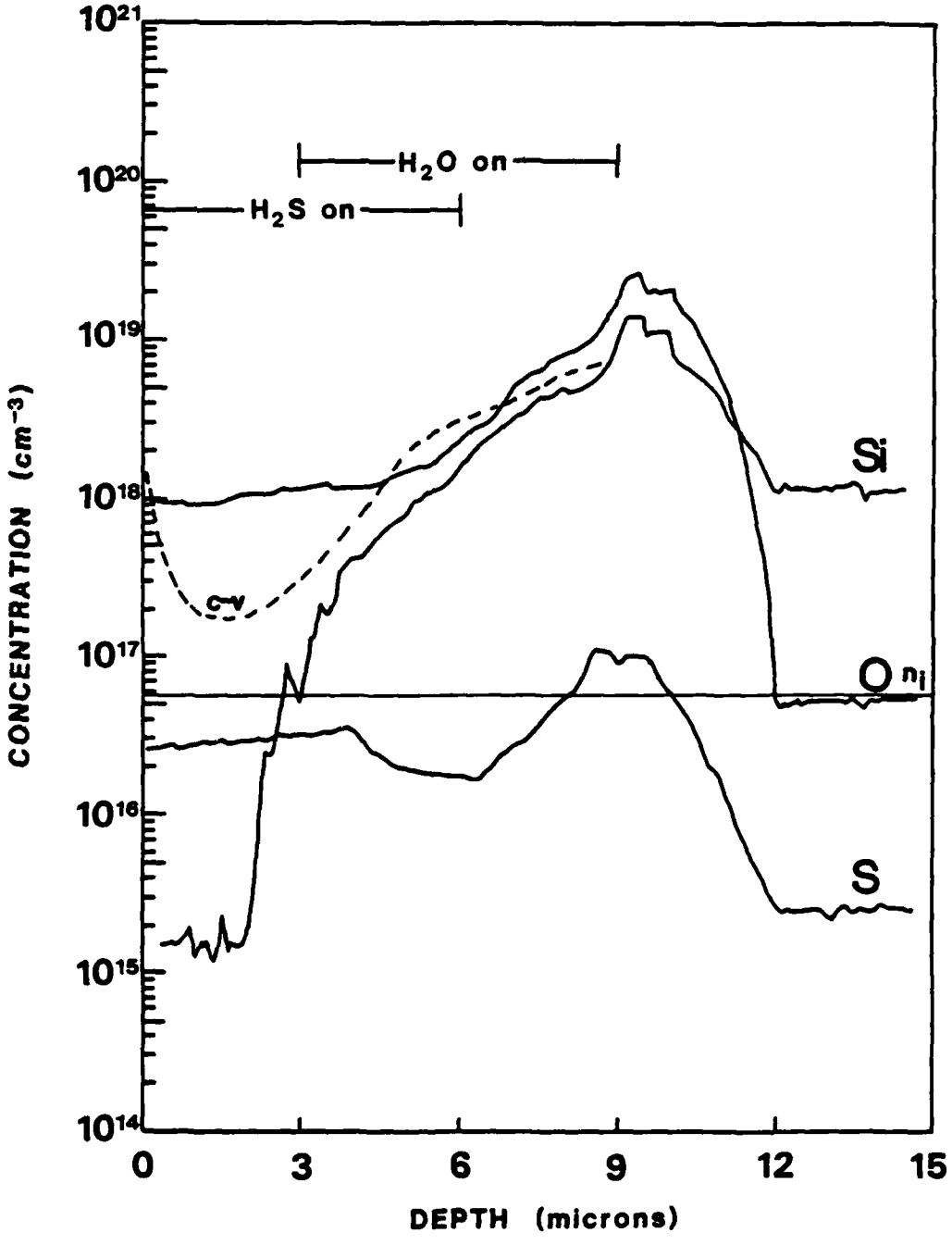

Figure 7. Self-calibrating layer grown with H_2O at -40°C.

Experiments with the homogeneously doped samples indicate that the first explanation is more plausible.

Examination of the behavior of the sulfur in the sulfur transition region shows a dependence of the sulfur turn-on profile on the input partial pressure of the H_2O. From the SIMS analysis, it is evident that the turn-on profile for the sulfur becomes more gradual. Associated with the more gradual turn-on of sulfur is the elevation of the sulfur concentration in the H_2O and H_2S calibration regions.

Some increase in the sulfur concentration with increased H_2O partial pressure in the sulfur calibration region was expected from the work done with the homogeneously doped layer and this was observed. The increase of sulfur in the H_2O calibration region, however, was unexpected. Fig. 5 shows the sulfur concentration in the H_2O calibration region as $1x10^{15}cm^{-3}$ and Fig. 6 shows an order of magnitude increase of sulfur for an increase in H_2O temperature of $10^{o}C$. There are two possible explanations for this behavior. One explanation is, as before, that O_2 may be mistaken for S in the SIMS analysis. The other possibilty is reactive diffusion of sulfur with the impurity introduced or defect induced by the H_2O. The corresponding softening of the sulfur turn-on profile favors the latter explanation.

Finally, notice must be taken of the large concentration of Si throughout the layers of Figs. 6 and 7. It is believed that the source of Si is the substrate and that the profile is the result of autodoping or H_2O enhanced outdiffusion.

The C-V profiles confirm that Si is the major contributor to the carrier concentration when incorporated at such a high concentration.

C.2.3 DISCUSSION

Experiments performed with homogeneously doped layers demonstrate that H_2O introduces some impurity or defect into the growing layer and that there are two interactions which should be considered. These are (1) the H_2O-residual or intentionally-added impurity interaction responsible for the highly compensated H_2O doped samples and deep donor behavior and (2) the H_2O-H_2S interaction responsible for the change in the sulfur distribution or diffusion. Analysis of self-calibrating layers yields more evidence that H_2O increases the distribution or diffusion of sulfur in GaAs and, at high input partial pressures, contributes significantly to the free carrier concentration.

C.2.4 REFERENCES

1. L.J. van der Pauw, Philips Res. Repts. 13, 1, (1958).

2. Handbook of Chemistry and Physics 54th edition, CRC Press, 1973.

3. D.P. Kennedy, P.C. Murley, W. Kleinfelder, IBM J. Res. Dev. 13, 409B (1968).

4. T. Ambridge, C.R. Elliott, and M.M. Faktor, J. Appl. Electrochem. 3, 1(1973).

5. T. Ambridge and M.M. Faktor, J. Appl. Electrochem. 5, 319 (1975).

6. T. Ambridge and M.M. Faktor, Electronic Lett. 10, 204 (1974).

7. D.G. Fiddyment and M.R. Taylor, J. Electrochem. Soc. 122, 1567 (1975).

8. T. Ambridge, D.J. Ashen, Electronic Lett. 15, 647 (1979).

9. K.H. Nichols, Camellia M.L. Yee, and C.M. Wolfe, Solid State Electronics 23, 109 (1980).

10. Charles Evans and Associates, private communication.

PHYSICAL REVIEW B VOLUME 25, NUMBER 1 1 JANUARY 1982

D.1 Effects of interactions between hopping particles on T_1 relaxation rates at low concentrations

Peter A. Fedders
Department of Physics, Washington University, St. Louis, Missouri 63130
(Received 4 May 1981)

We calculate the correlation function for a pair of specific particles making nearest-neighbor jumps in a simple-cubic lattice. Short-ranged interactions are included by allowing one jump rate when the particles are separated and arbitrary jump rates into and out of configurations where the particles are nearest neighbors. This correlation function is then used to calculate the effects of particle repulsion (or attraction) on $T_1(I\text{-}I)$, the motionally altered spin relaxation time due to the dipolar interaction between the hopping particles. The frequency or magnetic-field dependence of this relaxation time is not what one would expect from simply doctored second-moment arguments.

I. INTRODUCTION

The problem of nuclear spin relaxation due to the motionally altered dipolar interactions between atoms hopping in a crystal has been studied for many years. However, until now, it has almost always been assumed (explicitly or implicitly) that the hopping particles did not interact with each other except that multiple occupancy of a single site was forbidden. In this paper we shall investigate the effects of particle interactions on the spin relaxation for a small concentration of particles hopping in a simple-cubic lattice.

In the simple hopping problem one assumes that the probability per unit time for a particle to hop from one site to a neighboring vacant site is a constant. The first treatment of this problem was by Bloembergen, Purcell, and Pound,[1] who employed a single-relaxation-time approximation which usually yields qualitatively correct and quantitatively reasonable results. The random-walk approximation, first employed by Torrey,[2] was a significant improvement in that correlations due to specific lattices were incorporated.

More recently virtually exact results for spin relaxation with the simple hopping model have been obtained. This includes the mean-field approximation which is exact for low concentrations of particles and the multiple scattering approximation employed by Sankey and ourselves which is virtually exact at all concentrations.[3,4] Further, Wolf[5] has performed numerous computer simulations for the monovacancy limit where the concentration of particles approaches one and Bustard[6] has performed computer simulations at a number of concentrations for a simple-cubic lattice. In a number of cases these calculations and simulations have been in excellent agreement with each other and with experimental results.

For atomic migration in "hot solids" the monovacancy regime almost always obtains and thus any interactions will only lead to a modified hopping rate. The possibility of interactions among the hopping protons in metallic hydrides has been mentioned from time to time although only very recently has good evidence for their existence been obtained. In some cases discrepancies between theory and experiment have been shown to be due to inadequate theories.[4,7] However, recent[8] NMR and diffusion measurements on Ta-H_x along with calculations[4] on the relaxation rates due to $I\text{-}I$ and $I\text{-}S$ interactions present very strong evidence for the existence of repulsive interactions. In addition, fitting model calculations to phase diagrams in bcc metal hydrides also suggests extensive repulsive interactions.[9]

In this paper we consider the specific problem of the T_1 dipolar spin relaxation for a small concentration of interacting particles hopping in a simple-cubic lattice. In the rest of this section we define the model more exactly. Section II contains an outline of the calculation and some of the details. It can be omitted by a reader who is interested in the results but not the details of the calculation. The results are described and discussed in Sec. III.

Specifically, our model is that the probability per unit time for a particle to hop from site α to a vacant site β is $\Gamma_{\alpha\beta}$ where

$$\Gamma_{\alpha\beta} = \Gamma_0 f_{\alpha\beta} \ , \tag{1}$$

with $f_{\alpha\beta} = 1$ if α and β are nearest neighbors and $f_{\alpha\beta} = 0$ otherwise. Equation (1) will obtain if no other particles occupy sites neighboring either the site α or the site β. If the site α has an occupied neighboring site (not site β) and site β has no occupied neighboring site (except α), then Γ_0 is replaced by Γ_{in}, where

$$\Gamma_{in} = r_i \Gamma_0, \quad 0 \leq r_i \leq \infty \ . \tag{2}$$

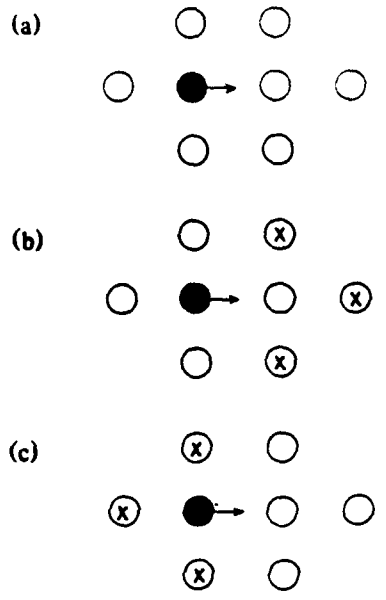

FIG. 1. Two-dimensional analog of the configurations considered. Open circles represent vacant sites, the shaded circle represents the particle under consideration with an arrow pointing toward the site that it will hop to. One and only one of the three circles with ×'s are occupied. (a), (b), and (c) refer to Eqs. (1), (2), and (3), respectively.

Further, if the site α has no occupied neighboring sites and site β has an occupied neighboring site (besides α) then Γ_0 is replaced by Γ_{out}, where

$$\Gamma_{out} = r_o \Gamma_0, \quad 0 \leq r_0 \leq \infty \ . \tag{3}$$

Since we are only considering low concentrations of particles we ignore any effects due to three or more particles. Further, in the sc lattice, no site can be a nearest neighbor to both sites α and β. Thus, the above equations completely define our system. A two-dimensional analog of the three cases considered above is shown in Fig. 1. Finally, with no interactions, the probability that a given site is occupied is c, the concentration of particles. However, in the present case, the probability of a site being occupied if one of its neighbors is occupied is pc where, by detailed balance,

$$r_i = p r_o \ . \tag{4}$$

Since the calculation is limited to the low-concentration limit, it reduces to following the motion of a pair of distinguishable particles. Therefore, it is exactly soluble, although the analytic solution is messy.

The model which we solve here is probably not applicable to any real systems because the substances that are the best candidates for the effects of interactions are not simple cubic but are bcc metal hydrides with the tetrahedral sites occupied. These sites are extremely close together. Further, except for host materials with very small magnetic moments, T_1 due to I-S interactions will tend to dominate the T_1 calculated here due to I-I interactions if the concentration of I spins is very low.

In this paper, the hopping particles are labeled by spin I and the host particles are denoted by spin S. Nevertheless, we believe the calculation is important in at least two respects. First, it can serve as an exactly soluble limit for calculations that are not limited to low concentrations. Second, it points up trends and frequency dependences that would be expected at higher concentrations. In fact, as discussed in Sec. III, the effects are far from uniform as a function of frequency or temperature.

II. CALCULATION

In this section we present the derivation of the T_1 relaxation time. The notation and some of the details are the same as in Ref. 3. The correlation function describing the motion of a pair of specific particles i and j is defined as

$$D(\alpha, \beta; \bar{\alpha}, \bar{\beta}; t) = \langle \rho_{i\alpha}(t) \rho_{j\beta}(t) \rho_{i\bar{\alpha}}(0) \rho_{j\bar{\beta}}(0) \rangle \Theta(t) \ , \tag{5}$$

where Θ is the step function, the greek letters α and β denote lattice sites, and $\langle x \rangle$ denotes the ensemble average of x. Further, as in Ref. 3,

$$\rho_{i\alpha} = N^{1/2} p_{i\alpha} \ , \tag{6}$$

where N is the number of sites and $p_{i\alpha}$ is a stochastic variable whose value is 1 if the particle i is at the site α and is zero otherwise. Expressions for T_1 in terms of D are available in the literature[3] and will not be repeated here.

As in earlier work, it is convenient to define a self-energy or mass operator K and express D in terms of it as

$$\frac{\partial}{\partial t} D(\alpha, \beta; \bar{\alpha}, \bar{\beta}; t) + \sum_{\gamma, \bar{\gamma}} \int d\bar{t} \, K(\alpha, \beta; \gamma, \bar{\gamma}; t - \bar{t}) D(\gamma, \bar{\gamma}; \bar{\alpha}, \bar{\beta}) = \delta_{\alpha\bar{\alpha}} \delta_{\alpha\bar{\beta}} (1 - \delta_{\alpha\beta}) [1 - (1 - p) f_{\alpha\beta}] \delta(t) \ . \tag{7}$$

This equation is identical to forms used earlier except for the factor in the square brackets of the inhomogeneous term which reflects the nonrandom probability of nearest-neighbor sites being occupied as discussed in Sec. I. In the present case we are only considering the motion of two particles and K can be written down exactly and rather easily using methods described earlier. That is, $K(\alpha,\beta;\bar{\alpha},\bar{\beta};t)$ is just the probability per unit time that the pair of particles can hop from the configuration where i is at α and j is at β to the configuration where i is at $\bar{\alpha}$ and j is at $\bar{\beta}$. For the sc lattice, one easily obtains the expression

$$K(\alpha,\beta;\bar{\alpha},\bar{\beta};t)=\Lambda_0\Big\{\delta_{\alpha\bar{\alpha}}\delta_{\beta\bar{\beta}}[12-2f_{\alpha\beta}(5r_e-6)+2\sum_{\gamma}f_{\alpha\gamma}f_{\alpha\beta}(r_i-1)$$
$$-\delta_{\beta\bar{\beta}}\delta_{\alpha\bar{\alpha}}[1+f_{\alpha\beta}(r_i-1)+f_{\bar{\alpha}\beta}(r_e-1)]$$
$$-\delta_{\alpha\bar{\alpha}}f_{\beta\bar{\beta}}[1+f_{\alpha\beta}(r_i-1)+f_{\alpha\bar{\beta}}(r_e-1)]\Big\}(1-\delta_{\alpha\beta})(1-\delta_{\bar{\alpha}\bar{\beta}}) \quad . \tag{8}$$

At this point it is convenient to Fourier transform in both space and time. All quantities $A(t)$ are transformed as

$$A(\omega)=\int_{-\infty}^{\infty}dt\,A(t)e^{i\omega t} \quad , \tag{9}$$

and quantities $A(\vec{R}_\alpha)$ depending on a single space coordinate difference $\vec{R}_\alpha$ are transformed as

$$A(\vec{q})=\sum_{\alpha}A(\vec{R}_\alpha)e^{-i\vec{q}\cdot\vec{R}_\alpha} \quad , \tag{10}$$

where $\vec{R}_\alpha$ is the lattice position of the site α. The function D defined in Eq. (5) contains more information than is needed and we define

$$D(\alpha,\beta,t)=N^{-2}\sum_{\gamma,\bar{\gamma}}D(\alpha+\gamma,\gamma,\beta+\bar{\gamma},\bar{\gamma};t) \quad , \tag{11}$$

which is proportional to the probability that the particles i and j are separated by $\vec{R}_\beta$ at time zero and $\vec{R}_\alpha$ at time t. Functions $A(\vec{R}_\alpha,\vec{R}_\beta)$ are transformed as

$$A(\vec{q},\vec{q}')=\sum_{\alpha,\beta}A(\vec{R}_\alpha,\vec{R}_\beta)\exp(-i\vec{q}\cdot\vec{R}_\alpha+i\vec{q}'\cdot\vec{R}_\beta) \quad . \tag{12}$$

From these definitions and Eqs. (7) and (8) one easily obtains the equations

$$i\omega D(\vec{q}',\vec{q}'',\omega)+N^{-1}\sum_{\vec{q}}K(\vec{q}',\vec{q},\omega)D(\vec{q},\vec{q}'',\omega)=N[\delta(\vec{q}'-\vec{q}'')-1-(1-p)f(\vec{q}'-\vec{q}'')] \quad , \tag{13}$$

$$K(\vec{q}',\vec{q}'',\omega)=N\delta(\vec{q}'-\vec{q}'')2\omega_0(\vec{q}')+2\Gamma_0[-6r_i+r_if(\vec{q}')+r_ef(\vec{q}'')+(5r_e-6)f(\vec{q}'-\vec{q}'')+(r_i-1)f^2(\vec{q}'-\vec{q}'')$$
$$+(1-r_e)f(\vec{q}')f(\vec{q}'-\vec{q}'')+f(\vec{q}'')f(\vec{q}'-\vec{q}'')(1-r_i)] \quad , \tag{14}$$

where

$$\omega_0(\vec{q})=\Gamma_0[6-f(\vec{q})] \quad . \tag{15}$$

The first term in Eq. (14) describes the random-walk approximation where each particle moves independently of the other.

Equations (13) and (14) describe an exactly soluable integral equation because the kernel is a sum of separable

kernels. After a bit of algebra one can show that

$$D(\vec{q}', \vec{q}'', \omega) = d_0(\vec{q}', \omega)[N\delta(\vec{q}' - \vec{q}'') - 1 - 1(1-p)f(\vec{q}' - \vec{q}'')]$$
$$-4d_0(\vec{q}', \omega)\Gamma_0\Big[\sum_i D(C_i, \vec{q}'', \omega)\Big[r_e + (5r_e - 6)\cos q_i' + 2(1-r_e)\cos q_i' \sum_j \cos q_j'\Big]$$
$$+ \sum_i D(S_i, \vec{q}'', \omega)\sin q_i'\Big[(5r_e - 6) + 2(1-r_e)\sum_j \cos q_j'\Big]$$
$$+2(r_l - 1)\sum_{i \neq j} D(S_iS_j, \vec{q}'', \omega)\sin q_i' \sin q_j'$$
$$+ \sum_{ij} D(S_iC_j, \vec{q}'', \omega)\sin q_i'[4(r_l - 1)\cos q_j' + 2(1-r_l)]$$
$$+ \sum_{ij} D(C_iC_j, \vec{q}'', \omega)\cos q_i'[2(r_l - 1)\cos q_j' + 2(1-r_l)]$$
$$-2(r_l - 1)\sum_i \sin^2 q_i' D(C_i^2, \vec{q}'', \omega)\Big] \quad . \tag{16}$$

where

$$d_0(\vec{q}, \omega) = [-i\omega + 2\omega_0(\vec{q})] \quad , \tag{17}$$

$$D(t_i, \vec{q}'', \omega) = N^{-1}\sum_{\vec{q}'} t_i(\vec{q}')D(\vec{q}', \vec{q}'', \omega) \quad , \tag{18}$$

where t_i is a trigonometric function such as C_i for $\cos q_i$, and S_i for $\sin q_i$.

Although Eq. (16) is exactly soluble, the solution is very long and messy. A significant simplification can be obtained by noting that certain terms in $D(\vec{q}', \vec{q}'', \omega)$ will not contribute to T_1. For example, terms that are odd in q_i' or in q_i'' will not contribute nor will terms whose only q' dependence is

$$\sum_i \cos q_i' \quad .$$

Thus such terms can be projected out of the solution. After the solution of D is obtained T_1 is rather easily obtained.[10] The results of these calculations are presented in the next section.

III. RESULTS AND CONCLUSIONS

In this section we shall present and discuss the results derived in the preceding section. Most of the discussion will be limited to the more interesting limiting cases.

In the high-frequency (or low-temperature) limit, where $\omega >> \Gamma_0$, the results are easily expressed analytically as

$$1/T_1 = (\Gamma_0 A/\omega^2)[(8.77 + 43.76r_l) + (1.37 - 35.40r_l)h]\omega >> \Gamma_0 \quad , \tag{19}$$

where

$$A = I(I+1)\hbar^2\gamma^4 c/a^6 \quad ,$$

$$h = \sum_i l_i^4 - \tfrac{3}{5} \quad , \tag{20}$$

where γ is the gyromagnetic moment of the spin I, ω is the frequency of the experiment, l_i are the direction cosines of the external magnetic field with respect to the cubic axes, and the angular average of h vanishes.

It should be observed that the relaxation rate in this limit depends only on r_l and not on r_e or p. This obtains because in the high-frequency limit the relaxation rate depends only on what happens in a single hop. The terms independent of r_l in Eq. (21) arise from configuration where two particles are not nearest neighbors either before or after the hop. The other terms which are proportional to r_l come from configurations where the particles are nearest neighbors (probability p) and one hops away (rate $\Gamma_0 r_e$) with a net rate proprotional to $pr_e = r_l$ and from configurations where the particles are not nearest neighbors (probability 1) and one hops to a nearest-neighbor site of the other (rate $\Gamma_0 r_l$).

The single most interesting and instructive case to consider is the one where nearest-neighbor occupancy is absolutely forbidden, $r_l = p = 0$. Normally, for the mobile protons in a metal hydride, one might expect nearest-neighbor occupancy to be reduced because the conduction electrons cannot screen out the Coulomb repulsion in short enough distances. In Fig. 2 we express the angular average of $1/T_1$ as

$$1/T_1 = (A/\omega)g(\omega\tau_c) \quad . \tag{21}$$

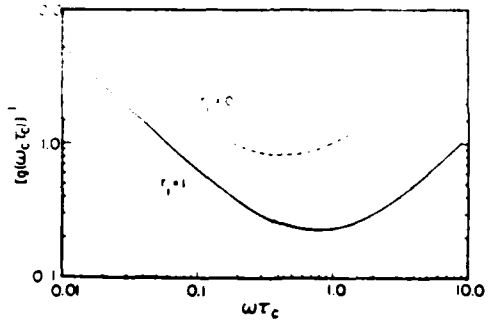

FIG. 2. Dimensionless function $[g(\omega\tau_c)]^{-1}$ vs $\omega\tau_c$ for $r_f = 0$ and 1 with $r_e = 1$.

where $\tau_c = 1/6\Gamma_0$.

At high frequencies the effects of the repulsion are most dramatic. T_1 is increased by a factor of 6.00 by the repulsion from its value for noninteracting particles. This is fairly close to the value of 5.27 that one could estimate by the fact that the appropriate second dipolar moment reduction.

At the other extreme, at low frequencies ($\omega << \Gamma$) or high temperature, T_1 is increased by only a factor of 1.66. This is far less than one would expect from naive arguments. The reason for this is that at low frequencies the hop where the pair of particles are not nearest neighbors contribute over half the relaxation rate.

---

[1]N. Bloembergen, E. M. Purcell, and R. V. Pound, Phys. Rev. 73, 679 (1948).
[2]H. C. Torrey, Phys. Rev. 92, 962 (1953); 96, 960 (1954).
[3]See, for example, O. F. Sankey and P. A. Fedders, Phys. Rev. B 18, 5938 (1978); 20, 39 (1979).
[4]O. F. Sankey and P. A. Fedders, Phys. Rev. B (in press).
[5]See, for example, D. Wolf, Phys. Rev. B 10, 2710 (1974); D. Wolf, D. R. Figueroa, and J. H. Strange, *ibid.* 15, 2545 (1977), and references therein.
[6]L. D. Bustard, Phys. Rev. B 22, 1 (1980).
[7]O. J. Zogal and R. M. Cotts, Phys. Rev. B 11, 2443 (1975).
[8]P. E. Mauger, W. D. Williams, and R. M. Cotts (unpublished).
[9]Heing Horner and Herbert Wagner, J. Phys. C 7, 3305 (1974).
[10]The analytical form of the results covers numerous pages. They are available from the author upon request.

PHYSICAL REVIEW B VOLUME 25, NUMBER 6 15 MARCH 1982

D.2 Electrostatic effects of hydrogenic donor complexes on magneto-optical spectra

Peter A. Fedders
Department of Physics, Washington University, St. Louis, Missouri 63130
(Received 9 November 1981)

We investigate the electrostatic effects on the energy of a hydrogenic donor complex in the presence of an externally applied magnetic field. The complex is defined as an impurity of net charge one whose charge distribution is not equivalent to a single point charge. The results are discussed with respect to photoconductivity measurements of the $1s$-$2p_-$ shallow-donor lines in GaAs.

I. INTRODUCTION

Although the study of the spectra of shallow donors in semiconductors is a rather old subject, many problems of understanding the linewidths, line shapes, and even the line positions remain unsolved. This is somewhat unfortunate since photoconductivity experiments cannot only detect shallow-donor impurities that have densities of 10^{12} cm^3 or less, but can also yield resolvable line shapes. With such a fantastically sensitive spectroscopic tool, one might hope to obtain a wealth of information about the structure and environment of shallow donor impurities.

One major difficulty is that different species of shallow donors ought to yield identical line shapes whose positions are controlled by central-cell corrections and whose intensities are proportional to the densities of the species.[1] As has been discussed in the literature, this is not the case quantitatively and is sometimes not even the case qualitatively. For example, linewidths for different species in GaAs are usually different[1-3] and often even line shapes are grossly different.[4-6]

Towards a partial understanding of these discrepancies we investigate the electrostatic effects on the energy levels of a hydrogenic shallow-donor complex in the presence of an applied magnetic field. For our purposes here, a simple shallow donor is described by an effective-mass Hamiltonian where the potential is due to a point charge of magnitude e. A complex (or complex shallow donor) is also described by an effective-mass Hamiltonian but the potential is due to a charge density $\rho(\vec{r})$ whose integrated weight is e but which, in general, is not the charge density of a single point charge.

In the rest of this section we shall more fully describe our model, its limitations, and its applicability to GaAs. Section II contains all the essential elements of the calculation of the energy levels of a complex in the presence of an externally applied magnetic field and other electrical disturbances generated far from the complex. The results for the $1s$ and $2p_-$ levels are presented and discussed in Sec. III.

The Hamiltonian for an electron in the field of a donor and a magnetic field $\vec{B}$ which defines the z axis is

$$H=(p^2/2m^*)+\tfrac{1}{2}\omega_c(xp_y-yp_x)+\tfrac{1}{8}m^*\omega_c^2(x^2+y^2)-(e/\epsilon_0)\int d^3r'\rho(\vec{r}')/|\vec{r}-\vec{r}'|\ , \qquad \int d^3r'\rho(\vec{r}')=e \tag{1}$$

where $\omega_c=eB/m^*c$ is the cyclotron frequency. We are assuming that the effective-mass approximation is valid and thus m^* and ϵ_0 are the effective mass and dielectric constants of the medium. We shall further assume that $\rho(\vec{r})$ is zero outside of a volume whose dimensions are small compared to a Bohr radius. The effects of charged impurities many Bohr radii from the center of the charge distribution can be treated as perturbations.

The effective-mass approximation yields excellent results in a wide variety of semiconductors[7] and its validity will not be discussed here. Of

course, in a real material, $\rho(\vec{r})$ is not the actual charge distribution but is the actual charge distribution minus the charge distribution of the perfect lattice. Further, the use of a dielectric constant in and very near the charge distribution is clearly not valid. The details of the interactions in this volume are contained in the central-cell correction to the energy of the 1s state which we shall assume to be given. These corrections are quite small in GaAs because the effective Bohr radius is 99 Å.

II. CALCULATION

In this section we outline the calculation of the effects of a complex on the energy levels of a shallow donor. Initially, we ignore the effects due to any remote charges. In reduced units, the zero-order Hamiltonian H_0 is that for a simple donor at the origin,

$$H_0=-\nabla^2+\left[\frac{\gamma}{i}\right]\left[\frac{\partial}{\partial\phi}\right]+\tfrac{1}{4}\gamma^2\rho^2-\frac{2}{r}\,, \tag{2}$$

where lengths and energies are taken in units of the effective Bohr radius, $a_0=\epsilon_0\hbar^2/m^*e^2$, and the effective rydberg, $R=m^*e^4/2\epsilon_0^2\hbar^2$. The dimensionless magnetic field strength is γ where $\gamma=\hbar\omega_c/2R$, $\rho^2=r^2\sin^2\theta$, and the magnetic field $\vec{B}$ defines the z direction. In what follows, we shall always assume γ is much larger than any other (dimensionless) perturbation.

We define the complex by a set of charges Z_ie at the points $\vec{r}_i$ where

$$\sum_i Z_i=1\,. \tag{3}$$

(If the charge distribution is a continuum, the appropriate sums can trivially be converted to integrals.) Thus H', the perturbation due to the complex, can be written as a sum of terms, one from each member of the complex,

$$H'=\sum_i V_i\,, \tag{4}$$

$$V_i=-2Z_i(\,|\,\vec{r}-\vec{r}_i\,|^{-1}-r^{-1})\,.$$

At this point it is important to note that the origin of the charge distribution is irrelevant. Thus, if we translate all of the charges by $\vec{r}_0$ so that

$$\vec{r}_i\rightarrow\vec{r}_i+\vec{r}_0\,, \tag{5}$$

the problem remains unchanged.

Using the usual multipole expansion, V_i can be expanded as

$$V_i=\begin{cases}-8Z_i\pi\displaystyle\sum_{l=1}\sum_m\frac{r_i^l}{r^{l+1}}\frac{Y_{lm}^*(\Omega_i)Y_{lm}(\Omega)}{2l+1}\,, & r>r_i \qquad (6a)\\[2ex] -2Z_i\left[\left[\dfrac{1}{r_i}-\dfrac{1}{r}\right]+4\pi\displaystyle\sum_{l=1}\sum_m\frac{r^l}{r_i^{l+1}}\frac{Y_{lm}^*(\Omega_i)Y_{lm}(\Omega)}{2l+1}\right], & r<r_i \qquad (6b)\end{cases}$$

where the $Y_{lm}(\Omega)$ are the usual spherical harmonics and Ω and Ω' refer to the solid angles for $\vec{r}$ and $\vec{r}_i$, respectively. As noted earlier, we have assumed that the charge distribution has dimensions d and that $d\ll 1$ in reduced units. Assuming that the origin in the problem is chosen to lie within a distance d of the charge distribution, the contribution to the energy of an s state from $r<r_i$ will be of order d^2 and will be independent of the angles Ω_i. The corresponding energies of other states will be proportional to the fourth or higher powers of d. Such contributions can be lumped into a central-cell correction and will temporarily be ignored while we concentrate on the contributions from Eqs. (4) and (6a).

Although the final answers must be independent of origin, some choices are more convenient than others. The perturbations described by Eq. (6a) contain a sum over l and the lth term is proportional to d^l. If we chose the origin to eliminate the $l=1$ term, then first-order perturbation theory will yield the correct answer to order d^2. Any other choice will require second-order perturbation theory to obtain answers to order d^2. This choice is accomplished by choosing the origin so that

$$\sum_i Z_i\vec{r}_i=0\,, \tag{7}$$

that is, so that the dipole moment of the charge distribution vanishes. Now, to order d^2, H' can be written with only the $l=2$ terms as

$$H' = -(8\pi/5)\sum_m \left| \sum_i Z_i r_i^2 Y^*_{2m}(\Omega_i) \right| Y_{2m}(\Omega)/r^3 . \tag{8}$$

Only the $m=0$ term in Eq. (8) will contribute in lowest-order perturbation theory. The energy shift of the state x can be written as

$$\Delta E_x = -\alpha_Q(x) Q(\Omega_i) , \tag{9a}$$

$$\alpha_Q(x) = \langle x | (3\cos^2\theta - 1)/r^3 | x \rangle , \tag{9b}$$

$$Q(\Omega_i) = \tfrac{1}{2}\sum_i Z_i r_i^2 (3\cos^2\theta_i - 1) . \tag{9c}$$

The $\vec{r}_i$ in Eq. (9c) are determined by Eq. (7) and θ_i refers to the ith charge in the coordinate system defined by the magnetic field. Equation (9c) will be presented in a more convenient form in the Sec. III. Before presenting our calculations of $\alpha_Q(x)$ for the $1s$ and $2p_-$ states, we wish to briefly comment on the coupling of terms arising from the complex with terms describing the electric field from remote charges.

The Hamiltonian describing an electron interacting with an electric field $\vec{E}$ generated by remote charges is

$$\mathcal{H}_s = -e\vec{E}\cdot\vec{r} . \tag{10}$$

Since this term has an odd parity, bound states (in the presence of a magnetic field) are unaffected by $\mathcal{H}_s$ to first order. They are, of course, affected to second order and this Hamiltonian gives rise to the second-order Stark shift. As has been extensively discussed in the literature, different donors are under the influence of different electric fields generated by remote defects. This leads to a characteristic line shape that is usually observed in photoconductivity experiments.

Since, in general, there will be a "length" vector $\vec{d}$ associated with the charge distribution of a complex, one might have expected a term in the complex Hamiltonian that was linear in d and had odd parity. If such a term existed, the cross term of it and the Stark term in second-order perturbation theory would lead to an energy shift proportional to Ed, i.e., an effective first-order Stark shift. In fact, such a term did exist in the Hamiltonian for a complex before we transformed it to zero via Eq. (7). If we had not transformed this dipole term to zero, every energy level would have been shifted by a term proportional to Ed. However, the multiplicative coefficient would be the same for all states and thus the term would cancel out for any energy difference.

A term linear in E whose coefficient depends on the charge configuration could be useful in trying to explain anomalous linewidths from different donor species. However, our argument does not rule out such a term,[8] it merely rules it out for a medium described by only an isotropic dielectric constant.[9] Terms depending on other less isotropic properties of the media may yield such terms.

III. RESULTS

The energy shift of a shallow-donor state due to the electrostatic effects of a complex is given by Eqs. (9) in the reduced units discussed at the beginning of Sec. II. For GaAs, lengths are measured in terms of the Bohr radius $a_0 = 99$ Å, energies are measured in terms of the rydberg $R = 5.77$ meV $= 46.5$ cm^{-1}, and γ is the dimensionless magnetic field strength where B (in kG) $= 65.6\gamma$. In this section we present and discuss the results of our calculations for the energy difference of the $1s$ and $2p_-$ states since this is the most important spectroscopic transition.

The wave functions of the $1s$ and $2p_-$ states for the zero-order Hamiltonian, Eq. (2), describing a hydrogenic atom in a magnetic field were obtained by variational calculations. The trial wave functions used were

$$\psi_{1s}(\vec{r}) = A\exp(-ar - b^2\rho^2 - c^2z^2) , \tag{11a}$$

$$\psi_{2p_-}(\vec{r}) = A\rho\exp(-ar - b^2\rho^2 - c^2z^2 - i\phi) , \tag{11b}$$

where a, b, and c were varied in each case to minimize the energy. One reason for the choice in Eqs. (11) is that all radial integrals can be expressed in terms of the parabolic cylinder function and only the θ integrals had to be performed numerically. Thus, the energies and all derivatives with respect to a, b, and c are easily computed and one can minimize the energies with very few iterations. The energies obtained are not quite as low as have been obtained with better trial wave functions. For example, we obtain

$$\left| \frac{E_h(\gamma) - E_L(\gamma)}{E_L(\gamma) - E(0)} \right| \leq 2\times 10^{-3} , \tag{12}$$

for all values of γ less than 10. In this expression $E_h(\gamma)$ is our computed energy as a function of γ for the $1s$ state, $E_L(\gamma)$ is the energy as a function of γ as obtained by Larsen[10] using better trial wave

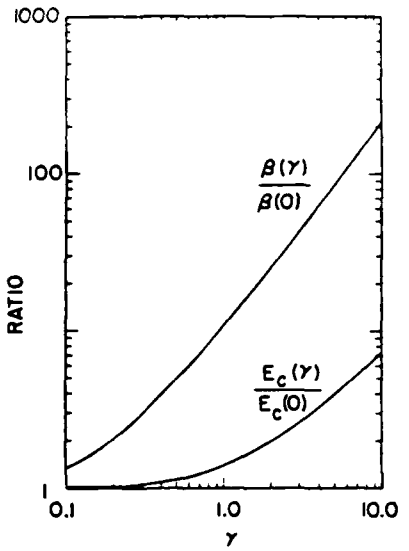

FIG. 1. Magnetic field dependence of $\beta(\gamma)$. The quantity plotted in $\beta(\gamma)/\beta(0)$ vs the magnetic field in dimensionless units. For purposes of comparison, the magnetic field dependence of the central-cell correction is also given.

functions, and $E(0)$ is the $1s$ energy in zero magnetic field.

Using the above wave functions we have calculated $\alpha_Q(x)$ where x refers to the $1s$ and $2p_-$

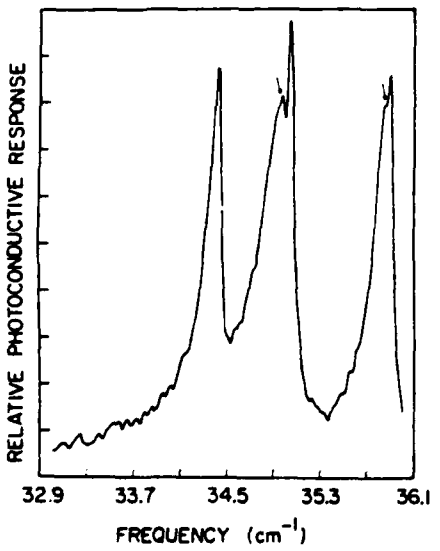

FIG. 2. High-resolution photoconductivity spectra of a GaAs epitaxial layer at a magnetic field of 50 kG and a temperature of 42 K (see Ref. 1). The arrows point to a structure that could be interpreted as resolved and partially resolved splittings due to complexes.

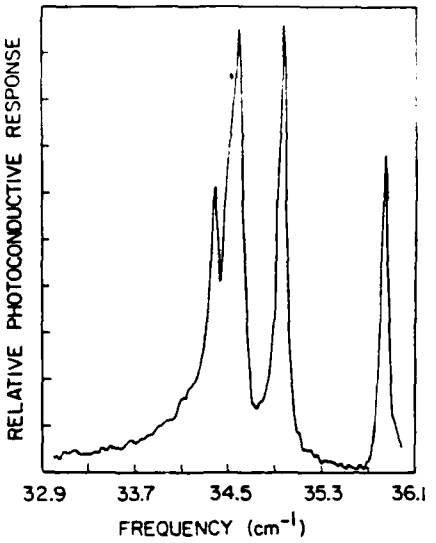

FIG. 3. High-resolution photoconductivity spectra of a GaAs epitaxial layer at a magnetic field of 50 kG and a temperature of 4.2 K (see Ref. 1). The arrow points to a structure that could be interpreted as an unresolved splitting due to a complex.

states. Since it is the energy shift between the $1s$ and $2p_-$ states that is important, we write

$$\Delta E(\gamma)=\beta(\gamma)Q(\Omega_i)\,,$$
$$\beta(\gamma)=\alpha_Q(1s)-\alpha_Q(2p_-)\,, \tag{13}$$

where $\Delta E(\gamma)$ is the shift in $E_{2p_-}-E_{1s}$ due to the complex. $Q(\Omega_i)$, given by Eq. (9b) in reduced units, depends only on the structure of the complex and its orientation. At $\gamma=0$,

$$\beta(0)=\tfrac{1}{60}\,. \tag{14}$$

The quantity $\beta(\gamma)$ is plotted versus γ in Fig. 1. For purposes of comparison the magnetic field dependence of the central-cell correction $E_c(\gamma)$ is also plotted in Fig. 1 where

$$E_c(\gamma)\propto 1/|\psi_{1s}(r=0)|^2\,. \tag{15}$$

There are two features that distinguish the complex shift from the central-cell shift. Firstly, the complex shift changes much more rapidly with magnetic field. Secondly, and more important, the complex shift depends on the orientation of a complex with respect to the magnetic field. As can be seen from Fig. 1, the effects of a complex as a function of field orientation can best be observed at highest magnetic fields.

As an example consider a complex consisting of

two charges $Z_1=2$ and $Z_2=-1$ separated by a dimensionless distance a. Using Eqs. (7) and (9c) we obtain

$$Q(\Omega)=a^2(3\cos^2\theta-1)\,, \tag{16}$$

where θ is the angle between the magnetic field and a line connecting the two charges. Suppose, for instance, such a complex could be oriented along any one of the four independent $\langle 111\rangle$ axes. If $\vec{B}$ was pointing along one of the three independent $\langle 100\rangle$ axis, Q would be zero in all cases. On the other hand, if $\vec{B}$ were pointing along one of the $\langle 111\rangle$ axes, complexes pointing along that axis would have $Q=2a^2$ and complexes pointing along the other three axes would have $Q=-\frac{2}{3}a^2$. Numerically, for GaAs in a magnetic field of 65.6 kG, the above complex with a length of one lattice spacing, 5.65 Å, could give rise to a shift that moves over a range of 0.0816 cm^{-1} as a function of magnetic field angle.

There is, of course, no guarantee that a given complex of net charge one is a shallow donor. The question of whether it is or not is beyond the scope of this paper and will not be discussed further. Besides substitutions of two or more atoms to form a complex there could be configurations where a single substitution plus a shift in position forms one. For example, suppose a C atom replaces an As atom but, because of its small size, the C atom moves slightly from the normal As position. Such a complex might be described by a charge Z_c at the C site and a charge $1-Z_c$ at the old As site where Z_c is an effective charge for the C.

Figures 2 and 3 exhibit photoconductive response data of doped GaAs epitaxial layers.[11] The arrows in the figures point to structures that could be interpreted as resolved, partially resolved, and unresolved splittings due to a complex. These data exist only at one orientation and therefore it is not known whether the structure shifts with magnetic field angle. Thus, one could also obviously interpret the data as structure due to different chemical species.

ACKNOWLEDGMENTS

This work was sponsored in part by the Office of Naval Research under Contract No. N00014-80C-0762. We wish to acknowledge useful and stimulating conversations with T. S. Low, G. E. Stillman, and C. M. Wolfe and to thank G. E. Stillman for use of his data prior to publication.

[1]D. M. Korn and David M. Larsen, Solid State Commun. 13, 807 (1973).
[2]David M. Larsen, Phys. Rev. B 8, 535 (1973).
[3]David M. Larsen, Phys. Rev. B 13, 1681 (1976).
[4]C. M. Wolfe, D. M. Korn, and G. E. Stillman, Appl. Phys. Lett. 24, 78 (1974).
[5]C. M. Wolfe, G. E. Stillman, and D. M. Korn, in *Gallium Arsenide and Related Compounds, 1976*, edited by L. F. Eastman (Institute of Physics, London, 1977), p. 119.
[6]G. E. Stillman, (private communication).
[7]With respect to GaAs see, for example, G. E. Stillman, David M. Larsen, C. M. Wolfe, and R. C. Brandt, Solid State Commun. 9, 2245 (1971).
[8]The Hamiltonian used here does contain an odd-parity term proportional to d^3. This term is too small to exhibit observable effect.
[9]Preliminary calculations that such a term is generated by strains emanating from the defect in conjunction with the piezoelectric effects.
[10]David M. Larsen, Phys. Rev. B 25, 1126 (1981).
[11]G. Stillman (private communication).

D.3

Potential fluctuations in high-purity *n*-type III-V semiconductors

Peter A. Fedders
Department of Physics, Washington University, St. Louis, Missouri 63130

(Received 2 April 1982; accepted for publication 10 May 1982)

We investigate the effects of fluctuations in the Coulomb potential due to charged impurities in high-purity *n*-type III-V semiconductors at low temperatures. Assuming that charged donors and acceptors are randomly distributed at high temperatures, we conclude that the donors are selectively filled at low temperatures leaving nonrandom distributions of charged and filled donors. The potential fluctuations from these distributions can approximately account for a number of experimental observations on low-temperature high-purity GaAs including the apparent decrease of donor binding energy with increasing impurity concentration observed in Hall measurements, the sharpness and temperature dependence of the *ls*-2*p* transition along with the diffuse *ls*-conduction band edge observed in photoconductivity experiments, and the fact that experimentally observed photoconductivity line shapes are narrower than those previously predicted.

PACS numbers: 61.70.Wp, 72.40. + w, 72.80.Ey

I. INTRODUCTION

For years it has been known that a random distribution of equal concentrations of fixed positive and negative charges will yield infinite fluctuations in the Coulomb potential in the limit of an infinite volume.[1] These fluctuations can be damped, of course, by screening due to additional mobile charges or by a rearrangement of the fixed charges themselves. In light of this, consider a high-purity *n*-type semiconductor at low temperatures. As the temperature is lowered, the number of free carriers is reduced toward zero, and thus the screening or Debye radius tends toward infinity.[2] Since one does not normally think of the charged donors and acceptors as being mobile, one would naively expect the Coulomb fluctuations to become huge and finally infinite.

However, there is another available mechanism for partially screening these fluctuations that consists of the spatially selective filling of donor states rather than the usual picture of filling these states randomly. That is, the Coulomb fluctuations, and of course the free energy, will be lowered by selectively filling the charged donor states. The purpose of this paper is to investigate theoretically this process including the magnitude and consequences of the remaining finite fluctuations. We shall limit our discussion and arguments to *n*-type III-V semiconductors with low impurity concentrations of shallow donors and acceptors. For the purposes of this paper, low concentrations mean $n_d^{1/3}a_0 \ll 1$, where n_d is the number density of donors and a_0 is the Bohr radius of a shallow donor. Thus, for GaAs with $a_0 = 99$ A, our limit would include samples with $n_d \lesssim 10^{15}$ cm^{-3}. These concentrations are low enough so that impurity band conduction becomes very difficult.[3]

Given a random distribution of donors and acceptors, finding the actual distribution of filled and empty donors from first principles is an extremely difficult problem that will not be attempted here. Instead we approach the problem in a much more phenomenological (and less rigorous) way as follows. We asume that each acceptor can be paired with an unfilled or charged donor. This pairing radius is described by the probability distribution function for being able to construct a charge neutral volume around an acceptor with that radius. The distribution of Coulomb potentials can then be obtained and used to deduce various properties of the system.

The picture that emerges from our analysis of the system at low temperatures is as follows. There must, of course, be fluctuations in the Coulomb potential due to the charged impurities. However, these fluctuations are quite different from those which one would obtain from a random distribution of charged impurities. This nonrandom distribution of fluctuations due to the selective filling of donors has two important aspects. In the first place, the average potential energy that electrons feel from charged donors and acceptors is negative in regions of the crystal near filled donors even though the average Coulomb potential throughout the crystal is, of course, zero. Secondly, there are finite fluctuations in the potential energy of an electron about this mean value that are smaller than the average fluctuations in the crystal as a whole.

Further, our analysis provides at least an approximate explanation of a number of puzzling phenomena observed in relatively pure *n*-type GaAs at low temperatures. These include the apparent decrease in E_d, the donor binding energy, with increasing n_d as observed in Hall measurements[4,5] and the decrease in mobility of many samples below about 10 K.[5] It also includes the sharpness and temperature dependence of the *ls*-2*p* transition along with the lack of a sharp *ls*-conduction band edge observed in photoconductivity experiments.[5,6] Finally, it gives an explanation for the fact that experimentally observed photoconductivity line shapes are narrower than those predicted theoretically[7,8] using the familiar Holzmark distribution of electric fields in a sample.

There have been a number of previous explanations of some of the above phenomena that depend on the banding of impurity states.[5] However, as will be discussed, the Coulomb fluctuations are much greater than typical overlap integrals at low concentrations of impurities which should preclude banding.[3]

In the next section we present the basic model and cal-

 0021-8979/82/096154-07$2.40

culations used in our analysis of Coulomb fluctuations screened by the selective filling of donor states. Section III contains a discussion of our results and their applicability to experimental results. Appendices A and B contain some of the calculational details.

II. CALCULATIONS

First, it is instructive to pursue the concept of the random filling of charged donor states in somewhat more detail. Thus, we consider the distribution of electric potentials at a given point due to a random distribution of point charges with a density n_t. The potential at the origin due to single positive charge at r is the screened Coulomb potential

$$\phi(\mathbf{r}) = (e/\epsilon_0 r)\exp(-r/r_s), \tag{1}$$

where ϵ_0 is the static dielectric constant of the medium and r_s is a screening radius. We assume that the system is charge neutral so that the number of positively charged impurities is equal to the number of negatively charged impurities plus the number of conduction electrons. Finally, we take the low-concentration limit where n_t is much smaller than the density of lattice points.

The calculation of the distribution of potentials for the above system is easily obtained as a special case of the calculation described in Appendix B. For our purposes here it is sufficient to characterize the Coulomb potential fluctuations by their second moment and one obtains

$$\phi_r^2 = \langle \phi^2 \rangle = 2\pi n_t r_s e^2/\epsilon_0^2. \tag{2}$$

In order to apply this to an n-type semiconductor we take r_s to be the Debye screening radius,

$$r_s = (kT\epsilon_0/4\pi n e^2)^{1/2}, \tag{3}$$

where n is the density of conduction electrons (assumed nondegenerate) and

$$n_t = (2n_a + n), \tag{4}$$

where n_a is the density of charged acceptors and $n_a + n$ is equal to the density of charged donors. At this point one can see that as the density of conduction electrons tends toward zero, the Debye radius and ϕ_r tend toward infinity.

To proceed further we assume a crude model where the charged donors have only one bound state with binding energy E_d and, using effective mass theory,

$$E_d = e^2/2a_0\epsilon_0. \tag{5}$$

Since the potential energy fluctuations at different donor sites span a width in energy of order $e\phi_r$ we approximate these fluctuations by a band of width U_0 where

$$U_0 = \alpha e\phi_r, \tag{6}$$

and α is a constant of order one. Thus, assuming that the conduction band and edge lie at the potential energy, the bound donor states have energies with respect to the lowest part of conduction band edge of

$$E(x) = -E_d + U_0 x, \tag{7}$$

where x lies between zero and one. From Eqs. (2)–(6) we obtain

$$(U_0/E_d) = \alpha[(8\pi kT/E_d)(n_t^2 a_0^3/n)]^{1/4}. \tag{8}$$

Now, as n decreases, U_0 increases. However, if U_0 becomes too large, many of the charged donor states will no longer bind an electron because $E > 0$ in Eq. (7). This will self-consistently stabilize the Coulomb fluctuations at $U_0 \sim E_d$. One can obtain quantitative results from this model by performing the standard calculation[2] for n using Eq. (7) with x taking on all values between zero and one with equal probabilities. The results of this calculation show that if $E_d \gg kT$, the number of conduction electrons will not decrease exponentially as the temperature is lowered but will be proportional to kT. Since this argument does not depend on the density of donors or acceptors, it predicts impurity-induced conduction electrons at low temperatures for any concentration of impurities. Further, n will be proportional to kT and thus the effective E_d measured in Hall measurements would be zero.

At least for small enough concentrations of charged impurities the above scenario does not occur. In our picture we still assume that the original distribution of donors and acceptors is random since at the temperatures at which materials are usually synthesized there are plenty of conduction electrons available to screen the fluctuations. However, as the temperature is lowered and donor states start to fill, they will not be filled at random. Instead they will fill in such a manner as to lower the Coulomb fluctuations and also the energy of the system.

We now consider in more detail a system with a density of n_d of shallow donors, a density n_a of charged acceptors, and a compensation ration,

$$K = n_a/n_d, \tag{9}$$

less than one. Both types of charged impurities are distributed at random. If at low temperatures all of the conduction electrons are frozen out, then there must be n_a unfilled or charged donors and $(K^{-1} - 1)n_a$ filled or neutral donors. The large fluctuations discussed earlier are due to the long-range nature of the Coulomb potential and arise from regions of the sample that are not charge neutral. They are in no way due to the divergence of the Coulomb potential at the origin.

In order to understand the length scale of these fluctuations we ask the following question: Given a charged acceptor at the origin, what is the probability $P(r)$ of being able to enclose that acceptor in a charge-neutral sphere of radius r. Besides the acceptor at the origin the sphere may enclose k other acceptors and n donors. Since the number of charged donors must be equal to the number of acceptors, all integral values of n and k with

$$n - 1 \geq k \geq 0 \tag{10}$$

are allowed. This is a well-defined mathematical problem whose solution will yield some information about how small the Coulomb fluctuations can be made.

The solution to this problem is obtained in Appendix A and the result is

$$P(r) = 1 - Q(r),$$

$$Q(r) = e^{-x} + (2xK^{1/2})e^{-x}\int_0^1 dz I_1(2xzK^{1/2})\exp(-z^2 xK),$$

$$x = (r/r_d)^3, \tag{11}$$

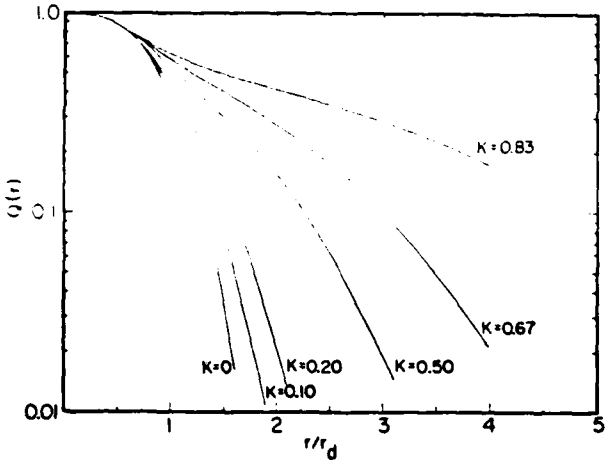

FIG. 1. $Q(r)$, the probability of not being able to enclose an acceptor in a charge neutral volume of radius r, vs r in units of an average interdonor spacing n_d. $Q(r)$ is plotted for various values of the compensation ratio $K = n_a/n_d$.

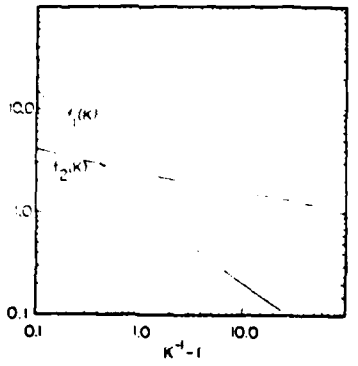

FIG. 2. The quantities $f_1(K)$ and $f_2(K)$ defined by Eqs. (15), describing the average and rms fluctuations of the potential energy of an electron, vs K.

where I_1 is the modified Bessel function and r_d is the average distance between donors

$$r_d = (3/4\,\pi n_d)^{1/3}. \tag{12}$$

Plots of $Q(r)$ for various values of K are given in Fig. 1 and, for very large values of r one can easily derive the asymptotic expression

$$Q(r) \simeq (K\,16\,\pi^2 z^2)^{-1/4} e^{-z},$$
$$z = (r/r_d)^3 (1 - K^{1/2})^2. \tag{13}$$

For small values of r/r_d or for small values of K, $P(r)$ is dominated by the probability of enclosing a single donor in the volume. However, as K increases, it is increasingly difficult to enclose more donors than acceptors and thus the probability of large positively charged volumes increases.

On one hand the above results are exact and do yield useful information about the distribution of Coulomb potentials. On the other hand they do not give any quantitative measurable properties of the system. Therefore, in order to make quantitative calculations, we assume that at low temperatures each acceptor can be associated with an unfilled or charged donor and that the probability density $p(r)$ that the two are separated by a distance r is related to $P(r)$ by the equation

$$4\,\pi r^2 p(r) = dP(r)/dr. \tag{14}$$

Further, we assume that a filled donor cannot be closer to an acceptor than the acceptor's partner is because otherwise the acceptor would have paired with the filled donor. Although the actual situation is far more complex than our simple model suggests, our model does correctly reflect the basic physics discussed in Sec. I.

With this model we can calculate the distribution of potentials in the sample due to the acceptors and charged donors. This is done in Appendix B. The distribution function itself can only be expressed in terms of several integrals, so we have computed the first two moments of the distribution. These results are plotted in Fig. 2 in the form

$$\langle U \rangle / E_d = -(U_1/E_d) = -y_a f_1(K),$$
$$\langle (U - \langle U \rangle)^2 \rangle^{1/2} / E_d = (U_2/E_d) = y_a f_2(K), \tag{15}$$

where the functions f_1 and f_2 are defined in Appendix B, Eq. (B8). Further, U_1 and U_2 are both positive, E_d is given by Eq. (5), y_a is a dimensionless measure of the average spacing between acceptors.

$$y_a = a_0/r_a,$$
$$r_a = (3/4\,\pi n_a)^{1/3}, \tag{16}$$

and K is the compensation ratio. The quantity $-U_1$ is the average potential energy of an electron near a filled donor due to charged donors and acceptors and U_2 is the rms potential energy fluctuation about $-U_1$ for the electron. The average potential energy of an electron anywhere in the sample is, of course, zero and the rms fluctuations about this value are $\sqrt{2}U_2$. Thus, because of the spatially nonrandom distribution of charged donors and acceptors, electrons in regions of the sample near filled donors have a lower (more negative) average potential energy with smaller rms fluctuations than electrons at arbitrary positions.

III. RESULTS

Based on the ideas and calculations of the previous sections we can now present an approximate picture of a low-temperature n-type III-V semiconductor with a low concentration of impurities and compare this picture to experimental observations on GaAs. When discussing shallow donors we shall use effective mass theory and, unless discussing transitions between hydrogenic states, we shall ignore any excited states of the donors. Including other hydrogenic states is not warranted by the accuracy of our model.

As discussed at the end of Sec. II, the potential energy of an electron due to charged donors and acceptors is zero with a rms fluctuation equal to $\sqrt{2}U_2$. Because of these fluctuations the bottom of the conduction band is not a well-defined quantity. However, we view it as a spatially varying quantity with minimum value denoted by E_c,

$$E_c = -\sqrt{2\alpha}U_2, \tag{17}$$

where α is a constant of order one. Electrons that are bound at donor sites feel an average potential energy of $-U_1$ with a

rms fluctuation of U_2. Thus we take the binding energy of these electrons to be

$$E_B(x) = E_d + U_1 + \alpha x U_2, \tag{18}$$

where x varies between plus and minus one and E_d is the effective mass binding energy. Therefore the binding energy of an electron with respect to the minimum of the conduction band is given by $E(x)$ where

$$E(x) = E_d + U_1 + \alpha U_2(-\sqrt{2} + x), \quad -1 \leqslant x \leqslant 1. \tag{19}$$

That is, the energy of a bound electron is an amount $E(x)$ below the minimum of the conduction band.

Thus we predict a spread or distribution of donor binding energies with

$$E_{max} = E_d + U_1 - (\sqrt{2} - 1)\alpha U_2$$
$$E_{av} = E_d + U_1 - \sqrt{2}\alpha U_2$$
$$E_{min} = E_d + U_1 - (\sqrt{2} + 1)\alpha U_2, \tag{20}$$

where E_{max}, E_{av}, and E_{min} are the maximum, average, and minimum binding energies, respectively. At temperatures such that U_2 is of order kT but not much less than kT we would expect E_{av} to control the temperature dependence of n in a Hall measurement. For $U_2 \gg kT$ we would expect E_{min} to be the controlling factor assuming that $E_{min} > 0$. If $E_{min} < 0$ the whole picture breaks down, although there may be a temperature range where the analysis is partly valid.

Of course the potential energy distribution of electrons averaged over the whole crystal or averaged over regions near filled donors does not cut off sharply in our model. The cutoff at energies of order the rms fluctuation is taken as a convenience. Since the distribution of potential energy involves simplifying assumptions anyway, we feel that little is lost by taking this convenience. However, we note that our distribution predicts an exponentially small probability for large potential energies and we believe that the exact distribution would also have this property. This means that a few electrons could never be bound to donors, although they could be trapped in regions of very small potential energy. We shall not pursue this fact in the remainder of this paper.

We now consider a qualitative and quantitative comparison of our theory with some experimental observations on GaAs. First we consider the dependence of the donor binding energy observed in Hall measurements on the concentrations of donor and acceptors. Table I contains values of impurity concentrations, observed donor binding energies, and computed values of K, U_1, and U_2 for various samples of high-purity GaAs. According to Eq. (20) and the ensuing discussion the observed donor binding energy, E_{do}, should be E_{av} which is related to U_1, U_2, and the effective mass donor binding energy, E_d, by the equation

$$(E_d + U_1 - E_{do})/E_d = \sqrt{2}\alpha U_2/E_d. \tag{21}$$

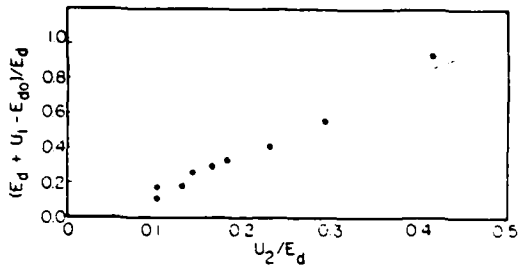

FIG. 3. Plot of $(E_d + U_1 - E_{do})/E_d$ vs U_2/E_d for the samples in Table I.

In order to check this and to determine the parameter α discussed above we have plotted $(E_d + U_1 - E_{do})/E_d$ vs U_2/E_d in Fig. 3 using the values in Table I and $E_d = 5.8$ meV.

The experimental points fall on a remarkably straight line with a slope corresponding to a value for α of 1.26. The fact that a line through the points does not pass through the origin indicates a value for E_d of 6.6 meV. This is somewhat higher than the 5.8 meV effective mass energy and the difference is larger than any expected central cell correction. However, in view of the straight line fit, this discrepancy appears to be independent of charged impurities. Since U_1, which is not an adjustable parameter, varies between 20% and 50% of $E_d - E_{do}$, we regard the excellent fit as evidence that our model has a reasonable quantitative validity.

In photoconductivity experiments on high-purity GaAs at low temperatures one observes a very sharp $1s$-$2p$ transition whose magnetic field dependence is in excellent agreement with effective mass theory with no corrections for fluctuations.[9] On the other hand, the $1s$-conduction band edge is either nonexistent or very diffuse. Photoconduction from the $1s$-$2p$ transition is believed to be thermally activated from the $2p$ level to the conduction band. However, the acti-

TABLE I. The quantities n_a, n_d, E_{do}, and K are the observed acceptor concentrations, donor concentrations, observed donor binding energies, and compensation ratios. The quantities U_1/E_d and U_2/E_d were computed using Eqs. (15).

Ref.	$n_a \times 10^{-12}$ cm^3	$n_d \times 10^{-12}$ cm^3	E_{do} in meV	K	U_1/E_d	U_2/E_d
a	21.3	48.0	5.52	0.44	0.046	0.103
a	40.7	204	5.09	0.20	0.022	0.103
a	136	502	4.51	0.27	0.045	0.166
a	327	1060	3.88	0.31	0.069	0.230
b	200	860	4.3	0.23	0.043	0.182
b	390	490	4.2	0.80	0.641	0.414
b	350	610	3.8	0.57	0.192	0.293
c	37.6	72.5	5.30	0.52	0.190	0.132
c	104	489	4.59	0.21	0.031	0.143

[a] G. E. Stillman, C. M. Wolfe, and J. O. Dimmock, Proc. 3rd Int. Conf. Photocond., Stanford, 1969 (Pergamon, Oxford, 1971), p. 265.
[b] Reference 11.
[c] G. E. Stillman and C. M. Wolfe (private communication).

vation energy of the strength of the transition is less than either $E_{do}/4$ or $E_d/4$ as would be expected from effective mass theory.[10]

Our picture is in agreement with all of these observations. Since the Coulomb fluctuations take place on a length scale much greater than a_0, they will have little effect on the low lying hydrogenic states and thus $E_{1s} - E_{2p}$ will be little affected as is observed.[8] However, the conduction band edge is spatially varying on a length much greater than a_0 and thus the *ls*-conduction band transition will have a spread of order $2\alpha U_2$ which will smear it considerably as is observed. For the first sample in Table I, $2\alpha U_2$ is 1.5 meV. This is quite close to the observed smearing for this sample.[11] Further, the 2*p*-conduction band energy gap will be given by Eqs. (19) and (20) with E_d replaced by $E_d/4$. Using the same analysis as that leading up to Eq. (21) we obtain

$$E_{av}(2s) = (E_d/4) + U_1 - \sqrt{2}\alpha U_2. \tag{22}$$

For the first sample in Table I this yields an activation energy of 0.65 meV which is reasonably close to the measured value[10] of 0.47 meV and much closer than the effective mass value of 1.45 meV.

Next, we consider what we consider a most puzzling and most underrated piece of evidence obtained from high-purity GaAs at low temperatures. It is apparently widely believed that the Holtzmark distribution describing the distribution of electric fields from a random distribution of charged impurities explains the line shapes observed in photoconductivity experiments. However, in the few careful comparisons between theory and experiment it has been noted that while the line shape predicted by the theory is fairly good, the number density of charged impurities necessary for quantitative agreement is considerably smaller than that obtained from transport measurements.[7,8] This is particularly disturbing since the observed line is *narrower* than the predicted line and thus additional broadening mechanisms cannot be invoked to explain the discrepancy.

Our picture provides a qualitative and even a semiquantitative explanation of this behavior. Although the charged acceptors do constitute a random distribution, the charged donors do not because they are more likely to lie near an acceptor than one would deduce from a random distribution. Further, the filled donors, which photoconductivity experiments sample, are not randomly placed either but are likely to be further from an acceptor than one would deduce from a random distribution. Both of these effects tend to decrease the electric fields at filled donor sites. Preliminary calculations on the distribution of electric fields have been performed with the following results. As K approaches one, the distribution of electric fields is exactly a Holtmark distribution with the effective number of impurities reduced by a factor of four. For values of K nearly one the distribution of electric fields is nearly Holtzmark with the effective number of impurities reduced to somewhat more than four.

Of course for small values of K the distribution of electric fields will more closely resemble a distribution from dipoles with a density n_a and a dipole moment of $r_d = K^{1/3} r_a$. We consider these line shape effects to be the strongest evidence in support of our picture because they most clearly depend on the nonrandomness of the distribution of charges.

Finally, we briefly consider the mobility of samples where $E_d > kT$ but at temperatures high enough so that hopping conduction can be ignored. At temperature $kT \sim U_2$ and below, the fluctuations in the Coulomb potential should constitute a significant scattering mechanism for the conduction electrons that is not included in the potential scattering due to charged impurities. In fact when kT is considerably less than U_2 there must be significant volumes of the sample that are virtually inaccessible to the electrons. Since U_2 depends on K for fixed n_a, this mechanism should be more pronounced as K approaches one. In fact this sort of behavior is observed, for example, with sample P128(b) and P121(a) of Ref. 11 which have almost identical values of n_a. However, the above argument only indicates that our theory has the trend correct. Actual calculations on this effect would be very useful.

ACKNOWLEDGMENTS

This work was sponsored in part by the Office of Naval Research under contract N00014-80C-0762. We wish to acknowledge useful and stimulating conversations with D. L. Rode.

APPENDIX A

In this Appendix we sketch the solution to the following mathematical problem. We are given a lattice with probabilities c_1 and c_2 of having particles of type 1 (donors) and type 2 (acceptors), respectively, on a given site where

$$c_2 < c_1 \ll 1. \tag{A1}$$

We wish to find $Q(N)$, the probability that a volume of N lattice sites does not contain more particles of type 1 than of type 2. Thus,

$$Q(N) = \sum_{m_1=0}^{N} \sum_{m_2=m_1}^{N} \binom{N}{m_1}\binom{N}{m_2} c_1^{m_1}(1-c_1)^{N-m_1} c_2^{m_2} \times (1-c_2)^{N-m_2}, \tag{A2}$$

$$\binom{N}{m} = \frac{N!}{m!(N-m)!}$$

The summation over m_2 can be expressed in terms of the incomplete beta function yielding

$$Q(N) = \sum_{m=0}^{N} Q_m(N),$$

$$Q_0(N) = (1-c_1)^N,$$

$$Q_m(n) = c_1^m (1-c_1)^{N-m} \binom{N}{m}^2 m \int_0^{c_2} t^{m-1}(1-t)^{N-m}\, dt, \quad m > 1. \tag{A3}$$

The summation over m can be performed exactly by constructing the sum

$$[(1+xe^{i\theta})(1+xe^{-i\theta})]^N = \sum_{m_1=0}^{N} \sum_{m_2=0}^{N} \binom{N}{m_1}\binom{N}{m_2} x^{m_1+m_2} e^{i\theta(m_1-m_2)}, \tag{A4}$$

integrating θ from 0 to 2π, and taking a derivative to obtain

$$\frac{x}{4\pi}\frac{d}{dx}\int_0^{2\pi} d\theta\,[1+x^2+2x\cos\theta\,]^N$$

$$=\sum_{m=1}^{\infty}\binom{N}{m}^2 m x^{2m}. \tag{A5}$$

Thus we can write

$$Q(N)=(1-c_1)^N+\int_0^{c_2} dt\int_0^{2\pi}\frac{d\theta}{4\pi}\frac{(1-c_1)^N(1-t)^N}{t}$$

$$x\frac{d}{dx}[1+x^2+2x\cos\theta\,]^N,$$

$$x=(c_1 t/(1-c_1)(1-t))^{1/2}. \tag{A6}$$

Since c_1 and c_2 are much less than one we can expand

$$[1+x^2+2x\cos\theta\,]^N=\exp(N\ln(1+x^2+2x\cos\theta))$$
$$\cong\exp(2Nx\cos\theta), \tag{A7}$$

the expansion being valid if $x^2N\ll 1$. One can easily check that values of N violating this restriction would constitute 10^{14} atoms for concentrations of impurities of order 10^{15} cm^{-3}. For N this large $Q(N)$ is ridiculously small. Further, by similar arguments,

$$(1-c)^N\cong\exp(-Nc),$$

$$(1-t)^N\cong\exp(-Nt),$$

$$x\cong(c_1 t)^{1/2}. \tag{A8}$$

When Eqs. (A6)–(A8) are combined, the θ integration can be expressed exactly in terms of a Bessel function of imaginary argument and one obtains

$$Q(N)=e^{-Nc_1}\left[1+\int_0^{c_2}\frac{dt}{t}e^{-tN}(c_1 t)^{1/2}NI_1[2(c_1 t)^{1/2}N\,]\right]. \tag{A9}$$

Equation (11) can be obtained by a simple change of variables and by noting that

$$(Nc_1)=(r/r_d)^3 \tag{A10}$$

for a sphere of radius r containing N lattice points.

APPENDIX B

In this Appendix we derive the distribution function and first two moments for the Coulomb potential of an electron due to the nonrandom distributions of chargerd donors and acceptors. We consider a random distribution of a small concentration of acceptors where $U_a(\mathbf{r})$ is the potential energy of an electron at the origin due to an acceptor at $\mathbf{r}$. Further, for each acceptor, there is a donor with a probability density $p(\mathbf{r})$ that the donor is at a position $\mathbf{r}$ away from the acceptor. The contribution to the potential energy of an electron at the origin from a donor at $\mathbf{r}$ is $U_d(\mathbf{r})$. By a straightforward generalization of a method used earlier,[13] one can easily obtain $F(U)dU$, the probability than an electron at the origin has a poetntial energy between U and $U+dU$.

$$F(U)=\int_{-\infty}^{\infty}\frac{dt}{2\pi}e^{iUt}e^{-I(t)},$$

$$I(t)=n_a\int d^3r\,d^3r'p(\mathbf{r}-\mathbf{r}')\{1-\exp[it(U_a(\mathbf{r})+U_d(\mathbf{r}'))]\}, \tag{B1}$$

where n_a is the density of acceptors.

In this case,

$$U_a(\mathbf{r})=-U_d(\mathbf{r})=e^2/\epsilon_0 r. \tag{B2}$$

For an electron at an arbitrary position Eqs. (B1) are correct as they stand. However, for an electron bound (or near to) a filled donor, the acceptor must be closer to its paired donor than to the filled donor and thus there is a restriction on the $\mathbf{r}$ and $\mathbf{r}'$ integrations such that

$$|\mathbf{r}|>|\mathbf{r}-\mathbf{r}'|. \tag{B3}$$

The moments of the distribution can be obtained by expanding $I(t)$ in a power series to obtain

$$M_k=n_a(e^2/\epsilon_0)^k\int d^3r\,d^3r'p(\mathbf{r}')(r^{-k}-|r-r'|^{-k}),r>r'. \tag{B4}$$

for $k=1,2$, one of the integrals in (B4) can easily be performed yielding

$$M_1=-(2\pi n_a e^2/3\epsilon_0)J_2=\langle U\rangle$$

$$M_2=(2n_a\pi e^4/\epsilon_0^2)J_1=\langle(U-\langle U\rangle)^2\rangle$$

$$J_k=\int d^3r r^k p(\mathbf{r}). \tag{B5}$$

By using Eq. (14), integrating by parts once, and changing variables from r to $N=4\pi\rho r^3$, where ρ is the density of lattice points we obtain

$$J_k=(3/4\pi\rho)^{k/3}(k/3)\int_0^{\infty}N^{(k-3)/3}Q(N)\,dN, \tag{B6}$$

where $Q(N)$ is in Appendix A. By using Eq. (A9) for $Q(N)$, the N integral is a tabulated Laplace transform of a Bessel function and we obtain

$$J_k=(3/4\pi\rho)^{k/3}(k/3)[\Gamma(k/3)c_1^{-k/3}+\Gamma(2+k/3)(c_1c_2)^{1/2}$$

$$\times\int_0^1 dx\,x^{-1/2}(c_1-c_2x)^{-1-k/3}P_{k/3}^{-1}((c_1+c_2x)/(c_1-c_2x))], \tag{B7}$$

where c_1 and c_2 are defined in Appendix A, $\Gamma(z)$ is the gamma function, and $P_{k/3}^{-1}$ is the Legendre function. By combining Eqs. (B7) with Eqs. (B5) and making another change of variables one obtains Eqs. (15) with

$$f_1(K)=(2K^{2/3}/3)\Gamma(2/3)[1+(10/9)L_2(K)],$$

$$(f_2(k))^2=(2K^{1/3})\Gamma(1/3)[1+(4/9)L_1(K)], \tag{B8}$$

$$L_k(K)=\int_0^{K/1-K}(x+1)^{(k-3)/3}F(-k/3,1+k/3;2,-x)\,dx,$$

where $F(a,b;c,z)$ is the hypergeometric function. The integral is performed numerically to obtain Fig. 2.

[1] B. I. Shklovskiĭ and A. L. Éfros, Zh. Eksp. Teor. Fiz. 60, 867 (1971) [Sov. Phys. JETP 33, 468 (1971)].

[2] See, for example, J. S. Blakemore, *Semiconductor Statistics* (Pergamon, Oxford, 1962).

[3] N. F. Mott and E. A. Davis, *Electronic Processes in Non-Crystalline Materials* (Clarendon, Oxford, 1971).

[4] C. M. Wolfe and G. E. Stillman in *Gallium Arsenide and Related Compounds* (Proc. 3rd Int. Symp., Aachen, 1970) Inst. Phys. and Phys. Soc., London, 1971.

[5]G. E. Stillman, C. M. Wolfe, and O. J. Dimmock, in "Far Infrared Photoconductivity in High Purity GaAs" in *Semiconductors and Semimetals*, Vol. 12 (Academic, New York, 1977).
[6]G. E. Stillman, D. M. Wolfe, and D. M. Korn, in *11th Conf. Phys. Semicond.* Warsaw, Poland, 1972, p. 863. Polish Sci. Publ., Warsaw, 1973.
[7]D. M. Korn and David M. Larsen, Solid State Commun. **13**, 807 (1973).
[8]David M. Larsen, Phys. Rev. B **13**, 1681 (1976).
[9]G.E. Stillman, David M. Larsen, C. M. Wolfe, and R. C. Brandt, Solid State Commun. **9**, 2245 (1975).
[10]G. E. Stillman, C. M. Wolfe, and O. J. Dimmock, in "Far Infrared Photoconductivity in High Purity GaAs" *in Semiconductors and Semimetals*, Vol. 12 (Academic, New York, 1977), p. 226.
[11]G. E. Stillman, C. M. Wolfe, and J. O. Dimmock, Proc. 3rd Int. Conf. Photocond., Stanford, 1969 (Pergamon, Oxford, 1971), p. 265.
[12]J. Whitaker and D. E. Bolger, Solid State Commun. **4**, 181 (1966).
[13]P. A. Fedders, Phys. Rev. B **11**, 1020 (1975).

Inst. Phys. Conf. Ser. No. 65: Chapter 6
Paper presented at Int. Symp. GaAs and Related Compounds, Albuquerque, 1982

D.4 Coulomb potential fluctuations in high-purity n-type III–V semiconductors

Peter A. Fedders

Department of Physics, Washington University, St. Louis, Missouri 63130

Abstract. We investigate the effects of fluctuations in the Coulomb potential due to charged impurities in high-purity n-type III-V semiconductors at low temperatures. Assuming that charged donors and acceptors are randomly distributed at high temperatures, we conclude that the donors are selectively filled at low temperatures leaving non-random distributions of charged and filled donors. The potential fluctuations from these distributions can approximately account for a number of experimental observations on low-temperature high-purity GaAs.

1. Introduction

For years it has been known that a random distribution of equal concentrations of fixed positive and negative charges will yield infinite fluctuations in the Coulomb potential in the limit of an infinite volume (Shklovskii and Effros 1971). These fluctuations can be damped, of course, by screening due to additional mobile charges or by a rearrangement of the fixed charges themselves. In light of this, consider a high-purity n-type semiconductor at low temperatures. As the temperature is lowered, the number of free carriers is reduced toward zero, and thus the screening or Debye radius tends toward infinity (Blakemore 1963). Since one does not normally think of the charged donors and acceptors as being mobile, one would naively expect the Coulomb fluctuations to become huge and finally infinite.

However, there is another available mechanism for partially screening these fluctuations that consists of the spatially selective filling of donor states rather than the usual picture of filling these states randomly. That is, the Coulomb fluctuations, and of course the free energy, will be lowered by selectively filling the charged donor states. The purpose of this paper is to theoretically investigate this process including the magnitude and consequences of the remaining finite fluctuations. We shall limit our discussion and arguments to n-type III-V semiconductors with low impurity concentrations of shallow donors and acceptors. For the purposes of this paper, low concentrations mean $n_d^{1/3} a_0 \ll 1$ where n_d is the number density of donors and a_0 is the Bohr radius of a shallow donor. Thus, for GaAs with $a_0 \approx 99$ A, our limit would include samples with $n_d \lesssim 10^{15}$ cm^{-3}. These concentrations are low enough so that impurity band conduction becomes very difficult (Mott and Davis 1971).

Given a random distribution of donors and acceptors, finding the actual distribution of filled and empty donors from first principles is an extremely difficult problem that will not be attempted here. Instead

0305-2346/83/0065-0545 $02.25

we approach the problem in a much more phenomenological (and less rigorous) way as follows. We assume that each acceptor can be paired with an unfilled or charged donor. This pairing radius is described by the probability distribution function for being able to construct a charge neutral volume around an acceptor with that radius. The distribution of Coulomb potentials can then be obtained and used to deduce various properties of the system.

The picture that emerges from our analysis of the system at low temperatures is as follows. There must, of course, be fluctuations in the Coulomb potential due to the charged impurities. However, these fluctuations are quite different from those which one would obtain from a random distribution of charged impurities. This non-random distribution of fluctuations due to the selective filling of donors has two important aspects. In the first place, the average potential energy that electrons feel from charged donors and acceptors is negative in regions of the crystal near filled donors even though the average Coulomb potential throughout the crystal is, of course, zero. Secondly, there are finite fluctuations in the potential energy of an electron about this mean value that are smaller than the average fluctuations in the crystal as a whole.

As will be discussed, our analysis provides at least an approximate explanation of a number of puzzling phenomena observed in relatively pure n-type GaAs at low temperatures.

2. Calculations

In our picture we assume that the original distribution of donors and acceptors is random since at the temperatures at which materials are usually synthesized there are plenty of conduction electrons available to screen the fluctuations. However, as the temperature is lowered and donor states start to fill, they will not be filled at random. Instead they will fill in such a manner as to lower the Coulomb fluctuations and also the energy of the system.

We now consider in more detail a system with a density n_d of shallow donors, a density n_a of charged acceptors, and a compensation ratio,

$$K = n_a/n_d \quad , \tag{1}$$

less than one. Both types of charged impurities are distributed at random. If at low temperatures all of the conduction electrons are frozen out, then there must be n_a unfilled or charged donors and $(K^{-1}-1)n_a$ filled or neutral donors. The large fluctuations discussed earlier are due to the long-range nature of the Coulomb potential and arise from regions of the sample that are not charge neutral. They are in no way due to the divergence of the Coulomb potential at the origin.

In order to understand the length scale of these fluctuations we ask the following question: Given a charged acceptor at the origin, what is the probability P(r) of being able to enclose that acceptor in a charge-neutral sphere of radius r. Besides the acceptor at the origin the sphere may enclose k other acceptors and n donors. Since the number of charged donors must be equal to the number of acceptors, all integral values of n and k with $n-1 \geq k \geq 0$ are allowed. This is a well defined mathematical problem whose solution will yield some information about how small the Coulomb fluctuations can be made. The solution to this problem is presented elsewhere (Fedders 1982).

Plots of Q(r) vs. r_d for various values of K are given in Figure 1 where

$$Q(r) = 1 - P(r) \ , \quad r_d = (3/4\pi n_d)^{1/3} \ . \tag{2}$$

For small values of r/r_d or for small values of K, P(r) is dominated by the probability of enclosing a single donor in the volume. However, as K increases, it is increasingly difficult to enclose more donors than acceptors and thus the probability of large positively charged volumes increases.

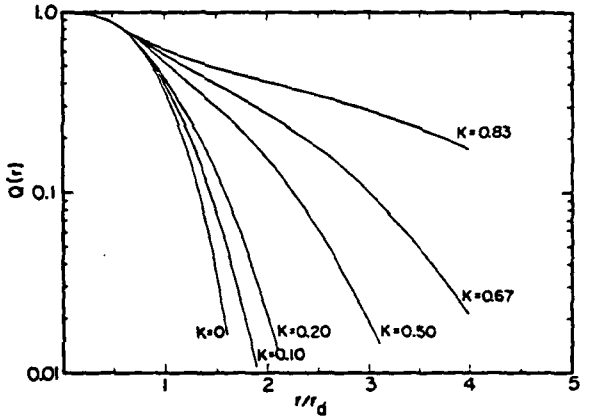

Figure 1
Q(r), the probability of not being able to enclose an acceptor in a charge neutral volume of radius r, vs. r in units of an average interdonor spacing r_d. Q(r) is plotted for various values of the compensation ratio $K = n_a/n_d$.

On one hand the above results are exact and do yield useful information about the distribution of Coulomb potentials. On the other hand they do not give any quantitative measurable properties of the system. Therefore, in order to make quantitative calculations, we assume that at low temperatures each acceptor can be associated with an unfilled or charged donor and that the probability density p(r) that the two are separated by a distance r is related to P(r) by the equation

$$4\pi r^2 \, p(r) = dP(r)/dr \tag{3}$$

Further, we assume that a filled donor cannot be closer to an acceptor than the acceptor's partner is because otherwise the acceptor would have paired with the filled donor. Although the actual situation is far more complex than our simple model suggests, our model does correctly reflect the basic physics discussed in Sect. 1.

With this model we can calculate the distribution of potentials in the sample due to the acceptors and charged donors. The distribution function itself can only be expressed in terms of several integrals so we have computed the first two moments of the distribution. These results are plotted in Figure 2 in the form

$$\begin{aligned} \langle U \rangle / E_d &= -(U_1/E_d) = -y_a \, f_1(K) \ , \\ \langle (U - \langle U \rangle)^2 \rangle^{1/2} / E_d &= (U_2/E_d) = y_a \, f_2(K) \ , \end{aligned} \tag{4}$$

where the functions f_1 and f_2 are given elsewhere (Fedders 1982). Further, U_1 and U_2 are both positive, E_d is the effective mass binding energy, y_a is a dimensionless measure of the average spacing between acceptors,

$$y_a = a_0/r_a \quad , \quad r_a = (3/4\pi n_a)^{1/3} \tag{5}$$

and K is the compensation ratio. The quantity $-U_1$ is the average potential energy of an electron near a filled donor due to charged donors and acceptors and U_2 is the rms potential energy fluctuation about $-U_1$ for the electron. The average potential energy of an electron anywhere in the sample is, of course, zero and the rms fluctuations about this value are $\sqrt{2}U_2$. Thus, because of the spatially non-random distribution of charged donors and acceptors, electrons in regions of the sample near filled donors have a lower (more negative) average potential energy with smaller rms fluctuations than electrons at arbitrary positions.

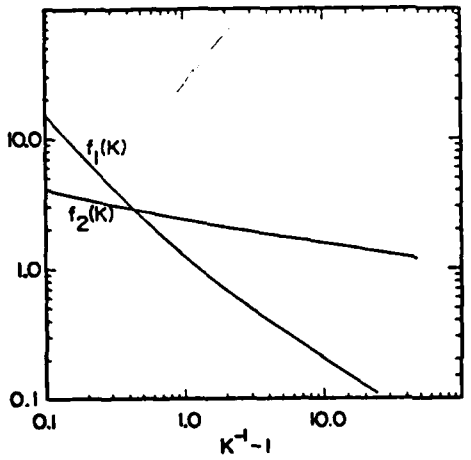

Figure 2

The quantities $f_1(K)$ and $f_2(K)$ defined by Eqs. (4) describing the average and rms fluctuations of the potential energy of an electron, vs. K.

3. Results

Based on the ideas and calculations of the previous sections we can now present an approximate picture of a low-temperature n-type III-V semiconductor with a low concentration of impurities and compare this picture to experimental observations on GaAs. When discussing shallow donors we shall use effective mass theory and, unless discussing transitions between hydrogenic states, we shall ignore any excited states of the donors. Including other hydrogenic states is not warranted by the accuracy of our model.

As discussed at the end of Sect. 2, the potential energy of an electron due to charged donors and acceptors is zero with an rms fluctuation equal to $\sqrt{2}U_2$. Because of these fluctuations the bottom of the conduction band is not a well defined quantity. However, we view it as a spatially varying quantity with minimum value given by $-\sqrt{2}\,\alpha\,U_2$ where α is a constant of order one. Electrons that are bound at donor sites feel an average potential energy of $-U_1$ with an rms fluctuation of U_2. Thus E_{av}, the average binding energy of an electron with respect to the minimum of the conduction band, is given by

$$E_{av} = E_d + U_1 - \sqrt{2}\,\alpha U_2 \quad , \tag{6}$$

with rms fluctuations of order U_2. At temperatures such that U_2 is less than or of order kT we expect E_{av} to control the temperature dependence of n in Hall measurements. When kT becomes less than U_2 substantial parts of the sample are virtually inaccessible to the conduction electrons and the effective mass picture is no longer valid. Of course the potential energy distribution of electrons averaged over the whole crystal or averaged over regions near filled donors does not cut off sharply in our model. The cut-off at energies of order the rms fluctuation is taken as a convenience.

We now consider a qualitative and quantitative comparison of our theory with some experimental observations on GaAs. First we consider the dependence of the donor binding energy observed in Hall measurements on the concentrations of donor and acceptors. Table I contains values of impurity concentrations, observed donor binding energies, and computed values of U_1, and U_2 for various samples of high-purity GaAs. According to Eq. (6) and the ensuing discussion the observed donor binding energy, E_{do}, should be E_{av} which is related to U_1, U_2, and the effective mass donor binding energy, E_d by the equation

$$(E_d + U_1 - E_{do})/E_d = \sqrt{2}\,\alpha U_2/E_d \quad . \tag{7}$$

In order to check this and to determine the parameter α discussed above we have plotted $(E_d + U_1 - E_{do})/E_d$ vs. U_2/E_d in Figure 3 using the values in Table I and E_d = 5.8 meV.

Table I: Observed values of n_a (in 10^{-12} cm^3), n_d (in 10^{-12} cm^3), K, and E_{do} (in meV) and computed values of U_1/E_d and U_2/E_d.

Ref.	n_a	n_d	E_{do}	U_1/E_d	U_2/E_d	K
a	21.3	48.0	5.52	0.046	0.103	0.44
a	40.7	204	5.09	0.022	0.103	0.20
a	136	502	4.51	0.045	0.166	0.27
a	327	1060	3.88	0.069	0.230	0.31
b	200	860	4.3	0.043	0.182	0.23
b	390	490	4.2	0.641	0.414	0.80
c	37.6	610	3.8	0.192	0.293	0.57
c	104	489	4.59	0.031	0.143	0.21

[a] G. E. Stillman, C. M. Wolfe, and J. O. Dimmock, Proc. 3rd Int. Conf. Photocond., Stanford, 1969, p. 265, Pergamon, Oxford, 1971.

[b] G. E. Stillman, C. M. Wolf, and J. O. Dimmock, Proc. 3rd Int. Conf. Photocond., Stanford, 1969, p. 265, Pergamon, Oxfore, 1971.

[c] G. E. Stillman and C. M. Wolfe, private communication.

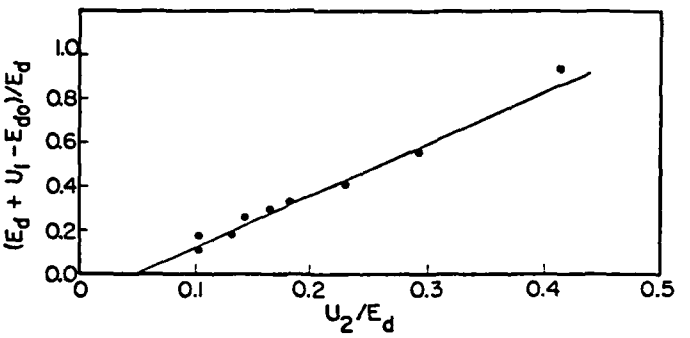

Figure 3: Plot of $E_d + U_1 - E_{do}/E_d$ vs. U_2/E_d for the sample in Table I.

The experimental points fall on a remarkably straight line with a slope corresponding to a value of of 1.26. The fact that a line through the points does not pass through the origin indicates a value for E_d of 6.6 meV. This is somewhat higher than the 5.8 meV effective mass energy and the difference is larger than any expected central cell correction. However, in view of the straight line fit, this discrepancy appears to be independent of charged impurities. Since U_1, which is not an adjustable parameter, varies between 20% and 50% of $E_d - E_{do}$, we regard the excellent fit as evidence that our model has a reasonable quantitative validity. Further, from Eqs. (4), (6), and Figure 2 one can see that observed donor binding energy is predicted to increase as K increases for fixed n_a. This is in at least qualitative agreement with observations on transmutation doped Ge (Cuevas 1967).

In photoconductivity experiments on high-purity GaAs at low temperatures one observes a very sharp 1s-2p transition whose magnetic field dependence is in excellent agreement with effective mass theory with no corrections for fluctuations (Stillman et al. 1975). On the other hand, the 1s-conduction band edge is either non-existent or very diffuse. Photoconduction from the 1s-2p transition is believed to be thermally activated from the 2p level to the conduction band. However, the activation energy of the strength of the transition is less than either $E_{do}/4$ or $E_d/4$ as would be expected from effective mass theory (Stillman et al. 1974).

Our picture is in agreement with all of these observations. Since the Coulomb fluctuations take place on a length scale much greater than a_0, they will have little effect on the low lying hydrogenic states and thus E_{1s}-E_{2p} will be little affected as is observed (Larsen 1976). However, the conduction band edge is spatially varying on a length much greater than a_0 and thus the 1s-conduction band transition will have a spread of order $2\alpha U_2$ which will smear it considerably as is observed. For the first sample in Table I, $2\alpha U_2$ is 1.15 meV. This is quite close to the observed smearing for this sample (Stillman et al. 1971). Further, the 2p-conduction band energy gap will be given by Eq. (6) with E_d replaced by $E_d/4$. Using the same analysis as that leading up to Eq. (7)

we obtain an activation energy of 0.65 meV for the first sample in Table I which is reasonably close to the measured value (Stillman et al. 1977) of 0.47 meV and much closer than the effective mass value of 1.45 meV.

Next, we consider what we consider a most underrated piece of evidence obtained from high-purity GaAs at low temperatures. It is apparently widely believed that the Holtzmark distribution describing the distribution of electric fields from a random distribution of charged impurities explains the lineshapes observed in photoconductivity experiments. However, in the few careful comparisons between theory and experiment it has been noted that while the lineshape predicted by the theory is fairly good, the number density of charged impurities necessary for quantitative agreement is considerably smaller than that obtained from transport measurements (Korn and Larson 1973; Larsen 1979). This is particularly disturbing since the observed line is narrower than the predicted line and thus additional broadening mechanisms cannot be invoked to explain the discrepancy.

Our picture provides a qualitative and even a semiquantitative explanation of this behavior. Although the charged acceptors do constitute a random distribution, the charged donors do not because they are more likely to lie near an acceptor than one would deduce from a random distribution. Further, the filled donors, which photoconductivity experiments sample, are not randomly placed either but are likely to be further from an acceptor than one would deduce from a random distribution. Both of these effects tend to decrease the electric fields at filled donor sites. Preliminary calculations on the distribution of electric fields have been performed with the following results. As K approaches one, the distribution of electric fields is exactly a Holtzmark distribution with the effective number of impurities reduced by a factor of four. Four values of K nearly one the distribution of electric fields is nearly Holtzmark with the effective number of impurities reduced by somewhat more than four. Of course for small values of K the distribution of electric fields will more closely resemble a distribution from dipoles with a density n_a and a dipole moment of $r_d = K^{1/3} r_a$.

Kogan (1980) has performed computer simulations on the selective filling of donor states and his numerical results and our analytic results on the distribution of electric fields agree quite well for $K < 0.9$. Thus it now appears that observed photoconductivity lineshapes are too broad to be explained entirely by ionized impurities.

Acknowledgments

This work was sponsored in part by the Office of Naval Research under contract N0014-80C-0762.

References

Blakemore, J.S. Semiconductor Statistics, (Pergamon Press, Oxford, 1962).
Cuevas, M. (1967) Phys. Rev. 164, 1021.
Mott, N.F. and Davis, E.A., Electronic Processes in Non-Crystalline Materials, (Clarendon Press, Oxford, 1971).
Fedders, P.A. (1982) to be published in J. Appl. Phys.
Korn, D.M. and Larsen, David M. (1973) Solid State Commun. 13, 807.
Larson, David M. (1976) Phys. Rev. B 13, 1681.
Shklovskiĭ, B.I. and Éfros, A.L. (1971) Zh. Eksp. Teor. Fiz 60, 867 (Sov. Phys. -JETP 33, 468 (1971).

Stillman, G. E., Wolfe, C. M., and Dimmock, O. J. (1977) in Far Infrared Photoconductivity in High Purity GaAs in Semiconductors and Semimetals, Vol. 12, Academic Press, New York.
Stillman, G. E., Wolf, C. M., and Dimmock, O. J. (1977) in Far Infrared Photoconductivity in High Purity GaAs in Semiconductors and Semimetals, Vol. 12, Academic Press, New York, p. 226.
Stillman, G. E., Wolfe, C. M., and Dimmock, J. O. (1971) Proc. 3rd Int. Conf. Photocond., Stanford, 1969 , p. 265, Pergamon, Oxford.

PHYSICAL REVIEW B VOLUME 27, NUMBER 8 15 APRIL 1983

D.5 Energy shift of hydrogenic donors in a magnetic field due to electric and strain fields

Peter A. Fedders
Department of Physics, Washington University, St. Louis, Missouri 63130
(Received 2 December 1982)

We calculate the second-order shifts in the energies of the 1s and $2p_-$ states of hydrogenic donors in a magnetic field due to electric fields and combination of electric and strain fields in a piezoelectric medium. The results are discussed as a possible explanation of different line shapes and linewidths associated with different donors as observed in photoconductivity experiments on GaAs.

I. INTRODUCTION

In this paper we calculate the second-order shifts in the energies of the 1s and $2p_-$ states of hydrogenic donors in a magnetic field due to electric fields and due to a combination of electric and strain fields in a piezoelectric medium. Given a distribution of electric fields or a distribution of electric fields and the strain field of a donor impurity, one can use these shifts to calculate donor line shapes as measured in photoconductivity experiments.

Recently there has been a lot of interest in the identification of various shallow donor impurities in GaAs by photoconductivity measurements on the $1s$-$2p_-$ transition in high magnetic fields. These measurements[1-5] have been made on samples fabricated by different growth techniques at different growth temperatures and correlations between these factors and relative concentrations of different donor impurities have been obtained. In addition, these experiments have exhibited a wide variety of line shapes and linewidths that appear to be as strongly correlated with the growth technique as with concentrations of charged impurities or mobilities.

In the past it has been widely believed that line shapes of shallow donor hydrogenic transitions were controlled by the concentrations of charged impurities and, in particular, that the $1s$-$2p_-$ line shape at high magnetic fields is primarily determined by second-order Stark shifts caused by a distribution of electric fields generated by the charged impurities.[6] Although this mechanism is undoubtedly an important one, experimental evidence shows that other mechanisms must play a role. For example, different donors in the same sample routinely exhibit different linewidths or line shapes and donors in samples with similar electrical properties exhibit different donor line shapes that appear to be correlated with the manner in which the sample was fabricated.

In an earlier paper[7] we investigated the electrostatic effects on the energy of a hydrogenic donor complex in the presence of an externally applied magnetic field and noted that there can be no cross terms in the energy shift that is linear in the electric field and in the dimensions of the complex. In this paper we note that a substitutional or interstitial donor will in general have a strain field associated with it and, in a piezoelectric medium, there will be an electrostatic potential associated with that strain field. However, in this case, there is a cross term in the energy shift that is linear in the electric field and in the strength of the strain field generated by the donor.

The method used in the calculation is based upon one used recently by Larsen[8] to calculate the second-order shift in energy of the 1s state to an applied electric field. Some modifications are necessary because the $2p_-$ state is degenerate with other states in the absence of a magnetic field. In addition, the method is easily extended to include cross terms between an electric field and other perturbations. In Sec. II we shall describe the basic model and perturbations arising from electric and strain fields. The actual calculations and their relationship to previous work are contained in Sec. III. Section IV contains the presentation and a discussion of our results.

II. MODEL

In reduced units the zero-order Hamiltonian H_0 is that of a simple hydrogenic donor at the origin interacting with an external magnetic field:

$$H_0 = -\nabla^2 + \frac{\gamma}{i}\frac{\partial}{\partial\phi} + \tfrac{1}{4}\gamma^2\rho^2 - \frac{2}{r}, \tag{1}$$

where lengths and energies are taken in units of the effective Bohr radius $a_0 = \epsilon_0\hbar^2/m^*e^2$ and the effective Rydberg $R = m^*e^4/2\epsilon_0^2\hbar^2$. The dimensionless magnetic field strength is $\gamma = \hbar\omega_c/2R$, where $\omega_c = eB/m^*c$, the magnetic field $\vec{B}$ defines the z

direction, θ and ϕ are the usual polar and azimuthal angles, and $\rho = r\sin\theta$. We consider two perturbations on this system. The first perturbation is the usual Stark term described by the Hamiltonian

$$H_1' = \vec{F}\cdot\vec{r}, \tag{2}$$

where the dimensionless vector $\vec{F}$ is given by $\vec{F} = ea_0\vec{E}/R$ where $\vec{E}$ is a uniform electric field. Equation (2) can also be written in a far more convenient spherical form as

$$H_1' = (F_+ e^{-i\phi} + F_- e^{i\phi})\rho + F_z z. \tag{2'}$$

where $z = r\cos\theta$ and $F_\pm = \frac{1}{2}(F_x \pm iF_y)$.

The second perturbation is far more complicated. In our picture an impurity donor is the source of a strain field and that strain field generates an electrostatic potential because of the piezoelectric coupling. According to elastic continuum theory a defect will produce a material displacement proportional to r^{-2} and a strain field proportional to r^{-3} at distances r that are large compared to the size of the defect. A fairly common model[9] is one where $\vec{u}(\vec{r})$, the displacement of a material point $\vec{r}$ due to a defect at the origin, is given by the equation

$$\vec{u}(\vec{r}) = b^3\vec{r}/\vec{r}, \tag{3}$$

where b has the units of length and is related to the size of the defect. The model defect defined by Eq. (3) is easy to manipulate analytically and reflects the correct r dependence at large distances which will dominate our results if the Bohr radius is much larger than the defect. However, the angular dependence predicted by Eq. (3) is far too simple to be realistic.

For a sphalerite structure the potential energy of an electron interacting with the electric potential generated by the model defect is[10]

$$V(\vec{r}) = 36\pi b^3 \frac{ee_{14}}{\epsilon_0}\frac{xyz}{r^5}, \tag{4}$$

where e_{14} is the piezoelectric coupling constant and where spatial directions refer to the crystalline axes. If $V(\vec{r})$ is expressed in the coordinate system defined by the magnetic field, then it will possess terms proportional to $e^{im\phi}$ with $m = \pm 2, \pm 1$, and 0. Since we are primarily interested in cross terms between this and the Stark effect, only the terms with $m = \pm 1, 0$ are relevant and we obtain the second-perturbation Hamiltonian in reduced units,

$$H_2' = [(G_+ e^{-i\phi} + G_- e^{i\phi})\rho + G_z z]z^2/r^5. \tag{5}$$

The G_m, dimensionless measures of the coupling strength, can be written as

$$G_m = (36\pi b^3 ee_{14}/\epsilon_0 a_0^2 R)\xi_m, \tag{6}$$

where $m = 0, \pm 1$, $\xi_1 = \xi_{-1}^*$, and all of the ξ_m are of order one.

In general the G's in Eq. (5) will depend on the orientation of the magnetic field with respect to the crystal axes. However, Eq. (3) is far too simple to describe a realistic material displacement and thus any detailed angular dependence cannot be viewed as reliable. Thus Eq. (5) will yield only an estimate of the effects due to strains and the b's must be estimated or obtained from other measurements.

III. CALCULATIONS

For a perturbation Hamiltonian H' that possesses no diagonal elements, the energy shift of a state x to second order in H' is ΔE_x,

$$\Delta E_x = \sum_{n\neq x} \frac{|\langle n|H'|x\rangle|^2}{E_x - E_n}, \tag{7}$$

where $|n\rangle$ and E_n are the eigenvectors and energies of the states of H_0. There are a number of ways of evaluating Eq. (7) including the summation over a few states n that are believed to be most important. Another way is to find a function $h_x(\vec{r})$ such that

$$\begin{aligned} &\langle n|h_x(\vec{r})|x\rangle = \langle n|H'|x\rangle/(E_x - E_n), \\ &\langle x|h_x(r)|x\rangle = 0. \end{aligned} \tag{8}$$

In this case Eq. (7) reduces to

$$\Delta E_x = \langle x|H'h_x(r)|x\rangle. \tag{9}$$

Of course the difficulty is in finding a function $h_x(\vec{r})$ that satisfies Eqs. (8). If the perturbation Hamiltonian H' contains two distinct terms

$$H' = \lambda_1 H_1' + \lambda_2 H_2', \tag{10}$$

then similarly one obtains

$$\Delta E_x = \lambda_1^2\alpha_{11}(x) + 2\lambda_1\lambda_2\alpha_{12}(x) + \lambda_2^2\lambda_{22}(x), \tag{11}$$

where

$$\begin{aligned} \alpha_{ij}(x) &= \langle x|H_i' h_{jx}(\vec{r})|x\rangle \\ &= \langle x|H_j' h_{ix}(\vec{r})|x\rangle, \\ \langle n|h_{ix}(\vec{r})|x\rangle &= \langle n|H_i'|x\rangle/(E_x - E_n), \\ \langle x|h_{ix}(\vec{r})|x\rangle &= 0. \end{aligned} \tag{12}$$

Thus in order to obtain α_{11} and α_{12}, only $h_{1x}(\vec{r})$ must be obtained, but not $h_{2x}(\vec{r})$.

The second-order Stark shift for the 1s hydrogenic donor in a magnetic field has been calculated by a number of authors[8,11,12] and our treatment follows Larsen's[8] quite closely. To our knowledge the method has not been used to calculate the energy shifts of any excited states. Stark-shift calculations of the $1s$-$2p_-$ energy difference by summing over a

few states have been performed as part of a line-shape analysis,[13] but ΔE has not been presented. As we shall see, summing over a few states appears to give reasonably good results for the quadratic Stark shift but terrible results for perturbations involving H_2'.

Larsen has recently described a variational method for obtaining $h_x(\vec{r})$ when Eqs. (8) cannot be solved exactly; the details are contained in Ref. (8). In this method one assumes a trial solution of the form

$$h_x(\vec{r})=\sum_i a_i f_i(\vec{r}), \tag{13}$$

where the $f_i(\vec{r})$ are chosen functions and the a_i are determined variationally by the equations

$$\begin{aligned}&\langle x \mid f_i(H'-A) \mid x\rangle=0,\\ &A \mid x\rangle=[h_x(r),H_0] \mid x\rangle.\end{aligned} \tag{14}$$

Equation (13) is then used in Eq. (9) to determine ΔE_x.

The wave functions used for the $1s$ and $2p_-$ states of H_0 were obtained by variational calculations with trial functions of the form

$$\begin{aligned}&\psi_{1s}(\vec{r})=A\exp(-ar-b^2\rho^2-c^2z^2),\\ &\psi_{2p_-}(r)=A\rho\exp(-ar-b^2\rho^2-c^2z^2-i\phi).\end{aligned} \tag{15}$$

These wave functions are discussed in Ref. (7) and are both lowest energy states with quantum numbers $m=0,-1$, respectively. In the calculations terms from H_1' and H_2' with different spherical components do not mix and thus each contribution can be computed separately. Further, since we are primarily interested in terms linear and quadratic in the electric field, we need only calculate the three spherical components of $h_{1x}(\vec{r})$ for $x=1s$ and $2p_-$. The trial functions $f_i(\vec{r})$ will be described in this section but the results will be presented in Sec. IV.

For the $1s$ state the functions chosen for the $m=0$ part of h_1 were of the form

$$f_{kn}(0)=r^n\cos^{2k+1}\theta, \tag{16}$$

and for the $m=\pm 1$ part of the h_1 the functions chosen were of the form

$$f_{kn}(m)=r^n\sin^{2k+1}\theta e^{-im\phi}. \tag{17}$$

In all cases the results at $\gamma=0$ were exact, the results converged rapidly as more terms were added, and f_{kn} with $k=0$, $n=1$–4 and $k=1$, $n=3$ and 4 are included in the final results. The $m=0,-1$ parts of H_1' for the $2p_-$ state were also perfectly straightforward and the same f_{kn} with the same values of k and n were used.

A problem arises with the $m=+1$ part of H_1' for the $2p_-$ state because this perturbation connects the $2p_-$ state with the $2s$ state and these are degenerate at $\gamma=0$. Thus this part of $\alpha_{11}(T)$ will be proportional to γ^{-1} as γ approaches zero. However, an $h_{1x}(\vec{r})$ constructed from f_{kn} with $(k,n)=(-1,-1)$, $(-1,0)$, $(0,1)$, $(0,2)$, and $(-1,1)$ can be found which satisfies Eqs. (12) to leading order in γ. By adding to this set, the results at finite γ converge quickly and our results include the functions f_{kn} with $k=-1$, $n=-1$–3 and $k=0$, $n=1$–4. The contribution to $\alpha_{12}(T)$ does not diverge as γ approaches zero because the appropriate matrix element between the $2p_-$ and $2s$ states vanishes.

IV. DISCUSSION

The shift in energy between the $1s$ and $2p_-$ states of a hydrogenic donor due to the perturbations H_1' and H_2' that was calculated in the last section can be written as

$$\begin{aligned}\Delta E&=\Delta E(2p_-)-\Delta E(1s)\\ &=\alpha_{11}(z)F_z^2-\alpha_{11}(T)F_T^2-\alpha_{12}(z)G_zF_z\\ &\quad-\alpha_{12}(T)\vec{G}_T\cdot\vec{F}_T\end{aligned} \tag{18}$$

in dimensionless units, where $\vec{F}_T=F_x\hat{x}+F_y\hat{y}$, and similarly for $\vec{G}_T$. As discussed earlier $\vec{F}$ is a dimensionless vector that is proportional to an applied electric field and $\vec{G}$ is a dimensionless measure of the strain field generated by the donor. The four coefficients α in Eq. (18) are plotted as a function of the dimensionless magnetic field strength in Figs. 1 and 2. As one would have expected $\alpha_{11}(z)$ and

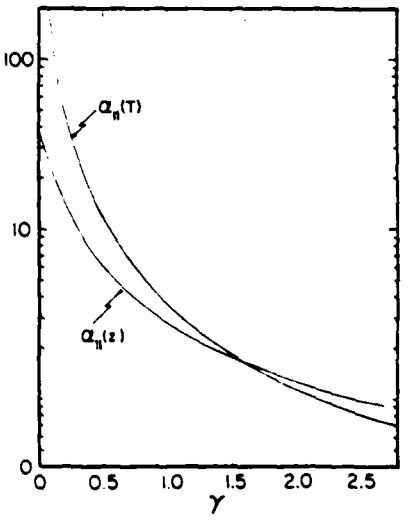

FIG. 1. Plot of the dimensionless coefficients $\alpha_{11}(T)$ and $\alpha_{11}(z)$ vs the dimensionless magnetic field γ.

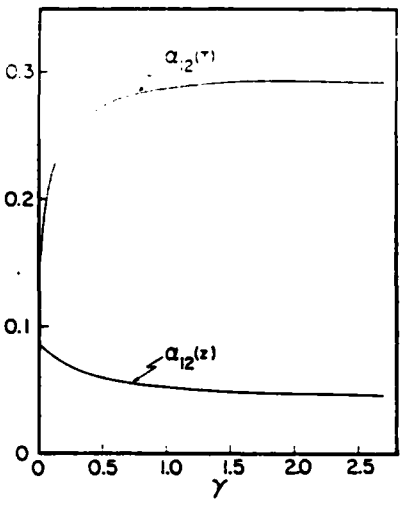

FIG. 2. Plot of the dimensionless coefficients $\alpha_{12}(T)$ and $\alpha_{12}(z)$ vs the dimensionless magnetic field γ.

$\alpha_{11}(T)$ are strongly decreasing functions of magnetic field strength and, in addition, the $2p_-$ contribution is much greater than the $1s$ contribution. On the other hand $\alpha_{12}(z)$ and $\alpha_{12}(T)$ depend rather weakly on the magnetic field and the contributions of the $1s$ and $2p_-$ states are of the same order of magnitude. For this reason we have included the contribution from the $2p_-$ state in Table I.

It is quite difficult to assess the accuracy of matrix elements computed by variational methods. Thus we shall limit the discussion on the precision of our results to a comparison of the $1s$ contributions to $\alpha_{11}(z)$ and $\alpha_{11}(T)$ to the recent results obtained by Larsen.[8] Larsen used variational wave functions of a more complex nature than ours that yielded slightly lower energies and, in addition, employed several corrections to the α's that we did not use. Nevertheless, our values are quite close to his in that our values of the $1s$ part of $\alpha_{11}(z)$ were 1.8%, 3.5%, 5.8%, and 6.7% lower than his at values of $\gamma=$ 0.5, 1.0, 2.0, and 3.0, respectively. The discrepancy between our values of the $1s$ contribution to $\alpha_{11}(T)$ were slightly less. The above errors are probably a reasonable measure of the error in all of our values of the α's even though the $2p_-$ state dominates the values of $\alpha_{11}(z)$ and $\alpha_{11}(T)$. This obtains because both the $1s$ and $2p_-$ are ground states in the manifold of states with $m=0$ and -1, respectively, and thus there is no reason to expect the $2p_-$ calculation to be significantly better or worse than the $1s$ calculations.

TABLE I. Contribution of the $2p_-$ state to $\alpha_{12}(z)$ and $\alpha_{12}(T)$ as a function of the dimensionless magnetic field strength γ.

γ	$[\alpha_{12}(z)]_{2p_-}$	$[\alpha_{12}(T)]_{2p_-}$
0.0	−0.214	0.041
0.1	−0.223	0.118
0.3	−0.237	0.158
0.5	−0.246	0.171
0.8	−0.255	0.179
1.0	−0.259	0.182
1.5	−0.267	0.183
2.0	−0.273	0.182
2.5	−0.278	0.180

We have also performed a few calculations for the energy shift to second order in H_2'. At $\gamma=0$ we obtain

$$\Delta E=0.124G_z^2+0.58G_\tau^2. \tag{19}$$

This shift is almost entirely due to the $1s$ state because the perturbation is proportional to r^{-2}. The degeneracy of the $2p_-$ states with other $n=2$ states is not a factor in this case because all matrix elements between degenerate states vanish. The magnetic field dependence of Eq. (19) is not very great; less than that of a central cell correction. Further, it is interesting to compare our results with the results that one would obtain by summing over a few exact states. We have done this for the $1s$ state at zero magnetic field where there are no degeneracy problems and where wave functions are known exactly. For α_{11} summing Eq. (7) over a few states gives an excellent approximation to the exact results. Conversely, the values of α_{12} and α_{22} obtained this way are only small fractions of the exact results. This indicates that the continuum or scattering states of the hydrogen atom contribute significantly to or even dominate the results in these cases.

We shall now comment briefly on the magnitudes of the terms that we have calculated with physical constants appropriate for GaAs. The magnitude of H_1' in units of the rydberg is

$$H_1' \sim e^2 a_0/\epsilon_0 r_i^2, \tag{20}$$

where r_i is an average spacing between charged impurities. Similarly, the magnitude of H_2' in units of the rydberg is

$$H_2' \sim 36\pi b^3 e_s/\epsilon_0 a_0^2. \tag{21}$$

The ratio of the magnitudes, H_2'/H_1', is about 10^2 for $b=10^{-8}$ cm and $n_i=10^{15}$ cm^{-3}, and is about 1 for $b=10^{-8}$ cm and $n_i=10^{12}$ cm^{-3} where n_i is the density of charged impurities. Further, α_{12} is about 0.1 of α_{11} at $\gamma\sim 1$ or a magnetic field of about 65 kG. Thus assuming that a substitutional donor creates a reasonable (but not huge) strain field, the cross term may have an appreciable effect. The rel-

ative importance of the effect should be greater at larger magnetic fields because the α_{11} decrease as the field is increased and the α_{12} are roughly constant.

We have performed a number of line-shape calculations including both the Stark and cross terms in order to assess the effects of the cross term on photoconductivity line shapes. In these calculations we have used a Holtzmark distribution of electric fields and have also assumed that $\alpha_{11}(z)=\alpha_{11}(T)$ and $\alpha_{12}(z)=\alpha_{12}(T)$. Thus the line shape as a function of energy $F(\epsilon)$ is easily seen to be

$$F(\epsilon)=\int P(\vec{E})\delta(\epsilon-AE^2-\vec{B}\cdot\vec{E})d^3E, \quad (22)$$

where $P(\vec{E})$ is the isotropic distribution of electric fields $\vec{E}$, while A and $\vec{B}$ are related to α_{11} and α_{12}, respectively. While neither of the above approximations is correct, they are good enough to see the effects of the cross term. For example, the characteristic very asymmetric line shape usually associated with photoconductivity lines is caused largely because of a second-order shift and the details of the electric field distribution are not of overwhelming importance.

Our results show that the second-order Stark distribution can be broadened by a factor of 2 or 3 by the cross term without its shape being significantly altered, except in the far wings. Thus to within experimental error, our calculations provide a mechanism whereby different donors could yield different linewidths even if they felt the same distribution of electric fields. However, as a function of magnetic field strength γ, the α_{11} decrease quite rapidly while the α_{12} are roughly constant. Thus as a function of increasing field strength the line would narrow as fast as predicted by including just the Stark term, and the line would eventually become more symmetric. This behavior was not noticed in Ref. 13. Finally, the cross term should yield a line shape that is angle dependent. However, as noted in Sec. II, our model of the strain is far too simple to yield believable angular dependences and thus we cannot estimate the size of this anisotropy.

ACKNOWLEDGMENTS

This work was sponsored in part by the U.S. Office of Naval Research under Contract No. NO0014-80C-0762.

[1]C. M. Wolfe, G. E. Stillman, and J. O. Dimmock, J. Appl. Phys. 41, 504 (1970).

[2]M. Ozeki, K. Kitaphara, K. Nakai, A. Stibatomi, K. Dazai, S. Okawa, and O. Ryuzan, Jpn. J. Appl. Phys. 16, 1617 (1977).

[3]T. S. Low, G. E. Stillman, D. M. Collins, C. M. Wolfe, S. Tiwari, and L. F. Eastman, Appl. Phys. Lett. 40, 1034 (1982).

[4]T. S. Low, G. E. Stillman, T. Nakanisi, T. Udagawa, and C. M. Wolfe, Appl. Phys. Lett. 41, 183 (1982).

[5]T. S. Low, B. J. Skromme, and G. E. Stillman, in *Proceedings of the 10th International Symposium on GaAs and Related Compounds, Albuquerque, 1982*, edited by J. A. Revill (IOP, London, 1983).

[6]David M. Larsen, Phys. Rev. B 13, 1681 (1976).

[7]P. A. Fedders, Phys. Rev. B 25, 3846 (1982).

[8]David M. Larsen, Phys. Rev. B 25, 1126 (1981).

[9]C. P. Flynn, *Point Defects and Diffusion* (Clarendon, Oxford, 1972), Chap. 3.

[10]P. A. Fedders, J. Appl. Phys. (in press).

[11]D. L. Dexter, Phys. Rev. A 18, 862 (1978).

[12]N. O. Lipari and D. L. Dexter, Phys. Rev. B 18, 1346 (1978).

[13]D. M. Korn and David M. Larsen, Solid State Commun. 13, 807 (1973).

E. ELECTRON SCATTERING FROM IMPURITIES AND DEFECTS

E.1 Magnetic-field dependence of the Hall factor for isotropic media

D. L. Rode and C. M. Wolfe
Department of Electrical Engineering, Washington University, St. Louis, Missouri 63130
G. E. Stillman
Department of Electrical Engineering, University of Illinois at Urbana-Champaign, Urbana, Illinois 61801

(Received 5 May 1982; accepted for publication 21 September 1982)

The magnetic-field dependence of the Hall factor is investigated theoretically and experimentally. The theory includes arbitrary band structure, carrier degeneracy, and wave functions assuming isotropic media and carriers behaving as spinless Fermions without energy-level quantization. Comparisons between theory and experiments on high-purity GaAs from the low magnetic-field limit to the classical high magnetic-field limit agree to within 0.7 percent.

PACS numbers: 07.55. + x, 72.20.My

I. INTRODUCTION

The Hall effect[1] is widely used in semiconductor research and development to determine the free-carrier concentrations of doped materials at temperatures ranging from a few degrees Kelvin to the melting temperatures.[2,3]

From the time of the earliest successful theoretical interpretations of the Hall coefficient R_H by Gans,[4,5] it has been known that R_H is inversely proportional to free-carrier concentration n:

$$R_H = r_H/en, \tag{1}$$

where e is the electron charge and r_H is the Hall scattering factor. Since the late 1950's, it has been customary to assume that $r_H = 1$ for interpreting experimental results. Nevertheless, the scattering factor does not equal unity in general and, furthermore, r_H depends on the strength of the magnetic field used for the Hall measurement.

To our knowledge, there has never been a quantitative comparison between theory and experiment on the magnetic-field dependence of the Hall scattering factor as given in Sec. V. We review in Sec. II some of the historical background of the Hall effect with particular emphasis on the scattering factor. In Sec. III, we derive general results of the theory of the Hall effect. In Sec. IV, we investigate the classical strong magnetic-field limit. In Sec. V, detailed theoretical calculations of the scattering factor are compared to experiments on n-type GaAs for varying magnetic-field strengths.

II. HISTORICAL BACKGROUND

In Gans' treatment of the Hall effect, he assumed a single noninteracting free-carrier species (electrons) with a constant-mass dispersion relation and classical statistics.[4] Furthermore, the electrons were supposed to be scattered in such a manner that they experienced a constant mean-free-path, independent of electron energy. This treatment gave rise to one of the well-known equations for the scattering factor.[4,6,7]

$$r_H = \langle \tau^2 \rangle / \langle \tau \rangle^2 = 3\pi/8. \tag{2}$$

For a general power-law dependence of mean-free-path on energy and for classical particle behavior, one can calculate various scattering factors ranging between about unity (constant scattering rate) and $315\pi/512 \simeq 1.93$ (Coulomb scattering).[8,9]

It appears that Harding[10] was the first to correctly rederive Gans' results within the more general framework of Boltzmann's equation and quantum mechanics, albeit assuming constant-mass particle behavior. Harding also wrote scattering terms for the Boltzmann equation which correctly included *scattering-in* and *scattering-out* terms as well as *inelastic* scattering by lattice phonons. However, in order to derive analytical expressions for the magnetoresistance and Hall coefficient of semiconductors, Harding assumed the lattice phonon energy to be negligibly small in comparison to electron energy. This assumption is one of the approximation methods which leads to what is nowadays known as the relaxation-time approximation (RTA).[7]

One of the first calculations incorporating Fermi statistics and inelastic phonon scattering as well as realistic electronic band structure was carried out by Ehrenreich.[11,12] These calculations were performed for the zero magnetic-field limit including all the dominant electron scattering mechanisms for InSb at temperatures from 200 to 700 K. Corresponding experimental results are, however, unavailable.

Further theory and calculations of the Hall scattering factor for electrons in fifteen different pure direct-gap polar semiconductors and semimetals were published by Rode.[13] These results showed that calculated values for r_H lie between unity and about 1.3 for wide ranges of temperature with r_H reaching its maximum value at a temperature corresponding to about one-half the Debye temperature of the longitudinal polar-optical phonon.

III. HALL-EFFECT THEORY

A general equation for the electron probability function f_{total} which satisfies the classical Boltzmann equation in the presence of a small electric field **F** and an orthogonal magnetic field **B** of arbitrary strength can be written as follows for isotropic media[13]:

$$f_{\text{total}} = f_{FD}(k) + xg(k) + yh(k), \tag{3}$$

where f_{FD} is the Fermi-Dirac distribution, x and y are the direction cosines measured respectively from **F** to **k** and **B** × **F** to **k** and $\hbar\mathbf{k}$ is the crystal momentum and $k = |\mathbf{k}|$.

Solutions for the small (relative to f_{FD}) perturbation distributions g and h can be written in implicit closed form as finite-difference equations.[13] These solutions are applicable to any isotropic system of spinless Fermions without energy-

 0021-8979/83/010010-04$02.40

level quantization.

$$g = \frac{S_i(g + \beta h) - (eF/\hbar)(\partial f_{FD}/\partial k)}{(1 + \beta^2)S_o}, \tag{4a}$$

$$h = \frac{S_i(h - \beta g) - (e\beta F/\hbar)(\partial f_{FD}/\partial k)}{(1 + \beta^2)S_o}. \tag{4b}$$

S_i and S_o are *scattering-in* and *scattering-out* operators which contain arbitrary numbers of elastic and inelastic electron scattering mechanisms at thermal equilibrium[13]; e.g., piezoelectrically coupled phonons, deformation potential coupled phonons, polar-optical phonons, ionized centers, etc. Magnitudes are denoted by $F = |\mathbf{F}|$ and $B = |\mathbf{B}|$. The quantity β, in a thermally averaged sense, is roughly equal to the dimensionless product $\mu B = \omega_c/\nu$, where μ is electron drift mobility, ω_c is cyclotron resonance frequency, and ν is the average momentum relaxation rate. Precisely, we have

$$\beta(k) = evB/\hbar k S_o, \tag{5}$$

$$v = (1/\hbar)(\partial \mathscr{E}/\partial k) \equiv (\hbar k/md), \tag{6}$$

where v is electron-group velocity, $\mathscr{E}$ is electron kinetic energy, m is free-electron mass, and d is defined in terms of $\partial\mathscr{E}/\partial k$ for convenience. The band structure is given by the energy $\mathscr{E}$ *versus* crystal momentum $\hbar\mathbf{k}$ relationship. We are assuming an isotropic medium so that $\mathscr{E}(\mathbf{k}) = \mathscr{E}(k)$.

The small magnetic-field limit corresponds to $\mu B \ll 1$ (or, small β). The classical high-magnetic field limit corresponds to $\mu B \gg 1$ (or, large β). For example, very pure GaAs at room temperature with $\mu \simeq 0.9$ m^2/V sec has $\mu B = 0.9$ at $B = 10$ kG.

The perturbation distribution g gives rise to electric current parallel to electric field F. The perturbation h gives rise to current in a direction perpendicular to F. The geometrical configuration is illustrated in Fig. 1.

The Hall scattering factor for arbitrary magnetic field B is denoted by r_B whereas r_H denotes the $B = 0$ limit of r_B. In general, subscript B denotes a quantity measured with finite magnetic field, and subscript H denotes the zero magnetic-field limit of the quantity.

Now we relate the perturbation distributions g and h to experimental measurements of r_B. Denote the Hall voltage and Hall electric field strength by V_B and E_B.

$$V_B \equiv E_B w, \tag{7}$$

$$V_B \equiv R_B B J w, \tag{8}$$

$$= R_B B I/d, \tag{9}$$

$$= r_B B I/end, \tag{10}$$

where w is the specimen width between Hall voltage measurement points, R_B is the Hall coefficient, J is electric-current density, I is total electric current, d is specimen thickness, and n is uniform electron concentration.

The Hall mobility is defined as μ_B.

$$\mu_B \equiv R_B \sigma, \tag{11}$$

$$\sigma \equiv en\mu, \tag{12}$$

where σ is conductivity and μ is electron drift mobility measured with zero magnetic field.

Thus, we have the following results:

$$r_B = \mu_B/\mu, \tag{13}$$

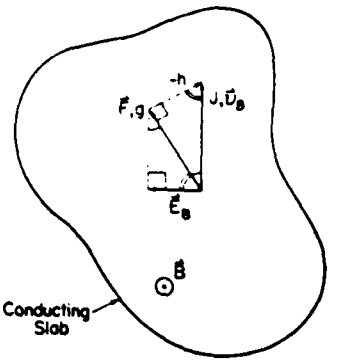

FIG. 1. Magnetic field B is applied normal to a conducting slab of thickness d. Current density J (transverse to B) induces average carrier drift velocity v_B and transverse Hall electric E_B. The total electric field is F. The perturbation distributions g and h give rise to carrier drift velocities directed as shown on the figure for positive charges.

$$r_B = endV_B/BI, \tag{14}$$

$$r_B = enE_B/BJ, \tag{15}$$

$$r_B = enE_B/env_B B, \tag{16}$$

$$r_B = (E_B/FB)/(v_B/F), \tag{17}$$

where v_B is the average electron drift velocity in the presence of electric field F and transverse magnetic field B. From Eqs. (4), (6), and (17), we obtain

$$r_B = -\left[(4\pi\hbar/3m)\int (k^3 h/FBd)\,dk \cdot (4\pi)\int k^2 f_{\text{total}}\,dk\right] \div (4\pi\hbar/3m)^2\left\{\left[\int (k^3 g/Fd)\,dk\right]^2 + \left[\int (k^3 h/Fd)\,dk\right]^2\right\}, \tag{18}$$

$$r_B = -(3mF/\hbar B)\left[\int k^3 h/d)\,dk \cdot \int k^2 f_{FD}\,dk\right] \div \left\{\left[\int (k^3 g/d)\,dk\right]^2 + \left[\int (k^3 h/d)\,dk\right]^2\right\}. \tag{19}$$

For the results given in Sec. V the exact expression (19) is solved numerically by iteration as discussed elsewhere.[13,14]

There are several features of Eq. (19) worth pointing out. First, according to Eqs. (4), h and g are linearly proportional to F. Hence, r_B is independent of F, as can be seen by inspection of Eq. (18).

Second, the algebraic sign of h given by Eq. (4b) is negative definite so that r_B is positive definite.

Third, nowhere have we assumed particle-like behavior (i.e., effective mass). Indeed, the band-structure and wave functions can be arbitrarily complicated provided the electron dispersion relation is isotropic and there are no electron-spin interactions. The formulation includes, as a special case, direct-gap semiconductors such as n-type GaAs, where the Γ conduction-band valley is approximately isotropic and spin degenerate.[14] Specifically excluded are cases where the band structure is anisotropic in k space, e.g., hexagonal ZnO or cubic indirect-gap semiconductors such as Si and Ge.

IV. CLASSICAL HIGH MAGNETIC-FIELD LIMIT

From Eqs. (4) in the limit of large magnetic field B, β is arbitrarily large and g vanishes as $1/B^2$. On the other hand, the perturbation h decreases as $1/B$.

$$Bh_x = \lim_{B=\infty} Bh = (eF/\hbar)(\partial f_{FD}/\partial k)/(evB/\hbar k),$$
$$Bh_z = (mdF/\hbar)(\partial f_{FD}/\partial k). \tag{20}$$

Note that h_x is proportional to electric-field strength F. From Eq. (19), we have

$$r_x = \lim_{B=\infty} r_B = -(3m/\hbar)\int k^2 f_{FD}\,dk \Big/ \int (k^3 Bh_x/Fd)\,dk,$$
$$r_\infty = -3\int k^2 f_{FD}\,dk \Big/ \int k^3(\partial f_{FD}/\partial k)\,dk. \tag{21}$$

With no loss of generality, Eq. (21) can be integrated by parts assuming that f_{FD} vanishes for large k.

$$r_\infty = -3\int k^2 f_{FD}\,dk \Big/ \left[k^3 f_{FD}\Big|_0^\infty - 3\int k^2 f_{FD}\,dk\right],$$
$$r_\infty = 1. \tag{22}$$

Therefore, it is proved that the classical strong magnetic-field limit of the Hall scattering factor is unity for any isotropic system of spinless Fermions at thermal equilibrium.

This conclusion is valid in the face of inelastic scattering, arbitrary isotropic band structure and wave functions, and arbitrary statistical degeneracy. Excluded are situations where electrons are scattered by spin interactions or where the band structure is anisotropic, i.e., cases where electron energy $\mathscr{E}(\mathbf{k}) \neq \mathscr{E}(k)$.

V. RESULTS

Hall-effect measurements were reported on a high-purity n-type GaAs sample labeled "Normal" by Wolfe *et al.*[15] Since it was anticipated that the Hall factor would fall to unity at large values of magnetic field, the results were presented assuming that $r_B = 1$ at the largest magnetic field used for the experiments (83 kG). Values for r_B at magnetic fields down to 0.44 kG were determined by assuming that variations of Hall coefficient with magnetic field are due entirely to the magnetic-field dependence of the Hall factor.

From Eqs. (4) and (19), it can be determined that r_B approaches unity asymptotically with $1/B^2$. The experimental data[15] have been corrected on this basis and are listed in Table I. Compared to the values given earlier,[15] the experimental data listed in Table I have been increased by 0.3 percent, which is within the estimated experimental error in r_B of ± 0.005 units. The experimental results and estimated error are plotted in Fig. 2.

Theoretical values of Hall factor were calculated from Eq. (19) with material parameters and band structure as given earlier for GaAs.[14] Experimental[15] donor and acceptor concentrations (N_D and N_A) measured from Hall freeze-out characteristics were included to provide a relatively small amount of ionized-purity scattering. Errors in N_D and N_A are estimated to be unimportant because of the relatively slight dependence of r_B on N_D and N_A under the present high-purity conditions. Electron scattering takes place primarily by fundamental lattice scattering mechanisms[14] in the present cases.

Theoretical calculations of r_B were carried out with an estimated error of less than ± 0.006. The results and estimated error are listed in Table I and plotted as the solid curve and vertical error bar in Fig. 2.

Sensitivity of the calculated results to the assumed values of effective mass at $k = 0$ was tested at 5 kG. A nine percent change in effective mass yields a 0.35 percent change in r_B. The assumed value of effective mass ($0.066m$) is thought to be accurate to within three percent, and r_B should be accurate to within about one-tenth percent on this basis.

Agreement between theory and experiment in Fig. 2 is within calculational and experimental error. The greatest discrepancies occur at the lowest magnetic fields, where the ratio of experimental to theoretical Hall factor is 1.0069.

We conclude that, within estimated errors of less than one percent, the agreement between theory and experiment verifies the classical theory of the Hall effect.

ACKNOWLEDGMENTS

It is a pleasure to acknowledge discussions of transport theory with Professor J. D. Wiley, University of Wisconsin, and with Dr. R. S. Allgaier, Department of the Navy (ret.), concerning the Hall anisotropy factor.

This research was partly supported by the Office of Naval Research under Contract No. 00014-80-C-0762.

APPENDIX I

The result that $r_\infty = 1$, even for the *classical* limit of $B = \infty$, is at first sight somewhat surprising. Alternatively, it might seem obvious that this result obtains. However, the latter notion is usually supported by an argument which runs as follows:

TABLE I. Magnetic-field dependence of Hall factor for high-purity n-GaAs at 295 K.

Magnetic field, B (kilogauss)	Scattering factor, r_B (experimental)	Scattering factor, r_B (theoretical)
0		1.164 ($\pm$ 0.006)
0.44	1.172 ($\pm$ 0.005)	1.164
1.00	1.170	1.163
2.30	1.158	
3.00	1.156	1.157
4.00	1.149	
5.00	1.139	1.146[a]
5.90	1.132	
8.00	1.119	
9.00	1.111	
10.0	1.104	1.111
11.5	1.100	
17.5	1.070	
20.0		1.060
23.5	1.049	
35.0	1.025	1.028
47.0	1.014	1.015
59.0	1.008	
70.0	1.007	
83.0	1.005	1.006
100.0		1.004

[a] Increasing effective mass at $k = 0$ from 0.066 to 0.072 increases r_B from 1.146 to 1.150.

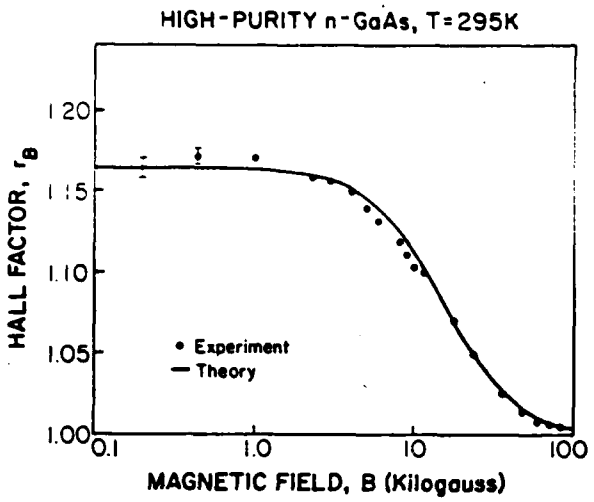

FIG. 2. Magnetic-field dependence of Hall factor for high-purity n GaAs at 295 K. Donor concentration ($N_D = 7.76\times10^{14}$ cm^{-3}) and acceptor concentration ($N_A = 1.86\times10^{14}$ cm^{-3}) are determined from Hall-effect freeze-out characteristics. Solid points are experimental results. The curve is theoretical.

Perceptibly all Fermions condense into a finite set of Landau levels at large enough values of B.[7] Furthermore, the energy spacing from the highest occupied Landau level measured to the lowest unoccupied Landau level increases with B and equals $eB\hbar/m^*$ where m^* is some effective mass.

Therefore, since $eB\hbar/m^*$ far exceeds the thermal energy κT at sufficiently large values of B, only those Fermions near the highest occupied Landau levels are free to participate in electrical conduction. However, these Fermions all have approximately the same energy and thus nearly the same scattering times. It then follows from Eq. (2) that $\langle\tau^2\rangle$ approaches $\langle\tau\rangle^2$ and therefore $r_\infty = 1$, Q.E.D.

The surprising aspect of $r_\infty = 1$ as given by Eq. (22) is that *no energy-level quantization* is taken into account. Therefore, the above argument based on Landau levels is not *a priori* relevant. Indeed, we assumed a smooth thermal distribution of Fermions (a Fermi-Dirac distribution) and a smooth density-of-states function [related to d of Eq. (6)].

Consequently, we are compelled to develop the following physical argument which does not rely on energy-level quantization. Note also that Lifshitz *et al.*[16] obtained the classical $r_\infty = 1$ limit for isotropic and anisotropic materials with closed orbits on the Fermi surface by assuming the relaxation approximation. The anisotropy factor, an additional correction to the Hall effect, has been examined extensively by Allgaier.[17]

At sufficiently large values of B, we note that a charged excitation will exhibit an average drift velocity $\mathbf{v}_d$ in the crossed electric field $\mathbf{F}$ and magnetic field $\mathbf{B}$ according to the Lorentzian force equation.[7]

$$\mathbf{v}_d = \mathbf{F}\times\mathbf{B}/B^2 . \tag{A1}$$

This is consistent, in the limit $B = \infty$, with Eqs. (4) and (20) which show that g vanishes relative to h, and hence $\mathbf{v}_d$, arising from h, is entirely orthogonal to $\mathbf{F}$ and $\mathbf{B}$ which are themselves mutually orthogonal. Furthermore, v_d decreases as $1/B$ in agreement with the $1/B$ dependence of h in the limit $B = \infty$. Finally, Eq. (20) can be used to show that $v_d = F/B$ in the limit $B = \infty$.

Now consider a Hall measurement with total electrical current I passing through a sample of thickness d and width w. We have

$$F/B = v_d \tag{A2}$$

$$= I/endw. \tag{A3}$$

However, the Hall voltage V_B developed between points spaced w apart is

$$V_B = R_B BI/d \tag{A4}$$

$$= r_B BI/end. \tag{A5}$$

Noting furthermore that $F = V_B/w$ we obtain $r_B = r_\infty = 1$, Q.E.D.

Even though the above argument leads to $r_\infty = 1$ in the *classical* limit $B = \infty$, one wonders whether the same $r_\infty = 1$ obtains if the density-of-states function d of Eq. (6) and the scattering rates of Eqs. (4) are altered to contain arbitrary energy-level quantization for only those components of $\mathbf{k}$ orthogonal to $\mathbf{B}$ provided merely that energy $\mathscr{E}$ be isotropic in components of $\mathbf{k}$ orthogonal to $\mathbf{B}$. If this is true, then one could prove that $r_\infty = 1$ for any isotropic thermal-equilibrium system of spinless Fermions with inelastic scattering and arbitrary degeneracy in both *classical* and *quantum* limits.

[1] E. H. Hall, Am. J. Math. **2**, 287 (1879).
[2] C. M. Wolfe and G. E. Stillman, in *Semiconductors and Semimetals*, edited by R. K. Willardson and A. C. Beer (Academic, New York, 1975), Vol. 10, Chap. 3.
[3] *ASTM Standard Method* (American Society for Testing Materials, Philadelphia, 1980), Pt. 43.
[4] R. Gans, Ann. Phys. (Paris) **20**, 293 (1906).
[5] L. L. Campbell, *Galvanomagnetic and Thermomagnetic Effects* (Longmans, Green, New York, 1923), p. 94 ff. The author reviews the dozen or so extant "theories" of the Hall effect.
[6] R. A. Smith, *Wave Mechanics of Crystalline Solids* (Chapman and Hall, London 1961), p. 333.
[7] K. Seeger, *Semiconductor Physics* (Springer, New York 1973) p. 61 ff.
[8] V. A. Johnson and K. Lark-Horovitz, Phys. Rev. **79**, 176 (1950).
[9] H. Brooks, Adv. Electron. Electron Phys. **7**, 85 (1955).
[10] J. W. Harding, Proc. R. Soc. London Ser. A **140**, 205 (1933).
[11] H. Ehrenreich, J. Phys. Chem. Sol. **9**, 129 (1959).
[12] S. S. Devlin, *Physics and Chemistry of II-VI Compounds*, edited by M. Aven and J. S. Prener (North-Holland, Amsterdam, 1967), p. 561.
[13] D. L. Rode, Phys. Status Solidi B **55**, 687 (1973).
[14] D. L. Rode, in *Semiconductors and Semimetals*, edited by R. K. Willardson and A. C. Beer (Academic, New York, 1975), Vol. 10, Chap. 1.
[15] C. M. Wolfe, G. E. Stillman, D. L. Spears, D. F. Hill, and F. V. Williams, J. Appl. Phys. **44**, 732 (1973).
[16] I. M. Lifshitz, M. Y. Azbel, and M. I. Kaganov, JETP **31**, 63 (1956).
[17] P. H. Cowley and R. S. Allgaier, Philos. Mag. **29**, 111 (1974) and references therein.

Inst. Phys. Conf. Ser. No. 65: Chapter 6
Paper presented at Int. Symp. GaAs and Related Compounds, Albuquerque, 1982

E.2 Magnetic-field dependence of the Hall factor of gallium arsenide

D.L. Rode*, C.M. Wolfe*,**, and G.E. Stillman+**

*Washington University, St. Louis, MO 63130 +University of Illinois, Urbana, IL 61801

Abstract. The magnetic-field dependence of the Hall factor from 0.44 to 83kG for electrons in n-GaAs at room temperature is examined experimentally and theoretically. Lateral uniformity of the moderately pure n-GaAs sample is determined from photoconductivity and infrared transmission measurements. Theoretical calculations include Kane bands, admixed wave functions, lattice scattering and Brooks-Herring scattering. Theoretical and experimental values of Hall factor agree to within 0.7 percent.

1. Introduction

The Hall effect is widely used to determine the free-carrier concentration and mobility of doped semiconductors (ASTM 1980). It is common practice to quote the free-electron concentration n derived from the Hall coefficient R_B under the assumption that the Hall factor r_B equals unity. In fact,

$$R_B = r_B/en \quad [MKS] \tag{1}$$

Subscript B denotes conditions of finite magnetic field B and unsubscripted symbols denote true values.

Thus, electron concentration derived under the assumption that $r_B = 1$ and denoted by n_B is related to actual electron concentration by the Hall factor which usually lies between unity and two (Rode 1973).

$$n = r_B n_B \tag{2}$$

In order to determine whether state-of-the art electron transport theory is adequate for more careful comparisons between theory and experiment, we compare the magnetic-field dependence of r_B measured and calculated for n-GaAs.

**Research supported by the Office of Naval Research, Contract No. 00014-80-C-0762.

0305-2346/83/0065-0569 $02.25

2. Experimental

A nominally undoped n-GaAs epitaxial layer 80 microns thick was grown on semi-insulating Cr-doped GaAs by $AsCl_3/Ga/H_2$ VPE (Wolfe et al. 1973). Lateral sample homogeneity was ensured from near-infrared transmission microscopy and from near-and far-infrared photoconductivity measurements.

Donor and acceptor concentrations N_D and N_A were determined from Hall freeze-out measurements and from mobility analyses at 5kG from liquid-Helium to room temperature after applying Hall-factor corrections.

For n-GaAs, the Hall factor approaches unity asymptotically as $1/B^2$ when μB is large compared to unity. Therefore, experimental values for r_B plotted in Fig. 1 are derived by assuming $r_B = 1.006$ at 83kG and Hall coefficient varies with B according to Eq. (1) with n constant. The value of r_B at 83kG was determined from asymptotic analysis of experimental R_B versus $1/B^2$ for large B values assuming $r_B = 1$ in the large -B limit.

The sample purity ($N_D = 7.76\times10^{14}/cm^3$ and $N_A = 1.86\times10^{14}/cm^3$) is such that electron transport at room temperature is determined predominantly by fundamental lattice scattering (i.e., mostly polar optical phonons). At small values of magnetic field B, the Hall factor r_B approaches 1.17 in Fig. 1. Near $\mu B = 1$ at B = 11.5kG, the Hall factor falls to about 1.10.

Accuracy of the experiments is estimated to be within 0.005 in units of r_B. Measurements for B less than 25kG were carried out with an iron-core solenoid magnet. Measurements for B greater than 10kG were performed at the Bitter National Magnet Laboratory.

3. Comparison With Theory

Hall factor was calculated from iterated contraction mapping solutions of the Boltzmann equation with an estimated accuracy within 0.006 in units of r_B (Rode 1973). The theory includes Kane-type non-parabolic band structure, admixed wave functions, lattice scattering, and Brooks-Herring ionized-impurity scattering in the Born approximation.

Calculated results using impurity concentrations determined from Hall freeze-out measurements are plotted as the solid curve in Fig. 1. Material parameters are the same as those given by Rode (1975).

It should be noted that the effect of changing electron effective mass from 0.066m to 0.072m at 5kG is to increase calculated r_B from 1.146 to 1.150. Thus, unlike carrier mobility, Hall factor is relatively insensitive to this parameter due to the fact that Hall factor depends predominantly on the momentum dependence rather than the absolute value of electron scattering rate.

The comparison between theory and experiment in Fig. 1 agrees to within 0.7 percent (worst case) and to within 0.2 percent (RMS).

4. Conclusion

While the agreement between theory and experiment shown in Fig. 1 is quite good, it does not strictly imply that the accuracy of the theory is as good as a few tenths of a percent of Hall factor in general, i.e., at other temperatures, or for larger dopant concentrations, etc.

Nevertheless, it is gratifying to see that close agreement obtains when comparison is made with experiments which are carefully designed for the purpose of determining the Hall factor.

Acknowledgements

It is a pleasure to acknowledge Prof. J.D. Wiley, University of Wisconsin, for discussion of electron transport theory.

References

ASTM Standard Method, Pt. 43 (1980)
Rode D L 1973 Phys. Stat. Sol. (b) 55 687
Rode D L 1975 Semiconductors and Semimetals 10 (eds. Willardson & Beer) Ch. 1
Wolfe, C M, Stillman G E, Spears D L, Hill D E, and Williams F V 1973 J. Appl. Phys. 44 732

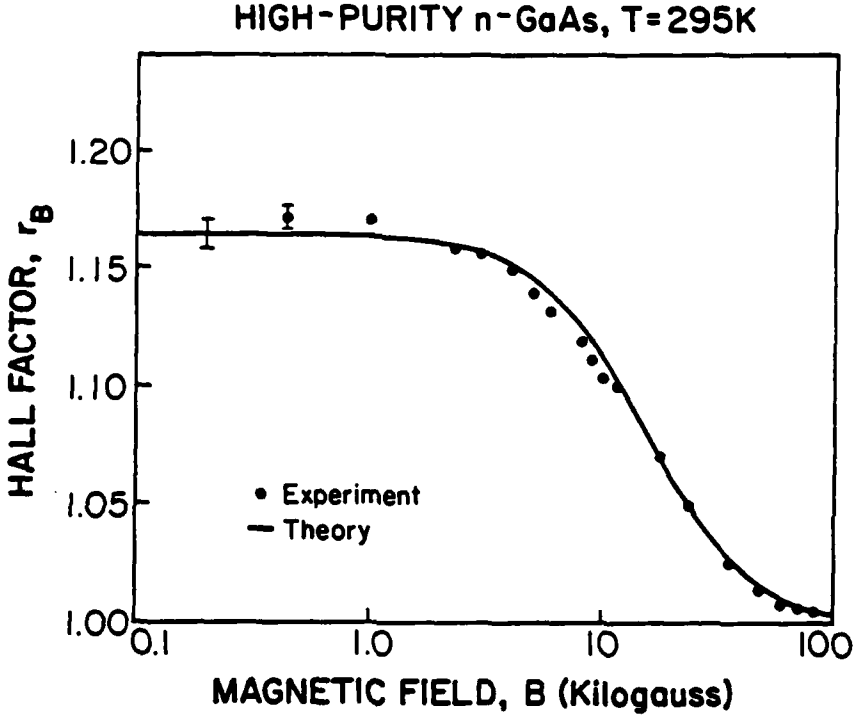

Fig. 1 Magnetic-field dependence of Hall factor for high-purity n-GaAs at 295K. Donor concentration ($N_D = 7.76\times10^{14}$ cm^{-3}) and acceptor concentration ($N_A = 1.86\times10^{14}$ cm^{-3}) are determined from Hall-effect freeze-out characteristics. Solid points are experimental results. The curve is theoretical.

E.3 Strain scattering of electrons in piezoelectric semiconductors

Peter A. Fedders
Department of Physics, Washington University, St. Louis, Missouri 63130

(Received 30 August 1982; accepted for publication 23 November 1982)

Static strains in piezoelectric semiconductors give rise to an electric field or potential which can have an effect on the electrical properties of the material. We have calculated the electric potential due to the strain field arising from a random distribution of point defects. This potential contributes a term to the mobility that is proportioned to $T^{1/2}$ and a Hall factor of 1.10. Crude estimates of strain strengths indicate that this scattering mechanism may contribute significantly to the mobility of electrically rather pure III-V semiconductors below room temperature when neutral impurity concentrations are greater than 10^{18} cm^{-3}. The mechanism may also constitute a dominant one in the mobility of some III-V alloys at fairly low temperatures. The existence of strain induced electric potentials also provides at least a possible mechanism whereby different donors can have different line shapes as measured in photoconductivity experiments.

PACS numbers: 61.70.Wp,72.20.Fr,72.80.Ey

I. INTRODUCTION

It is well known that static strains in piezoelectric materials give rise to an electric field or an electric potential. Thus in piezoelectric semiconductors, such as III-V compounds, static strains can have an effect on the electrical properties of the materials. In this paper we investigate some of these electrical effects that are due to a distribution of strains generated by a random distribution of point defects.

More particularly, we calculate the mobility due to a concentration of charge neutral defects that each produce a given strain field. The electric potential due to a strain producing point defect in a piezoelectric crystal is quite similar to the potential due to a point dipole and both will produce a mobility that is proportional to $T^{1/2}$ in the effective mass approximation. Except for scattering by ionized impurities, this is the only mechanism that produces a mobility that decreases as the temperature decreases. Crude estimates of the strain field associated with a single defect are estimated from linewidth measurements on a Si sample with a known concentration of specific impurities. These estimates indicate that the piezoelectric static strain scattering mechanism may contribute significantly to the mobility of electrically rather pure semiconductors below room temperature when neutral impurity concentrations are greater than 10^{18} cm^{-3}. Further, it could be a dominant mechanism in determining the mobility of III-V semiconducting alloys in some regimes. Other electrical effects, such as donor line shapes as measured in photoconductivity experiments, are also qualitatively discussed.

In the rest of this section we shall obtain the lattice displacement and strain for a model point defect. Section II contains the details of our calculations for the potential due to such a defect, the mobility due to a random concentration of such defects, and the distribution of strains due to these defects. Our results, their implications, and a limited comparison with experiments are contained in Sec. III.

According to elastic continuum theory[1] a defect will produce a lattice displacement proportional to r^{-2} and a strain field proportional to r^{-3} at distances r that are large compared to the size of the defect. In this paper we shall make use of a "model defect" defined so that $\mathbf{u}(\mathbf{r})$, the displacement of a material point at $\mathbf{r}$ due to a defect at the origin, is given by the equation

$$u(\mathbf{r}) = b^3\mathbf{r}/r^3, \tag{1}$$

where b has the units of length. This gives rise to a strain field

$$u_{ij}(\mathbf{r}) = \tfrac{1}{2}[(\partial u_i/\partial r_j) + (\partial u_j/\partial r_i)] = (r^2\delta_{ij} - 3r_i r_j)b^3/r^5. \tag{2}$$

Several cautionary and explanatory remarks are appropriate at this point. The model defect described by Eq. (1) is a fairly common model[2] because it is rather easy to manipulate analytically and it does, of course, possess the correct long range behavior which determines the dominant features of our results. However, Eq. (1) is not to be taken very seriously at distances within a few atomic spacings of the defect. In fact the displacement near the defect is a very difficult problem that is largely irrevelant to the present problem because the behavior of u_{ij} distances of a few atomic spacings will not contribute to any expressions in this paper. Further, although Eq. (1) implies a dilatation of volume change of order b^3, this is incidental to this paper. The piezoelectric coupling in III–V semiconductors occurs only through the shear strain components $u_{ij}(i \neq j)$ which describes a trigonal shape change of a material element and not a volume change. An appreciable shear strain in a crystal may or may not be accompanied by any volume change. Thus, while one expects b to be related to the dimensions of a defect, it cannot be related to a volume change or a nearest-neighbor displacement. In this paper b will be estimated by examining experimental determinations of strain fields in samples with known defect concentrations. We also note that Eq. (1) describes a spherically symmetric displacement. This is almost surely not the case in any real material. Even in an isotropic continuum no finite number of force pairs will produce a spherically symmetric displacement and the situation is worse in a nonisotropic material. In general

$$u_{ij}(\mathbf{r}) = f_{ij}(\Omega)/r^3, \tag{3}$$

where $f_{ij}(\Omega)$ is a very complicated function of angles. Thus,

 0021-8979/83/041804-04$02.40

any detailed angular dependence predicted by our model strain cannot be viewed as reliable.

II. CALCULATION

In this section we derive expressions for the quantities used in the rest of this paper. First we obtain an expression for the electric potential Φ due to the model defect described by Eq. (1). We use the notation and basic equations from Ref. 3 which includes cgs units and the summation convention for repeated indices. In the presence of a strain field (and to first order in the strains) the equation[3] connecting the electric and displacement fields is

$$D_i = \epsilon_0 E_i - 4\pi e_{ijk} u_{jk}, \tag{4}$$

where we assume an isotropic dielectric constant ϵ_0. For the cubic sphalerite structure the only nonzero element of the piezoelectric coupling constant e_{ijk} is e_{14} if i, j, and k are all distinct and is zero otherwise. The quantity e_{14} has the units of charge/length.[2] The equations $\nabla\cdot\mathbf{D} = 0$ and $\mathbf{E} = -\nabla\Phi$ together with Eq. (4) yield

$$\nabla^2\Phi(\mathbf{r}) = -4\pi\rho(\mathbf{r}), \tag{5}$$

where ρ is an effective charge density,

$$\rho(\mathbf{r}) = (\partial/\partial x_i)(e_{ijk} u_{jk}(\mathbf{r})/\epsilon_0). \tag{6}$$

Using Eq. (2) for our model defect yields

$$\rho(\mathbf{r}) = (90b^3 e_{14}/\epsilon_0)(xyz/r^7), \tag{7}$$

where spatial directions refer to the crystalline axes.

Equations (5) and (7) can be solved in a variety of different ways and we have found Fourier transforming the equations to be most convenient. Thus all functions $f(\mathbf{r})$ have a Fourier transform

$$f(\mathbf{k}) = \int d^3r f(\mathbf{r}) e^{-i\mathbf{k}\cdot\mathbf{r}},$$

$$f(\mathbf{r}) = \int \frac{d^3k}{(2\pi)^3} f(\mathbf{k}) e^{i\mathbf{k}\cdot\mathbf{r}}, \tag{8}$$

and Eq. (5) can be written as

$$k^2\Phi(\mathbf{k}) = 4\pi\rho(\mathbf{k}). \tag{5'}$$

The Fourier transform of $\rho(\mathbf{r})$ from Eq. (7) is obtained by first writing

$$\rho(\mathbf{k}) = (90b^3 e_{14}/\epsilon_0)(i\partial/\partial k_x)(i\partial/\partial k_y)(i\partial/\partial k_z)\int_0 d^3r e^{-i\mathbf{k}\cdot\mathbf{r}}(1/r^7), \tag{7a}$$

where the subscript 0 on the integral means that the radial part of the integral is restricted to values of $r > r_0$ where r_0 is arbitrarily small. After performing the angular part of the r integration in Eq. (7a) one obtains

$$\rho(\mathbf{k}) = (360\pi b^3 e_{14}/\epsilon_0)(i\partial/\partial k_x)(i\partial/\partial k_y)(i\partial/\partial k_z)\int_{r_0}^{\infty} dr \sin kr/r^6. \tag{7b}$$

By first performing the r integration, then taking the derivatives, and finally letting $r_0 \to 0$ one obtains

$$\rho(\mathbf{k}) = (24\pi i e_{14} b^3/\epsilon_0)(k_x k_y k_z/k^2). \tag{7c}$$

Thus, even though xyz/r^7 becomes infinite near the origin, its angular dependence is fast enough so that the Fourier integral exists. By use of the cutoff r_0, which is set equal to zero at the end, all of the integrals can be performed rigorously. Similarly one obtains

$$\Phi(\mathbf{k}) = (96\pi^2 i e_{14} b^3/\epsilon_0)(k_x k_y k_z/k^4),$$

$$\Phi(\mathbf{r}) = (36\pi b^3 e_{14}/\epsilon_0)(xyz/r^5). \tag{9}$$

The effects of Debye screening can also easily be included and the results are

$$\Phi(\mathbf{k}) = (96\pi^2 i e_{14} b^3/\epsilon_0\{k_x k_y k_z/[k^2(k^2 + k_s^2)]\}$$

$$\Phi(\mathbf{r}) = (-24\pi e_{14} b^3/\epsilon_0)(\partial/\partial x)(\partial/\partial y)(\partial/\partial z)(r_D^2) \times [(1 - \exp(-r/r_D))], \tag{9s}$$

where r_D is the Debye screening length and $k_s = 1/r_D$. Thus, $\Phi(\mathbf{r})$ is proportional to r^{-2} if $r \ll r_D$ and proportional to r^{-4} if $r \gg r_D$.

Given the electrical potential, the calculation for the elastic scattering relaxation rate and thus the mobility is perfectly straightforward, at least in the Born approximation. The calculation is virtually identical to the one described by Rode[4] for ionized impurities except that the Coulomb potential is replaced by the piezoelectric strain field potential and only one point needs further clarification. Where the $|\Phi(\mathbf{k})|^2$ enters the calculation we replace it by its angular average analogue $|\overline{\Phi}(\mathbf{k})|^2$ where

$$|\overline{\Phi}(\mathbf{k})|^2 = \langle|\Phi(\mathbf{k})|^2\rangle = 3\times 2^{10}\pi^4/35)(e_{14} b^3/\epsilon_0)^2/k^2 \tag{10}$$

for the unscreened version. This simplifying approximation is well within the spirit of neglecting any detailed angular dependence discussed in Sec. I. The relaxation rate in the effective mass approximation is

$$\nu = (3\times 2^9\times\pi^3/5\times 7)(ee_{14} b^3/\epsilon_0)^2 m^* n/\hbar^3 k, \tag{11}$$

where n is the density of model defects and e is the magnitude of the electronic charge. If this is the only scattering mechanism under consideration then the mobility is easily calculated to be

$$\mu = (5\times 7/2^6\times\pi^3\times 3^2)(\epsilon_0\hbar/em^* e_{14} b^3)^2(e/n)(2m^* kT/\pi)^{1/2}, \tag{12}$$

and the Hall factor r_H is

$$r_H = \Gamma(7/2)\Gamma(5/2)/\Gamma^2(3) \simeq 1.10. \tag{13}$$

Equations (11) through (13) were obtained by ignoring screening. The effects of screening can easily be added, if necessary, by starting with Eq. (9s) for $\Phi(\mathbf{k})$ instead of Eq. (9).

In order to make contact with other effects from the strains we consider the distribution of strains due to a random distribution of model defects. In the limit where the number of defects is a small fraction of the number of lattice sites the calculation is straightforward.[5] If $p(\xi)d\xi$ is the probability that the strain at a given point is between ξ and $\xi + d\xi$ then

$$p(\xi) = (\xi_0/\pi)(\xi^2 + \xi_0^2)^{-1},$$

$$\xi_0 = (4\pi/3)nb^3, \quad \text{for } \xi = u_{xy},$$

$$\xi_0 = (8\pi^2/9\sqrt{3})nb^3, \quad \text{for } \xi = u_{xx}. \tag{14}$$

Finally we note that if there are concentrations n_i of several

impurities with associated values of b_i then

$$\xi_0 \sim \sum_i n_i b_i^3,$$

$$\nu \sim \mu^{-1} \sim \sum_i n_i b_i^6. \tag{15}$$

These equations can also include the effects of more extended defects such as complexes or dislocation loops in which b^3 is roughly proportional to the volume of the loop. At distances far from the defect the same r dependence will obtain[1] and thus the k dependence of ν and the T dependence of μ will remain the same.

III. RESULTS

One major result of Sec. II is that the strains generated by point defects in a piezoelectric semiconductor produce a mobility that is proportional to $T^{1/2}$ and a Hall factor of $r_H = 1.10$. These are the same as would have been produced by a distribution of point dipoles. Except for scattering by ionized impurities, these are the only mechanisms that we know of that decrease the mobility as the temperature decreases.

The obvious question is whether the strength of the static strain piezoelectric scattering mechanism is large enough to cause a measurable effect in mobilities. Concentrations of neutral defects of order 10^{18} cm^{-3} are common in almost all materials. Further EPR, infrared, and optical measurements on defects in many materials yield splittings or inhomogeneous line broadening of about 1 cm^{-1}. Since splittings are typically of order 10^4 cm^{-1} per unit strain, this implies typical random strains of order 10^{-4}. Measurements of neutral impurity concentrations in well characterized III-V semiconductors are rare. There are, however, reports that concentrations of order 10^{18} cm^{-3} are quite common even in electrically rather pure GaAs.[6] However, we know of no quantitative analysis of strains in any III-V semiconductors. There is one quantitative determination of the strains due to oxygen impurities in Czochralski grown silicon that was obtained by their effect on the resonance lineshape of deep *In* acceptors. Mozurkewich,[7] using a backward wave phonon spectroscopy technique, measured linewidths corresponding to strains of about 0.5×10^{-4} in a sample with an oxygen content of 0.5×10^{18} cm^{-3}. Using Eq. (14) this implies a value of $b^3 \sim 0.3\times10^{-22}$ cm^{-3}.

From these numbers we estimate that $n = 10^{18}$ cm^{-3} and $b^3 = 0.3\times10^{22}$ cm^{-3} are at least not unreasonable. For GaAs with $\epsilon_0 = 12.5$, $e_{14} = 4.7\times10^4$ esu/cm^2, and $m^* \simeq 0.0665$ m, this yields a mobility of 1.5×10^5 cm^2/V sec at a temperature $T = 20$ °K. This is lower than the mobility of good samples whose mobilities are published. However, our numerical estimates for b^3 are uncertain to at least an order of magnitude which will lead to a change in the mobility of a factor of one hundred. We feel that our estimates are certainly no better than that but that they do show that the mechanism is worth considering.

We have included the possibility of static strain piezoelectric scattering in analyzing the mobility of one well studied very good sample of GaAs. Using reasonable parameters the fit could be made slightly better than without the mechanism. However, the fit could also be improved by changing the number of donors and acceptors by about 10% and thus we regard this attempt as inconclusive. Unfortunately, there is probably a tendency for data on well characterized samples with only the highest mobilities to reach the literature and these samples are the worst candidates for the effect.

One might expect strain effects to be more important in III-V semiconducting alloys than in the pure materials. Our analysis, of course, is valid only for rather dilute alloys although we expect the qualitative features to be present at all concentrations. We would also expect much smaller values for b^3 in alloys than for many impurities in purer substances. There have been a number of mobility measurements on $Ga_{1-x}Al_xAs$ at temperatures low enough so that static strain piezoelectric scattering might be detectable.[8–10] That is, at low enough temperatures the various lattice scattering mechanisms[4] should have become quite ineffective leaving only scattering by charged impurities, alloy scattering, and possibly static strain piezoelectric scattering. One expects a $T^{-1/2}$ temperature dependence in the mobility for what is usually called alloy scattering. Although the $T^{-1/2}$ really obtains from a weak scattering limit, it is difficult to see how scattering from short range fluctuations due to alloying could lead to a mobility that decreases as the temperature does. That is, as the temperature is decreased the conduction electrons average momentum is lowered and these electrons are less affected by spatially small potential variations. At still lower temperatures, of course, other impurity mechanisms will come into play and the mobility will cease to increase as the temperature is lowered.

GaAs and AlAs have almost identical lattice parameters and thus one might expect rather small effects for $Ga_{1-x}Al_xAs$. However, most mobility measurements do exhibit a low temperature regime where the mobility decreases with decreasing temperature and with increasing alloy concentration x. This is usually interpreted as an increasing number of donors and acceptors as x increases even though n (the number of conduction electron at 77 °K or at room temperature) is not correlated with the composition. We suggest that at least part of the decrease in mobility with decreasing temperature and increasing x may be due to static strain piezoelectric scattering. In oder to conclusively verify this independent determinations of N_A and N_D would have to be made.

We have crudely analyzed some of the mobility data of Chandra and Eastman[10] in order to see if static strain piezoelectric scattering could be a dominant mechanism. The analysis was limited to temperature between 25 °K and 45 °K so that lattice scattering mechanisms could be safely ignored. Assuming that inverse mobilities add and that the number of charged impurities was largely independent of x, one can obtain concentration or x dependent mobilities by subtracting inverse mobilities of different samples. This was done with the higher concentration sample pairs (F14,F16), (F14,F18), (F16,F18), and (F15,F19). The results yielded mobilities that varied by less than 5% over the temperature range. Either a $T^{1/2}$ or $T^{-1/2}$ temperature dependence would have given a mobility that varied by more than 30% over this range although the right combination of $T^{1/2}$ and $T^{-1/2}$

would be consistent with our analysis. Further, all pairs gave a μ^{-1} that was roughly proportional to x with a value of b^3 about one hundred times smaller than discussed earlier. We regard this analysis as suggestive but certainly not conclusive.

Finally we wish to make a few qualitative comments on the effect of strain produced electrostatic potentials on the donor line shapes measured in photoconductivity experiments. First we note that the $1s$–$2p$ line shapes measured in alloys are much broader and more symmetric than in pure compounds. The typical narrow asymmetric line obtains because the electric field from impurities separated by distances much greater than a Bohr radius contribute only to second order in the $1s$–$2p$ energy difference. This will not be true for the electric potential due to strain centers that are separated by distances small compared to the Bohr radius. Secondly we note that different donors are characterized by different linewidths (or even line shapes) in pure III–V semiconductors. A possible explanation of this is a strain generated potential from the donor defect itself contributes to the line shape. These ideas are presently being pursued quantitatively.

ACKNOWLEDGMENTS

This work was sponsored by the Office of Naval Research under Contract No. N00014–80C–0762. We wish to acknowledge useful and stimulating conversations with D. L. Rode and C. M. Wolfe.

[1]L. D. Landau and E. M. Lifshitz, *Theory of Elasticity* (Pergamon, London, 1959).
[2]C. P. Flynn, *Point Defects and Diffusion* (Clarendon, Oxford, 1972), Chap. 3.
[3]L. D. Landau and E. M. Lifshitz, *Electrodynami Continuous Media* (Pergamon, London, 1960), Chap. II.
[4]D. L. Rode in *Semiconductors and Semimetals*, edited by R. K. Willardson and Albert C. Beer (Academic, New York, 1975), Vol. 10, Chap. 1.
[5]See, for instance, P. A. Fedders, Phys. Rev. B **11**, 1020 (1975).
[6]C. W. Wolfe, G. E. Stillman, and E. B. Owens, J. Electrochem. Soc. **117**, 129 (1970).
[7]George Mozurkewich, Ph.D. thesis, Washington University, 1981 (unpublished).
[8]G. B. Stringfellow, J. Appl. Phys. **50**, 4178 (1979).
[9]K. Kaneko, M. Ayabe, and N. Watanabe, Inst. Phys. Conf. Ser. **33a**, 216 (1977).
[10]A. Chandra and L. F. Eastman, J. Appl. Phys. **51**, 2669 (1980); J. Electrochem. Soc. **127**, 211 (1980)

E.4

Electron scattering in semiconductor alloys

D. L. Rode[a] and P. A. Fedders[b]
Washington University, St. Louis, Missouri 63130

(Received 1 March 1983; accepted for publication 13 July 1983)

Suitability of the Born approximation and the Boltzmann equation is demonstrated for the scattering of free-carrier electrons by random-alloy atomic potentials in semiconductor alloys. Composition dependences of alloy-scattering potential strengths are hypothesized and electron scattering rates are derived. "Order parameters" are derived from scattering theory and compared to those derived previously from statistical and thermodynamic arguments by Warren and Cowley. The treatment is generalized to include ternary, quaternary, and lattice-matched alloys which, in general, show more complicated order-parameter dependencies than the previously known $x(1-x)$ dependence for ternary zincblende alloys. Electron-momentum relaxation-rate expressions are given, including nonparabolic Kane bands and admixed wave functions appropriate to small energy-gap semiconductors. Electron drift mobility, as determined by alloy scattering, is derived in the effective-mass limit which shows that *any* short-range alloy potential yields the experimentally observed $1/\sqrt{m^{*5}T}$ dependence reported in the literature. An effective-charge model for alloy scattering is compared to experiments on $Al_xGa_{1-x}As$. The magnitude of the effective charge on isolated Al atoms in GaAs is found to be 0.145 electron charges.

PACS numbers: 72.10.Bg, 72.15.Qm, 72.20.Dp, 72.20.Jv

I. INTRODUCTION

As interest has grown in the use of semiconductor alloys for high-speed electronics and optoelectronics technologies, there is increasing need to better understand free-carrier electron scattering due to the random alloy potentials of the crystalline lattice. This is particularly true for the partially ionic (mostly covalent) zincblende semiconductor alloys such as $Al_xGa_{1-x}As$ and $In_{1-x}Ga_xAs$ (ternaries), as well as for $In_{1-x}Ga_xAs_yP_{1-y}$ and $In_{1-x-y}Ga_xAl_yAs$ (Refs. 1–5) (quaternaries).

At first glance, it might seem doubtful that the Born approximation for electron scattering and the Boltzmann equation for electron transport can be accurately applied to the "alloy scattering" problem since free-carrier electron wave packets extend over a large number of lattice sites while alloy-scattering potentials must fluctuate over distances comparable to interatomic spacings. Applicability of the Born approximation relies on *binary* scattering processes and applicability of the Boltzmann equation requires quasiparticle carrier dynamics.[6]

However, the mere fact that an electron wave packet extends over many alloy sites does not necessarily imply that *multiple* scattering (as opposed to binary scattering) must be taken into account. To ensure binary scattering events, it is sufficient to require that the potential strength for each alloy site be weak enough to yield a relatively small probability of multiple scattering in comparison to the probability of binary scattering within a typical scattering interaction volume. We denote this condition by the term *weak scattering*.[7]

A convenient criterion to ensure weak scattering is to require the average electron deflection time (t_d) *within* a particular atomic alloy scattering potential to be small in comparison to the average time interval (t_a) *between* electron alloy scattering events.

$$t_d \ll t_a. \tag{1}$$

The time interval t_a is on the order of the mean time between scattering events and can be estimated in the effective-mass approximation.

$$t_a = \mu_a m^*/e, \tag{2}$$

where μ_a is the partial electron drift mobility due to alloy scattering alone, m^* is the electron effective mass, and e is the electron charge.

The deflection time t_d is not precisely defined, in general, but we can estimate its approximate value within the quasi-particle viewpoint as equal to the distance the electron travels during the scattering interaction divided by the average quasi-particle velocity. The velocity is approximately $\hbar k_{av_g}/m^*$ where $\hbar k_{av_g}$ is the average electron crystal momentum.

The appropriate value to use for the scattering interaction distance is likewise not well known, but we can estimate that it is on the order of twice $1/2k_{av_g}$ by analogy with the length-scale $1/2k$ which appears in the scattering formula for screened-Coulomb potentials. [See Eq. (90) of Ref. 6.] This estimate is not felt to limit the present treatment to any particular class of short-range alloy potential forms, such as screened Coulomb, but it is intended as an estimate to the otherwise unknown length scale.

From Eq. (1) and the above estimates, we obtain a criterion for weak scattering wherein the Born approximation and the Boltzmann equation are expected to be valid.

$$2\times(1/2k_{av_g})/(\hbar k_{av_g}/m^*) \ll \mu_a m^*/e. \tag{3}$$

[a] Department of Electrical Engineering.
[b] Department of Physics.

 0021-8979/83/116425-07$02.40

Alternatively, Eq. (3) can be usefully expressed in terms of the partial electron drift mobility for alloy scattering since this quantity is known approximately for several semiconductor alloys.

$$\mu_a > e/\hbar k_{avg}. \tag{4}$$

For nondegenerate semiconductors with constant mean-free-path scattering (which is known to be approximately true for alloy scattering), the drift-mobility average of $\hbar k$ is $\hbar k_{avg} = \sqrt{9\pi m^* \kappa T/8}$ where κ is Boltzmann's constant, T is absolute temperature, and we have used the effective-mass approximation. [See Eq. (46) of Ref. 6.] Thus, Eq. (4) can be written in terms of known semiconductor material parameters.

$$\mu_a > 8e\hbar/9\pi m^* \kappa T, \quad \text{weak scattering.} \tag{5}$$

For example, Eq. (5) applied to room-temperature $Al_xGa_{1-x}As$ with $m^* = 0.082\,m$ yields $\mu_a > 154\ cm^2/V\ sec$.

Since μ_a is typically greater than several thousand cm^2/V sec for zincblende semiconductor alloys,[1-4] Eq. (5) is usually satisfied, and the Born approximation and Boltzmann equation are applicable. Furthermore, the alloy-scattering partial mobility μ_a is known to depend on temperature as $T^{-1/2}$. Thus, Eq. (15) is satisfied for many temperatures of interest.

Having established the applicability of the Born approximation and Boltzmann equation, we treat alloy-scattering potential strengths and derive "order parameters" from scattering theory in Sec. II.

II. ALLOY SCATTERING

The treatment of ternary alloy scattering by Harrison and Hauser[6] introduces the alloy composition dependence $x(1-x)$ as an "order parameter" derived by statistical and thermodynamic arguments by Warren and Cowley.[9] In this section, we derive composition dependences from scattering theory and show how the simple $x(1-x)$ dependence results under certain assumptions. In general, the composition dependence is more complicated than $x(1-x)$.

Within the Born approximation, the electron differential scattering rate[6] (per unit of time per unit of k-space volume) is proportional to the absolute square of the matrix element of the alloy scattering potential ϕ_a. Since ϕ_a arises from short-range atomic disorder, the range of the potential ϕ_a is small (less than a couple of Angstroms) compared to the size of an electron wavepacket (several tens of Angstroms). The electron wave function is unable to probe the detailed structure of ϕ_a in this low-energy limit, and therefore the differential scattering rate is proportional to the square of a volume integral of the atomic scattering potential [see Eq. (19) below].

This volume integral is linearly proportional to the *potential strength* V_a. Furthermore, the local atomic scattering potential ϕ_a is linearly proportional to the potential strength V_a which we formulate below.

A. Quaternary alloy, $A_{1-x}B_xC_yD_{1-y}$

Consider the quaternary zincblende alloy $A_{1-x}B_xC_yD_{1-y}$ (e.g., $In_{1-x}Ga_xAs_yP_{1-y}$) where A and B atoms reside on one fcc sublattice, and C and D atoms reside on the other. Substitution of B atoms in the ternary BC_yD_{1-y} does not provide alloy scattering. On the other hand, substitution of an isolated B atom in the ternary AC_yD_{1-y} is expected to yield the maximum potential strength for alloy scattering by a B atom. Consequently, the alloy-scattering potential strength V_B is expected to increase monotonically with the *second-nearest-neighbor* alloy composition $(1-x)$.

Now consider the variation of V_B with the *nearest-neighbor* alloy compositions y and $(1-y)$. B atoms in the ternary alloy $A_{1-x}B_xC$ will have a potential strength for alloy scattering which we label $V_B(ABC)$. Similarly, B atoms in the ternary alloy $A_{1-x}B_xD$ will have potential strength $V_B(ABD)$. In general, $V_B(ABC)$ and $V_B(ABD)$ will differ from one another in magnitude and in sign.

In the present paper, *we assume that V_B varies linearly with both nearest-neighbor alloy compositions y and $(1-y)$ and with second-nearest-neighbor alloy compositions x and $(1-x)$.*

$$\begin{aligned} V_B &= yV_B(ABC) + (1-y)\,V_B(ABD) \\ &= y(1-x)\,V_B(AC) + (1-y)(1-x)\,V_B(AD), \end{aligned} \tag{6a}$$

where $V_B(AC)$ and $V_B(AD)$ are the alloy-scattering potential strengths of isolated B atoms in the endpoint binary compounds AC and AD, respectively.

The assumed linear variations of potential strengths are expected to be reasonable approximations provided the alloy is homogeneous (no correlation between atomic spatial compositions)[4] and provided there exist only small differences between A and B, or C and D atoms in terms of size, electronegativity, and valence electron concentration (i.e., Hume–Rothery Rule[10]).

Similarly, we derive the alloy-scattering potential strengths for A, C, and D atoms.

$$V_A = yxV_A(BC) + (1-y)\,xV_A(BD), \tag{6b}$$

$$V_C = x(1-y)\,V_C(BD) + (1-x)(1-y)\,V_C(AD), \tag{6c}$$

$$V_D = xyV_D(BC) + (1-x)\,yV_D(AC). \tag{6d}$$

In the Born approximation, the electron momentum *relaxation rate ν_a is proportional to a k-space integral over* the absolute square of the matrix element of the scattering potential.[6] Hence, ν_a is proportional to the potential strength squared. Furthermore, the matrix-element sum over all lattice positions A, for example, is uncorrelated with the sum over all lattice positions B, C, and D for homogeneous alloys (see Sec. III). Thus, the electron momentum relaxation rate due to A atoms is proportional to $(1-x)\,V_A^2$, where $(1-x)$ is the relative concentration of A atoms, and so on for B, C, and D atoms. Thus, from Eqs. (6),

$$\begin{aligned} \nu_a &= (1-x)\,V_A^2 + xV_B^2 + yV_C^2 + (1-y)\,V_D^2 \\ &= (1-x)\,x^2[\,yV_A(BC) + (1-y)\,V_A(BD)\,]^2 \\ &\quad + (1-x)^2\,x[\,yV_B(AC) + (1-y)\,V_B(AD)\,]^2 \\ &\quad + (1-y)^2\,y[\,xV_C(BD) + (1-x)\,V_C(AD)\,]^2 \\ &\quad + (1-y)\,y^2[\,xV_D(BC) + (1-x)\,V_D(AC)\,]^2. \end{aligned} \tag{7}$$

Equation (7) shows that in the case of potential strengths which are linearly dependent upon alloy compositions, there are eight unknown endpoint strengths $V_i(jk)$ in addition to linear, square, and cubic dependencies of scattering rate on alloy compositions x and y.

It seems unlikely that experiments will soon be available to determine all eight of the endpoint-binary strength parameters of Eq. (7) for a particular quaternary semiconductor alloy. In addition, several semiconductor alloys of interest rely on use of atomic species which are not too dissimilar from one another, as evidenced by nearly linear variations of measured material parameters with alloy composition.[11]

Therefore, we assume that the potential difference (which gives rise to the alloy-scattering potential strength V_A) between an A atom and the binary compound BC is equal in magnitude and opposite in sign to that for a B atom in the binary compound AC.

$$V_A(BC) = -V_B(AC). \tag{8a}$$

Similarly, we assume

$$V_A(BD) = -V_B(AD), \tag{8b}$$

$$V_C(BD) = -V_D(BC), \tag{8c}$$

$$V_C(AD) = -V_D(AC), \tag{8d}$$

Thus, the eight strength parameters of Eq. (7) are reduced to four and Eq. (7) can be simplified as follows:

$$\begin{aligned} v_a &= [yV_A(BC) + (1-y)V_A(BD)]^2[(1-x)x^2 + (1-x)^2x] \\ &+ [xV_D(BC) + (1-x)V_D(AC)]^2[(1-y)^2y + (1-y)y^2] \\ &= x(1-x)\{V_A(BD) + y[V_A(BC) - V_A(BD)]\}^2 \\ &+ y(1-y)\{V_D(AC) + x[V_D(BC) - V_D(AC)]\}^2. \end{aligned} \tag{9}$$

The relaxation rate of Eq. (9) exhibits the well-known dependences on $x(1-x)$ and $y(1-y)$.[8] However, the first term containing $x(1-x)$ is modified by a term linear and quadratic in y, and similarly for the second term.

Thus, within the assumption of Eqs. (8) with linearly dependent scattering-potential strengths the scattering rate varies linearly and quadratically with alloy composition x, provided y is held constant, but the dependence on x is different from the usual $x(1-x)$ behavior due to cross terms such as xy, xy^2, yx^2, and x^2y^2. [Note that the same result obtains if plus signs are substituted for minus signs in Eq. (8).]

Since the scattering rate of Eq. (9) for a ternary alloy (y equals zero or unity) is proportional to $x(1-x)$, one might be tempted to describe the scattering rate for a quaternary alloy as proportional to the *sum* of two terms: one term proportional to $x(1-x)$ and one term proportional to $y(1-y)$. Equation (9) demonstrates that this formulation might be accurate in the unlikely event that scattering-potential strengths are *independent* of *nearest-neighbor* compositions, i.e., $V_A(BC) = V_A(BD)$ and $V_D(BC) = V_D(AC)$.

B. Ternary alloy, $A_{1-x}B_xC$

Setting $y = 1$ in the above formulation, the assumed linear dependences of potential strengths V_A and V_B on second-nearest-neighbor compositions give the following relaxation rate from Eq. (7).

$$v_a = (1-x)x^2[V_A(BC)]^2 + (1-x)^2x[V_B(AC)]^2. \tag{10}$$

Thus, v_a varies linearly, quadratically, and cubically with alloy parameter x. However, the coefficients of these terms are interrelated since there are only two endpoint binary-compound parameters, $V_A(BC)$ and $V_B(AC)$.

As discussed in Sec. II A, if A and B atoms are not too dissimilar, we expect Eq. (8a) to apply. In this case, we obtain the well-known $x(1-x)$ behavior.

$$v_a = x(1-x)V_A(BC)^2. \tag{11}$$

Equation (11) exhibits precisely the $x(1-x)$ "order parameter" dependence discussed previously[8] and which was derived from statistical and thermodynamical arguments,[9] as opposed to the scattering-theory approach adopted here. Nevertheless, it is worth repeating that the simple result, Eq. (11) for ternary alloys, obtains from assuming both (a) linear variation of scattering-potential strength with x, and (b) the approximation wherein $V_A(BC) = -V_B(AC)$. [Note that identical results are obtained for $V_A(BC) = +V_B(AC)$].

C. Lattice-matched quaternary alloy, $y = f(x)$

In some cases, there is a need to "lattice match" the quaternary alloy such that the lattice parameter of a quaternary-alloy epitaxial layer is held constant and matched to that of a binary compound substrate.

For $In_{1-x}Ga_xAs_yP_{1-y}$ on InP, lattice matching dictates that[3,11] $x \simeq 0.47y$ while y varies from zero to unity. From Eq. (9), we see that the scattering rate in this case is dependent upon powers of x from unity through four. Thus, plots of scattering strength versus x should exhibit a fourth-order polynomial dependence on x. The corresponding four polynomial coefficients are uniquely specified by the four potential strengths appearing in Eq. (9).

The results of this section are derived more generally in Appendix A.

III. MATRIX ELEMENTS AND SCATTERING RATE

For the quaternary alloy $A_{1-x}B_xC_yD_{1-y}$, the local atomic potential at position $\mathbf{r}$ in the neighborhood of (and due to) an A atom, which gives rise to alloy scattering, is denoted by $\phi_A(\mathbf{r})$ and similarly for B, C, and D atoms. The potential $v(\mathbf{r})$ at position $\mathbf{r}$ equals the sum over all A, B, C, and D atoms.

$$\begin{aligned} v(\mathbf{r}) = \sum_{\mathbf{R}} &[\phi_A(\mathbf{r}-\mathbf{R}) + \phi_B(\mathbf{r}-\mathbf{R}) \\ &+ \phi_C(\mathbf{r}-\mathbf{R}) + \phi_D(\mathbf{r}-\mathbf{R})], \end{aligned} \tag{12}$$

where $\mathbf{R}$ is the set of all lattice sites in the crystal of volume V. We assume that the local potentials ϕ_A, ϕ_B, ϕ_C, and ϕ_D are isotropic and randomly situated so that $v(\mathbf{r}) = v(r)$, $\phi_A(\mathbf{r}) = \phi_A(r)$, etc.

The differential scattering rate between state $\mathbf{k}\beta$ and $\mathbf{k}'\beta'$, where β and β' are spin indices, is proportional to the absolute square of the matrix element of $v(r)$,[7]

$$s(\mathbf{k}',\mathbf{k}) = (2\pi/\hbar)|\langle \mathbf{k}'\beta' | v(r) | \mathbf{k}\beta \rangle|^2 \rho_{E'}\delta(E-E'), \tag{13}$$

where ρ_k is the k-space density-of-states function and the delta function of the difference between initial and final state kinetic energies E and E' describes elastic scattering.

Summing over spin indices and evaluating the matrix element for *normal* scattering, we obtain the following result.

$$\langle \mathbf{k}'|v|\mathbf{k}\rangle = (B_{k'k}/V)\int v(r)\exp[i(\mathbf{k}-\mathbf{k}')\cdot\mathbf{r}]\,d\mathbf{r}, \qquad (14)$$

where $|B_{k'k}|^2 \equiv G(\mathbf{k}',\mathbf{k})$ is the overlap integral for admixed s and p wave functions[6] and V is the volume of the crystal. We combine Eqs. (12) and (14) and denote the summand of Eq. (12) by $\phi(r')$ where $\mathbf{r}' = \mathbf{r} - \mathbf{R}$.

$$\langle \mathbf{k}'|v|\mathbf{k}\rangle = (B_{k'k}/V)\sum_{\mathbf{R}}\int \phi(\mathbf{r}-\mathbf{R})\exp[i(\mathbf{k}-\mathbf{k}')\cdot\mathbf{r}]\,d\mathbf{r}$$

$$= (B_{k'k}/V)\sum_{\mathbf{R}}\exp[i(\mathbf{k}-\mathbf{k}')\cdot\mathbf{R}]\int \phi(r')$$

$$\times\exp[i(\mathbf{k}-\mathbf{k}')\cdot\mathbf{r}']\,d\mathbf{r}'. \qquad (15)$$

The integrand in Eq. (15) is vanishingly small for r' much greater than an interatomic spacing since the local atomic potential is assumed to be short ranged. On the other hand, the average change in momentum measured by $|\mathbf{k}-\mathbf{k}'|$ is small compared to the large values of $1/r'$ for which $\phi(r')$ is significantly different from zero for a particular scattering site. Thus, the exponential term in the integrand is approximately unity.

$$\langle \mathbf{k}'|v|\mathbf{k}\rangle = (B_{k'k}/V)\sum_{\mathbf{R}}\exp[i(\mathbf{k}-\mathbf{k}')\cdot\mathbf{R}]\int \phi(r')\,d\mathbf{r}'. \qquad (16)$$

Thus, the local atomic scattering potential appears *only* as a local volume integral which removes effects of the detailed structure of the local potential. The volume integral of $\phi(r)$ for a given atom is proportional to the *potential strength* discussed in Sec. II.

Substituting Eq. (16) into Eq. (13) entails multiplying the sum over R by its complex conjugate, which converts the summand to unity at the various A, B, C, D atomic sites. Thus, the absolute square of the matrix element yields a count over the total number of A-atom sites N_A multiplied by $|\int\phi_A(r)\,d\mathbf{r}|^2$, plus like terms for B, C, and D atoms.

$$|\langle \mathbf{k}'|v|\mathbf{k}\rangle|^2 = (|B_{k'k}|^2/V^2)\left[N_A\left|\int\phi_A(r)\,d\mathbf{r}\right|^2 + N_B\right.$$

$$\times\left|\int\phi_B(r)\,d\mathbf{r}\right|^2 + N_C\left|\int\phi_C(r)\,d\mathbf{r}\right|^2$$

$$\left. + N_D\left|\int\phi_D(r)\,d\mathbf{r}\right|^2\right]. \qquad (17)$$

Equation (17) can be written in terms of volume concentrations $n_A = N_A/V$, $n_B = N_B/V$, etc.

$$|\langle \mathbf{k}'|v|\mathbf{k}\rangle|^2 = (|B_{k'k}|^2/V)\left[n_A\left|\int\phi_A(r)\,d\mathbf{r}\right|^2\right.$$

$$+ n_B\left|\int\phi_B(r)\,d\mathbf{r}\right|^2 + n_C\left|\int\phi_C(r)\,d\mathbf{r}\right|^2$$

$$\left. + n_D\left|\int\phi_D(r)\,d\mathbf{r}\right|^2\right]. \qquad (18)$$

The density-of-states function $\rho_k = V/8\pi^3$ since a sum over spin has already been taken into account. Thus, the differential scattering rate for alloy scattering is as follows:

$$s_a(\mathbf{k}',\mathbf{k}) = [c^2G(\mathbf{k}',\mathbf{k})\,\delta(E-E')/4\pi^2\hbar]$$

$$\times\left[n_A\left|\int\phi_A(r)\,d\mathbf{r}\right|^2 + n_B\left|\int\phi_B(r)\,d\mathbf{r}\right|^2\right.$$

$$\left. + n_C\left|\int\phi_C(r)\,d\mathbf{r}\right|^2 + n_D\left|\int\phi_D(r)\,d\mathbf{r}\right|^2\right]. \qquad (19)$$

The momentum relaxation rate for elastic scattering is ν_a.[6]

$$\nu_a = \int(1-X)\,s_a(\mathbf{k}',\mathbf{k})\,d\mathbf{k}', \qquad (20)$$

where X is the cosine of the angle between $\mathbf{k}'$ and $\mathbf{k}$. Thus, evaluating the overlap integral $G(\mathbf{k}',\mathbf{k})$ for nonparabolic Kane bands with zero spin-orbit splitting and admixed wave functions with $(1-c^2)$ proportion s character and c^2 proportion p character,[6] we obtain the momentum relaxation rate for alloy scattering ν_a.

$$\nu_a = (e^2mdk/3\pi\hbar^3)\cdot\left[n_A\left|\int\phi_A(r)\,d\mathbf{r}\right|^2 + n_B\left|\int\phi_B(r)\,d\mathbf{r}\right|^2\right.$$

$$\left. + n_C\left|\int\phi_C(r)\,d\mathbf{r}\right|^2 + n_D\left|\int\phi_D(r)\,d\mathbf{r}\right|^2\right]\cdot(3-8c^2+6c^4), \qquad (21)$$

where $1/d \equiv (m/\hbar^2k)\,\partial E/\partial k$ and m is free-electron mass in vacuum. Equation (21) is a general result applicable to static short-range potentials.

Two interesting features of Eq. (21) become readily apparent in the limit of parabolic bands where $md = m^*$ and $c = 0$. In this case, the relaxation rate is proportional to m^*k and the corresponding partial electron drift mobility is

$$\mu_a = (4\hbar^4/3e)\sqrt{\pi/2m^{*5}\kappa T}\Big/\left[n_A\left|\int\phi_A(r)\,d\mathbf{r}\right|^2\right.$$

$$+ n_B\left|\int\phi_B(r)\,d\mathbf{r}\right|^2 + n_C\left|\int\phi_C(r)\,d\mathbf{r}\right|^2$$

$$\left. + n_D\left|\int\phi_D(r)\,d\mathbf{r}\right|^2\right]. \qquad (22)$$

Therefore, *any* sufficiently short-ranged scattering potential leads to partial mobility decreasing as $1/\sqrt{m^{*5}T}$. The $T^{-1/2}$ mobility dependence is well known,[4] and the $m^{*-5/2}$ dependence is consistent with experiments on InGaAsP reported by Hayes *et al.*[3] Nevertheless, as Eq. (22) shows, electron transport experiments are incapable of revealing the actual local r-dependent structure of the alloy scattering potentials ϕ_A, etc.

We now consider two scattering-potential models for alloy scattering.

A. Square-well alloy-scattering potentials

Following Harrison and Hauser,[8] assume $\phi_A(r)$ is an isotropic square-well (or square-barrier) potential of amplitude ΔE and radius r_0. We evaluate the potential strength

appearing as the square of the volume integral in Eq. (18).

$$\left|\int \phi_A(r)\,d\mathbf{r}\right|^2 = \left|4\pi\int_0^{r_0^0} \Delta E\cdot r^2\,dr\right|^2$$

$$= 16\pi^2|\Delta E|^2 r_0^6/9. \tag{23}$$

Equation (23) is identical to the result derived by Harrison and Hauser[3] and, of course, the corresponding partial electron drift mobility varies as $1/\sqrt{m^{*5}T}$ for parabolic bands. The quantity $r_0^6|\Delta E|$ is linearly proportional to the potential strengths V_A, etc., discussed in Sec. II.

B. Effective-charge screened Coulomb potentials

The difficulty with the square-well model of Sec. III A is the conceptual problem of estimating what to use for the square-well amplitude and radius.[3]

While it hardly remedies the above difficulty, it is worthwhile noting that alloy scattering can be modeled in the following effective-charge model with local atomic potentials $\phi_A(r)$, etc., which are Coulomb potentials screened by high-concentration valence *bond* electrons.

$$\phi_A = (eZ_A/4\pi\epsilon r)\,e^{-\beta r}. \tag{24}$$

The dimensionless effective charge is eZ_A, ϵ is the free-space permittivity, and $1/\beta$ is the screening length. The quantity Z_A is expected to be less than unity. In the effective-charge model, the potential strengths discussed in Sec. II are proportional to the specific effective charges Z_A, Z_B, etc.

The volume integral of the potential ϕ_A appearing in Eq. (18) is as follows:

$$\left|\int \phi_A(r)\,d\mathbf{r}\right|^2 = \left|(eZ_A/4\pi\epsilon)\int\{\exp(-\beta r)/r\}\,d\mathbf{r}\right|^2$$

$$= \left|(eZ_A/\epsilon)\int r\cdot\exp(-\beta r)\,dr\right|^2$$

$$= (eZ_A/\epsilon\beta^2)^2. \tag{25}$$

The differential scattering rate follows from Eq. (19).

$$s_a(\mathbf{k}',\mathbf{k}) = [e^4 G(\mathbf{k}',\mathbf{k})\,\delta(E-E')/4\pi^2\epsilon^2\hbar\beta^4]$$

$$\times(n_A Z_A^2 + n_B Z_B^2 + n_C Z_C^2 + n_D Z_D^2). \tag{26}$$

The electron momentum relaxation rate follows from Eq. (21).

$$\nu_a(\mathbf{k}',\mathbf{k}) = [e^4 mdk/3\pi\epsilon^2\hbar^3\beta^4]$$

$$\times(n_A Z_A^2 + n_B Z_B^2 + n_C Z_C^2 + n_D Z_D^2)$$

$$\times(3-8c^2+6c^4). \tag{27}$$

The partial drift mobility for Eq. (27) cannot be evaluated analytically, in general, because of the k dependence of d and c for nonparabolic bands.[6] However, in the parabolic-band limit where $md = m^*$ and $c = 0$, Eq. (27) yields the partial electron drift mobility for alloy scattering μ_a.

$$\mu_a = \frac{(4\epsilon^2\hbar^4\beta^4/3e^3)\sqrt{\pi/2m^{*3}\kappa T}}{(n_A Z_A^2 + n_B Z_B^2 + n_C Z_C^2 + n_D Z_D^2)}. \tag{28}$$

As expected, μ_a exhibits the previously discussed $1/\sqrt{m^{*3}T}$ dependence.

IV. EFFECTIVE-CHARGE ALLOY SCATTERING

In this section, we combine the results of Secs. II and III utilizing the effective-charge model leading to Eq. (27). In order to include alloy compositions in the expression for momentum relaxation rate, we use the results expressed by Eqs. (6) and (8). The effective charge Z_A equals the potential strength V_A of Eq. (6), and so on for Z_B, Z_C, and Z_D.

For comparison to III-V alloys, such as $In_{1-x}Ga_xAs_yP_{1-y}$, the concentration n_A of Eq. (27) equals $(1-x)N_{III}$ where $N_{III} = 4/a^3$ is the concentration of group-III sublattice sites and a is the lattice parameter and so on for n_B, n_C, and n_D.

A further simplication results from specifying the screening length $1/\beta$ due to the high concentration of valence electrons as equal to half the interatomic spacing. The proper value to use for screening length is not known accurately and, furthermore, it needs to be specified self-consistently with the atomic potentials ϕ_A, etc. Our choice of half the interatomic spacing for $1/\beta$ is merely a qualitative first step in this problem.

From Eqs. (6) and (8), the effective charges for atoms in the quaternary alloy $A_{1-x}B_xC_yD_{1-y}$ are

$$Z_A = yxZ_A(BC) + (1-y)\,xZ_A(BD), \tag{29a}$$

$$Z_B = y(x-1)\,Z_A(BC) + (1-y)(x-1)\,Z_A(BD), \tag{29b}$$

$$Z_C = x(y-1)\,Z_D(BC) + (1-x)(y-1)\,Z_D(AC), \tag{29c}$$

$$Z_D = xyZ_D(BC) + (1-x)\,yZ_D(AC), \tag{29d}$$

where $eZ_A(BC)$ is the effective charge for alloy scattering by an isolated A atom in the binary compound BC, etc.

Combining Eqs. (27) and (29), we obtain

$$\nu_a = (3e^4 amdk/2^{10}\pi\epsilon^2\hbar^3)$$

$$\times\{x(1-x)[\,yZ_B(AC) + (1-y)\,Z_B(AD)]^2$$

$$+ y(1-y)[xZ_D(BC) + (1-x)\,Z_D(AC)]^2\}$$

$$\times(3-8c^2+6c^4). \tag{30}$$

Equation (30) indicates that alloy scattering in the quaternary alloy $In_{1-x}Ga_xAs_yP_{1-y}$, for example, is determined over the entire composition plane (x, y) by the four effective charges of dilute Ga atoms in InAs [i.e., $Z_B(AC)$] and InP, and by the effective charges of dilute P atoms in GaAs and InAs.

As an application of Eq. (30), consider the ternary alloy $Al_xGa_{1-x}As$ by setting $y = 1$. In this case, the magnitude of the effective charge of dilute Al in GaAs is $Z_B(AC) = Z_{Al}(GaAs)$ and this is the only effective-charge parameter appearing in Eq. (30) when $y = 1$. In Fig. 1 we show theoretical calculations of electron Hall mobility (solid curve) compared to measurements by Chandra and Eastman[2] on $Al_{0.155}Ga_{0.845}As$ from 26 to 300 K. The theoretical curve includes piezoelectric, acoustic, polar-optical, alloy, and Brooks–Herring ionized-impurity scattering with nonparabolic Kane bands and admixed electron wave functions.[9,12] The Boltzmann equation for galvanomagnetic transport is solved by the contraction mapping method discussed previously,[9] and numerical results are obtained by iteration of

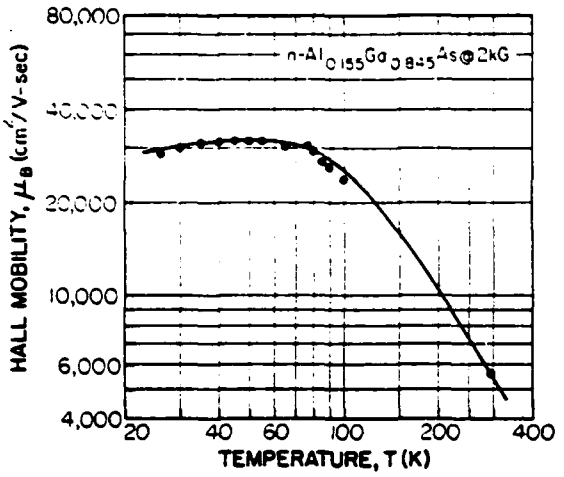

FIG. 1. Electron Hall mobility of $Al_{0.155}Ga_{0.845}As$ at 2-kG magnetic field vs lattice temperature from 26 to 300 K. Experimental points were measured by Chandra and Eastman (see Ref. 2). Theoretical curve is a best-fit obtained by varying alloy-scattering effective-charge eZ_{Al}(GaAs) and ionized-acceptor concentration. Best fit occurs for $Z_{Al}(GaAs) = 0.145e$.

the contraction mapping solution with finite magnetic field. Parameters used in the calculation are listed in Table I. We have corrected the experimental measurements[2] of electron concentration for finite Hall factor and assumed no freeze-out.

The effective-charge Z_{Al}(GaAs) and ionized-acceptor concentration were varied to achieve a best fit with experimental data.[2]

We obtained $|Z_{Al}(GaAs)| = 0.145$ which is satisfyingly less than unity. Nevertheless, the empirically derived effective charge is sensitive to the assumed screening length $1/\beta$ of Eq. (30). We set $1/\beta$ equal to half the interatomic spacing as discussed above.

V. CONCLUSION

A formulation for alloy scattering is derived for isotropic short-range scattering potentials of arbitrary form. The partial electron drift mobility, within the Born approximation, depends upon electron effective mass and temperature as $1/\sqrt{m^{*5}T}$ in the effective-mass limit.

TABLE I. Parameters used in the simulation[a] of $Al_{0.155}Ga_{0.845}As$.

Energy gap 1.76 eV
Effective mass 0.082 m
Optical dielectric constant 10.44
Static dielectric constant 12.53
Polar phonon energy 433 K
Longitudinal stiffness 1.4×10^{11} N/m²
Acoustic deformation potential 7.2 eV
Piezoelectric coefficient 0.052
Magnetic-field strength[b] 2 kG
Free-electron concentration[b] 2.9×10^{14} cm^{-3}
Ionized-acceptor concentration 2.9×10^{14} cm^{-3}
Ionized-donor concentration 5.8×10^{14} cm^{-3}

[a]SETA simulations (Semiconductor Electron Transport Analysis) were performed by Pendragon Associates, Nine Prado, St. Louis, MO 63124.
[b]From Ref. 2, including corrections for simulated values[12] of Hall factor.

The potential strength for alloy scattering is derived under the assumption that potential strength varies linearly with nearest-neighbor and second-nearest-neighbor lattice compositions. Under the additional assumption that the potential strength of an A atom in the binary compound BC is equal in amplitude to that of a B atom in the compound AC, the electron scattering rate for ternary alloys varies with composition x according to $x(1-x)$ in agreement with previous results.[8] For quaternary alloys, the corresponding dependence on composition x and y includes $x(1-x)$ and $y(1-y)$ terms as well as additional cross terms involving xy, x^2y, xy^2, and x^2y^2.

Local atomic alloy-scattering potentials are modeled in terms of screened-Coulomb potentials with fractional effective charges. The scattering rate for quaternary alloys is given in terms of the four effective charges of isolated atoms in the corresponding four endpoint binary compounds. For the ternary alloy $Al_xGa_{1-x}As$ the magnitude of the effective charge of isolated Al in GaAs is estimated to be $0.145e$ for screening length equal to half the interatomic spacing.

In future work, we hope to better define the local atomic potential for alloy scattering by finding potential functions which are derivable from measurements which are independent of electron transport measurements, e.g., Raman scattering and neutron-diffraction measurements of phonon spectra.

ACKNOWLEDGMENTS

We are grateful to Professor C. M. Wolfe of Washington University and Professor L. F. Eastman of Cornell University for comments on the manuscript and for discussing unpublished results on alloy-scattering research.

APPENDIX A

Within the assumption of alloy-scattering potential strength varying linearly with sublattice alloy compositions, a general equation can be written for the potential strength V_I of atomic species I. Suppose the crystal consists of atomic species A, B, and C on one sublattice, and atomic species D, E, and F on a second sublattice. Denote fractional sublattice compositions by a, b, and c (for species A, B, and C), and by x, y, and z (for species D, E, and F). By assumption, we have

$$\begin{aligned} V_I = {} & a[xV_I(AD) + yV_I(AE) + zV_I(AF)] \\ & + b[xV_I(BD) + yV_I(BE) + zV_I(BF)] \\ & + c[xV_I(CD) + yV_I(CE) + zV_I(CF)], \end{aligned} \tag{A1}$$

where $V_I(JK)$ is the alloy-scattering potential strength of dilute species I in the endpoint compound JK. Equation (A1) is written for three species on each of two sublattices. In general, for n sublattices, each endpoint potential strength is multiplied by n compositions and V_I has as many terms as there are endpoint compounds. We limit the present treatment to the nine-term expression given by Eq. (A1) for convenience.

The endpoint strength $V_I(JK)$ vanishes identically if I is *equivalent* to J or K (i.e., identical species and sublattice).

Consequently, the potential strength for species A follows by setting $\iota = A$ in Eq. (A1).

$$V_A = b\,[xV_A(BD) + yV_A(BE) + zV_A(BF)] + c[xV_A(CD) + yV_A(CE) + zV_A(CF)]. \quad \text{(A2)}$$

V_B, V_C, etc., follow in similar fashion.

For example, if the alloy is $A_{1-x}B_xC_yD_{1-y}$, Eq. (A1) yields V_A as follows:

$$V_A = xyV_A(BC) + x(1-y)\,V_A(BD). \quad \text{(A3)}$$

Equation (A3) is identical to Eq. (6b).

As another example, consider the zincblende alloy $In_{1-x-y}Ga_xAl_yAs$. The alloy-scattering potential strength for In atoms follows from Eq. (A1).

$$V_{In} = xV_{In}(GaAs) + yV_{In}(AlAs) \quad \text{(A4)}$$

and similarly for V_{Ga} and V_{Al}. Of course, V_{As} vanishes identically since there is only one As sublattice species.

[1] G. B. Stringfellow, J. Appl. Phys. **50**, 4178 (1979).
[2] A. Chandra and L. F. Eastman, J. Appl. Phys. **51**, 2669 (1980), and J. Electrochem. Soc. **127**, 211 (1980).
[3] J. R. Hayes, A. R. Adams, and P. D. Greene, *GaInAsP Alloy Semiconductors*, edited by T. P. Pearsall (Wiley, Chichester, 1982), p. 189.
[4] J. H. Marsh, Appl. Phys. Lett. **41**, 734 (1982).
[5] K. Alavi, H. Temkin, W. R. Wagner, and A. Y. Cho, Appl. Phys. Lett. **42**, 254 (1983).
[6] D. L. Rode, *Semiconductors and Semimetals*, edited by R. K. Willardson and A. C. Beer (Academic, New York, 1975), Vol. 10, p. 1.
[7] From the viewpoint of quantum field theory, quasi-particles characterized by wavemember k are "almost free" if kinetic energy $E(\mathbf{k}) = \hbar^2\mathbf{k}^2/2m^*$ is much greater than $\hbar/\tau(\mathbf{k})$ where $\tau(\mathbf{k})$ is the k-dependent scattering time. This condition is equivalent to Eqs. (3)–(5) in the limits considered in the text. In particular, Eq. (4) is equivalent to an "uncertainty relation" $E(\mathbf{k})\cdot\tau(\mathbf{k}) \gg \hbar/2$ if $\mathbf{k} = \mathbf{k}_{ave}$ and $\tau(\mathbf{k}_{ave}) = m^*\mu_e/e$ in the effective-mass approximation.
[8] J. W. Harrison and J. R. Hauser, Phys. Rev. B **13**, 5347 (1976).
[9] P. A. Flinn, Phys. Rev. **104**, 350 (1956).
[10] W. Hume-Rothery, *Electrons, Atoms, Metals and Alloys* (Dover, New York, 1963).
[11] S. Adachi, J. Appl. Phys. **53**, 8775 (1982).
[12] SETA simulations (Semiconductor Electron Transport Analysis) of electron Hall mobility were performed by Pendragon Associates, Nine Prado, St. Louis, MO 63124.

DISTRIBUTION LIST

CONTRACT N00014-80-C-0762

Office of Naval Research — 4
Code 414
Arlington, VA 22217

Naval Research Laboratory
4555 Overlook Avenue, S.W.
Washington, DC 20375
Code 6810 — 1
Code 6820 — 1
Code 6870 — 1

Defense Documentation Center — 12
Building 5, Cameron Station
Alexandria, VA 22314

Dr. Y. S. Park — 1
AFWAL/DHR
Building 450
Wright-Patterson AFB
OH 45433

Dr. W. Wisseman — 1
Texas Instruments
Central Research Lab
M.S. 134
13500 North Central Expressway
Dallas, TX 75265

Dr. R. Bierig — 1
Raytheon Company
141 Spring Street
Waltham, MA 02173

Dr. Mike Driver — 1
Westinghouse Research and
Development Center
Beulah Road
Pittsburgh, PA 15235

Dr. F. Eisen — 1
Rockwell International
Science Center
P.O. Box 1085
Thousand Oaks, CA 91360

Mr. Lothar Wandinger — 1
ECOM/AMSEL/TL/IJ
Fort Monmouth, NJ 07003

Dr. William Lindley — 1
MIT
Lincoln Laboratory
F124 A, P.O. Box 73
Lexington, MA 02173

Commander — 1
U.S. Army/ERADCOM
Attn: V. Gelnovatch, DELET-M
Fort Monmouth, NJ 07703

Dr. F. Sterzer — 1
RCA
Microwave Technology Center
Princeton, NJ 08540

Commander — 1
Naval Electronics Systems Command
Attn: J. P. Letellier, Code 6142
Washington, DC 20360

Commander — 1
Naval Air Systems Command
Attn: A. Glista, Jr., AIR 34
Washington, DC 20361

Dr. R. Bell, K-101 — 1
Varian Associates, Inc.
611 Hansen Way
Palo Alto, CA 94304

Dr. Robert Archer — 1
Hewlett-Packard Corporation
1501 Page Road
Palo Alto, CA 94306

Drs. E. J. Crescenzi, Jr. and — 1
K. Niclas
Watkins-Johnson Company
3333 Hillview Avenue
Stanford Industrial Park
Palo Alto, CA 94304

Commandant 1
Marine Corps
Scientific Adviser (Code AX)
Washington, DC 20380

Dr. W. Weisenberger 1
Communications Transistor Corp.
301 Industrial Way
San Carlos, CA 94070

Drs. F. A. Brand and 1
J. Saloom
Microwave Associates
Northwest Industrial Park
Burlington, MA 01803

Commander, AFAL 1
AFWAL/AADM
Attn: Dr. Don Rees
Wright-Patterson AFB
OH 45433

Professor Walter Ku 1
Cornell University
Phillips Hall
Ithaca, NY 14853

Mr. Horst W. A. Gerlach 1
Harry Diamond Laboratories
800 Powder Mill Road
Adelphia, MD 20783

A.G.E.D. 1
201 Varick Street
9th Floor
New York, NY 10014

Dr. Ken Weller 1
TRW Systems
MS/1414
One Space Park
Redondo Beach, CA 90278

Professor L. Eastman 1
Cornell University
Phillips Hall
Ithaca, NY 14853

Dr. T. J. Magee 1
Advanced Research and
Applications Corporation
Sunnyvale, CA 94086

Professors Hauser and 1
Littlejohn
North Carolina State University
Department of Electrical Engineering
Raleigh, NC 27607

Professor J. Beyer 1
University of Wisconsin
Department of Electrical and
Computer Engineering
Madison, WI 53706

Professors Rosenbaum and Wolfe 1
Washington University
Semiconductor Research Laboratory
St. Louis, MO 63130

Dr. W. H. Perkins 1
General Electric Company
Electronics Lab 3-115/B4
P.O. Box 4840
Syracuse, NY 13221

Dr. Bryan Hill 1
AFWAL/AADE
Wright-Patterson AFB
OH 45433

Dr. J. Schellenberg 1
Hughes Aircraft Company
Electron Dynamics Division
3100 W. Lomita Boulevard
P.O. Box 2999
Torrance, CA 90509

Mr. H. Willing 1
Radar Directorate
BMD - Advanced Technical Center
P.O. Box 1500
Huntsville, AL 35807

Dr. C. Krumm 1
Hughes Research Laboratory
3011 Malibu Canyon Road
Malibu, CA 90265

Dr. E. Silberg 1
Bell Telephone Laboratories
Holmdel, NJ 07733

Dr. Harvey Nathenson 1
Westinghouse Research and
Development Center
Beulah Road
Pittsburgh, PA 15235

Dr. S. Wanuga 1
General Electric Company
Electronics Lab 134
Electronics Park
Syracuse, New York 13221

Professor D. Navon 1
University of Massachusetts
Department of Electrical and
Computer Engineering
Amherst, MA 01003

Professor Dan Dapkus 1
SSC 502
Dept. of Electrical Engineering
University of Southern California
University Park
Los Angeles, CA 90089

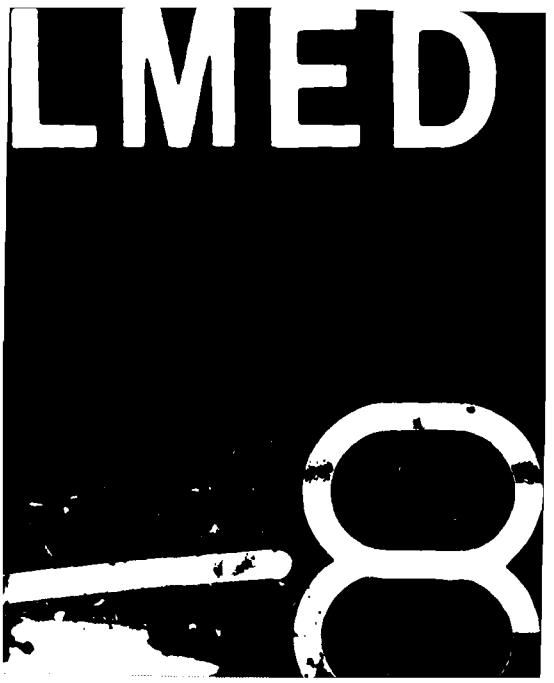
LMED